

DEEP GEOLOGIC

REPOSITORY

FOR OPG's LOW & INTERMEDIATE LEVEL WASTE

Postclosure Safety Assessment (V1): Gas Modelling

July 2009

Prepared by:

N Calder, J Avis, P Humphreys, F King, P Suckling and
R Walsh

NWMO DGR-TR-2009-07

Quintessa **INTERA**


SENE Consultants Limited

Note:

The Nuclear Waste Management Organization (NWMO) is managing the development of a Deep Geologic Repository for low and intermediate level radioactive waste, at the Bruce nuclear site, on behalf of Ontario Power Generation (OPG).

NUCLEAR WASTE MANAGEMENT ORGANIZATION

22 St. Clair Avenue East, Toronto, Ontario M4T 2S3 Canada
Toll Free: 1.866.249.6966
www.nwmo.ca

DEEP GEOLOGIC

REPOSITORY

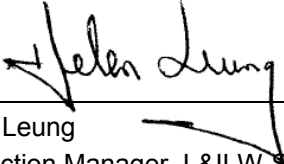
FOR OPG's LOW & INTERMEDIATE LEVEL WASTE

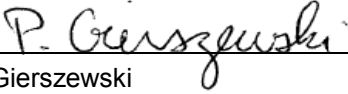
Preliminary

Postclosure Safety Assessment (V1): Gas Modelling

NWMO DGR-TR-2009-07

July 2009

Recommended by:  July 7, 2009
H. Leung Date
Section Manager, L&ILW Safety Assessment
NWMO

Accepted by:  July 7, 2009
P. Gierszewski Date
Director, Repository Safety
NWMO

DOCUMENT HISTORY

Title:	Postclosure Safety Assessment (V1): Gas Modelling		
Report Number:	NWMO DGR-TR-2009-07		
Revision:	0	Date:	7 th July 2009
Notes:	Initial release		
Prepared by:	N Calder, J Avis, P Humphreys, F King, P Suckling and R Walsh		
Reviewed by:	J Pickens (interim version) J Avis and R Little (final version)		
Approved by:	 R Little Project Manager Quintessa Limited		

EXECUTIVE SUMMARY

Ontario Power Generation (OPG) is proposing to build a Deep Geologic Repository (DGR) for Low and Intermediate Level Waste (L&ILW) near the existing Western Waste Management Facility at the Bruce Site in the Municipality of Kincardine, Ontario. The Nuclear Waste Management Organization, on behalf of OPG, is currently preparing an Environmental Impact Statement (EIS) and Preliminary Safety Report (PSR) for the proposed repository.

The project involves investigation of the site's geological and surface environmental characteristics, conceptual design of the DGR, and safety assessment. The postclosure safety assessment (SA) evaluates the long-term safety of the proposed facility. It will provide the basis for a future version of the safety assessment that will support the final EIS and the PSR.

The present report describes numeric modelling work undertaken to calculate the generation and build-up of gas in the repository, the two-phase exchange of gas and groundwater between the repository and the surrounding rock, and between the rock and the surface environment. The results are used to inform the Version 1 SA assessment modelling.

Models and Simulation Cases

Conceptual models for gas and groundwater flow in the geosphere were based on the repository design and descriptions of expected system evolution to create a high level description of the system to be modelled.

The modelling approach consists of a two dimensional radial and vertical axisymmetric grid encompassing the repository and 1.5 kilometres of geosphere around the repository. The repository representation has been simplified to comply with the radial model concept: the main and vent shafts have been combined to form a single shaft with properties representing the aggregate of both shafts, and the repository is represented by a radial segment of appropriate angle, thickness and volume.

The geosphere representation within the model focuses on two-phase flow transport in the lower permeability deep bedrock groundwater zone (the Ordovician sediments and below) and the intermediate bedrock groundwater zone (the Silurian sediments from the Salina F unit shale to the top of the Ordovician sediments).

The analyses considered two geospheres. The base case (BC) used low-permeability rock as described in the Phase I Geosynthesis report. The second "updated geosphere" (UG) model used much lower permeabilities, as implied by recent site characterization results.

A series of calculation cases based on the Normal Evolution Scenario were simulated. These include a base case and a number of sensitivity cases which address various parameter and conceptual model uncertainties. Additionally, a Disruptive Scenario considering severe shaft seal failure was simulated. Calculations were conducted using TOUGH2, coupled to a custom gas-generation module GGM. The coupled code is referred to as T2GGM.

In all cases, groundwater was assumed constant density; the gas species generated in the repository were converted to a single bulk gas of air for transport through the geosphere; no horizontal hydraulic gradients (e.g., in the Guelph unit) were implemented due to the limitations

of the 2D radial model; and climate change and glaciation related impacts were not addressed. The impacts of these are qualitatively addressed.

Results and Analysis

Modelling of the Normal Evolution (NE) Scenario base case and sensitivity cases indicate the following results.

- All cases with the base case geosphere show partial water saturation of the repository, to a saturation between 20 and 90%, before generation of gases increases pressures in the repository and expels water out of the repository. Eventually repository pressures decrease below pressures in the geosphere, and the repository begins to resaturate. Only the case with increased metal inventory (NE-GG1) expels all water from the repository to maintain a dry repository for the remainder of the simulation.
- All cases with the updated geosphere (UG cases) show very long delayed water saturation of the repository. Most show the beginning of water saturation late in the simulation, after 200 000 years, and by the end of the simulation, repository water saturations less than 15%. For the NE-UG-GT case (updated geosphere, initial gas content in the Ordovician), the repository does not begin to saturate within one million years.
- The different cases result in a range of peak repository pressures between 6.9 and 10 MPa, with the base case at 8.5 MPa at 2 000 years and the base case with an updated geosphere at 6.9 MPa at 1 000 000 years. Peak repository pressures are greatest for the cases based on the base case geosphere, as these cases have greater repository water saturation, reducing the void volume available for gas. All cases (except NE-UG-GT case as explained below) show peak pressures within about 1 MPa around the initial steady-state pressure at the repository horizon (7.6 MPa), and below the lithostatic pressure at the repository horizon (17 MPa).
- The two gas generation variants considered, NE-GG1 and NE-GG2, which investigate modified corrosion rates, degradation rates and increased metallic waste inventories, affected the peak pressure slightly, within 0.3 MPa.
- The NE-UG-GT case (updated geosphere, initial gas content in the Ordovician) has reached a pressure of 9.8 MPa by 1 Ma, the end of the simulation. This case starts with an assumed high gas pressure within the Ordovician rocks, due to the initial gas content and high capillary pressures in the Ordovician rocks, which will drive the steady-state pressure in the repository close to 12 MPa (the capillary pressure in the rock for a gas saturation of 4%, present at the end of the one million year simulation). For this case, the gas generation model conservatively allows water consuming reactions to proceed even once the water saturation has reached zero.
- The final gas composition, which is primarily determined by the initial waste inventories, was methane rich in all cases. The corrosion and microbial reaction rates are the main factors affecting the gas composition up until the time the waste is fully degraded/corroded. The microbial methane generation reaction from hydrogen and carbon dioxide was found to be the main reaction responsible for reducing the gas

pressure within the repository. Iron corrodes to form mostly magnetite (Fe_3O_4) and some siderite (FeCO_3).

- The results show that the rock mass forms a highly effective barrier to gas transport for the 1 Ma simulation period, preventing gas from migrating farther than a few meters from the repository. However, small amounts of dissolved gas eventually reach the top of the Intermediate Groundwater Zone (Salina F formation) in all cases from both shafts and rock mass.
- Only the NE-EDZ (high permeability in EDZ) case results in gas reaching the top of the Intermediate Groundwater Zone, due to the permeable shaft EDZ of this case.

The Severe Shaft Seal Failure (SF) Scenarios results show that:

- both gas and dissolved gas reach the top of the Intermediate Groundwater Zone (Salina F formation) and the amount of dissolved gas reaching the top of the Intermediate Groundwater Zone is much greater than in the NE cases;
- for cases with full shaft failure, most gas is transported upwards through the shafts with little to no gas through the rock mass ; and
- in all SF cases, repository water saturations at early times are increased, and repository peak gas pressures are about 8 MPa at 2 000 years.

Uncertainties

The sensitivity cases for the Normal Evolution Scenario considered in this report were intended to explore the range of responses to possible conceptual model or parameter uncertainty.

There are uncertainties with some parameters that potentially have a large impact on results: geosphere water and gas permeabilities; characterization of initial saturation and initial gas pressure conditions in host rock (including two-phase flow parameters); characterization of the shaft EDZ; and microbial activity under repository conditions. Where possible, conservative assumptions and bounding sensitivity cases address these uncertainties. Additional site characterization data will reduce uncertainties related to geosphere permeabilities and initial conditions. However, it is recommended that future studies consider the sensitivity to two-phase flow parameters (gas permeability and capillary pressure), considering their importance for the NE-UG-GT case, which provided results substantially different from the base case.

A conceptual model uncertainty relates to the spatial representation of the repository. For the repository, the gas generation model does not treat spatial heterogeneity within the repository directly. This conceptual simplification has allowed a detailed model to be used that separates the waste into waste streams that are subject to different degradation and corrosion processes and reaction rates, allowing all the major gas generation processes which might occur to be captured. Observed abrupt changes in gas generation behaviour are likely to result from the assumption of spatial and temporal constancy of corrosion rates for example. Considering variability in the repository for the gas generation model would likely improve the model and allow the impact of this variability to be assessed. As well, the modelling approach used is based on a dimensional simplification of the actual three-dimensional repository to an equivalent two-dimensional axisymmetric system, primarily to improve computational tractability.

Inherent uncertainties related to simplification of the repository and tunnel system could be addressed by future implementation of a fully 3D model as a sensitivity case.

Additional uncertainties in geosphere conceptual models will also affect results. Specifically, the time dependence and causal mechanisms for measured Cambrian overpressures and Ordovician underpressures are not completely understood. The base case assumes the Cambrian pressure is retained indefinitely, such that there is a net upward hydraulic gradient through the repository system. The base case also assumes a steady-state flow system and ignores the effect of Ordovician underpressures, which would generally tend to direct hydraulic gradients towards the repository for extremely long time periods. These assumptions are expected to be generally conservative. Future analyses considering possible time dependencies, such as incorporation of glacial loadings in coupled hydromechanical models, may provide additional insight into long-term system performance.

A number of issues were also identified for further improvement of the T2GGM model, including use of methane or a combination of gases, rather than air as the bulk gas; and differentiating between initial gas and gases potentially contaminated by waste degradation. While these issues are expected to have minimal impact on the results, resolution of these issues would improve the clarity of the results. In addition, the NE-UG-GT case highlights uncertainties in the modelling of the gas generation at zero saturation. While the current assumption that water-consuming reactions within the repository can continue is conservative, there is scope for model improvement.

CONTENTS

	<u>Page</u>
EXECUTIVE SUMMARY	v
1 INTRODUCTION.....	1
1.1 PURPOSE AND SCOPE	2
1.2 REPORT OUTLINE	3
2 CONCEPTUAL MODELS	4
2.1 T2GGM and GGM coupling	4
2.2 Gas Generation Overview	5
2.2.1 Classification of Organic and Metallic Wastes	5
2.2.2 Processes Not Included	6
2.2.3 Key Processes Included.....	6
2.2.4 Interaction between the Repository and Geosphere.....	9
2.3 Geosphere System Overview.....	9
2.4 Repository Location and Characteristics	12
2.5 Normal Evolution and Disruptive Scenarios.....	15
2.6 Modelling Approach	17
3 CALCULATION CASES	19
3.1 NORMAL EVOLUTION SCENARIO	19
3.2 DISRUPTIVE SCENARIOS	21
4 MODEL IMPLEMENTATION AND DATA	23
4.1 SOFTWARE CODES USED	23
4.2 DATA.....	23
4.2.1 Formation Properties.....	23
4.2.2 Shaft, Repository and Sealing Material Properties	33
4.2.3 Gas Generation Input Parameters	36
4.2.4 Gas Properties	36
4.3 MODEL IMPLEMENTATION	37
4.3.1 Model Structure	37
4.3.2 Model Discretisation and Property Assignment.....	40
4.3.3 Boundary and Initial Conditions	44
4.3.4 Gas and Water Source Terms	45
5 RESULTS FOR THE NORMAL EVOLUTION SCENARIO	47
5.1 Base Case (NE-BC)	48
5.1.1 Gas Generation	48
5.1.2 Gas and Water Flows	61
5.2 Case NE-GG1 – Increased rates and metal inventories	68
5.2.1 Gas Generation	68
5.2.2 Gas and Water Flows	72
5.3 Case NE-GG2 – Reduced organic degradation and hydrogen consumption rates	79
5.3.1 Gas Generation.....	79
5.3.2 Gas and Water Flows	81
5.4 Case NE-EDZ – High permeability EDZ	83

5.4.1	Gas Generation	83
5.4.2	Gas and Water Flows	86
5.5	Case NE-UG-BC – Updated geosphere Permeabilities	96
5.5.1	Gas Generation	96
5.5.2	Gas and Water Flows	99
5.6	Case NE-UG-EDZ – Updated Geosphere Permeabilities and High Permeability EDZ.....	106
5.6.1	Gas Generation	106
5.6.2	Gas and Water Flows	106
5.7	Case NE-UG-RD1 – Updated Geosphere Permeabilities and Backfilling of Tunnels	111
5.7.1	Gas Generation	111
5.7.2	Gas and Water Flows	113
5.8	Case NE-UG-GT – Updated geosphere Permeabilities and initial gas saturation in the Ordovician.....	117
5.8.1	Gas Generation	117
5.8.2	Gas and Water Flows	120
6	RESULTS FOR THE DISRUPTIVE SCENARIOS	127
6.1	Case SF-ES1: severe shaft failure	127
6.1.1	Gas Generation	127
6.1.2	Gas and Water Flows	129
6.2	Case SF-US: Upper shaft failure	138
6.2.1	Gas Generation	138
6.2.2	Gas and Water Flows	138
6.3	Case SF-UG-ES1: Severe shaft failure and updated geosphere data	141
6.3.1	Gas Generation	141
6.3.2	Gas and Water Flows	142
7	RESULTS ASSESSMENT AND COMPARISON	151
8	UNCERTAINTIES AND ISSUES FOR FURTHER WORK	161
8.1	GAS GENERATION MODEL.....	161
8.2	GAS TRANSPORT MODEL	164
8.2.1	MODELLING APPROACH	164
8.2.2	PARAMETER UNCERTAINTY	166
8.3	GEOSPHERE CONCEPTUAL MODEL UNCERTAINTY	166
9	SUMMARY AND CONCLUSIONS	169
	REFERENCES	172
	APPENDIX A: T2GGM V1.3 COMPUTER PROGRAM ABSTRACT.....	175
	APPENDIX B: SIMPLE GAS PRESSURE CALCULATION.....	179

LIST OF TABLES

	<u>Page</u>
Table 3-1: Gas modelling cases for the Normal Evolution Scenario	20
Table 3-2: Gas modelling cases for the SF Disruptive Scenario	22
Table 4-1: Geological Units and Model IDs	25
Table 4-2: Physical and hydrogeologic properties for each geological unit for the BC	26
Table 4-3: Two phase flow properties (Van Genuchten) for each geological unit.....	29
Table 4-4: Hydraulic conductivities of Silurian and Ordovician units for UG calculation cases. .	32
Table 4-5: Physical, hydrogeologic, and two phase flow properties for shaft, repository and EDZ for the BC.....	35
Table 4-6: Two phase flow $1/\alpha$ parameter (Van Genuchten) for inner and outer EDZ for the NE-EDZ case	36
Table 4-7: Cross-sectional areas of combined shaft (2DR model).	38
Table 7-1: Summary of Peak Repository Pressures and Water Saturations	154
Table 7-2: Summary of cumulative gas mass (in kg) crossing the SALF transport plane at the top of the detailed gas model	160
Table 7-3: Summary of cumulative dissolved gas mass (in kg) crossing the SALF transport plane at the top of the detailed gas model.....	160

LIST OF FIGURES

	<u>Page</u>
Figure 1-1: The DGR Concept at the Bruce Site	1
Figure 1-2: Document Structure for the Version 1 Postclosure Safety Assessment	2
Figure 2-1: T2GGM and GGM Coupling	4
Figure 2-2: Geological Stratigraphy from DGR Site Investigation Boreholes (Gartner Lee 2008b).....	10
Figure 2-3: Environmental head profile from DGR Site Investigation Boreholes based on May 2008 monitoring data.	12
Figure 2-4: Repository layout in UTM coordinate system.	13
Figure 2-5: Lithology and shaft sealing system (Walke et al. 2009b)	14
Figure 2-6: Conceptual illustration of the repository and shaft of the 2DR model. Mass flows are calculated using an area equivalent to a 90° angle as shown.....	18
Figure 4-1: Geologic layering in the gas transport model	24
Figure 4-2: Vertical permeability in the BC model, compared to the permeability for the full geological sequence.	27
Figure 4-3: Capillary pressure and relative permeability curves for limestone formations OLAR, SherR and CobR (which includes Cobourg and Collingwood). Due to the unavailability of data, OLAR has the same gas transport curves as SherR (Sherman Fall).....	30
Figure 4-4: Capillary pressure and relative permeability curves for shale formations OSAR and QueeR. Due to the unavailability of data, the formations above Queenston are set to the same gas transport curves as QueeR.	31
Figure 4-5: Vertical permeability in the BC and UG models.	33
Figure 4-6: Plan section of shaft in the 90° 2DR model.....	38
Figure 4-7: Plan section of repository in the 2DR model at the repository horizon	40

Figure 4-8: Detail of 2DR model property assignments. Note that ground surface is at 185.7 mASL (not shown).....	41
Figure 4-9: Detail of 2DR model discretization of repository, ring zone, monolith, shaft, EDZ, and lowest concrete bulkheads	43
Figure 4-10: Detail of discretization of asphalt waterstop system in 2DR model	44
Figure 5-1: NE-BC: Water Balance	49
Figure 5-2: NE-BC: Water Saturation.....	50
Figure 5-3: NE-BC: Amounts of Gases within the Repository	51
Figure 5-4: NE-BC: Amounts of Gases which have Left the Repository	52
Figure 5-5: NE-BC: Concentrations of Dissolved Gas within the Repository	52
Figure 5-6: NE-BC: Total and Partial Gas Pressures with the Repository	53
Figure 5-7: NE-BC: Amounts of Metallic Waste	56
Figure 5-8: NE-BC: Amounts of Corrosion Products	57
Figure 5-9: NE-BC: Iron Atom Stack Plot.....	57
Figure 5-10: NE-BC: Amounts of Organic Waste.....	58
Figure 5-11: NE-BC: Carbon Atom Stack Plot.....	58
Figure 5-12: NE-BC: Relative Humidity	59
Figure 5-13: NE-BC: Gas and Water Generation Rates.....	60
Figure 5-14: NE-BC: Dissolved gas flow rates across the ORD and SALF planes	61
Figure 5-15: NE-BC: Cumulative dissolved gas mass crossing the ORD and SALF planes.....	61
Figure 5-16: Evolution of conditions for the NE-BC at the start of the simulation (0 years), 800 years, and 1200 years. Gas saturation, and gas and water flow (outside repository) are shown in the figures on the left, and pressure and repository water saturation in the figures on the right.	63
Figure 5-17: Evolution of conditions for the NE-BC simulation at 2000 years, 3000 years, and 6000 years. Gas saturation, and gas and water flow (outside repository) are shown in the figures on the left, and pressure and repository water saturation in the figures on the right.	65
Figure 5-18: Evolution of conditions for NE-BC simulation at 600 000 years. Gas saturation and gas and water flows (outside repository) are shown in the figure above, and pressure and repository water saturation in the figure below.	66
Figure 5-19: Dissolved gas concentrations at 0, 2000, 100 000 and 600 000 years for the NE-BC. Note the different radial X and elevation scale at 0 years.	67
Figure 5-20: NE-GG1: Gas and Water Generation Rates	69
Figure 5-21: NE-GG1: Total and Partial Gas Pressures with the Repository.....	69
Figure 5-22: NE-GG1: Amounts of Gases which have Left the Repository	70
Figure 5-23: NE-GG1: Water Balance	70
Figure 5-24: NE-GG1: Water Saturation	71
Figure 5-25: NE-GG1: Amounts of Organic Waste	71
Figure 5-26: Dissolved gas flow rates across the ORD and SALF planes for the NE-GG1 case. Note different y-axis scale in comparison to the NE-BC.	72
Figure 5-27: Cumulative dissolved gas mass crossing the ORD and SALF planes for the NE-GG1 case. Note different y-axis scale in comparison to the NE-BC.	72
Figure 5-28: Evolution of conditions for the NE-GG1 case at the start of the simulation (0 years), 800 years, and 1500 years. Gas saturation, and gas and water flow (outside repository) are shown in the figures on the left, and pressure and repository water saturation in the figures on the right.	74
Figure 5-29: Evolution of conditions for the NE-GG1 case at 3000 years and 5000 years. Gas saturation, and gas and water flow (outside repository) are shown in the figures on the left, and pressure and repository water saturation in the figures on the right.	75

Figure 5-30: Evolution of conditions for the NE-GG1 case at 15 000 years. Gas saturation, and gas and water flows (outside repository) are shown in the figure above, and pressure saturation in the figure below. Note that there is no water saturation in the repository at this time.....76

Figure 5-31: Evolution of conditions for NE-GG1 simulation at 500 000 years. Gas saturation, and gas and water flows (outside repository) are shown in the figure above, and pressure and repository water saturation in the figure below.77

Figure 5-32: Dissolved gas concentrations at 0, 800, 45 000 and 378 000 years for the NE-GG1 case. Note the different radial X and elevation scale at 0 years.....78

Figure 5-33: NE-GG2: Amounts of Organic Waste80

Figure 5-34: NE-GG2: Total and Partial Gas Pressures with the Repository.....80

Figure 5-35: NE-GG2: Amounts of Corrosion Products.....81

Figure 5-36: Dissolved gas flow rates across the ORD and SALF planes for the GG2 case. ...82

Figure 5-37: Cumulative dissolved gas mass crossing the ORD and SALF planes for the GG2 case.82

Figure 5-38: NE-EDZ: Water Balance84

Figure 5-39: NE-EDZ: Water Balance - separate shaft/EDZ and rock mass flows.84

Figure 5-40: NE-EDZ: Water saturation85

Figure 5-41: NE-EDZ: Amounts of Gases which have Left the Repository.....85

Figure 5-42: NE-EDZ: Total and Partial Gas Pressures with the Repository86

Figure 5-43: Gas flow rates across the ORD and SALF planes for the NE-EDZ case (top: gas, bottom: dissolved gas).87

Figure 5-44: Cumulative gas mass crossing the ORD and SALF planes for the NE-EDZ case (top: gas, bottom: dissolved gas)88

Figure 5-45: Evolution of conditions for the NE-EDZ case at the start of the simulation (0 years), 500 years, and 1000 years. Gas saturation, and gas and water flow (outside repository) are shown in the figures on the left, and pressure and repository water saturation in the figures on the right.90

Figure 5-46: Evolution of conditions for the NE-EDZ case at 10 000 years, 15 000 years, and 1000 years. Gas saturation, and gas and water flow (outside repository) are shown in the figures on the left, and pressure and repository water saturation in the figures on the right.....91

Figure 5-47: Gas saturation for the NE-EDZ case at 25 000 years.93

Figure 5-48: Evolution of conditions for the NE-EDZ simulation at 1 000 000 years. Gas saturation is shown in the figure above, and pressure and repository water saturation in the figure below.....94

Figure 5-49: Dissolved gas concentrations at 0, 2000, 100 000 and 1 000 000 years for the NE-EDZ case. Note the different radial X and elevation scale at 0 years.95

Figure 5-50: NE-UG-BC: Water Balance.....97

Figure 5-51: NE-UG-BC: Water saturation.....97

Figure 5-52: NE-UG-BC: Total and Partial Gas Pressures with the Repository.....98

Figure 5-53: NE-UG-BC: Amounts of Gases which have Left the Repository98

Figure 5-54: Dissolved gas flow rates across the ORD and SALF planes for the NE-UG-BC. Note different y-axis scale in comparison to the NE-BC.100

Figure 5-55: Cumulative dissolved gas mass crossing the ORD and SALF planes for the NE-UG-BC. Note different y-axis scale in comparison to the NE-BC.....100

Figure 5-56: Evolution of conditions for the NE-UG-BC at the start of the simulation (0 years), 2000 years, and 10 000 years. Gas saturation, and gas and water flow (outside repository) are shown in the figures on the left, and pressure and repository water saturation in the figures on the right.102

Figure 5-57: Evolution of conditions for the NE-UG-BC at 25 000 years and 100 000 years. Gas saturation, and gas and water flow (outside repository) are shown in the figures on the left, and pressure and repository water saturation in the figures on the right.....	103
Figure 5-58: Evolution of conditions for NE-UG-BC simulation at 1 000 000 years. Gas saturation, and gas and water flows (outside repository) are shown in the figure above, and pressure and repository water saturation in the figure below.....	104
Figure 5-59: Dissolved gas concentrations at 0, 2000, 100 000 and 1 000 000 years for the NE-UG-BC. Note the different radial X and elevation scale at 0 years.	105
Figure 5-60: NE-UG-EDZ: Total and Partial Gas Pressures with the Repository.....	106
Figure 5-61: Dissolved gas flow rates across the ORD and SALF planes for the NE-UG-EDZ. Note different y-axis scale in comparison to the NE-UG-BC.....	107
Figure 5-62: Cumulative dissolved gas mass crossing the ORD and SALF planes for the NE-UG-EDZ. Note different y-axis scale in comparison to the NE-UG-BC.	107
Figure 5-63: Evolution of conditions for the NE-UG-EDZ at the start of the simulation (0 years), 2000 years, and 5000 years. Gas saturation, and gas and water flow (outside repository) are shown in the figures on the left, and pressure and repository water saturation in the figures on the right.	109
Figure 5-64: Repository water saturation for the NE-UG-EDZ case compared to the NE-UG-BC.....	110
Figure 5-65: Dissolved gas concentrations at 0, 2000, 100 000 and 1 000 000 years for the NE-UG-EDZ case. Note the different radial X and elevation scale at 0 years.....	110
Figure 5-66: NE-UG-RD1: Total and Partial Gas Pressures with the Repository.....	111
Figure 5-67: NE-UG-RD1: Water Balance	112
Figure 5-68: NE-UG-RD1: Water saturation.....	112
Figure 5-69: Dissolved gas flow rates across the ORD and SALF planes for the NE-UG-RD1 case. Note different y-axis scale in comparison to the NE-UG-BC.	113
Figure 5-70: Cumulative dissolved gas mass crossing the ORD and SALF planes for the NE-UG-RD1 case. Note different y-axis scale in comparison to the NE-UG-BC.....	114
Figure 5-71: Evolution of conditions for the NE-UG-RD1 case at the start of the simulation (0 years), 2000 years, and 10 000 years. Gas saturation, and gas and water flow (outside repository) are shown in the figures on the left, and pressure and repository water saturation in the figures on the right.	115
Figure 5-72: Evolution of conditions for NE-UG-RD1 simulation at 1 000 000 years. Gas saturation, and gas and water flows (outside repository) are shown in the figure above, and pressure and repository water saturation in the figure below.....	116
Figure 5-73: NE-UG-GT: Amounts of Gases which have Left the Repository. (Negative values indicate that gas has entered the repository.).....	118
Figure 5-74: NE-UG-GT: Amounts of Gases within the Repository	118
Figure 5-75: NE-UG-GT: Water Balance	119
Figure 5-76: NE-UG-GT: Relative Humidity	119
Figure 5-77: NE-UG-GT: Total and Partial Gas Pressures with the Repository.....	120
Figure 5-78: Conditions at the start and end of the simulation (0 and 1 000 000 years). Gas pressure is shown in the top two figures, water pressure in the middle two figures and gas saturation in the bottom two figures.....	122
Figure 5-79: Evolution of conditions for the NE-UG-GT case at the 10 000 years, and 140 000 years. Gas saturation, and gas and water flow (outside repository) are shown in the figures on the left, and pressure in the figures on the right. Note that pressures are water pressures, except in the repository, where they are gas pressures.	124

Figure 5-80: Evolution of conditions for the NE-UG-GT case at 1 000 000 years. Gas saturation is shown in the figure above, and gas pressure in the middle figure and water pressure below.....	125
Figure 5-81: Dissolved gas concentrations at 0, 2000, 100 000 and 1 000 000 years for the NE-UG-GT case. Note the different radial X and elevation scale at 0 years.....	126
Figure 6-1: SF-ES1: Water balance.....	128
Figure 6-2: SF-ES1: Total and Partial Gas Pressures with the Repository.....	128
Figure 6-3: SF-ES1: Amounts of Gases which have Left the Repository.....	129
Figure 6-4: Gas flow rates across the ORD and SALF planes for the SF-ES1 case (top: gas, bottom: dissolved gas).	130
Figure 6-5: Cumulative gas mass crossing the ORD and SALF planes for the SF-ES1 case (top: gas, bottom: dissolved gas). Note different y-axis scales to comparable figures. ...	131
Figure 6-6: Evolution of conditions for the SF-ES1 case at the start of the simulation (0 years), 200 years, and 600 years. Gas saturation, and gas and water flow (outside repository) are shown in the figures on the left, and pressure and repository water saturation in the figures on the right.	133
Figure 6-7: Evolution of conditions for the SF-ES1 case at 1400 years, 20 000 years, and 55 000 years. Gas saturation, and gas and water flow (outside repository) are shown in the figures on the left, and pressure and repository water saturation in the figures on the right.....	134
Figure 6-8: Evolution of conditions for the SF-ES1 simulation at 1 000 000 years. Gas saturation is shown in the figure above, and pressure and repository water saturation in the figure below.....	136
Figure 6-9: Dissolved gas concentrations at 0, 2000, 100 000 and 1 000 000 years for the SF-ES1 case. Note the different radial X and elevation scale at 0 years.....	137
Figure 6-10: Dissolved gas flow rates across the ORD and SALF planes for the SF-US case.	139
Figure 6-11: Cumulative dissolved gas mass crossing the ORD and SALF planes for the SF-US case.	139
Figure 6-12: Dissolved gas concentrations at 0, 2000, 100 000 and 1 000 000 years for the SF-US case. Note the different radial X and elevation scale at 0 years.	140
Figure 6-13: SF-UG-ES1: Water balance.....	141
Figure 6-14: SF-UG-ES1: Total and Partial Gas Pressures with the Repository.....	142
Figure 6-15: Repository gas pressures for the SF-UG-ES1 case, compared to the NE-UG-BC and SF-ES1 cases.	143
Figure 6-16: Repository water saturation for the SF-UG-ES1 case, compared to the NE-UG-BC and SF-ES1 cases.	143
Figure 6-17: Gas flow rates across the ORD and SALF planes for the SF-UG-ES1 case (top: gas, bottom: dissolved gas).....	144
Figure 6-18: Cumulative gas mass crossing the ORD and SALF planes for the SF-UG-ES1 case (top: gas, bottom: dissolved gas).	145
Figure 6-19: Evolution of conditions for the SF-UG-ES1 case at the start of the simulation (0 years), 200 years, and 600 years. Gas saturation and gas and water flow (outside repository) are shown in the figures on the left, and pressure and repository water saturation in the figures on the right.	147
Figure 6-20: Evolution of conditions for the SF-UG-ES1 case at 15 000, 25 000 and 45 000 years. Gas saturation, and gas and water flow (outside repository) are shown in the figures on the left, and pressure and repository water saturation in the figures on the right.....	148

Figure 6-21: Evolution of conditions for the SF-UG-ES1 simulation at 315 000 years. Gas saturation is shown in the figure above, and pressure and repository water saturation in the figure below. 149

Figure 6-22: Dissolved gas concentrations at 0, 2000 and 25 000 for the SF-UG-ES1 case. Note the different radial X and elevation scale at 0 years. 150

Figure 7-1: Average repository gas pressure for all cases based on the NE-BC geosphere. . 152

Figure 7-2: Average repository gas pressure for all cases based on the NE-UG-BC geosphere, as well as the NE-BC for comparison. 152

Figure 7-3: Average repository water saturation all cases based on the NE-BC geosphere... 153

Figure 7-4: Average repository water saturation all cases based on the NE-UG-BC geosphere. 154

Figure 7-5: Gas and dissolved gas flow rates crossing the SALF plane for all cases cases based on the NE-BC geosphere..... 156

Figure 7-6: Gas and dissolved gas flow rates crossing the SALF plane for all cases cases based on the NE-UG-BC geosphere. Note that all NE-UG-BC and NE-UG-RD1 case results are below the lower limit of the Y-axis..... 157

Figure 7-7: Gas and dissolved gas cumulative mass crossing the SALF plane for all cases based on the NE-BC geosphere..... 158

Figure 7-8: Gas and dissolved gas cumulative mass crossing the SALF plane for all cases based on the NE-UG-BC geosphere. 159

1 INTRODUCTION

Ontario Power Generation (OPG) is proposing to build a Deep Geologic Repository (DGR) for Low and Intermediate Level Waste (L&ILW) near the existing Western Waste Management Facility (WWMF) at the Bruce site in the Municipality of Kincardine, Ontario (Figure 1-1). The Nuclear Waste Management Organization, on behalf of OPG, is currently preparing an Environmental Impact Statement (EIS) and Preliminary Safety Report (PSR) for the proposed repository.

The project involves investigation of the site's geological and surface environmental characteristics, conceptual design of the DGR, and safety assessment. The Version 1 postclosure safety assessment (SA) evaluates the long-term safety of the proposed facility and will provide the basis for a future version of the safety assessment that will support the final EIS and PSR.

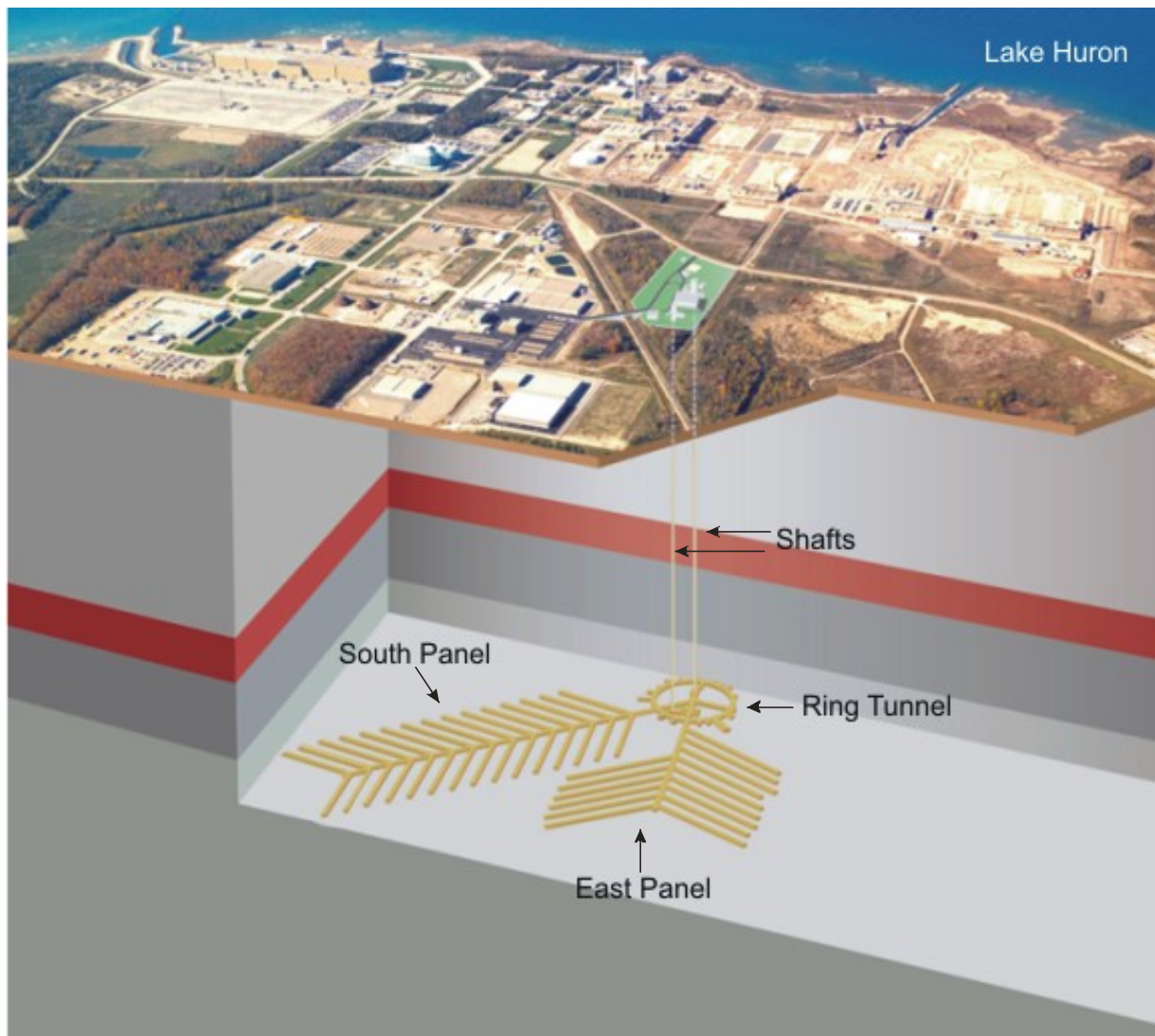


Figure 1-1: The DGR Concept at the Bruce Site

The Version 1 work builds upon a scoping assessment conducted by Quintessa in 2002 and 2003 (Penfold et al. 2003) and has been refined to take account of the revised waste inventory and repository design, and the greater understanding of the site that is being developed as the project proceeds.

This report (Gas Modelling) is one of a suite of documents that present the Version 1 SA studies (Figure 1-2), which also includes the Postclosure SA report (Quintessa et al. 2009), the Normal Evolution Scenario Analysis report (Walke et al. 2009a), the Human Intrusion and Other Disruptive Scenarios Analysis report (Penfold and Little 2009), the System and its Evolution (Little et al. 2009), the Features, Events and Processes report (Garisto et al. 2009), the Data report (Walke et al. 2009b), and the Groundwater Modelling report (Avis et al. 2009).

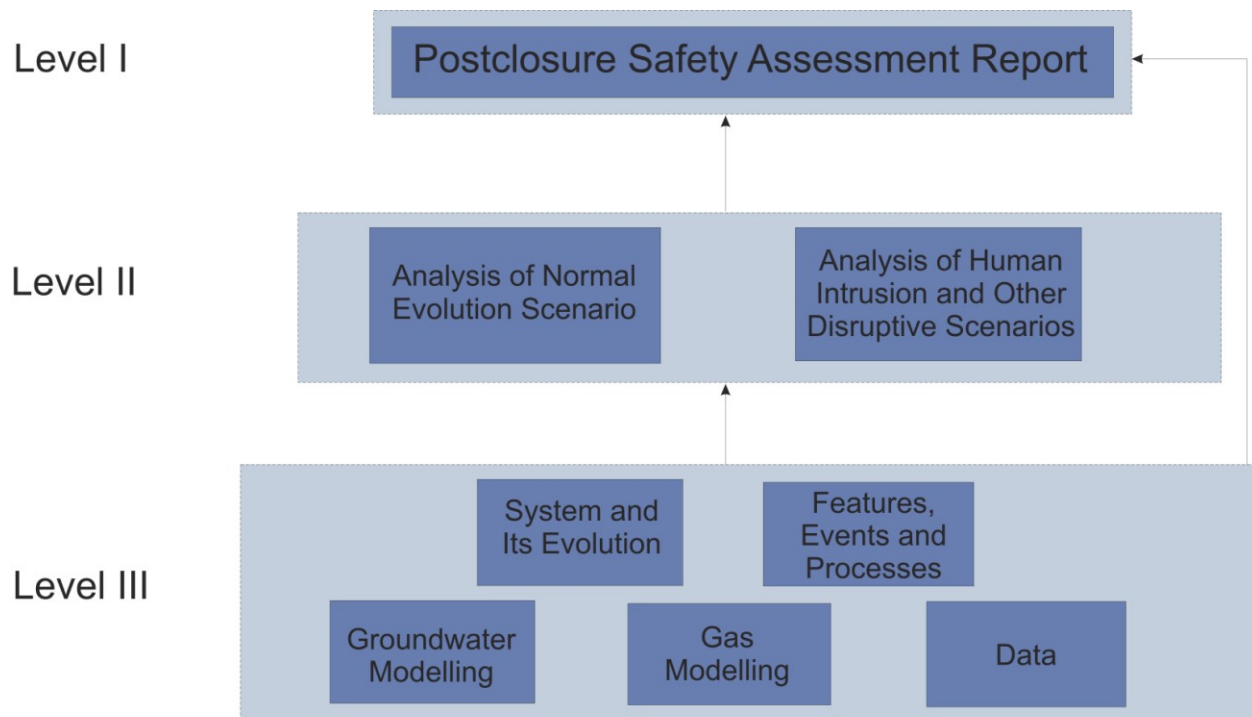


Figure 1-2: Document Structure for the Version 1 Postclosure Safety Assessment

1.1 PURPOSE AND SCOPE

This report describes numeric modelling work undertaken to calculate the generation and build-up of gas in the repository, and the two-phase flow of gas and groundwater from the proposed repository to the surface environment. The modelling was performed using a coupled gas generation and two-phase flow transport code that allows for detailed representation of repository and geosphere.

The detailed models are expected to capture most relevant aspects of overall system performance for both Normal Evolution Scenario and possible Disruptive Scenarios documented in Little et al. (2009). The detailed models were simulated for a base case set of parameters and initial conditions that approximate the Normal Evolution Scenario with the exception that glaciation cycle related impacts are not assessed. A number of calculation

cases addressing sensitivity to normal evolution scenario assumptions were also simulated, such as alternative geosphere boundary and initial conditions, engineered barrier system performance, and geosphere parameters. An additional calculation case was defined to simulate a “what if” disruptive scenario. Results of calculation cases are compared to the base case to provide a quantitative assessment of scenario significance.

Results from the detailed modelling provide input to the assessment modelling (Walke et al. 2009a, Penfold and Little 2009) and are also used to verify the mathematically less complex models of gas flow and transport used in the assessment modelling. The assessment modelling describes the performance of the total system (repository through biosphere) for all radionuclides, and calculates metrics that can be compared to regulatory standards, such as peak dose. This approach necessarily requires less numerically complex models which are abstractions of processes indicated as important by the detailed modelling presented in this report.

1.2 REPORT OUTLINE

The report is organised as follows:

- Section 2 describes the conceptual models of gas generation, flow and transport and the approach used to create numeric models representing the conceptual models;
- Section 3 describes the defined calculation cases;
- Section 4 provides an overview of the data used in the numeric modelling and the implementation of the detailed numeric models;
- Section 5 presents results of modelling for the Normal Evolution Scenario’s base and sensitivity calculation cases;
- Section 6 presents results for Disruptive Scenarios based on Severe Shaft Seal Failure Scenario;
- Section 7 presents graphical and tabular summaries and a discussion of all case results.
- Section 8 describes uncertainties in the modelling scenarios and results and enumerates issues for possible further consideration in subsequent version of the SA; and
- Section 9 provides overall conclusions on the detailed gas modelling results.

Appendix A provides a computer program abstract for the coupled generation and transport code used. This code is named T2GGM, and consists of TOUGH2 coupled to a custom gas-generation module. Appendix B provides a simple repository gas pressure calculation.

The report has been written for a technical audience that is familiar with the scope and objectives of the DGR project; the Bruce site; and the process of assessing the long-term safety of radioactive waste disposal.

2 CONCEPTUAL MODELS

This section of the report describes the general conceptual models of gas and water generation and consumption within the repository and the detailed modelling of the groundwater and gaseous pathways through the geosphere at the Bruce site. These conceptual models are generally consistent with the system and its evolution described in the Normal Evolution and Disruptive Scenarios. Differences required to best simulate the integrated repository and geosphere system while still maintaining computational tractability, are described.

2.1 T2GGM AND GGM COUPLING

The full model, T2GGM, comprises a TOUGH2 2-phase gas and water transport model, coupled to a custom gas generation model (Figure 2-1). Based on the current state of the repository as supplied by TOUGH2 and knowledge of the waste inventories, the gas generation model calculates the rate of generation of water and gas within the repository based on a model for corrosion and microbial degradation of the wastes. These rates are interpreted as sources for water and gas within TOUGH2's 2-phase flow model of the repository. TOUGH2 simulates the transport of gas and water through the repository and geosphere. TOUGH2 and the GGM are able to calculate the amount of bulk gas or the amounts of the individual gas components leaving the repository respectively. The following sections provide more detailed descriptions for the gas generation and gas and water transport models.

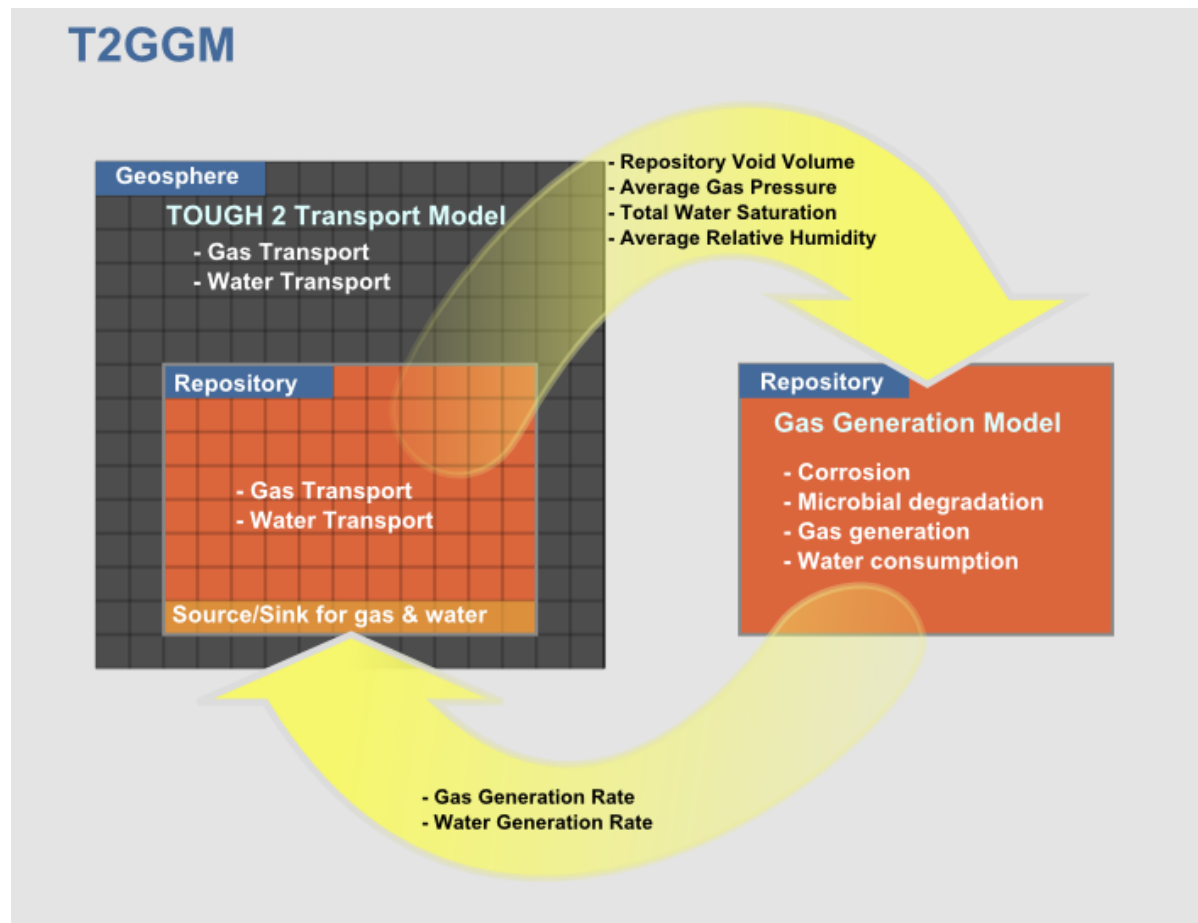


Figure 2-1: T2GGM and GGM Coupling

2.2 GAS GENERATION OVERVIEW

Gas generation within the repository is one of the key factors in the post-closure safety of the proposed facility. Gas is generated and consumed within the repository by various microbial and corrosion processes. The repository interacts with the geosphere through the fluxes of gas and water into and out of the repository. Following closure, the build-up of gas within the sealed repository affects the resaturation time and can lead to the release of gaseous radionuclides.

A gas generation model (GGM) has been developed to simulate various microbial and corrosion processes, and the gas evolution of the repository and its interaction with the geosphere. Using the GGM model it has been possible to establish which processes have only a relatively minor effect on the evolution of total gas pressure and gas saturation in the repository, and which are the key processes/factors determining the interaction of the repository with the geosphere. Thus, for simplicity, most of the results in this report are generated using a reduced version of the complete model, which only includes the key processes. The other processes are simply turned off by setting initial values to zero.

GGM tracks the production, consumption of the key chemical species (e.g., metals, organic wastes, gases, water) due to the gas generation reactions, and tracks the fluxes of the water and gases into and out of the repository. It is designed to fully conserve Fe and C, and to ensure that there is sufficient water to support reactions. Other elements are conservatively assumed not to be limiting and are not tracked to complete mass balance (e.g., N needed to support microbial reactions).

The following sections describe the waste streams and processes included in the simplified version of GGM used in the DGR Postclosure Safety Assessment. A complete description of all the processes included in GGM with supporting references, is given in the theory section of the software documentation (Suckling et al. 2009).

Note that for the simulations presented in this report, the GGM is implemented as part of T2GGM, a code that couples GGM and TOUGH2. TOUGH2 simulates multi-phase fluid flow in porous media and was developed by the Earth Sciences Division of Lawrence Berkeley National Laboratory (Pruess et al. 1999). Further information about T2GGM can be found in Section 4.1.

2.2.1 Classification of Organic and Metallic Wastes

The organic and metallic wastes are classified into a number of waste streams. This allows the degradation/corrosion of each waste stream to be modelled independently and assigned different reaction rates.

Organic wastes are classified into three groups: cellulosic wastes, ion-exchange resins, and plastics and rubbers.

Metallic wastes are classified into four groups: carbon and galvanised steels, passivated carbon steels, stainless steels and nickel alloys, and zirconium alloys.

2.2.2 Processes Not Included

Under ideal conditions, microbial systems employ a range of terminal electron acceptors in oxidation-reduction reactions which are consumed in a well-defined order depending on the amount of energy provided by each reaction: oxygen, nitrate, ferric ion, manganese, sulphate, and carbon dioxide. All of these stages apart from manganese are explicitly modelled in GGM. However, calculations found that all but the last methane generation stage complete very quickly under DGR conditions – within 10 to 20 years. This is because there are relatively small amounts of these terminal electron acceptors available initially within the DGR and host rock.

Furthermore, the reduction of the various terminal electron acceptors in the initial stages has minimal impact on the composition and amounts of the gases that play the main role in generating the peak gas pressures in the final stage: methane, hydrogen and carbon dioxide. Thus the gas modelling results presented here do not include the small initial amounts of terminal electron acceptors (oxygen, nitrate, ferric ion, manganese, and sulphate). GGM models only the final anaerobic methane generation stage.

The complete GGM model also includes provision for the growth of live biomass from cellulose, styrene and hydrogen, the death of biomass, and the recycling of a fraction of the dead biomass as organic matter with the remainder modelled as recalcitrant. The complete model shows that when biomass is included, the primary effect is that a small fraction of the carbon in the system becomes locked up as biomass. This reduces the amount of carbon available for methane and carbon dioxide, reducing peak pressures slightly. Since this effect is small and ignoring it results in a conservative outcome, biomass growth has been omitted from the modelling presented here. It is simply assumed that there is sufficient biomass to support the gas-generating reactions.

2.2.3 Key Processes Included

GGM includes four key mechanisms for the generation of gas and consumption of water (see Suckling et al. 2009 for complete supporting references):

1. the microbial degradation of organic wastes;
2. methanogenesis via the microbial hydrogen mechanism;
3. the corrosion of metallic wastes; and
4. the CO₂ enhanced corrosion of metallic wastes and formation of siderite (FeCO₃).

These processes may occur in either the saturated (water submerged) or vapour phases. Gases are modelled as partitioning between the saturated and vapour phases according to Henry's Law. The relative humidity of the vapour phase is calculated by TOUGH2 and provided as an input to the model (Figure 2-1). Microbial activity is expected to have completely ceased below a relative humidity threshold of 0.6. Since the relative humidity has remained sufficiently high (at 100% for most simulations), it has not been necessary to model the cessation of microbial activity. Aqueous corrosion processes are modelled as being active in the vapour phase provided the relative humidity is above a threshold of 0.6.

These four mechanisms are summarised in Sections 2.2.3.1 to 2.2.3.4 below.

2.2.3.1 Microbial Degradation of Organic Wastes

Cellulosic wastes are modelled as cellulose which degrade in the presence of water according to the following reaction:



The limiting reaction rate is that for cellulose hydrolysis.

Ion-exchange resins are modelled as styrene that has degraded from polystyrene, which degrade according to the following reaction:



The limiting reaction rate is that for styrene hydrolysis. The functional groups on the resins are an appreciable fraction of the resin mass, but do not contain carbon, and so do not contribute to the gas generation.

Plastics and rubbers represent a heterogeneous mix of materials such as PVC, polyethylene, neoprene, nitrile and latex. In order to assess the impact of potential plastic and rubber degradation on the overall gas generation these components are modelled in the same manner as ion-exchange resins.

The degradation of polymeric organic substrates is modelled as being first order with respect to their amounts.

2.2.3.2 Methanogenesis via the Microbial Hydrogen Mechanism

In radioactive waste disposal sites, significant amounts of hydrogen may be produced via anaerobic corrosion. This can be consumed anywhere in the system via the methanogenic reaction:



provided that there is sufficient humidity to support microbial processes. The minimum relative humidity required for microbial activity is approximately 0.6. It has been found in the cases analysed here that the relative humidity is almost always above this limit. The rate for this reaction is modelled as being first order with respect to CO_2 concentration, but limited by the availability of hydrogen.

2.2.3.3 Corrosion of Metallic Wastes

Corrosion of metallic wastes and container materials occurs within the saturated (water submerged) and vapour phases. Aqueous corrosion processes are possible in the vapour phase provided the relative humidity exceeds a threshold value of 0.6.

The inventory of carbon and galvanized steels in the repository will comprise various carbon steel wastes, as well as carbon and galvanized steel waste containers. Galvanized and carbon steels are treated as a single metallic source, represented by the corrosion of Fe as carbon

steel (C-steel). The initial presence of ferric corrosion products (rust) due to corrosion in air is neglected – all steel is conservatively assumed available for anaerobic corrosion.

The overall reaction for the anaerobic corrosion of C-steel is given below:



The reaction proceeds at a rate determined by the C-steel corrosion rate.

Passivated carbon steel comprises waste forms grouted in cementitious materials and structural steel (rebar, rails, etc.) in contact with concrete. These materials are treated separately from the plain carbon and galvanized steel inventories because of the effect of the cementitious material on the corrosion rate. Although the rate of corrosion of passivated carbon steel is lower, the mechanism is treated in exactly the same fashion as for the plain carbon and galvanized steel.

Stainless steels and nickel alloys are present as container materials and waste from steam generators and end fittings from pressure tubes, as well as miscellaneous waste forms. These materials contain Fe, Ni, Cr, Mo, and other minor alloying elements, in amounts dependent on the composition of the particular alloy.

For simplicity, the corrosion of the passive materials is treated in the same manner as carbon steel (i.e., Eqn 2-4). The passive materials and stainless steels/nickel alloys are modelled as 100% Fe and as fully reacting at a slower rate based on the effective corrosion rate of each type of metal.

Zirconium alloy waste comprises pressure tubes and other components of the decommissioned reactors. Typically these alloys contain small amounts of Nb, which is approximated as corroding similar to Zr. The corrosion of zirconium alloys is given by the following reaction:



2.2.3.4 CO₂ Enhanced Corrosion of Metallic Wastes

Carbon steel undergoes accelerated corrosion in the presence of high CO₂ partial pressures. The enhanced corrosion rate is primarily a consequence of the decrease in pH that accompanies the dissolution of CO₂ in water to form carbonic acid (H₂CO₃). However, because of the high HCO₃⁻ concentration, the stable corrosion product is siderite (FeCO₃) rather than Fe₃O₄. The corrosion rates for metallic wastes undergoing CO₂ enhanced corrosion are taken to be a function of the CO₂ partial pressure, with the overall corrosion reaction given by the following reaction (EU 1999):



Although the pH of the environment is not specifically calculated within the model, the use of an enhanced corrosion rate in the presence of CO₂ implicitly takes into account the acidification resulting from the dissolution of CO₂ in the aqueous phase. In terms of the model, the rate of reaction is treated as a multiplier of the anaerobic corrosion rate. Therefore, depending upon

the partial pressure of CO₂, the anaerobic corrosion rate is enhanced by an appropriate factor:

$$1 + \left(\frac{P_{\text{CO}_2}}{P_{\text{CO}_2}^{\text{ref}}} \right)^q \quad (2-7)$$

where P_{CO_2} is the partial pressure of CO₂, $P_{\text{CO}_2}^{\text{ref}}$ is a reference partial pressure of CO₂ and q is the reaction order with respect to the partial pressure of CO₂ and has a value of 0.67. If there is no CO₂ present, the factor is 1. The relative amounts of Fe₃O₄ and FeCO₃ formed are determined by the values of the respective rate constants which, in the case of FeCO₃, is the enhanced additional corrosion rate due to the partial pressure of CO₂.

In addition to the carbon and galvanised steels, the stainless steels and nickel alloys are also modelled as undergoing enhanced CO₂ corrosion and forming carbonate-containing corrosion products based on the experience of using these materials in CO₂-containing environments in the oil and gas industry. No CO₂ enhancement is included for Zr alloys.

2.2.4 Interaction between the Repository and Geosphere

The GGM model of the repository and TOUGH2 model of the geosphere are coupled via the total gas pressure, repository gas/water saturation, relative humidity, and repository void volume. These couplings determine the flows of water and of gas into and out of the repository. The TOUGH2 model simulates a single bulk gas (air) only. For the purpose of modelling the fluxes of individual gas components into and out of the repository, it is assumed that the composition of gas leaving or entering the repository is the same as that currently in the repository.

2.3 GEOSPHERE SYSTEM OVERVIEW

As described in Little et al. (2009), groundwater flow at the Bruce site can be divided into four basic zones, delineated by stratigraphy. The stratigraphic column at the Bruce site is based on results from boreholes DGR-1 and DGR-2 described in Gartner Lee (2008a), and presented in Figure 2-2. The groundwater zones are:

1. Surficial deposits (overburden) groundwater zone – Local flow of fresh water providing precipitation driven recharge to the underlying shallow groundwater zone. The surficial zone is approximately 20 metres thick.
2. Shallow bedrock groundwater zone – The relatively high permeability sequence consisting of Devonian and Upper Silurian (to Salina G) sediments to an approximate depth of 185 metres below ground surface (mBGS), or an elevation of 0 metres above sea level (mASL). Groundwater in this zone is fresh to brackish and flow is primarily horizontal, driven by topographic features with discharge to Lake Huron. Hydraulic gradients in this zone are sufficiently high to create advective dominated flow.

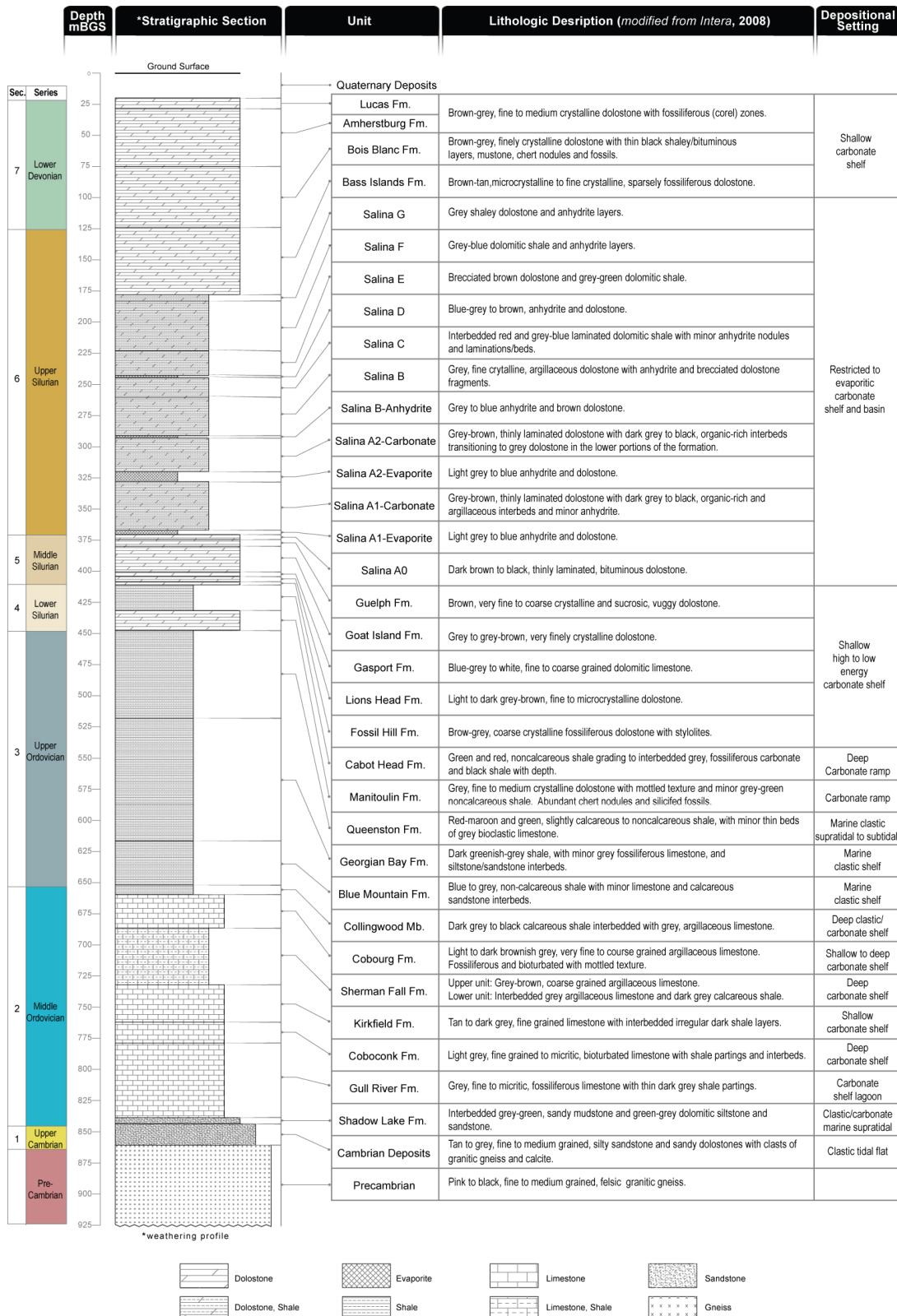


Figure 2-2: Geological Stratigraphy from DGR Site Investigation Boreholes (Gartner Lee 2008b)

3. Intermediate bedrock groundwater zone – The Silurian sediments from the Salina F down to the Manitoulin. Some zones of medium permeability exist in this sequence (Salina A2, Guelph/Salina A0), but the formations are primarily low-permeability shales and dolostones, with some extremely low permeability anhydrite beds. Regional horizontal groundwater flow is posited to exist in the medium permeability units, albeit under very low horizontal gradients. Groundwater in the zone is extremely saline (20 to 310 g L⁻¹). The intermediate zone is approximately 265 m thick (to an approximate depth of 450 mBGS, or an elevation of -265 mASL).
4. Deep bedrock groundwater zone - All stratigraphic units below the Manitoulin. Transport in the low-permeability Ordovician shales and limestones is expected to be diffusion dominated. Site characterization results (Figure 2-3) show elevated environmental heads in the Cambrian sandstones and underpressured conditions throughout the Ordovician sequence, indicating that the system is not in hydrodynamic equilibrium. Groundwater in the zone is extremely saline (150 to 350 g L⁻¹).

There are significant uncertainties associated with hydrogeologic characterization of the intermediate and deep bedrock groundwater zones. Estimates of formation hydraulic conductivity have not been finalized (see Section 4.2.1). Horizontal gradients in the more permeable intervals in the intermediate zones have not been determined at the site scale. Isolated zones of overpressure within the Silurian and Ordovician sediments shown in Figure 2-3 may represent the presence of a separate gas phase. The full extent of underpressures in the Ordovician sequences has yet to be determined, and the underlying cause of the non-equilibrium conditions is under investigation. The existence of the Cambrian overpressure is certain; however, neither its cause nor time dependence are currently known.

However, many of these features are indicative of a low vertical permeability host rock, and many of the uncertainties are essentially on "how low is low". The modelling approach and calculation cases presented in this report use conservative approaches which neglect the possible reductions in gas transport associated with the uncertainties.

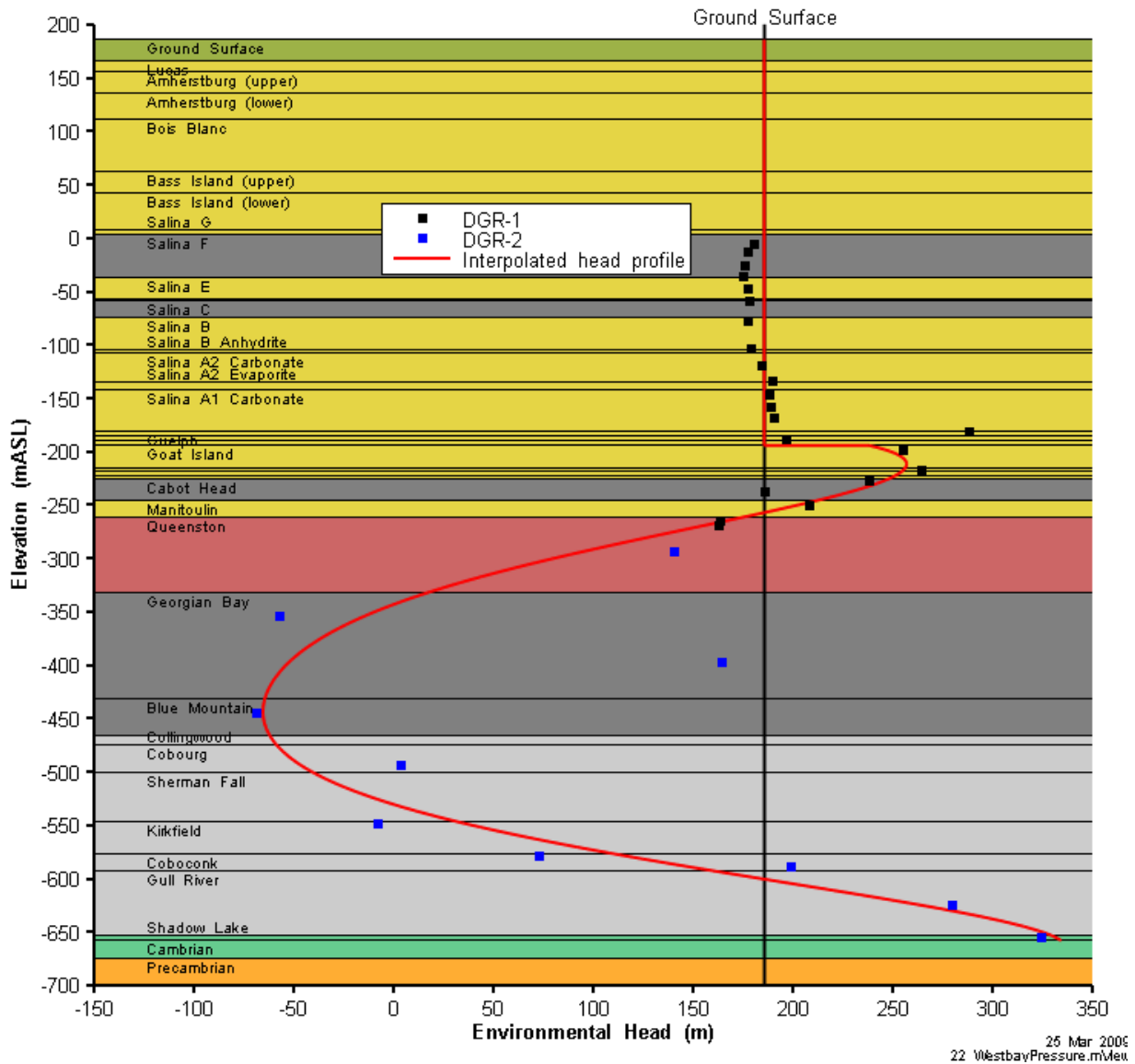


Figure 2-3: Environmental head profile from DGR Site Investigation Boreholes based on May 2008 monitoring data.

2.4 REPOSITORY LOCATION AND CHARACTERISTICS

The current repository design (adapted from Hatch, 2008) is shown in Figure 2-4 in relation to the site Universal Transverse Mercator (UTM) coordinate system. The figure also shows the location of current site characterization deep boreholes.

The repository design includes two waste emplacement panels (East and South) and two shafts; a main access shaft (8 m diameter at closure) and a smaller vent shaft (5.95 m diameter at closure). Both shafts are located within the area bounded by the 120 m diameter ring tunnel.

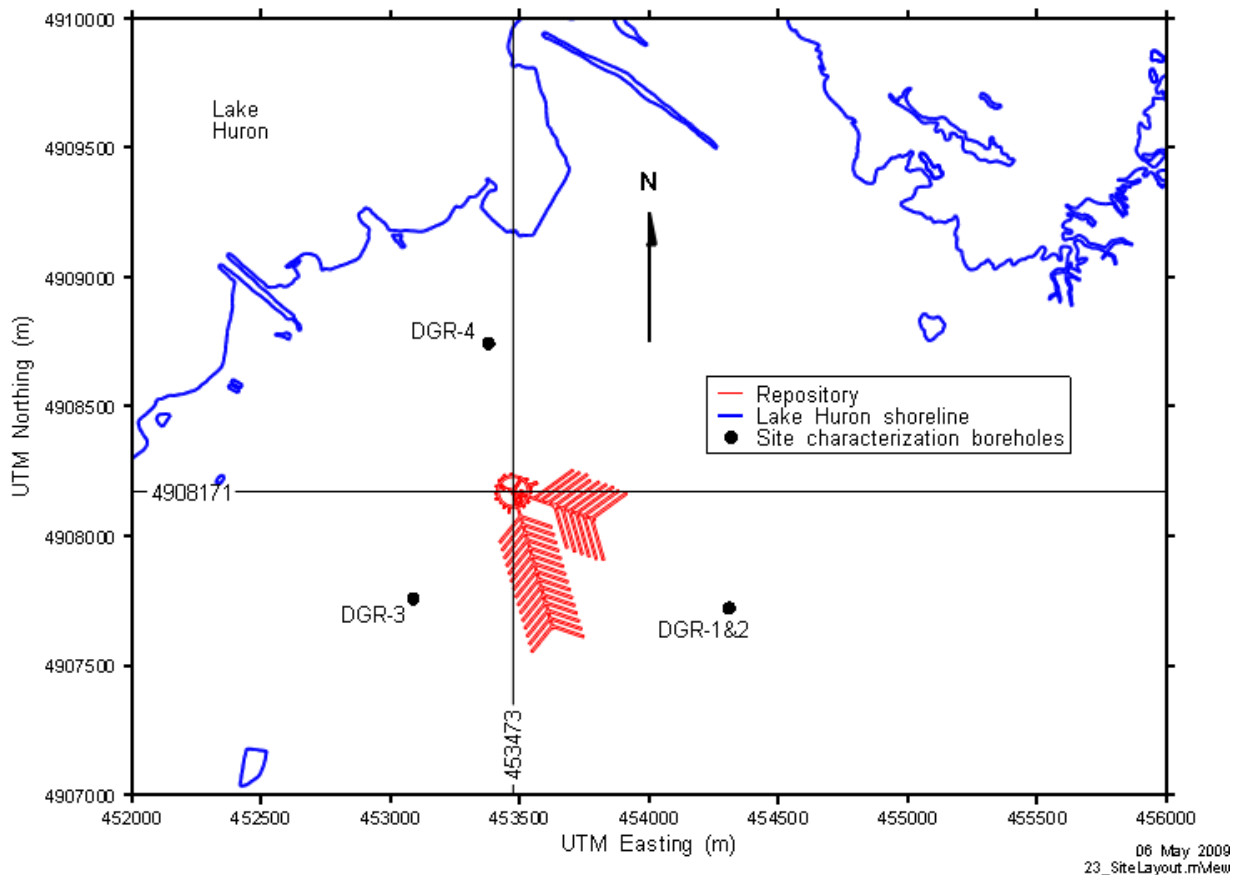


Figure 2-4: Repository layout in UTM coordinate system.

The repository is located at a depth of approximately 680 mBGS in the Cobourg Formation.

Hatch (2008) describes a post-closure shaft seal design consisting of compacted bentonite sand and asphalt waterstops seals separated by concrete bulkheads. The shaft sealing system isolates the repository from the biosphere by preventing groundwater and gas flow through the shafts and through the excavation damage zone (EDZ) surrounding each shaft.

The EDZ is described in detail in Little et al. (2009). Within the EDZ, permeability of the rock mass will increase due to horizontal stress relaxation. The EDZ is conceptualized as consisting of two zones, an inner EDZ extending from the shaft wall to an additional radius equal to one half the shaft radius; and an outer EDZ extending an additional one half shaft radius beyond the inner EDZ. The permeability of the inner EDZ is higher than the outer EDZ, reflecting increased stress relaxation in immediate proximity to the shaft.

The shaft seal design analysed in this report is described in Walke et al. (2009b) and is shown in Figure 2-5. The same sealing system is to be applied to both shafts. This design moves the location of some seals relative to the Hatch 2008 design to take advantage of newer information on site characteristics in order to improve overall system performance. It also includes cautious assumptions about the inner EDZ.

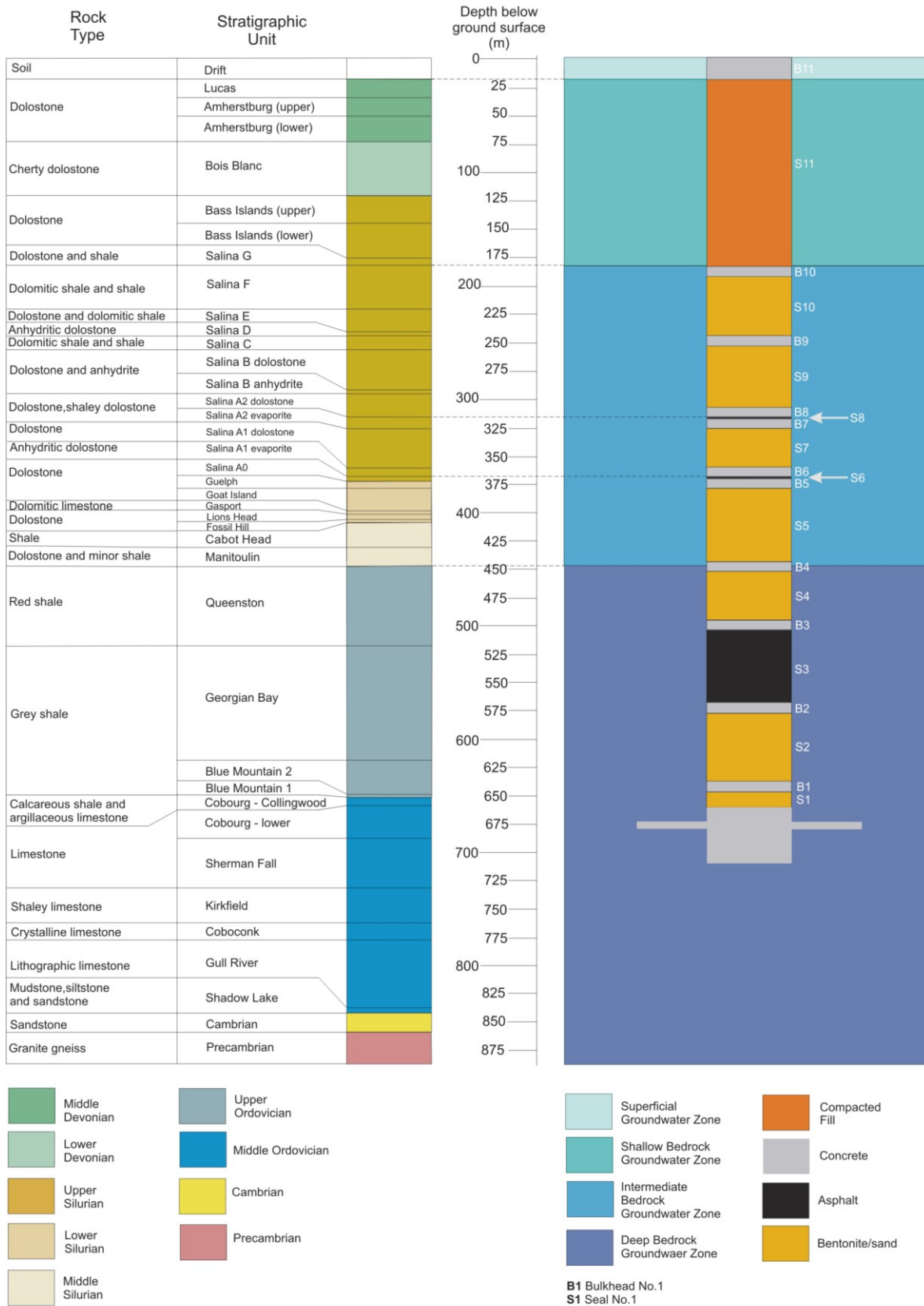


Figure 2-5: Lithology and shaft sealing system (Walke et al. 2009b)

2.5 NORMAL EVOLUTION AND DISRUPTIVE SCENARIOS

The Normal Evolution Scenario, described in detail in Little et al. (2009), is the consensus description of expected evolution of the geosphere and repository system as a function of time. It includes a detailed description of evolution of changes in the waste forms, repository conditions, geosphere evolution and climate conditions.

Ideally, a numeric model would incorporate all features, events, and processes (FEPs). However, limitations in numeric model capabilities preclude an all inclusive approach. Consequently, the scenario must be simplified, while still considering key FEPs.

The Normal Evolution Scenario implemented in the detailed gas modelling makes the following assumptions and simplifications.

1. Climatic impacts due to glaciation are not modelled. From a hydrogeologic modelling perspective, the impact of glaciation events can be extensive. Glacial advance and retreat provide large transient changes in mechanical and hydraulic loading of the geosphere system. However, regional data and modelling indicate (Gartner Lee, 2008a), and site characterization work is expected to confirm that this hydraulic loading has little influence on the deep groundwater system. The mechanical loading would reach the repository level, and the aggregate geomechanical impacts of multiple glacial cycles on the repository are included by making conservative assumptions about rockfall within the facility.
2. For the modelling presented in this report, the flow system is conservatively assumed to be at steady-state, with vertical gradients driven by a constant head boundary condition at the Cambrian. The steady-state flow system assumptions results in a prevailing upwards vertical gradient driven by the constant Cambrian head boundary condition. If the underpressures were incorporated in the analyses, the prevailing gradients within the Ordovician system would be towards the repository.
3. Groundwater is constant density. Preliminary site characterization results indicate that (as described in Section 2.3) extremely saline waters are found in the deep and intermediate systems. Ignoring salinity profiles simplifies the modelling approach and allows for use of steady-state models and in general is conservative. Furthermore, the Cambrian boundary condition heads used in the steady-state and transient modelling are based on the same density compensations. Modelling of salinity and variable density flow is important in systems with topographic driving forces for horizontal groundwater flow as increases in density with depth tend to decrease the depth of penetration of topographic induced heads and consequently moderates horizontal gradients, thus reducing transport. However, in the current local site system, where flow is primarily vertical due to the Cambrian overpressure and Ordovician underpressures, environmental head gradients already effectively incorporate the salinity profile.
4. Geosphere is assumed to be water saturated. Water saturation is the volumetric proportion of the porosity occupied by water. Characterization of initial gas saturations (proportion of the porosity occupied by gas, equal to one minus the water saturation) in the geosphere at the Bruce site is ongoing as part of the site characterization program. A sensitivity case in this report examines the impact of small initial gas saturations in the

geosphere. Note that desaturation of the rock mass and EDZ surrounding shafts and tunnels during the operational period are not considered. This is expected to have negligible impact on results, due to the relatively quick shaft resaturation times observed during all simulations (for the base case, shaft is fully saturated with water by 3000 years, with the shaft at the repository horizon fully water saturated by 800 years, see Section 5.1.2).

5. While the gas generation model considers multiple gas species, the model for two-phase transport considers only a single bulk gas of air. The generation rate of the multiple gas species is converted to a molar equivalent air generation rate. Note that air has different transport properties than the dominant gas leaving the repository, methane. Transport properties of air and methane are similar, except for solubility, with air solubility twice that of methane.

Four Disruptive Scenarios were also identified in which various scenarios were considered in which the major geosphere barriers could be breached (Little et al. 2009). Briefly stated, the scenarios and their treatment in the detailed groundwater modelling are as follows.

- Human Intrusion – An exploration borehole penetrates the repository and is abandoned. The intrusion is assumed to occur once institution control over the site is no longer effective. A steady-state saturated flow system is assumed to be established immediately after the borehole intersects the repository.
- Severe Shaft Seal Failure Scenario – The shaft seals (including the EDZ) perform much poorer than expected, possibly due to poor installation undetected by quality control and/or unexpected natural processes which results in more rapid and more extensive seal degradation. The scenario is conservatively modelled by setting the properties of all shaft sealing material at high permeabilities (at least four orders of magnitude greater than base case permeabilities). In addition, shaft seals do not intersect the EDZ and therefore do not impede flow through the EDZ. The EDZ permeability is assumed to be at the upper estimated value.
- Open Borehole Scenario – An exploration or monitoring borehole near, but not intersecting, the repository is not decommissioned properly. Standard practice is that exploration or water wells that are no longer to be used are sealed with bentonite or cement to prevent contamination of potable water supplies. If this step is not undertaken or is improperly performed, the abandoned well can provide a preferential path for the flow of contaminated groundwater.
- Extreme Earthquake Scenario – An extreme seismic event causes the reactivation of a fault in the vicinity of the repository, but outside the area assessed in detail by site characterization. An enhanced permeability vertical fault extending from the Cambrian to surface is assumed to reactivate at a location downgradient of the repository.

Only the Severe Shaft Seal Failure Scenario is considered in the present report on detailed gas transport modelling.

The Human Intrusion Scenario was not considered as gases would vent to surface upon intersection of the borehole with the repository, negating the requirement for a detailed gas model. The release rate of gas would be controlled by the operation of a blow-out preventor

normally installed on such deep boreholes. The other two Disruptive Scenarios (Open Borehole and Extreme Earthquake) were also not considered in this report, as inclusion of a borehole or fault within the current 2D radial gas transport model is not possible. A 3D model is required, which is currently not tractable given the very long run times of the detailed gas transport model. However, these scenarios are treated in assessment-level modelling (Penfold and Little 2009).

2.6 MODELLING APPROACH

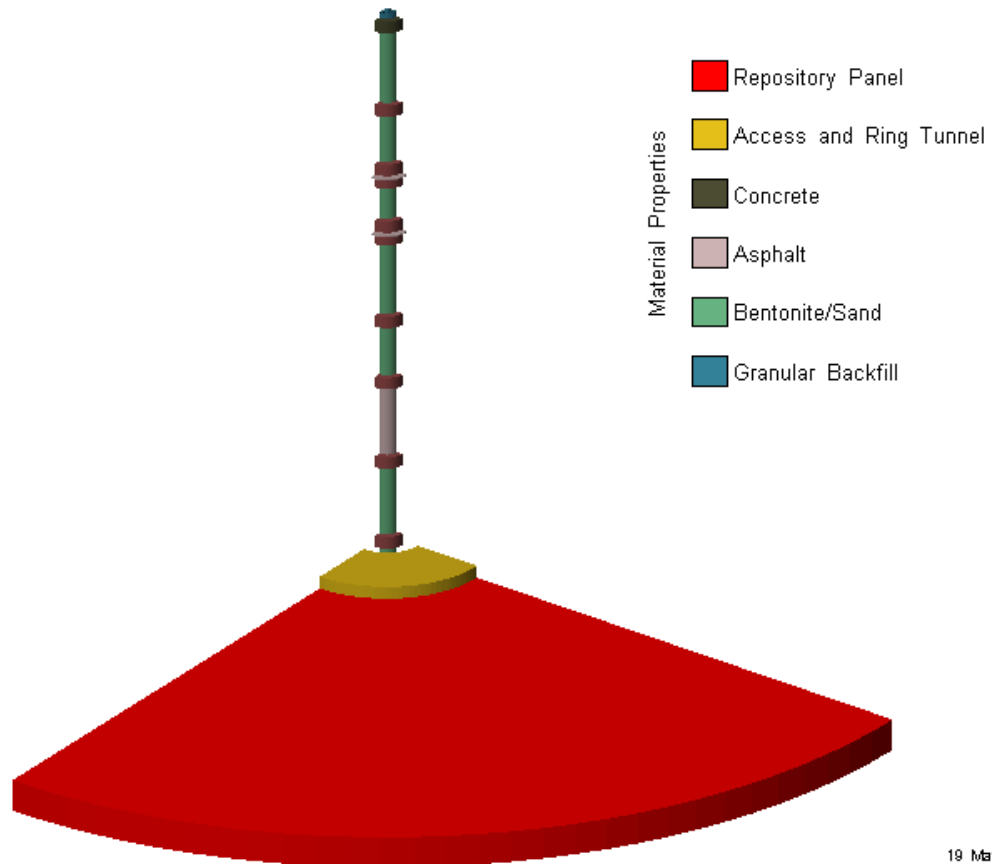
The model domain for the detailed two-phase flow and transport modelling presented in this report encompasses the repository and a several kilometre radius around the repository. This allows the modelling to focus on the impact of the repository on gas flow and transport and to effectively represent the relatively small scale features of the repository design such as shafts and shaft seals.

One effect of this limited domain is to require that regional flow processes be incorporated as boundary conditions. Regional flow modelling is being undertaken to support the Phase I site Geosynthesis (Sykes et al. 2008). Results of this modelling, and indications from site characterization, show that regional gradients and flow within the deep and intermediate bedrock groundwater zones are extremely low, and that transport within these zones is likely to be diffusion dominated. Consequently, the domain selected is appropriate for modelling transport in the vicinity of the repository with most vertical boundary conditions specified as zero-flow.

The approach to modelling two-phase flow and transport consists of a two dimensional radial and vertical axisymmetric grid (2DR) used to represent the repository and geosphere. The main and vent shafts have been combined to form a single shaft with properties representing the aggregate of both shafts. The conceptualisation is based on the 2DR detailed groundwater flow representation, presented in Avis et al. (2009), with modifications to alleviate numeric problems with the two-phase flow model. The conceptualization of the repository and shaft is shown in Figure 2-6.

The geosphere is described as horizontal layers with properties varying on a formation basis. Horizontal formations are a minor simplification of actual stratigraphy given the model domain and relatively shallow dip of formations at the Bruce site.

The 2DR model has significant computational advantages over a 3D model as significantly fewer nodes are required to accurately discretize the system. However, the 2DR model is incapable of representing horizontal gradients across the model domain as all horizontal flow is radial, relative to the central shaft. Furthermore, impacts of different spatial allocations of waste in the South or East panels cannot be represented. Finally, as will be shown later, the 2DR model overstates the importance of the central shaft and EDZ.



19 May 2008
Gas_2DRConcept.mView

Figure 2-6: Conceptual illustration of the repository and shaft of the 2DR model. Mass flows are calculated using an area equivalent to a 90° angle as shown.

3 CALCULATION CASES

Calculation cases were derived for the Normal Evolution scenario and for the disruptive event scenarios. A common calculation case naming convention has been specified for the detailed groundwater, detailed gas and assessment modelling. The calculation case identifier is made up of the scenario (NE – normal evolution, SF – shaft failure), additional identifiers describing the case (described below) and a suffix describing the model to be used (F2 – Groundwater 2DR, F3 – Groundwater 3DS, T – gas 2DR, A – assessment).

An additional modifier, -UG-, is used to indicate cases that are based on an “updated geosphere”. Recent preliminary site characterization information from boreholes DGR-3 and DGR-4 indicate that permeability in the Silurian and Ordovician sediments may be significantly lower than shown by DGR-1 and DGR-2 testing, which serves as the basis for the current permeability data outlined in Walke et al. (2009b). These lower permeabilities have significant impact on gas transport, and are therefore incorporated in the current assessment as an indicator of likely performance. However, until the preliminary DGR-3 and DGR-4 data are verified and accepted, the current base case permeability data will be used for most models, consistent with the Phase I Geosynthesis report (Gartner Lee 2008a) and the use of higher permeabilities is more conservative for transport. Hydraulic conductivity data for the updated geosphere are presented in Section 4.2.1.

3.1 NORMAL EVOLUTION SCENARIO

Detailed modelling was performed for a base case (BC) model and for a number of parameter and conceptual model sensitivity cases. The BC is characterized as follows:

- constant present-day climate conditions, no change in boundary condition during the simulation period;
- 1 000 000 year simulation period;
- stratigraphic, hydrogeologic, and transport properties as outlined in the Data report (Walke et al. 2009b);
- rockfall extends 20 m above repository and 30 m above central access and ring tunnels;
- EDZ zone with increased permeability (K) and porosity surrounding shaft and repository elements¹;
- removal of shaft inner EDZ where concrete bulkheads are to be installed;
- higher permeability of concrete bulkheads in shallow aquifer zone due to presumed partial degradation;
- 140 m hydraulic head fixed boundary at the bottom of the modelled system (the top of the Cambrian geological unit);
- 0 m fixed head boundary at the top of the upper bedrock unit (top of Salina F geologic unit for the detailed gas model);
- no flow boundaries on all vertical model boundaries;
- no horizontal gradient in the more permeable Silurian units (due to the limitations of a 2D radial model);

¹ The shaft EDZ is described as two zones (Inner and Outer) while a single EDZ zone is defined for the repository and tunnels. All EDZ zones are isotropic and are parameterized with hydraulic conductivity calculated as a multiple on the associated rock mass vertical hydraulic conductivity

- constant density water;
- single bulk gas of air;
- Initial gas saturation 98.3% in the repository (based on initial water content of waste), 50% in shaft, and 0% in rock mass;
- Initial inventory of metal mass is 5.8×10^7 kg and of organic mass is 2.2×10^7 kg, as reported in Table 4-10 of the Data Report (Walke et al. 2009b).
- Initial repository void volume of 3.3×10^5 m³ (based on emplacement rooms, access tunnels and ring tunnels), as reported in Table 4-5 of the Data Report (Walke et al. 2009b).
- Microbial hydrogen consumption rate is 1 y^{-1} , as reported in Section 3.6.6.2 of the Data Report (Walke et al. 2009b).

Detailed parameters, e.g., permeabilities, are presented in Section 4.2.

Table 3-1 describes the modelling cases for the Normal Evolution Scenario.

Table 3-1: Gas modelling cases for the Normal Evolution Scenario

Case ID	Case Description
NE-BC-T	Base case (BC) parameters, as described above.
NE-GG1-T	NE-BC except increased gas generation achieved by increasing the inventory of metals in the repository to 7.3×10^7 together with a corresponding increase in surface areas, and increasing corrosion and degradation rates using the maximum values given in the V1 Data Report (Walke et al. 2009b).
NE-GG2-T	NE-BC except use reduced degradation rates (i.e., minimum values from V1 data report (Walke et al. 2009b) which for anaerobic conditions are an order of magnitude less than the best estimate values) and a lower hydrogen consumption rate (0.01/yr).
NE-EDZ-T	NE-BC except permeability for inner EDZ assumed to be four orders of magnitude greater than the rock mass, and permeability for outer EDZ assumed to be two orders of magnitude greater than the rock mass. Interruption of inner EDZ by concrete bulkheads and asphalt waterstops is assumed to be ineffective. Reduced $1/\alpha$ values for the EDZ calculated using the Davies relationship (Davies 1991), which suggests that air-entry pressures are highly inversely correlated with permeability.
NE-UG-BC-T	NE-BC with updated geosphere data from DGR-3 and DGR-4 (DGR 2009).
NE-UG-EDZ-T	NE-UG-BC with the same adjustments to the EDZ as NE-EDZ.
NE-UG-RD1-T	NE-UG-BC except backfill access tunnels and ring tunnels filled with low permeability concrete (rockfall only in emplacement rooms). Resulting void volume is 3.0×10^5 m ³ .
NE-UG-GT-T	NE-UG-BC except initial gas saturations in Ordovician sediments of 10% (consistent with site characterization results).

The NE-GG1 modelling case examines the effect of increased metallic waste inventories due to additional overpacking of carbon and stainless steel wastes, increased corrosion rates and degradation rates. The overpacking only has a significant effect on the total mass of the unpassivated C-steel waste stream, which increases to 3.8×10^7 kg. The inventories of the other waste streams are unchanged to within the precision of the calculation. The increased metal inventories result in an increase in the surface areas exposed to corrosion processes. The procedure used to calculate the surface areas for the base case is reapplied to obtain the

following surface areas for the NE-GG1-T case: $1.2 \times 10^6 \text{ m}^2$ for unpassivated carbon steel, and $3.8 \times 10^5 \text{ m}^2$ for passivated alloys. The passivated C-steels and zirconium alloys are unaffected. Note that the overpacking and container wastes are treated separately in the analysis. The degradation rates are all increased by a factor of 10.

The NE-GG2 case is as described in Table 3-1.

The NE-EDZ modelling case examines the impact if the maximum EDZ hydraulic conductivity estimates from Walke et al. (2009b) are applied and the air-entry pressure of the EDZ is reduced (by reducing $1/\alpha$ values). Additionally, this scenario assumes that the interruption of the inner EDZ by the concrete bulkheads and asphalt waterstops does not function as planned, such that the excavation of the inner EDZ simply generates new inner EDZ around the larger cavity prior to installation and curing the concrete bulkheads.

Reduction of air-entry pressures ($1/\alpha$) for the NE-EDZ case was accomplished by applying the Davies relationship (Davies 1991) to the formation permeability:

$$P_{ae} = 5.6 \times 10^{-7} k^{-0.346} \quad (3-1)$$

where:

P_{ae} is the air entry pressure, MPa; and
 k is the rock permeability, m^2 .

For example, the revised air-entry pressure for the Inner EDZ in the Cobourg Formation is 0.75 MPa, compared to 50 MPa for the NE-BC. The same air-entry pressure was applied to both the Inner and Outer EDZ.

Modelling case NE-UG-RD1 examines the effect of sealing the access and ring tunnels with concrete, essentially extending the monolith out to the repository panels.

The NE-UG-GT examines the impact of potential initial gas saturations in the Ordovician sediments. As described in Section 2.3, initial gas saturations may explain the existence of the underpressures currently observed at the Bruce site. Initial gas saturations of 10% are assumed in the Ordovician sediments.

3.2 DISRUPTIVE SCENARIOS

Three calculation cases are considered for the Disruptive Scenarios, all based on the Severe Shaft Seal Failure Scenario (SF). Other scenarios are not considered due to the limitations of the 2D radial gas transport model (i.e., features such as open boreholes or fractures, required by the Human Intrusion, Open Borehole and Extreme Earthquake Scenarios cannot be modelled with a 2D radial model; a 3D model would be required). The SF calculation cases are enumerated in Table 3-2.

The SF cases simulate improper repository closure or other unexpected events that lead to very poor shaft seal performance. In the SF-ES1 case, all shaft and seal materials are assigned an extremely high hydraulic conductivity of 10^{-7} m/s , and the inner EDZ permeability is assumed to be four orders of magnitude greater than for rock mass. Concrete bulkheads, as well as the asphalt waterstops, are not keyed into the inner EDZ, resulting in a continuous flow path up the inner EDZ. As well, air-entry pressures of the EDZ are reduced (by reducing $1/\alpha$ values), in the

same manner and the NE-EDZ case. The SF-UG-ES1 case simulates the same sealing failure within the updated geosphere system. The SF-US case assumes the seal failure zone is restricted to the Silurian formations. Failure of the seals is assumed to occur instantly for all three cases.

Table 3-2: Gas modelling cases for the SF Disruptive Scenario

Case ID	Case Description
SF-ES1-T	As NE-BC but with hydraulic properties of all seals, backfill and inner EDZ set to extreme values and seals not keyed into EDZ.
SF-UG-ES1-T	SF-ES1 with updated geosphere data.
SF-US-T	As SF-ES1 but with failure only for those seal system components located above the top of the Queenston shale.

4 MODEL IMPLEMENTATION AND DATA

4.1 SOFTWARE CODES USED

All detailed gas modelling presented in this report has been performed using T2GGM (Version 1.3), a code coupling the Gas Generation Model (GGM, Version 3.0) and TOUGH2 (Version 2.0, EOS3 equations of state). GGM models the generation of gas within the DGR due to corrosion and microbial degradation of the various waste streams present, and TOUGH2 models the subsequent two-phase transport of the gas through the geosphere. GGM, a project-specific model, was written and is maintained by Quintessa Limited. TOUGH2 is a general-purpose numerical simulation program for multi-phase fluid and heat flow in porous and fractured media developed by the Earth Sciences Division of Lawrence Berkeley National Laboratory (Pruess et al. 1999), and the EOS3 equation of state module simulates the transport of air and water. The EOS3 equation of state module uses the steam table equations for the properties of water and assumes that air is an ideal gas. Integration of the TOUGH2 and GGM codes was performed by and is maintained by Intera Engineering Ltd. Quality assurance documentation for T2GGM is provided in Suckling et al. (2009) and Appendix A. A summary of GGM is provided in Section 2.1 and 2.2.

Model pre- and post-processing has been performed using mView 4.02, a proprietary modelling support tool developed by Intera Engineering Ltd. Pre-processing procedures consist primarily of discretization and property assignment. Post-processing includes all summary calculations and visualizations. mView 4.00A has been qualified to Yucca Mountain Project (YMP) Software Quality procedures. Additional capabilities added to mView since the YMP qualification have been verified in compliance with Intera's internal, ISO 9001 compliant, software development procedure.

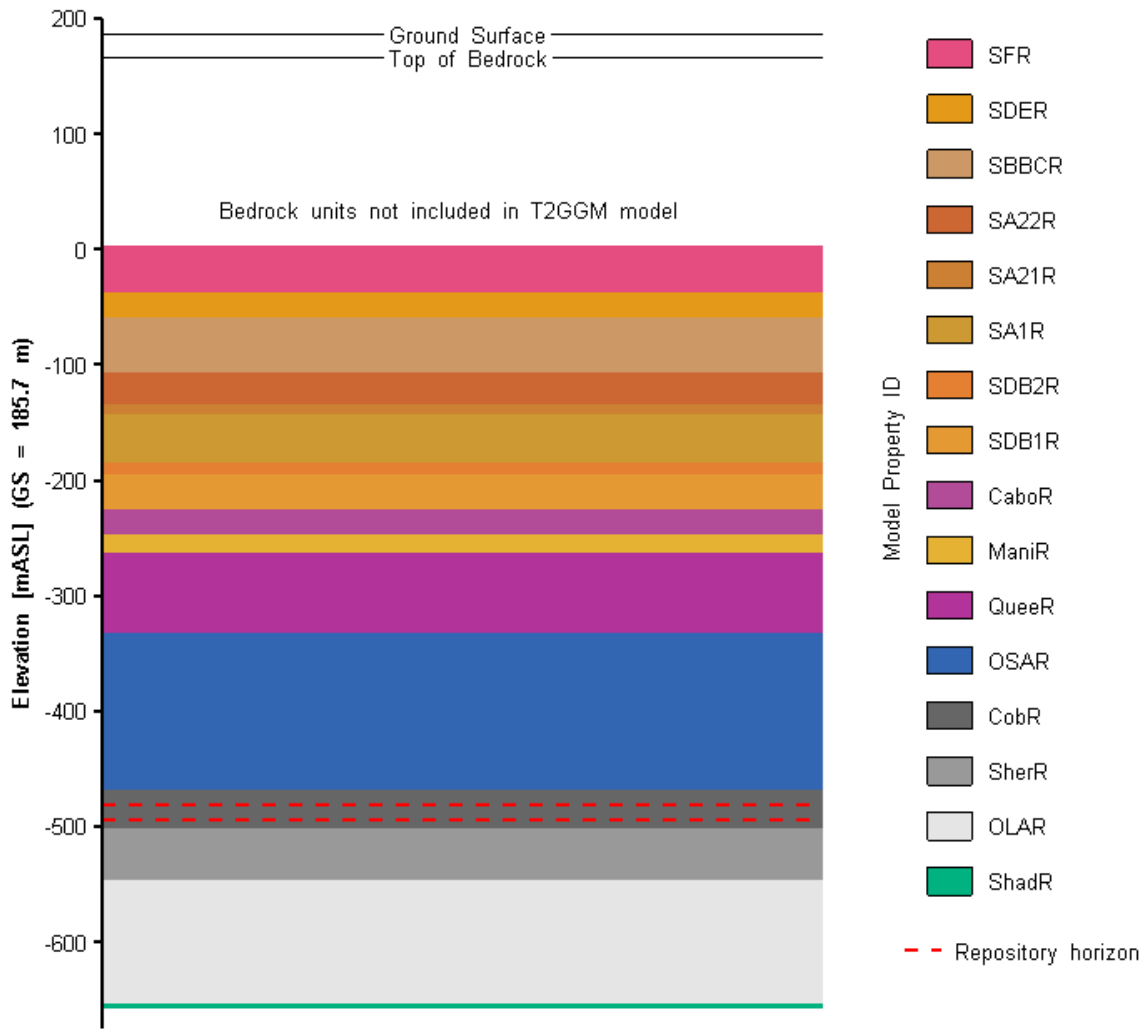
The detailed gas calculations have been conducted to standards specified in the Intera Engineering ISO 9001 Registered Quality Management System. There is a specific Work Instruction (WI), Numeric Modelling, which describes model input file management and archiving using a version control system.

4.2 DATA

This section presents the rock property data from Walke et al. (2009b) and describes how the data are used to delineate model units.

4.2.1 Formation Properties

Stratigraphy outlined in the Data report (Walke et al. 2009b) serves as the basis for the assignment of properties to the layers of the numerical model. The numerical models extend from the top of the Intermediate Bedrock Groundwater Zone (Salina F) at a depth of 183 m (elevation 3 mASL) to the bottom of the Ordovician Shadow Lake formation at a depth of 844 m (elevation -658 mASL), as shown in Figure 4-1. As will be discussed in Section 4.3.1 below, ignoring the Shallow Bedrock Groundwater Zone will provide a conservative estimate on the gas flows reaching the surface, while improving model stability. As well, a 3D model, rather than the current 2D model, would be required to represent flow through the Shallow Bedrock Groundwater Zone. Assessment modelling has considered the Shallow Bedrock Groundwater Zone pathway for gas release to the surface (Walke et al. 2009a).



GeologicLayersAndK.mView
31 Mar 2009

Figure 4-1: Geologic layering in the gas transport model

Simplification of the geologic layering was required for numeric tractability. Table 4-1 describes the combined stratigraphic geologic units of the gas transport model. Stratigraphic nomenclature in Table 4-1 is taken from Walke et al. (2009b). The table column “Model ID” designates the material property name used for the geologic units, and indicates the geologic units combined for simplification in the detailed gas transport model. The Model ID is limited to a maximum of five characters for the T2GGM model, and the text “R” indicates rock mass rather than the EDZ.

Table 4-1: Geological Units and Model IDs

Age	Stratigraphic Unit	Hydro-stratigraphic unit	Model ID	Top Elevation	
				mBGS	mASL
Quaternary	Various	Surficial	Not used	0	185.7
Devonian	Various	Shallow	Not used	20	165.7
Upper Silurian	Salina F	Intermediate	SFR	183	3
Upper Silurian	Salina E		SDER	223	-37
Upper Silurian	Salina D			243	-57
Upper Silurian	Salina C		SBBCR	245	-59
Upper Silurian	Salina B			260	-75
Upper Silurian	Salina B Anhydrite			291	-106
Upper Silurian	Salina A2 Carbonate		SA22R	293	-107
Upper Silurian	Salina A2 Evaporite		SA21R	320	-134
Upper Silurian	Salina A1 Carbonate		SA1R	328	-142
Upper Silurian	Salina A1 Evaporite			367	-181
Upper Silurian	Salina A0		SDB2R	371	-185
Middle Silurian	Guelph			375	-189
Middle Silurian	Goat Island			380	-194
Middle Silurian	Gasport		SDB1R	401	-215
Middle Silurian	Lions Head			404	-219
Middle Silurian	Fossil Hill			408	-223
Lower Silurian	Cabot Head	411		-225	
Lower Silurian	Manitoulin	ManiR	432	-246	
Upper Ordovician	Queenston	Deep	QueeR	448	-262
Upper Ordovician	Georgian Bay		OSAR	518	-332
Upper Ordovician	Blue Mountain			617	-431
Middle Ordovician	Collingwood		CobR	652	-466
Middle Ordovician	Cobourg			660	-474
Middle Ordovician	Sherman Fall		SherR	687	-501
Middle Ordovician	Kirkfield		OLAR	732	-546
Middle Ordovician	Coboconk			762	-576
Middle Ordovician	Gull River			779	-593
Middle Ordovician	Shadow Lake		ShadR	839	-653
Cambrian	Cambrian		Not used	844	-658
Precambrian	Precambrian		Not used	861	-675

Table 4-2 provides the physical and hydrogeologic properties for each model unit obtained from the Data report (Walke et al. 2009b), with properties for consolidated geologic layers represented by an average of the member geologic layers (log-average for permeability and pore compressibility) for the detailed gas model. Vertical permeability (K_v) values for the model layers are shown graphically in Figure 4-2, in comparison to the K_v values for the full geologic sequence (the full geologic sequence was used in the 2DR groundwater model). The comparison of K_v values illustrates the minimal impact of geologic layer simplification in the gas transport model. Within two units, SBBCR and SA1R, consolidated permeabilities for the gas transport model appear to be greater than those for the full geologic sequence, due to the presence of thin higher permeability units (SB1R and SA11R) within these consolidated units.

Table 4-2: Physical and hydrogeologic properties for each geological unit for the BC

Unit	Top Elevation (mASL)	Porosity (-)	Horizontal Permeability (K_h) (m^2)	Vertical Permeability (K_v) (m^2)	Pore Compressibility* (Pa^{-1})
SFR	3	0.03	2.81E-19	2.81E-20	9.33E-09
SDER	-37	0.06	9.39E-19	9.39E-20	2.02E-09
SBBCR	-59	0.08	2.99E-19	6.44E-20	2.99E-09
SA22R	-107	0.08	1.26E-17	1.26E-18	6.25E-10
SA21R	-134	0.08	8.23E-16	8.23E-16	4.38E-10
SA1R	-142	0.08	9.39E-20	2.97E-20	5.12E-10
SDB2R	-185	0.08	1.26E-15	1.26E-16	6.00E-10
SDB1R	-215	0.08	1.84E-18	1.84E-19	6.00E-10
CaboR	-225	0.03	9.39E-20	9.39E-21	8.33E-08
ManiR	-246	0.01	2.81E-19	2.81E-20	2.30E-08
QueeR	-262	0.09	5.33E-19	5.33E-20	4.82E-09
OSAR	-332	0.09	1.04E-18	1.04E-19	1.62E-08
CobR	-466	0.02	1.94E-18	1.94E-19	6.92E-09
SherR	-501	0.01	1.55E-18	1.55E-19	2.38E-08
OLAR	-546	0.02	4.17E-18	4.17E-19	4.62E-09
ShadR	-653	0.01	9.68E-17	9.68E-18	1.30E-08

*Pore compressibilities are calculated from rock compressibility divided by porosity.

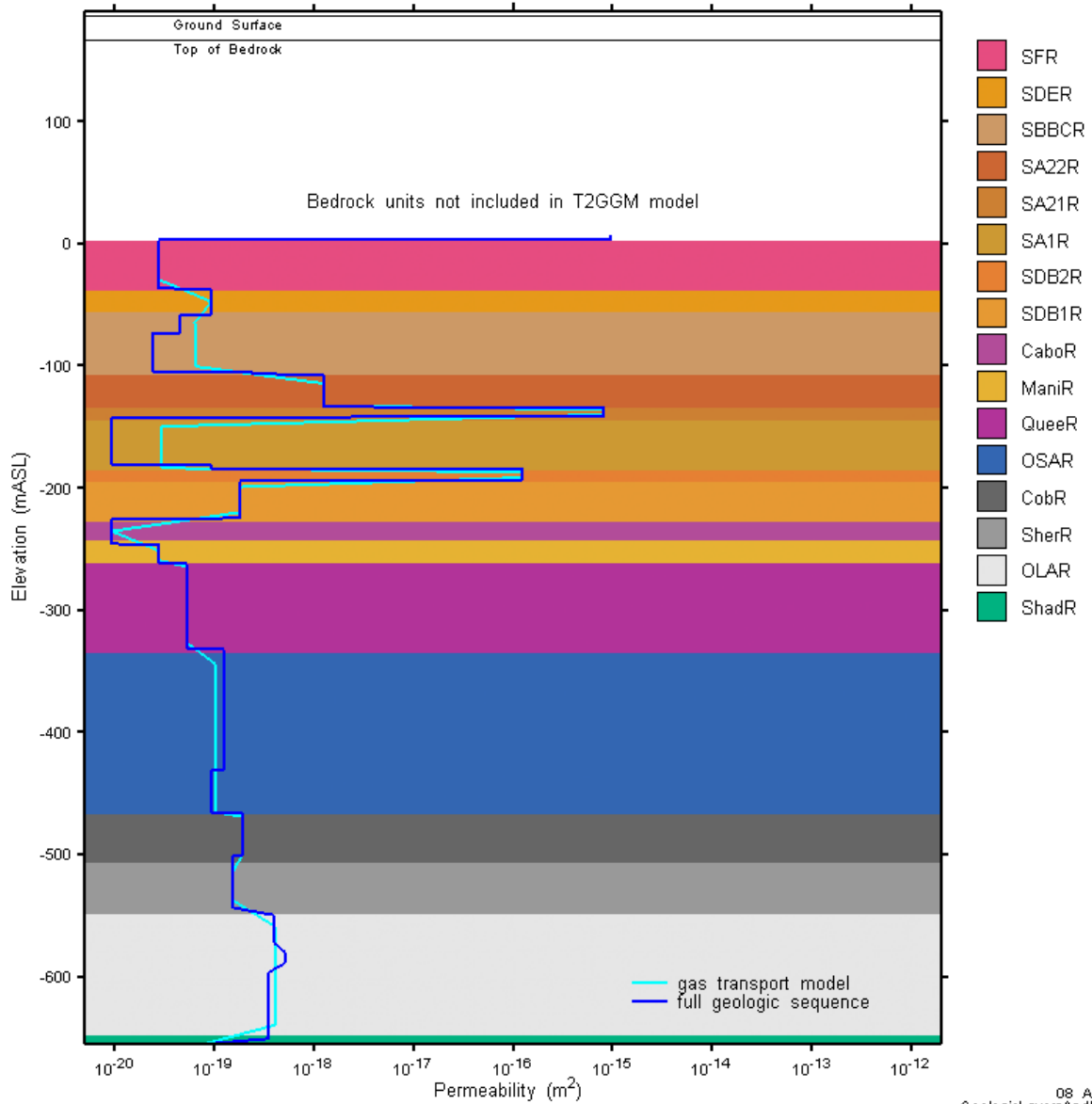


Figure 4-2: Vertical permeability in the BC model, compared to the permeability for the full geological sequence.

Two phase flow properties, which define the capillary pressure and relative permeability curves, are based on values reported in the Data report (Walke et al. 2009b), with modification to improve numeric stability as described in detail below. The values in the Data report were calculated by fitting equations to laboratory petrophysical data calculated from Ordovician core samples.

Capillary pressure and relative permeability curves are represented using the Van Genuchten equations as a function of the water saturation fraction S_i :

$$S_{ec} = \frac{S_l - S_{lr}}{1 - S_{lr}} \quad (4-1)$$

$$S_{ek} = \frac{S_l - S_{lr}}{1 - S_{lr} - S_{gr}} \quad (4-2)$$

$$P_c = \frac{1}{\alpha} [S_{ec}^{-1/m} - 1]^{1/n} \quad (4-3)$$

$$k_{rl} = S_{ek}^{1/2} [1 - (1 - S_{ek}^{1/m})^m]^2 \quad (4-4)$$

$$k_{rg} = (1 - S_{ek})^{1/3} [1 - S_{ek}^{1/m}]^{2m} \quad (4-5)$$

where:

- P_c is the capillary pressure, Pa;
- k_{rl} is the water phase relative permeability (ratio);
- k_{rg} is the gas phase relative permeability (ratio);
- S_{ec} is the effective saturation for the capillary pressure relationship (volume ratio);
- S_{ek} is the effective saturation for the relative permeability relationship (volume ratio);
- S_l is the water saturation (volume ratio);
- S_{lr} is the residual water saturation (volume ratio), the water saturation below which water does not flow;
- S_{gr} is the residual gas saturation (volume ratio), the gas saturation below which gas does not flow;
- m is a van Genuchten fitting parameter (unitless);
- n is a van Genuchten fitting parameter (unitless); and
- α is a van Genuchten fitting parameter, Pa^{-1} . $1/\alpha$ is analogous to the air entry pressure.

Two phase flow properties for the consolidated layers are presented in Table 4-3. Note that no data is available for units above the Queenston, and consequently two phase flow properties for the Silurian units above the Queenston are based on the values for the Queenston, except that, as reported in Walke et al. (2009b), α values for the Silurian dolostones were modified according to the Davies relationship.

Modifications to the two phase flow properties were required due to the numeric limitations of the TOUGH2 code and van Genuchten equations; without these modifications, the TOUGH2 code is unable to resolve the very large capillary pressures provided by the van Genuchten model at very low gas saturations. Note that two phase flow properties for ShadR were not modified (i.e., they are the same as presented in Walke et al. 2009b), as capillary pressures for this unit are relatively low.

While these modified curves present a departure from the original analysis of the laboratory petrophysics data (as reported in the Data report, Walke et al. 2009b), the modified characteristic curves are very similar and within range of the original petrophysical data upon which these curves are based, as shown in Figure 4-3 and Figure 4-4. The modified characteristic curves are also within range of the curves derived for the Opalinus Clay (Marschall 2006), also shown in Figure 4-3 and Figure 4-4.

Table 4-3: Two phase flow properties (Van Genuchten) for each geological unit

Unit	Top Elevation (mASL)	$1/\alpha$ (MPa)	m (-)	n (-)	S_{lr} (-)	S_{gr} (-)
SFR	3	32	0.90	1.70	0.02	0.01
SDER	-37	26	0.90	1.70	0.02	0.01
SBBCR	-59	32	0.90	1.70	0.02	0.01
SA22R	-107	11	0.90	1.70	0.02	0.01
SA21R	-134	3	0.90	1.70	0.02	0.01
SA1R	-142	32	0.90	1.70	0.02	0.01
SDB2R	-185	2	0.90	1.70	0.02	0.01
SDB1R	-215	21	0.90	1.70	0.02	0.01
CaboR	-225	32	0.90	1.70	0.02	0.01
ManiR	-246	32	0.90	1.70	0.02	0.01
QueeR	-262	32	0.90	1.70	0.02	0.01
OSAR	-332	40	0.80	1.60	0.00	0.01
CobR	-466	50	0.80	1.60	0.00	0.01
SherR	-501	24	0.80	1.70	0.00	0.01
OLAR	-546	24	0.80	1.70	0.00	0.01
ShadR	-653	0.13	0.35	1.54	0.00	0.00

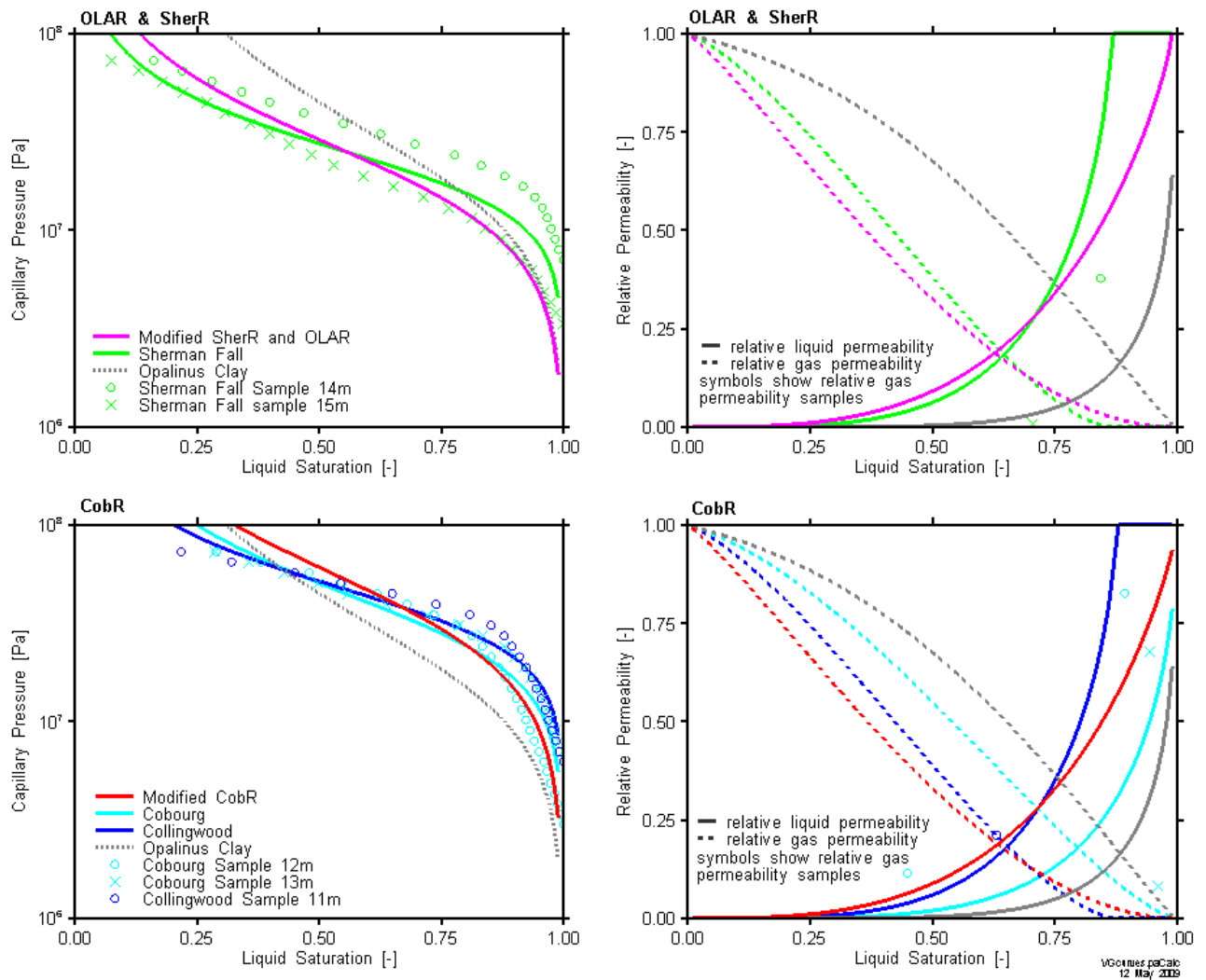


Figure 4-3: Capillary pressure and relative permeability curves for limestone formations OLAR, SherR and CobR (which includes Cobourg and Collingwood). Due to the unavailability of data, OLAR has the same gas transport curves as SherR (Sherman Fall).

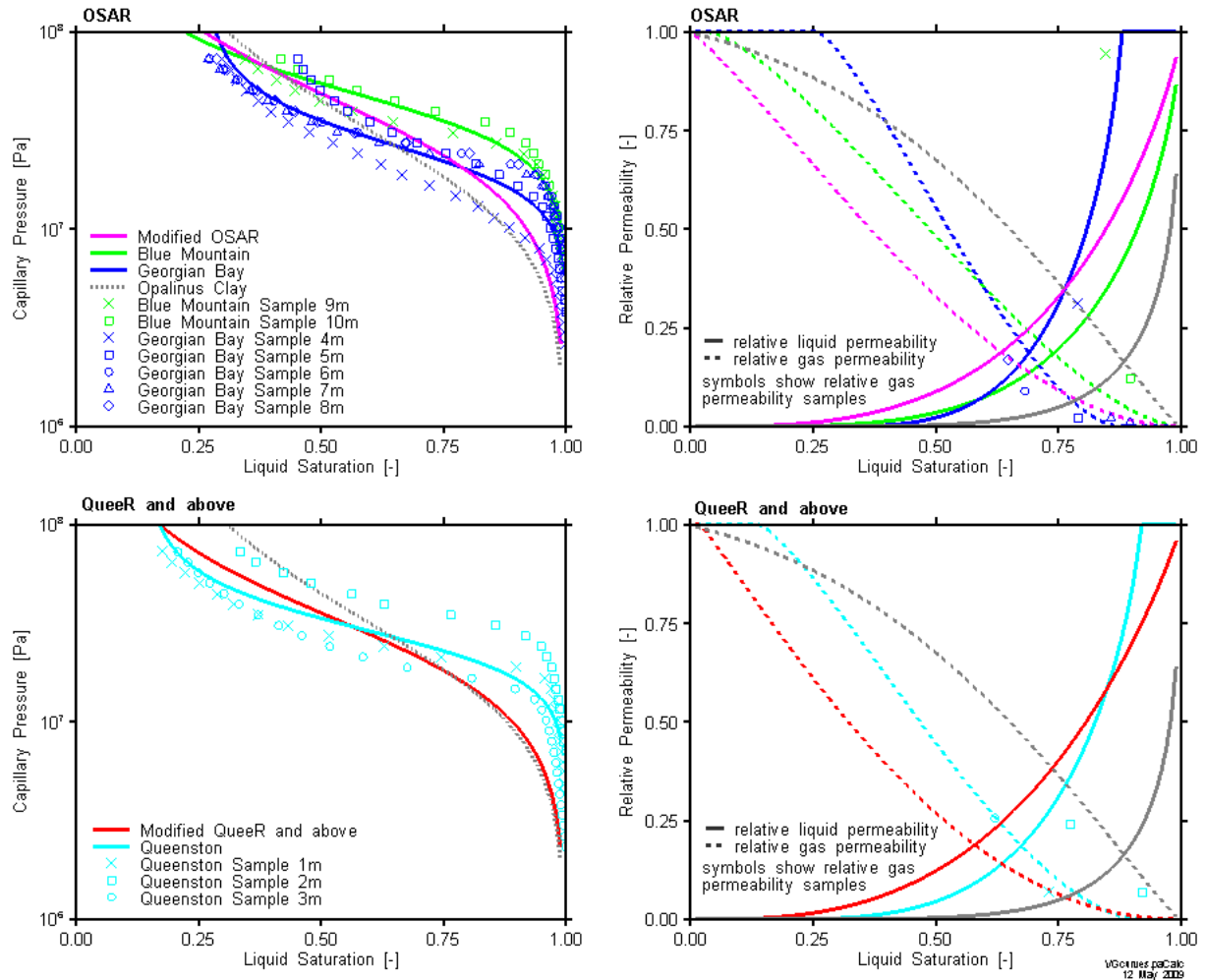


Figure 4-4: Capillary pressure and relative permeability curves for shale formations OSAR and QueeR. Due to the unavailability of data, the formations above Queenston are set to the same gas transport curves as QueeR.

The updated geosphere (all UG cases) permeabilities (DGR 2009) are presented in Table 4-4. All other parameters remain the same as for the base case, except for $1/\alpha$ values for the Silurian dolomites, which were calculated explicitly based on the permeability (note that all other gas transport properties are based on sample data, independent of permeability measurements).

Table 4-4: Hydraulic conductivities of Silurian and Ordovician units for UG calculation cases.

Unit	Horizontal Permeability (K_h) (m^2)	Vertical Permeability (K_v) (m^2)
SFR	5.81E-21	5.81E-22
SDER	5.81E-20	5.81E-21
SBBCR	6.78E-20	1.46E-20
SA22R	4.84E-17	4.84E-18
SA21R	6.78E-15	6.78E-15
SA1R	8.66E-19	2.74E-19
SDB2R	1.50E-16	1.50E-17
SDB1R	1.94E-19	1.94E-20
CaboR	1.94E-20	1.94E-21
ManiR	1.94E-20	1.94E-21
QueeR	1.94E-21	1.94E-22
OSAR	2.91E-21	2.91E-22
CobR	1.37E-21	1.37E-22
SherR	1.94E-21	1.94E-22
OLAR	2.91E-20	2.91E-21
ShadR	9.68E-17	9.68E-18

Vertical permeability (K_v) values for the BC and UG cases are shown graphically in Figure 4-5. As described previously, UG case permeabilities are significantly lower than base case within the Ordovician sequence. Within the Silurian formations they are lower in some cases, and higher in others. The most significant differences in the Silurian formations are increased permeabilities within the sequence from the Guelph upwards to the Salina A2 evaporite, with the exception of the Salina A0, which is not considered a high-permeability unit in the UG cases.

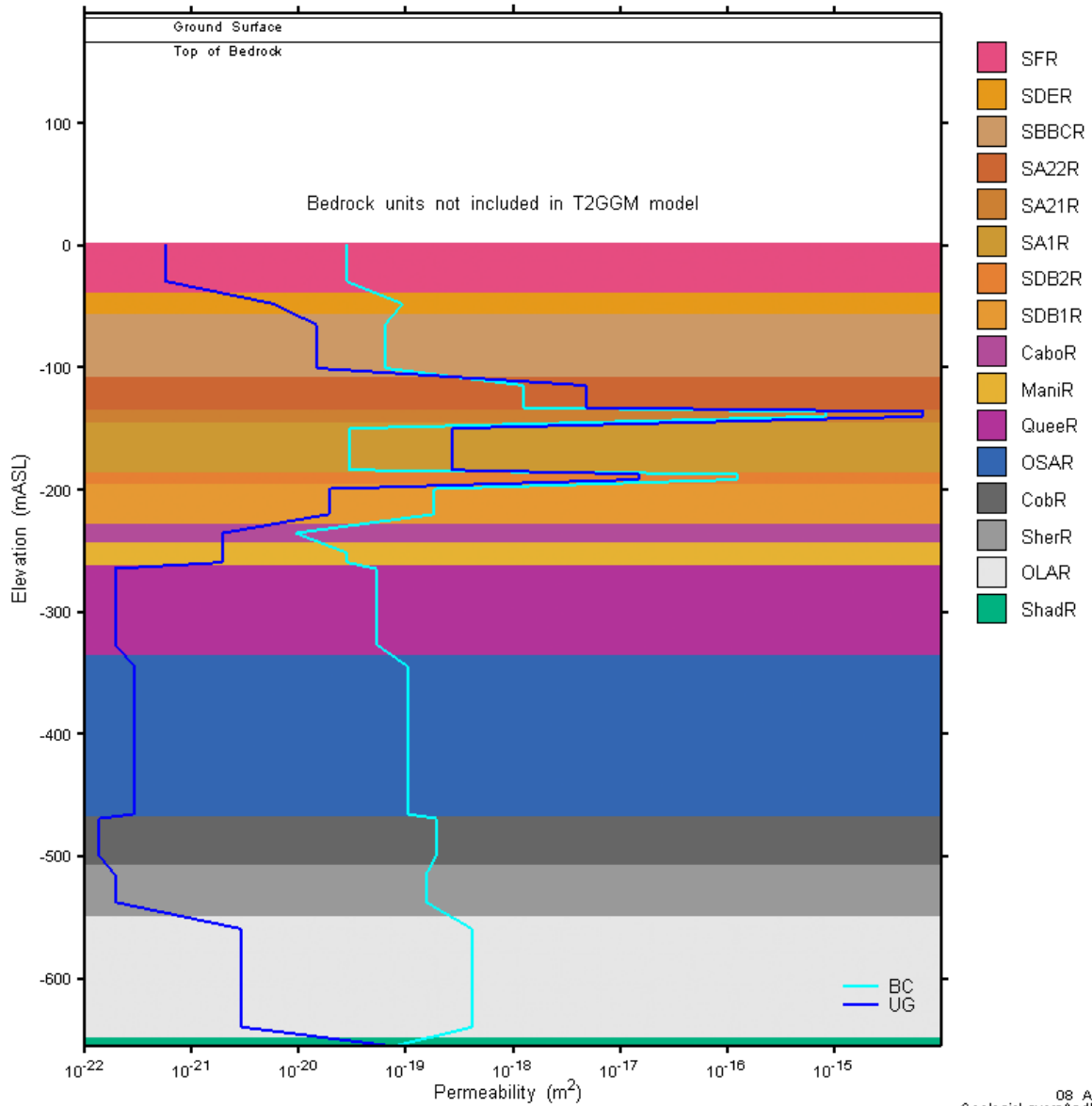


Figure 4-5: Vertical permeability in the BC and UG models.

4.2.2 Shaft, Repository and Sealing Material Properties

The emplacement rooms, access tunnels, ring tunnel, Main Shaft, the Ventilation Shaft, and their associated EDZ and sealing systems form the engineered portion of the modelled system. For these components of the model, there is no directionality to the material and the vertical and horizontal permeabilities are equal. Model IDs in this section are shown in bold text to make them easily distinguishable.

As described in Section 4.3.1, the repository is conceptually divided into two components, each with slightly different properties: the waste disposal area, consisting of emplacement rooms and

access tunnels joining the emplacement rooms (referred to as **repo** for repository); and the ring tunnels and the access tunnels joining the ring tunnel to the waste disposal area (referred to as **ring**). Note that for simplicity, discussion of results often refers to **repo** and **ring** as simply the repository. The porosity for both these components is calculated from the ratio of the total void volume of repository, access tunnels and ring tunnels and the total model volume assigned to each model property (repo and ring). The porosity of the rock pillars and the rock above the repository (rockfall) is low and therefore neglected in this calculation. The resulting calculated porosity is 0.061 for the repository zone and 0.184 for the ring zone.

The EDZ surrounding the monolith, ring tunnels, access tunnels and the repository (referred to as repository EDZ or **rpEDZ**) is assumed to be entirely within the Cobourg unit (CobR), and is assumed to have uniform properties. Repository EDZ properties are based on the Cobourg rock mass properties, with a uniform permeability 1000 times the horizontal permeability of the Cobourg and a porosity two times the porosity of the Cobourg rock mass.

A concrete monolith at the base of the shaft extends 20 m beyond the edge of the shaft (see Figure 2-6). The shafts are backfilled with a series of compacted bentonite/sand seals (**bentS**), separated by concrete bulkheads. The primary seal also contains a section of asphalt (**asph**) and two asphalt waterstops separated by concrete bulkheads. The monolith and concrete bulkheads in the deep and intermediate groundwater zones within the shaft are assumed to have identical properties and are designated as lower concrete (**concl**). The concrete bulkheads above -10 mASL (only one of which is within the gas transport model) are assumed to have degraded slightly and therefore have somewhat higher permeabilities (Walke et al. 2009b), and are designated shallow concrete (**concs**).

The shaft has an inner and outer EDZ, with separate model properties defined for each geologic unit intersected by the shaft. EDZ property IDs are identical to the geologic unit IDs, with the "R" in the model ID replaced by an "I" for the inner EDZ and an "O" for the outer EDZ. For example, the Cobourg unit has rock, inner EDZ and outer EDZ model property IDs, labelled respectively of CobR, CobI and CobO.

Physical, hydrogeologic and two-phase flow properties for these materials, based on data in the Data report (Walke et al. 2009b), are given in Table 4-5. Due to the large number of geologic units, and consequently the large number of inner and outer EDZ material types, Table 4-5 does not provide the properties for each EDZ material. Except for permeability and porosity, EDZ properties are identical to rock mass given in Table 4-2. In the BC, the inner EDZ has a vertical hydraulic conductivity 100 times greater than the associated rock mass K_v , and outer EDZ has a vertical hydraulic conductivity 10 times greater. Inner EDZ has twice the porosity of the associated rock mass. For example, the Cobourg unit Inner EDZ has a vertical permeability of $1.94\text{E-}17\text{ m}^2$ and a porosity of 0.03, and the Cobourg unit outer EDZ has a vertical permeability of $1.94\text{E-}18\text{ m}^2$ and a porosity of 0.015. Within the EDZ it is assumed that vertical and horizontal permeability are equal. As well, it should be noted that the repository and ring tunnel will have a very high permeability as it is primarily void space. However, numeric issues associated with permeability contrasts required that a nominal permeability be present for the code to execute successfully. A value of 10^{-6} ms^{-1} was chosen as an acceptable value that would not materially impact flow or transport results.

Two phase flow properties are not provided in Table 4-5 for the repository or ring tunnels as a different approach was taken to describe the two-phase flow behaviour for these components to recognize that they are actually a void space without porous media type behaviour. Capillary

pressure is assumed to be zero, and relative permeability is modelled using a simple linear model. In the linear model selected, relative permeability of gas is assumed to be one, unless the gas saturation is less than 0.0001; and the relative permeability of water is assumed to be one, unless the water saturation is less than 0.1. The relative permeability of gas increases linearly from 0 to 1 between a gas saturation of 0 and 0.0001; and the relative permeability of water increases linearly from 0 to 1 between a water saturation of 0.01 and 0.1. This allows gas and water to move freely within the repository void, except at low gas and water saturations where the movement of gas and water is limited. Since the relative permeability of water is zero below a water saturation of 0.01, this effectively specifies a residual water saturation of 0.01 in the repository. Note that this residual water saturation was initially introduced in early testing of the model to improve numeric stability. Only relevant in cases where the repository becomes fully gas saturated (NE-GG1, NE-UG-RD1 and NE-UG-GT), the residual water saturation assumes that this water is not available to gas generation processes. This assumption will be revisited in future assessment modelling.

Table 4-5: Physical, hydrogeologic, and two phase flow properties for shaft, repository and EDZ for the BC

Unit	Porosity (-)	Permeability (m ²)	Pore Compressibility (Pa ⁻¹)	1/α (MPa)	m (-)	n (-)	S _{lr} (-)	S _{gr} (-)
repo	0.06	1.00E-13	1.65E-08					
ring	0.18	1.00E-13	5.43E-09					
rpEDZ	0.03	1.94E-15	5.77E-09	50	0.80	1.60	0.00	0.00
bentS	0.30	9.68E-19	1.43E-09	43	0.69	1.47	0.00	0.00
asph	0.02	9.68E-20	1.49E-08	1	0.50	2.00	0.25	0.00
concl	0.15	9.68E-19	3.87E-10	1	0.50	2.00	0.25	0.00
concS	0.25	9.68E-16	2.32E-10	1	0.50	2.00	0.25	0.00

For the EDZ sensitivity case NE-EDZ, the inner EDZ and outer EDZ permeability are 10 000 and 100 times the rock mass vertical conductivity, respectively. Inner and outer EDZ 1/α parameters were reduced according to Davies permeability relationship, and are detailed in Table 4-6. This approach addresses the basic assumption that air entry pressures in the EDZ for the NE-EDZ case should be lower than those of the rock mass. In general, further work needs to be performed to determine the appropriate gas transport parameters for the EDZ and the application of laboratory results to rock mass and EDZ.

For the shaft failure cases SF-ES1 and SF-UG-ES1, the shaft is assumed to be filled with a sand/granular material with a conductivity of 10⁻⁷ m s⁻¹ and a porosity of 0.40. Inner EDZ permeability is 10 000 times the rock mass vertical permeability.

Table 4-6: Two phase flow $1/\alpha$ parameter (Van Genuchten) for inner and outer EDZ for the NE-EDZ case

Unit	$1/\alpha$ (MPa)
SherI/SherO	0.81
Cobl/CobO	0.75
OSAI/OSAO	0.94
Queel/QueeO	1.18
Manil/ManiO	1.47
Cabol/CaboO	2.15
SDB1I/SDB1O	0.77
SDB2I/SDB2O	0.08
SA1I/SA1O	2.15
SA21I/SA21O	0.09
SA22I/SA22O	0.39
SBBCI/SBBCO	1.44
SDEI/SDEO	0.97
SFI/SFO	1.47

4.2.3 Gas Generation Input Parameters

The GGM requires information about: the initial surface areas of the metallic wastes, the inventories of metals and organic wastes in all waste groups; the reaction rates for the corrosion and degradation reactions under the various conditions (saturated phase, vapour phase); and physical properties such as densities, molar masses and solubility constants. All such parameters are documented in the Data report (Walke et al. 2009b).

4.2.4 Gas Properties

The TOUGH2 (EOS3 module) component of the T2GGM model simulates transport of a single bulk gas, and uses air as the bulk gas. Consequently, the gas transport properties defined in this section are for air used in the TOUGH2 component of the model. As will be discussed below, the GGM component of the T2GGM model simulates multiple gas components, which are then converted to the single bulk gas for transport in the TOUGH2 component of the model.

Air was selected as the bulk gas in the TOUGH2 component of the T2GGM model since the predominant gas was not known before the start of the T2GGM model development. The consequences of using air depend on the differences in gas transport properties to the predominant gas present in the repository over the course of the simulation, methane. Methane has a similar molar mass and viscosity to air, however, solubility is half that of air (e.g., at a given pressure, air will have twice the dissolved mass in water than methane). Future simulations should use methane or a combination of other gases as the bulk gas (T2GGM code changes will be required if another gas is used).

The GGM component of T2GGM converts the volume of individual gas components generated at each time step to an equivalent volume of air for injection into the TOUGH2 model. The

volume of individual gas components is converted to an equivalent volume of air by multiplying the sum of the molar rate (mol/s) of individual gas components by the molar mass of air.

The diffusion coefficient of water vapour and air in gas at 20°C is $2.1 \times 10^{-5} \text{ m}^2/\text{s}$ (Pruess et al. 1999; and Incropera and DeWitt 1996), and the diffusion coefficient of dissolved air in water is $2.5 \times 10^{-9} \text{ m}^2/\text{s}$ (Incropera and DeWitt 1996). As water is the main component of the water (i.e., dissolved gas is a dilute solution), the diffusion coefficient of water (in water) is zero.

The solubility of air is currently hard-coded into the TOUGH2 model, with a value of 1×10^{-10} mole fraction/Pa. Solubilities for the different gases modelled in the GGM component of the model, as reported in the Data report (Walke et al. 2009b), are similar within a factor of three (greater or smaller solubility), except for CO_2 , which is 12 times more soluble than air.

4.3 MODEL IMPLEMENTATION

4.3.1 Model Structure

The 2DR model provides a dimensionally simplified representation and computationally efficient model of the system. The 2DR model cannot account for lateral advective flow. All flow is radial, vertical, or a combination of the two. This means that this model is not suitable for any conceptual model that includes horizontal gradients or a water abstraction well (unless the abstraction well is located at the centre of the repository shaft). For such problems a 3D model is required. The advantage of the 2DR model is that it allows a much greater mesh resolution than the 3D model, leading to significantly improved computational performance and the ability to assess the impact of much smaller features of the repository sealing system and the rock formation.

Geology is represented as a flat “layer cake” system in the 2DR model. The model domain extends from the top of the Intermediate Bedrock Groundwater Zone (Salina F formation at 3 mASL or 183 mBGS) down to the top of the Cambrian sandstone at an elevation of -658 mASL (or 844 mBGS). The choice of the Cambrian sandstone as the lower boundary was dictated by a requirement to simulate pressurised conditions within this unit. The top boundary was selected based on recommendations for improving model stability: the high permeability units in the Shallow Bedrock Groundwater Zone add instability to the model, and ignoring these units will provide a conservative estimate on the gas flows reaching the surface in a 2D model, especially since groundwater flow is expected to be 3D in nature within the Shallow Bedrock Groundwater Zone.

The repository conceptual design (Hatch 2008) contains a central ring tunnel system with the access tunnels and emplacement panels to the south and east radiating outward from the centre of this ring at an offset of approximately 55° (see Figure 2-4).

The engineered components of the repository are simplified to comply with the radial model concept. The two shafts (Main and Ventilation) are merged into a single shaft which combines the cross-sectional area of the Main and Ventilation shafts in the Hatch (2008) repository design. The repository is modelled as a radial segment of appropriate angle, thickness and volume.

In a 2DR model, only a very thin slice of the repository is modelled. Subsequently, the fluxes crossing this slice are multiplied by the ratio of the slice area to the total area of the repository

to get the total flow and the mass flow from the repository. It is possible to distribute the repository area over any angle, if the radial extents are chosen consistently. Given the repository conceptual design, with the main and ventilation shafts close together and two repository panels radiating outward, a 90° 2DR model is appropriate.

In the 2DR model, the repository area is distributed over 90 degrees and the combined shaft is located at the corner of the model (see Figure 4-6). The combined shaft represents the effective combined response of the Main and Ventilation Shafts. Table 4-7 shows the cross-sectional areas of the combined shaft and shaft EDZ. EDZ radii are defined in terms of the shaft radius (R_{shaft}), with the inner EDZ extending from the shaft wall to a radius of 1.5 R_{shaft} , and the outer EDZ extending from 1.5 R_{shaft} to 2.0 R_{shaft} . Table 4-7 also shows the actual shaft dimensions used in the mesh. The mesh dimensions differ in two ways. (1) The 90 degree model represents the shaft as a wedge rather than a cylindrical object, and the wedge radius is calculated assuming an equivalent area. This approximation is reasonable because flow in the shafts will largely be vertical, driven by the Cambrian overpressure at the bottom of the model domain. (2) The radii dimensions are rounded to the nearest integer in order to make meshing tractable. This will not introduce significant additional error.

Table 4-7: Cross-sectional areas of combined shaft (2DR model).

Shaft	Shaft radius m	Inner EDZ Radius m	Outer EDZ Radius m	Shaft Area m ²	Inner EDZ Area m ²	Outer EDZ Area m ²
Main shaft	4.00	6.00	8.00	50.3	62.8	88.0
Ventilation shaft	3.00	4.50	6.00	28.3	35.3	49.5
Combined shaft	5.00	7.50	10.00	78.5	98.2	137.4
Combined shaft 90° wedge	10.00	15.00	20.00	78.5	98.2	137.4

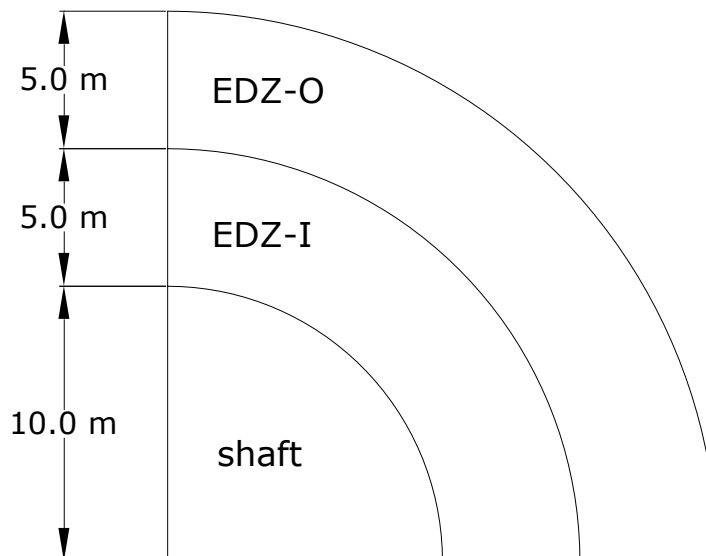


Figure 4-6: Plan section of shaft in the 90° 2DR model

In the repository plan, there is a concrete “monolith” at the base of each shaft extending up to 20 m beyond the edge of the shaft. In the model, the areas of the two monoliths are not combined, as horizontal flow and transport in the monolith and in the EDZ surrounding the monolith are the relevant processes. Combining the two monoliths (as was done for the shaft components) would increase the horizontal path length from the access and ring tunnel system to the shaft. As a conservative simplification the combined monolith uses the 20 m distance rather than the corrected (larger) combined distance. The monolith EDZ extends 4 m beyond the monolith into the surrounding rock on all sides.

The closure plan for the ring tunnels calls for using these tunnels to dispose of concrete debris from the shaft liner removal and to dispose of all used equipment. However, there will still be open space, and the model assumes rockfall into the ring tunnels, and that this collapse occurs immediately after closure. For the BC, it is assumed that there is 30 m of roof collapse above the top of the ring tunnel (Walke et al. 2009b). Consequently, the tunnels will be filled with rubble, with a very high effective permeability. These tunnels have been modelled simply as a high permeability and porosity zone. The thickness of the quarter ring representing the ring tunnel zone is based on the average distance between the edge of the repository and the centre of the ring tunnel. For this model, the EDZ on all sides of the access and ring tunnels extends 7 m into the surrounding rock (Walke et al. 2009b).

The repository is located in the Cobourg (CobR) unit, with the bottom of the repository at an elevation of -494.2 mASL. For the repository, the volume of the two repository panels has been calculated (including access tunnels, emplacement rooms, and pillars) and, using an average repository height of 6.7 m plus 20 m of rockfall (less than the ring tunnel because the rooms are partially filled with waste packages) (Walke et al. 2009b). This volume has been distributed in a quarter ring outside the ring tunnel zone. The resulting maximum path length from the repository to the ring tunnel is 404 m. The path length from the repository (and the repository EDZ) to the shaft is somewhat shorter than the actual path length in the proposed repository. A plan section of the model representation of the repository is shown in Figure 4-7.

The repository EDZ is 7 m thick above and below the repository.

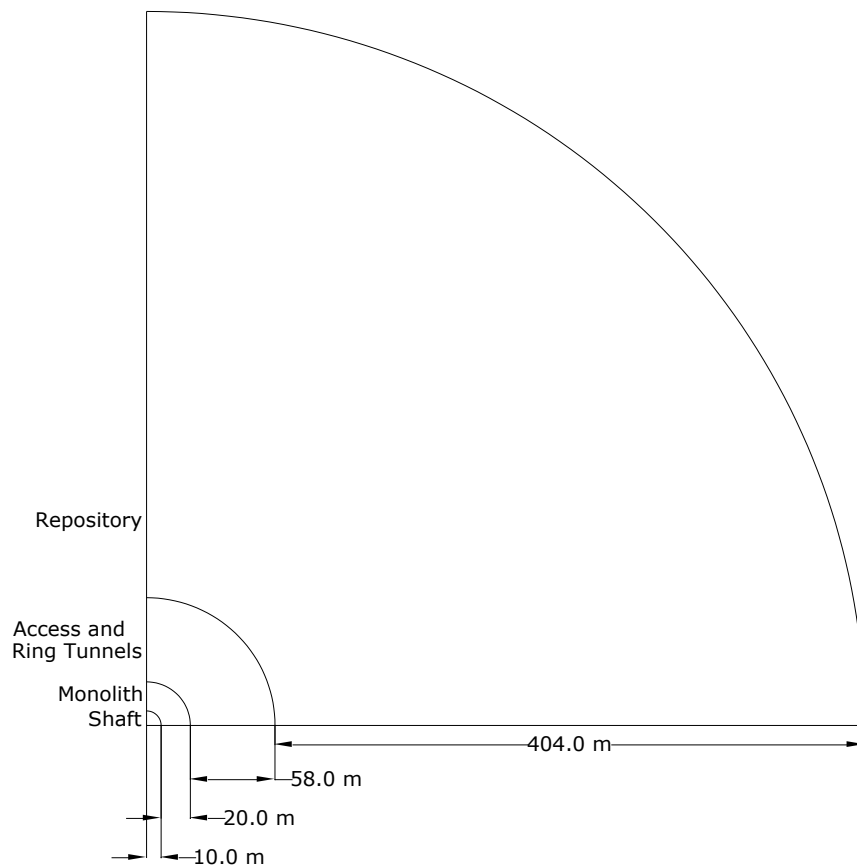


Figure 4-7: Plan section of repository in the 2DR model at the repository horizon

4.3.2 Model Discretisation and Property Assignment

In plan section, the 2DR grid is constructed of a radial slice of 4-sided elements. The one element thick slice is then projected vertically to obtain an array of 6-sided elements. The total included angle of 0.0349 radians (2.0 degrees) represents 1/45th of a quarter circle. Flows from the model must be multiplied by a factor of 45 to obtain the total flow from the system.

Vertically, the model is divided into 60 layers. The model grid spans the formations from the top of the Cambrian (-658 mASL) to the top of the Salina F formation (3 mASL), as shown in Figure 4-8. Note that discretization is not shown in the figure as it would completely obscure property assignments at the figure scale.

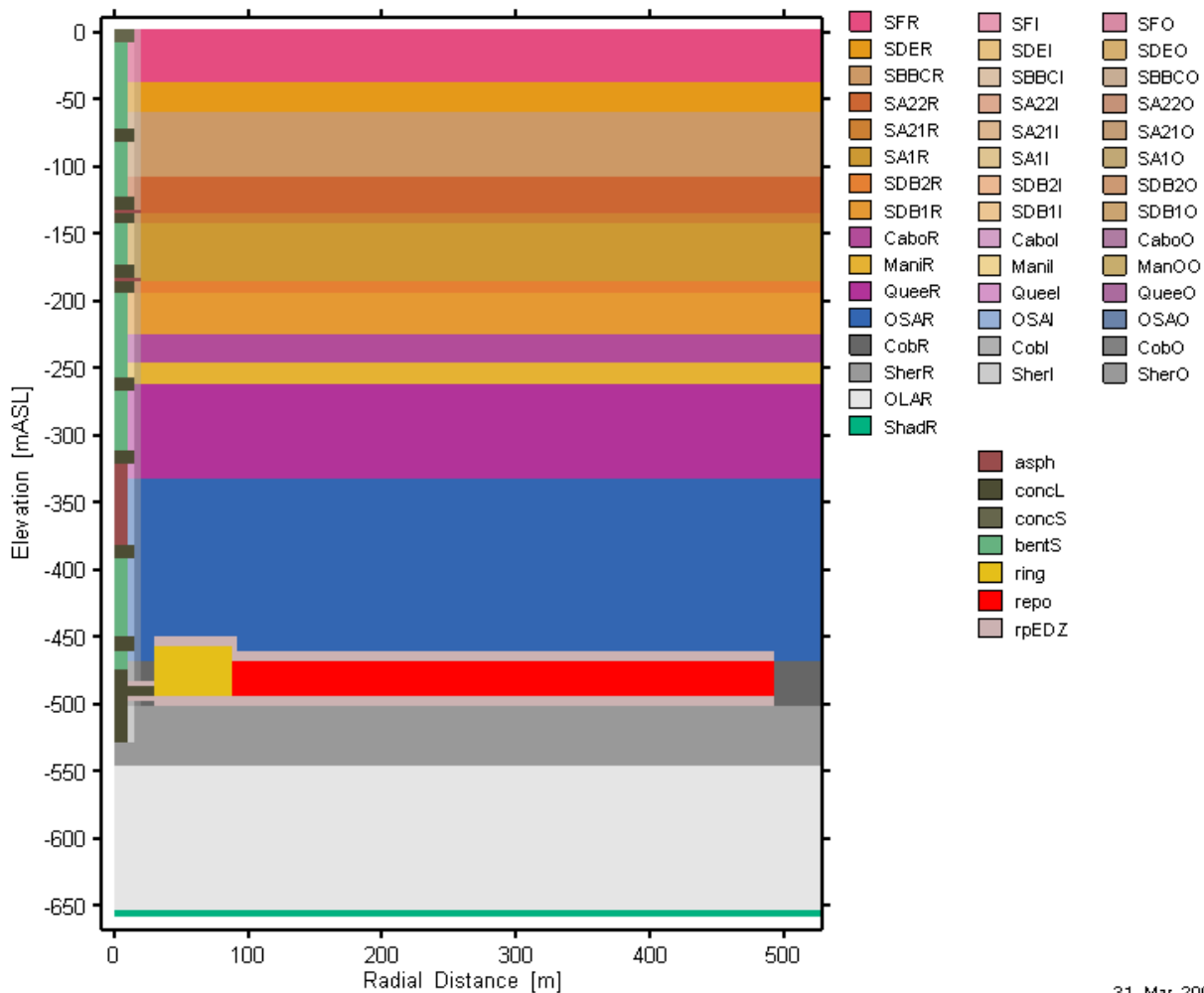


Figure 4-8: Detail of 2DR model property assignments. Note that ground surface is at 185.7 mASL (not shown).

Horizontally, the mesh is finest near the shaft centre, to resolve the shaft, the inner and outer EDZ, and the concrete monolith. The discretization remains relatively fine past the end of the repository, beyond which the mesh size increases. The 2DR model is discretized with a total of 96 radial increments out to an external boundary radius of 1500 m. The horizontal and vertical discretization results in a mesh with 5820 nodes.

Access tunnel EDZ was not included in the zone between the access tunnel and the shaft, as the geometric approximations of the 2DR model had already increased the size of the access tunnel system wider than that of the ring tunnel alone. The EDZ surrounding the monolith is directly in contact with the high permeability access zone.

In comparison to the 2DR detailed groundwater model (Avis et al. 2009), the discretization is considerably coarser and the model spans a smaller area. Analysis found numeric stability improved by:

- reduced discretization in the shaft/EDZ area and reduced radial extents (eliminating very small and very large blocks reduces the ratio of smallest to largest element volumes, which improves matrix solver performance); and
- reduced vertical extents, removing the high permeability Shallow Bedrock Groundwater Zone.

In addition, a larger node block size reduces simulation times for the execution time-intensive two-phase flow TOUGH2 model.

The coarse discretization required slight adjustments in the assignment of properties, mainly the location of concrete bulkheads and the asphalt waterstops, with adjustments less than 1 m. The asphalt waterstops were also assumed to be twice as thick as the thickness given in Walke et al. (2009b), 2.4 m, to prevent large changes in element volume and minimize the model instabilities observed during initial modelling.

Figure 4-9 and Figure 4-10 show details of the grid discretization.

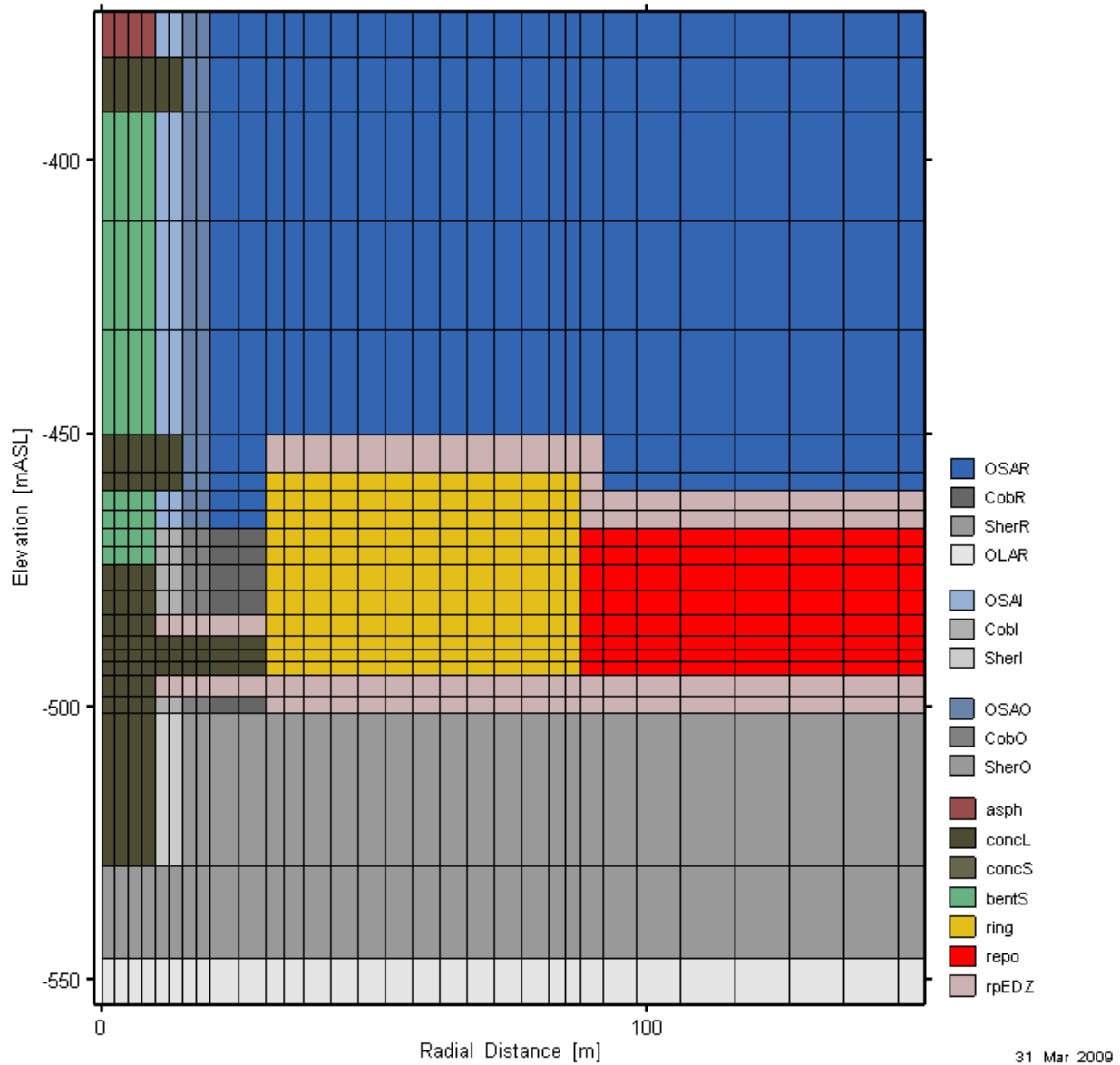


Figure 4-9: Detail of 2DR model discretization of repository, ring zone, monolith, shaft, EDZ, and lowest concrete bulkheads

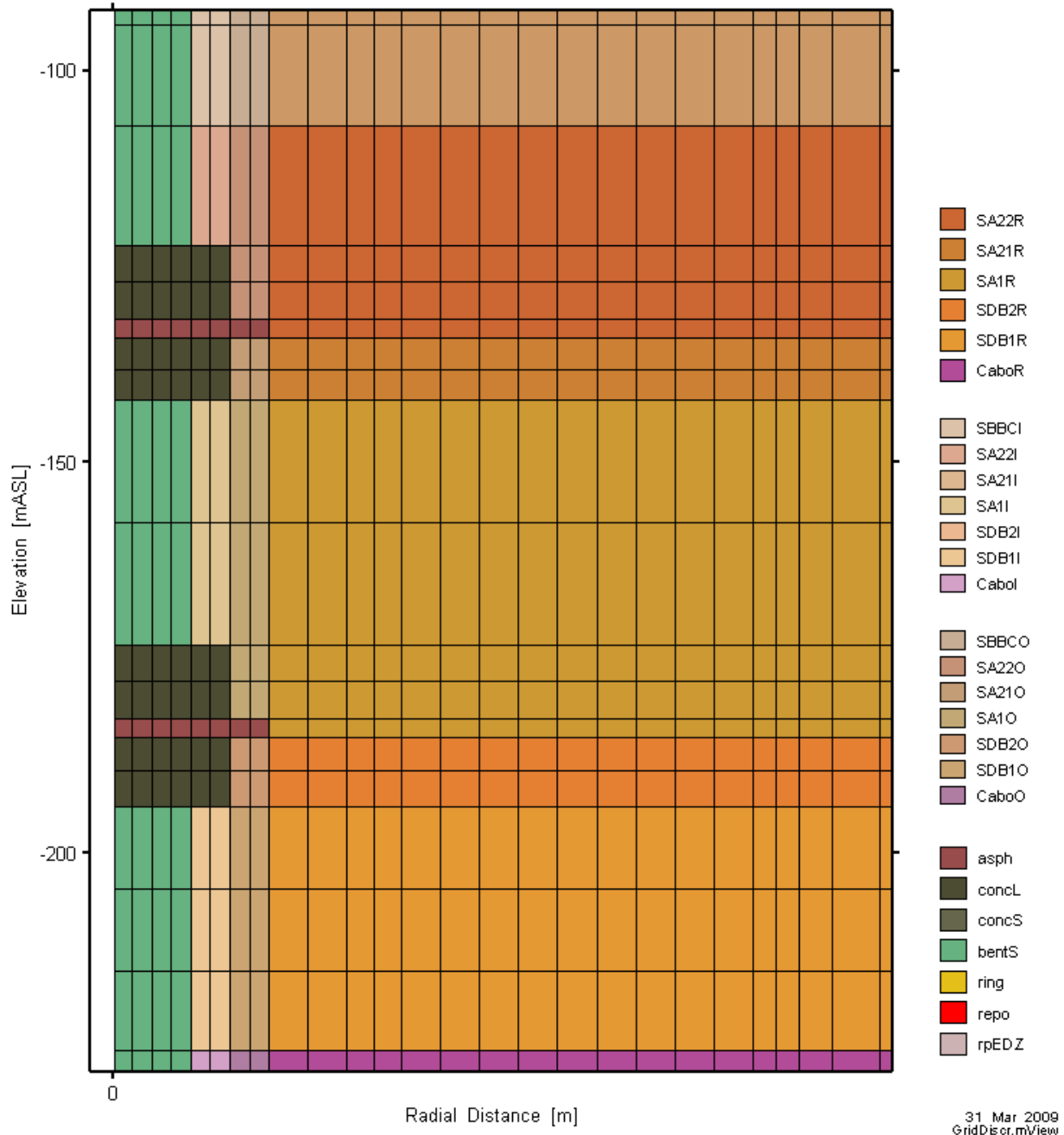


Figure 4-10: Detail of discretization of asphalt waterstop system in 2DR model

4.3.3 Boundary and Initial Conditions

4.3.3.1 Flow Boundaries and Initial Conditions

The model has fixed head boundary conditions on the top and bottom layers of the model, defining a vertical gradient in the system. The base case (BC) assumes a 140 m total gradient, with the top model surface (at 3 m ASL) defined with a head of 0.0 m, and the bottom surface

(at -658 mASL) defined with a head of 140.0 m. The value of zero at the top of the Salina F Formation assumes no substantial vertical gradients in the Devonian system. These heads are converted to absolute pressures required by TOUGH2 based on the depth below ground surface plus imposed head converted to pressures, assuming a density of 1000 kg m^{-3} . Atmospheric pressure is taken to be 101.3 kPa. The value of 140 m represents the environmental head calculated from measured Cambrian overpressures, presented previously in Figure 2-3, and thus implicitly includes the effects of salinity on the boundary condition.

The 2DR model cannot account for lateral advective flow in the model domain. All flow is radial, vertical, or a combination of the two. The reference case external boundary at $R = R_{\text{max}}$ (where $R_{\text{max}} = 1500 \text{ m}$) is zero-flow, for both gas and groundwater. The boundary is sufficiently distant so as not to significantly affect simulation results.

The model is simulated without the repository and shaft to obtain a steady-state head profile for the initial conditions in the rock mass, prior to construction of the repository. These steady state heads in the rock mass are combined with atmospheric pressures in the repository, ring tunnel and shaft to provide the initial pressure conditions. This assumes no operational period (as an operation period would affect pressures in the rock mass adjacent to the repository, ring tunnels and shaft), which was considered acceptable given the brief duration of the operational period (less than 100 years) relative to the 1 million year run times. Initial conditions were generated for both the BC and UG geospheres.

4.3.3.2 Gas Saturation Initial Conditions

The rock mass was assumed fully saturated with water. While small initial gas saturations might be expected in the rock mass, this simplifying assumption was made due to the uncertainty in the magnitude of initial gas saturations and the negative impact of initial gas saturations on simulation times. This simplifying assumption is expected to have minimal impact on results; it is expected to be conservative with respect to gas pressures in the repository, and non-conservative with respect to gas fluxes to surface. Case NE-UG-GT further investigates this assumption.

The repository and ring tunnel were assumed to be initially saturated with gas, except for the bottom layer of the repository. The bottom layer of the repository was set to an initial water saturation that results in a water saturation for the entire repository of 0.017 (volumetric fraction), equivalent to the initial mass of water in the waste of $5.2 \times 10^6 \text{ kg}$ (Walke et al. 2009b).

The shaft was assumed initially saturated with gas at fifty percent. This represents the partial saturation of the shaft materials when emplaced².

4.3.4 Gas and Water Source Terms

The GGM component of the T2GGM model calculates the gas generation and water consumption rates within the repository. These source terms are then applied to the TOUGH2 component of the T2GGM model. TOUGH2 is responsible for simulating the flow of water and bulk gas into and out of the repository (see Figure 2-1).

² The 70/30 bentonite/sand shaft seal material will likely be placed at a somewhat higher saturation.

Unlike TOUGH2, the GGM does not model any spatial dependence within the repository. Instead it treats it as an arbitrary volume within which the time dependence of the gas generation processes are modelled in detail. The following are explicitly modelled within the repository: the evolution of the individual gas components (partial pressures, concentrations in the saturated phase and total amounts within the repository and leaked from the repository); the generation/consumption of water due to the reactions; metallic wastes and their corrosion; organic wastes and their degradation; and corrosion and degradation products. See Section 2.1 and Section 2.2 for further details.

As input, the GGM takes information about the current (repository averaged) total gas pressure, saturation, relative humidity, and repository void volume from TOUGH2. The gas pressure and saturation are used to determine the flux of gas out of the repository.

As output, the GGM calculates the rates of gas and water production within the repository as a whole. Note that for gas, GGM calculates gas generation rates for individual gas components, and calculates a molar equivalent rate of air for the TOUGH2 source term. These rates for the whole repository are distributed spatially by TOUGH2, with gas injected into or withdrawn from the top row of repository elements (repo), and water injected into or withdrawn from the bottom row of all repository elements.

5 RESULTS FOR THE NORMAL EVOLUTION SCENARIO

This section will present the detailed modelling results for normal evolution scenarios. For each case, results are presented for:

- gas generation, as determined by the GGM component of the T2GGM model; and
- transport of gas, both in gaseous form and dissolved form, out of the repository and into the shaft and rock mass, and water flow from the rock mass into the repository. Gas and water transport is calculated by the TOUGH2 component of the T2GGM model.

The base case is presented in detail, and all other normal evolution cases are then compared.

It is useful to briefly describe some terminology and visualization conventions here before actual results are presented.

For gas generation figures, the evolution of all quantities is given as a function of time in years on a logarithmic scale. All concentrations are given per volume of water unless otherwise stated. Stack plots are used to demonstrate mass balance. Each band on the stack plot represents a different form that the given quantity can be in. The thickness of a band on a stack plot shows the number of moles of the quantity that is currently in the given form. Mass balance is demonstrated by the sum of all contributions – that is the height of the stack – being constant.

The term “repository” refers to the repository and ring tunnels, unless specified otherwise, as the gas and water flow processes in the two model zones are generally the same.

Use of the term “gas” refers to the bulk gas in gaseous form, and does not include water vapour. “Dissolved gas” refers to the bulk gas dissolved in the water. “Water” refers to the groundwater present in the geosphere. While water includes dissolved gas, the dissolved gas is a dilute component of the water. Current T2GGM simulations assume non-saline water as the water.

Gas saturation is the volumetric proportion of the porosity occupied by gas. Gas saturations are presented to show the extent of gas transport within the shaft and geosphere, and gas saturations greater than 10^{-6} are shown in all figures unless otherwise noted. Water saturation is the volumetric proportion of the porosity occupied by water, and is equal to one minus the gas saturation. Consequently, figures showing a gas saturation of less than one percent (fraction of 0.01), have a water saturation greater than 99 percent.

Gas and dissolved gas flow rates are extracted and presented for two horizontal planes.

1. At -262 mASL, the interface between the Queenston and Manitoulin units (denoted ORD). This interface was selected as it is the interface between the Deep and Intermediate Groundwater Zones.
2. At 2.7 mASL, the top of the Salina F unit (denoted SALF) and the top of the detailed gas transport model. Upward flow through this interface represents flow into the Shallow Groundwater Zone.

At each elevation, the transport planes are divided into two regions representing the shaft and the EDZ (denoted Shaft and EDZ) and the rest of the model domain (denoted Rock).

In describing gas and water flows, time in years are provided. Note that these times are restricted to the time resolution available for results. GGM results have a greater time resolution than spatial TOUGH2 results, and consequently TOUGH2 results are typically rounded to the closest 1000 years.

5.1 BASE CASE (NE-BC)

The NE-BC is only complete to 600 000 years due to numeric issues with the TOUGH2 model. The TOUGH2 model stalls at this point due to very small timesteps; an issue that will be resolved for future safety assessments. While the NE-BC results are incomplete, they are sufficient for analysis, particularly considering C-14 has decayed by approximately 100 half lives by this time.

5.1.1 Gas Generation

5.1.1.1 Water Balance and Saturation

Figure 5-1 provides a water balance for the repository for the base case (NE-BC). Shown are: the cumulative amount of water produced by the corrosion and microbial processes within the repository (green); the cumulative amount of water that has entered the repository from the geosphere (blue); and the total amount of water in the repository (red). The initial water content, cumulative amount produced and cumulative amount entered sum to give the total amount of water in the repository. Water vapour entering or leaving the repository is negligible (less than 10^5 mol).

The evolution of water saturation (fraction of the void volume in the repository occupied by water) is shown in Figure 5-2. Water seeps slowly from the surrounding host rock and shafts into the repository. Repository water saturation peaks at 72% at approximately 1200 years. After peak saturation is reached, gas generation begins to push water out of the repository until the repository reaches a water saturation of 18%. The double peak is related to the pressure profile (see Section 5.1.1.2). There is a large drop in the hydrogen production rate once all the carbon and galvanised steels have been completely corroded at approx. 2×10^3 years. This causes the pressure to drop to below the initial steady state pressure at the repository horizon, allowing a net influx of water into the repository until approx 4×10^3 years. The pressure recovers as gas continues to be produced, and water continues to be forced out of the repository. Investigation using TOUGH2 shows that towards the end of the simulation the amount of water that has left the repository through the shaft is approximately 9% of the cumulative amount of water that has entered the repository.

The implication of the expulsion of potentially contaminated water is studied in the assessment modelling (Walke et al. 2009a).

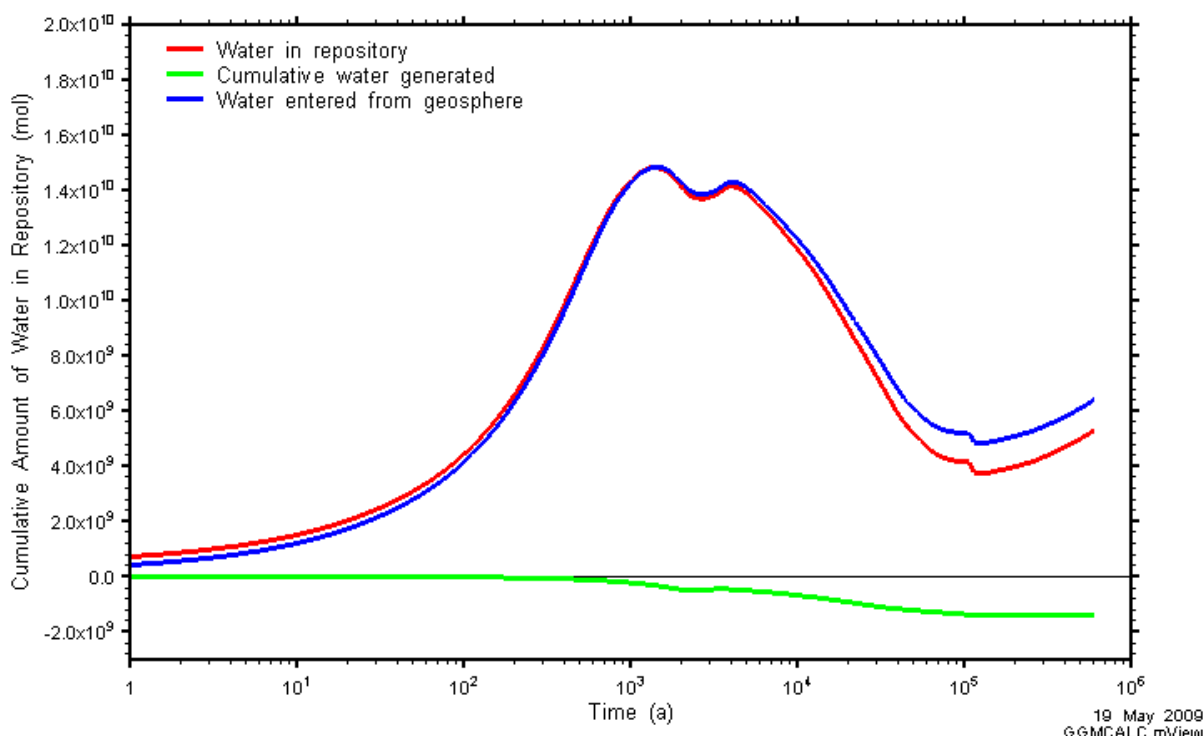


Figure 5-1: NE-BC: Water Balance

It is possible to estimate the total number of moles of water required to corrode all metallic wastes. The anaerobic corrosion of 3 moles of the carbon and galvanised steels and passivated steels and stainless steels all require 4 moles of water (producing Fe_3O_4). See equation (2-4). Similarly, the anaerobic corrosion of 1 mol of Zirconium alloy requires 2 moles of water producing ZrO_2 . See equation (2-5). Based on the initial number of moles of each metallic waste (4.12×10^8 , 3.04×10^8 , 3.02×10^8 and 6.68×10^6 respectively), this implies that the total number of moles of water required to corrode all metallic waste is 1.4×10^9 mol.

Similarly, the total number of moles of water required to degrade all the organic wastes is estimated. Methane production from cellulosic materials requires one mole of water for every one of cellulose as in equation (2-1), whereas 6 moles of water are required for every mole of styrene as in equation (2-2), which is used to represent ion-exchange resins and plastics and rubbers. Based on the initial number of moles of each type of organic waste (5.25×10^7 , 3.85×10^7 and 7.60×10^7 respectively), this implies that the total number of moles of water required to degrade all organic waste is 0.7×10^9 mol.

Finally, the degradation of 1 mole of cellulose, ion-exchange resin, or plastics and rubbers each lead to the generation of 3 moles of carbon dioxide. Thus a total of 5×10^8 moles of carbon dioxide are produced. If this is all consumed via the microbial methane generation reaction, this will produce twice as many moles of water: 10^9 moles - see equation 2-3).

Thus, the net amount of water expected to be consumed is approximately $1-2 \times 10^9$ mol. This is compatible with the total amount consumed shown in Figure 5-1.

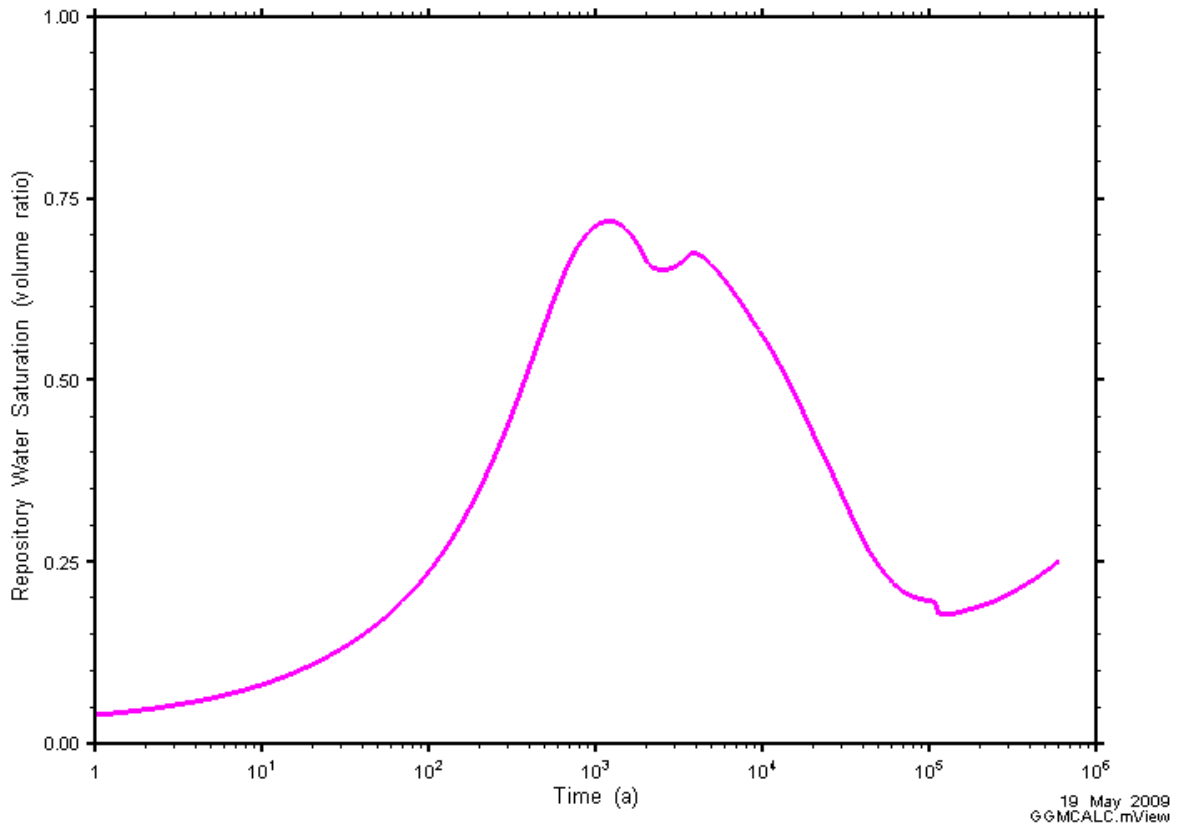


Figure 5-2: NE-BC: Water Saturation

5.1.1.2 Gases

Figure 5-3 shows the evolution of the amounts of the gases (in gaseous form) in the repository and Figure 5-4 shows the amounts of the gases which have left the repository. Figure 5-5 gives the concentrations of the gases dissolved in the saturated part of the repository. Information about water vapour is calculated by TOUGH2 and provided in Figure 5-12.

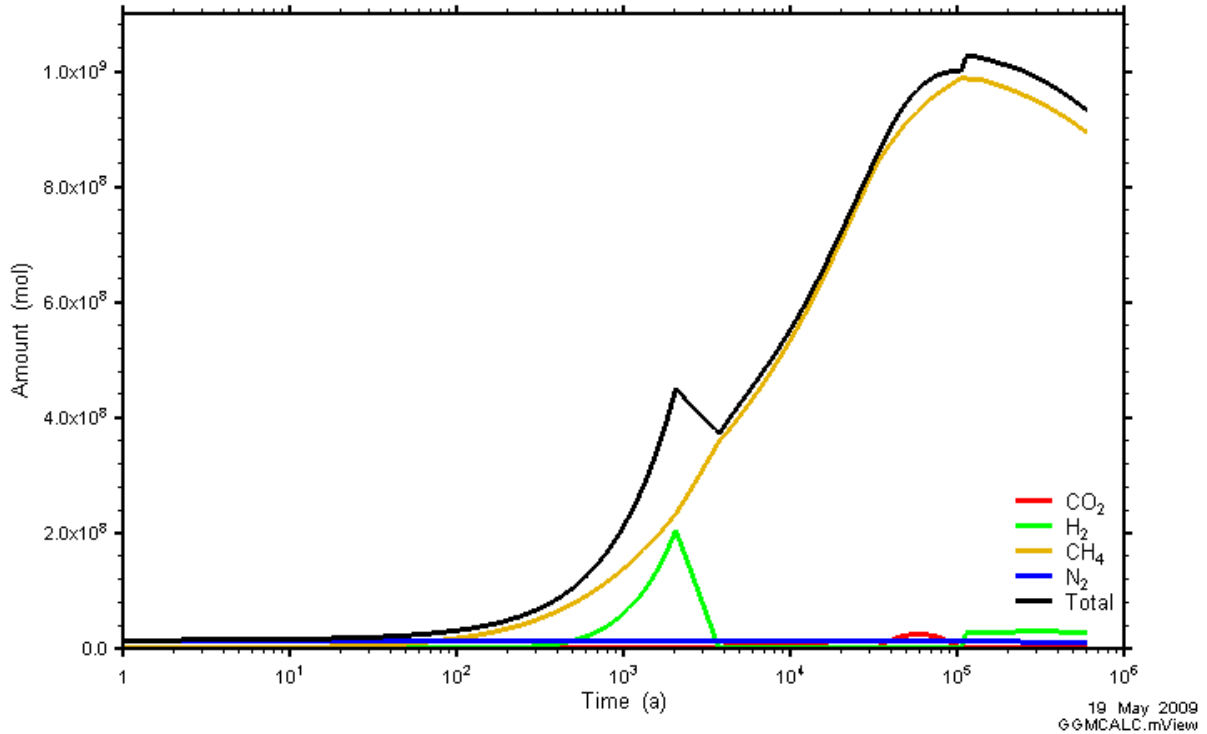


Figure 5-3: NE-BC: Amounts of Gases within the Repository

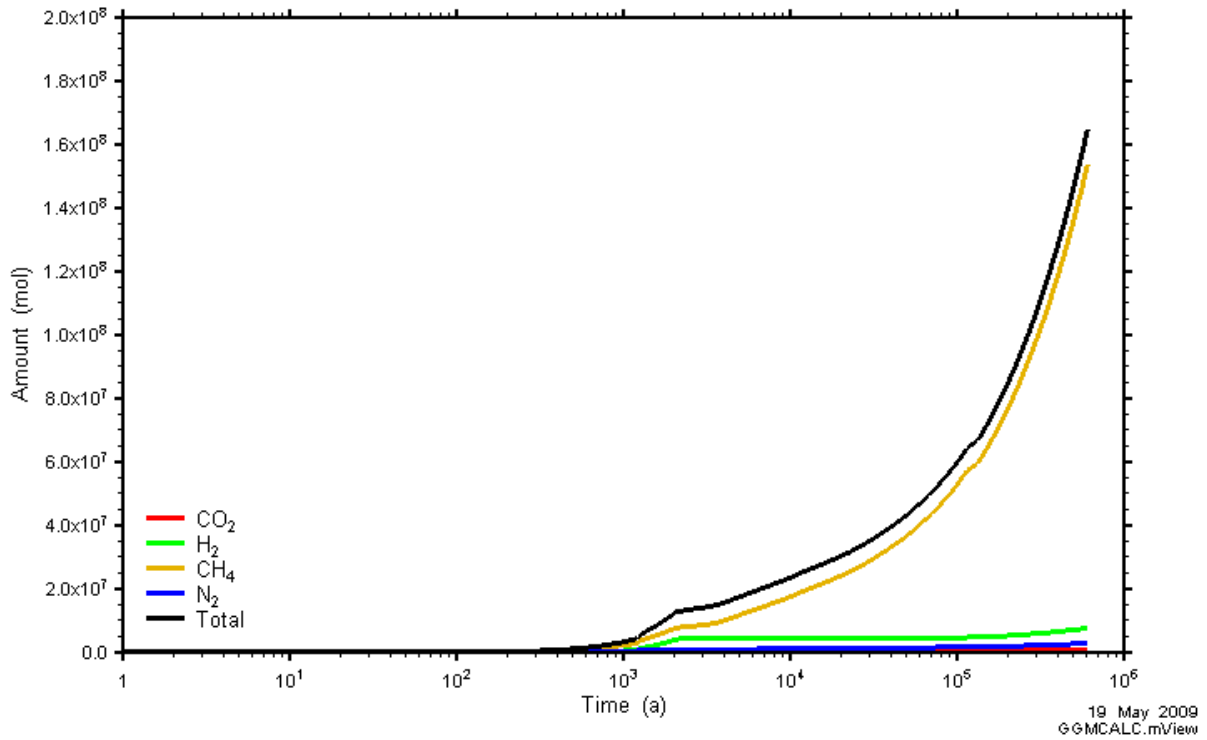


Figure 5-4: NE-BC: Amounts of Gases which have Left the Repository

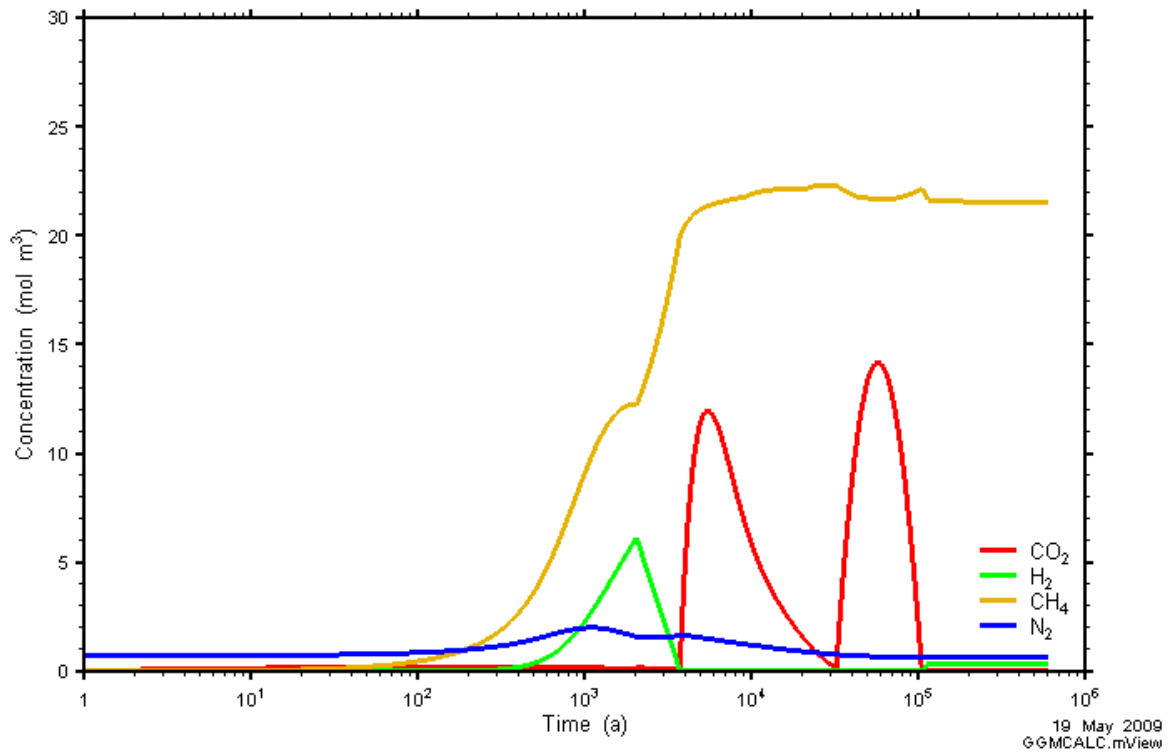


Figure 5-5: NE-BC: Concentrations of Dissolved Gas within the Repository

The gas partial pressures and total gas pressure within the repository are given in Figure 5-6. The total gas pressure undergoes its biggest rise during a phase of methane and hydrogen generation, achieving a peak pressure of 8.5 MPa at 2100 years. Initial steady state pressure in the geosphere at repository depth is indicated as two horizontal lines, representing the range of pressure observed at the top and bottom horizon of the repository. The peak pressure is confirmed by a simple calculation check using the ideal gas law ($PV=nRT$); the void volume of the repository ($V = 1.29 \times 10^5 \text{ m}^3$, for the repository and ring tunnel with a water saturation of 0.66); the total number of moles of gas in the repository at the time of peak pressure, determined from Figure 5-3 ($n = 4.50 \times 10^8 \text{ mol}$); and a temperature of 20 degrees Celsius. This calculation yields a pressure of 8.5 MPa.

The evolution of the individual gas components will now be described in turn.

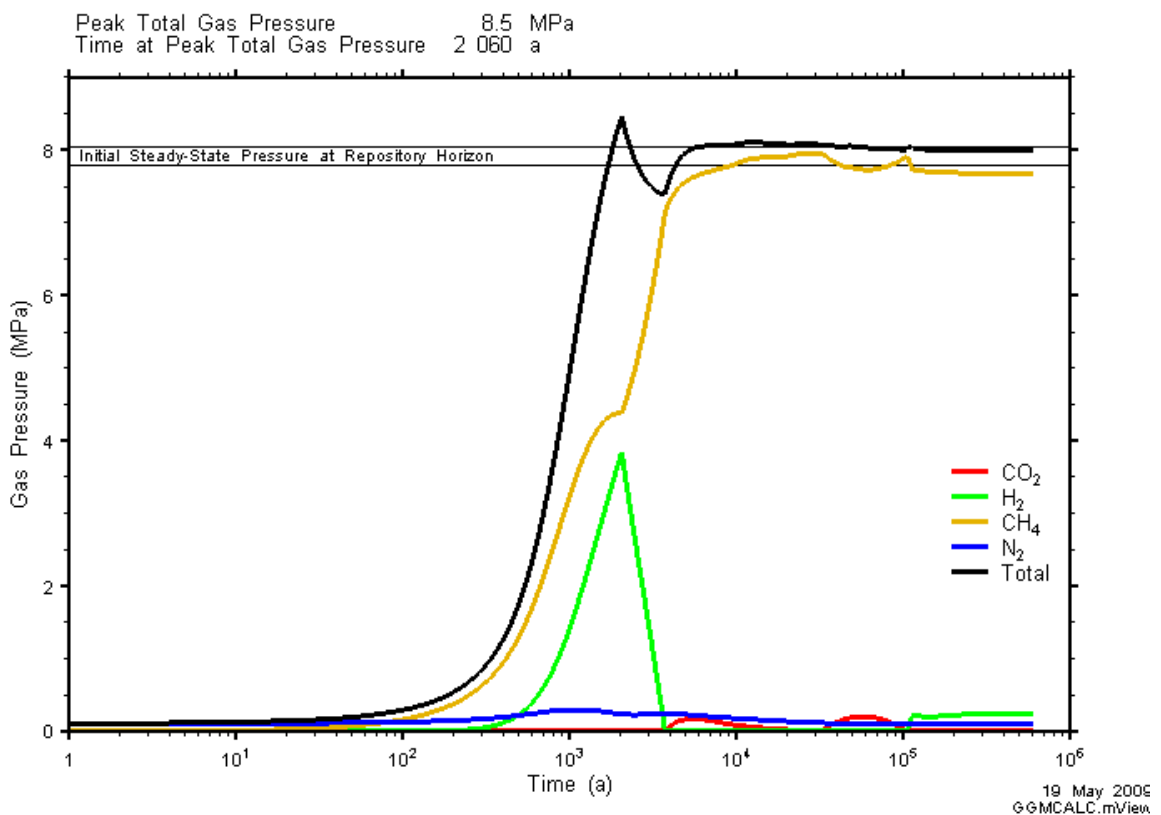


Figure 5-6: NE-BC: Total and Partial Gas Pressures with the Repository

5.1.1.2.1 Nitrogen

Nitrogen gas is not involved in any of the corrosion, degradation or microbial reactions within the repository. As the total gas pressure within the repository increases, nitrogen is transported out of the repository. Approximately one tenth of the original amount leaves in total (Figure 5-4 and Figure 5-3). The concentration and partial pressure of nitrogen within the repository remain fairly constant.

5.1.1.2.2 Methane

Methane is the dominant gas within the repository, produced by both the microbial degradation of organic wastes and the metabolism of carbon dioxide and hydrogen (Figure 5-3).

Most of the carbon initially in the organic waste streams is finally converted to methane gas. See the carbon atom stack plot, Figure 5-11. No mechanisms for the consumption of methane are modelled.

Methane generation through the degradation of organic wastes decreases as the organic wastes become degraded. This methane generation path ceases once all organic wastes have been degraded at 4×10^5 years (Figure 5-10).

Methane generation via the microbial metabolism of carbon dioxide and hydrogen given in equation (2-3) can proceed very rapidly. However, this reaction is limited by the availability of both hydrogen and carbon dioxide. Between 4×10^3 years and 10^5 years for example, methane generation is limited by the availability of hydrogen and the rate at which it is produced through the corrosion of metallic wastes. At 10^5 years it becomes limited by the availability of carbon dioxide and the rate at which it is produced through the degradation of organic wastes.

The microbial methane generation reaction acts to reduce the total number of moles of gas, converting hydrogen and carbon dioxide to methane and water. If methanogens are present and active, it occurs relatively quickly. If conditions are not favourable for methanogens, then even the base degradation of organics would also proceed slowly. The implication of this case is examined later in the NE-GG2-T case.

In the base case, only 20% of the available carbon in the system has taken the form of methane by the peak pressure time (see Figure 5-11). It takes almost 10^5 years for the remaining carbon to be converted to methane.

5.1.1.2.3 Carbon Dioxide

Carbon dioxide is produced via the microbial degradation of organic wastes. Carbon dioxide production decreases as the organic waste streams are degraded and ceases once all the organic waste has been degraded – which occurs at 4×10^5 years for the base case NE-BC (see Figure 5-10).

Carbon dioxide is consumed via the microbial generation of methane and via the enhanced corrosion of metallic wastes.

Enhanced corrosion of the carbon and galvanised steels and the stainless steels and nickel alloys leads to a more rapid consumption of carbon dioxide when pressures are significantly higher than the reference partial pressure for enhanced CO₂ corrosion; 0.05 MPa (Walke et al. 2009b). Partial pressures of carbon dioxide are sufficiently high for this to occur twice, at 5×10^3 and 5×10^4 years (see Figure 5-6). However, by the time the second peak has arrived, those metallic waste streams susceptible to enhanced corrosion have already been completely corroded (see Figure 5-7). The enhanced corrosion which occurs during the first carbon dioxide partial pressure peak shows up as a more rapid increase in the corrosion product FeCO₃ at that time (see Figure 5-8).

It is methane generation via the microbial metabolism of carbon dioxide and hydrogen which has the greatest impact on the evolution of CO₂. Provided there is sufficient hydrogen being generated to sustain this reaction it proceeds rapidly, keeping the amount of CO₂ in the repository at a low level. This is the case until 4×10^3 years (see Figure 5-3). Production of hydrogen slows as the metallic waste streams are corroded and at 4×10^3 years hydrogen is completely consumed. The methane generation reaction then becomes limited by the rate at which hydrogen can be produced through corrosion. Since the microbial methane generation reaction becomes hydrogen limited, CO₂ consumption is reduced and the balance switches back in favour of CO₂ production at this time.

Hydrogen also undergoes step decreases in production each time a metallic waste stream is completely exhausted. This occurs at 2×10^3 years, 3×10^4 years and 10^5 years (Figure 5-7). These step decreases in hydrogen production cause step decreases in the amount of CO₂ that is being consumed through the methane generation reaction – particularly when this microbial methane generation reaction is hydrogen limited as is the case between 4×10^3 and 10^5 years. This can cause the balance to switch back in favour of CO₂ generation through degradation of organic wastes. This can be seen to occur in the small jump in the amount of CO₂ at 2×10^3 years and the larger one at 3×10^4 years (Figure 5-6).

At 10^5 years all carbon dioxide is consumed and the microbial methane generation reaction becomes carbon dioxide limited until such time that all organic wastes have been exhausted, carbon dioxide production ceases and hence methane generation ceases, creating a final state with mostly methane, and some hydrogen but no carbon dioxide.

5.1.1.2.4 Hydrogen

Hydrogen is produced by corrosion of metallic wastes. Hydrogen production decreases as the metallic waste streams are corroded and ceases once they are completely exhausted at 3×10^5 years (Figure 5-7 and Figure 5-3). Hydrogen production undergoes step decreases as each metallic waste stream is completely exhausted³. For example, at 2×10^3 years, the time of the peak pressure, the carbon and galvanised steel wastes are exhausted (Figure 5-7). In this case, the rate of generation of hydrogen drops sufficiently to change the balance to net consumption of hydrogen.

Hydrogen is rapidly consumed via the microbial generation of methane from carbon dioxide and hydrogen. Once all hydrogen has been consumed, this reaction becomes limited by the rate at

³ Note that these appear as step decreases on the timescale of interest. In practice we expect variability within the waste and the rates at which it corrodes to smooth these transitions to a certain extent.

which hydrogen is produced through corrosion. Provided sufficient carbon dioxide is available this microbial methane generation reaction will continue to consume all hydrogen made available through corrosion. This occurs between 4×10^3 and 10^5 years (Figure 5-3).

5.1.1.3 Metallic Wastes

The different types of metallic wastes can be seen to be consumed over time scales varying from 2×10^3 to more than 10^5 years in Figure 5-7. The various corrosion products are given in Figure 5-8. Figure 5-9 shows the complete balance of Fe atoms on a stack plot. It can be seen that only approximately 20% of the iron in the metallic waste ends up as FeCO_3 produced through enhanced carbon dioxide corrosion, with most ending up as Fe_3O_4 .

The generation of corrosion products slows each time a metallic waste stream is completely corroded. The complete consumption of the carbon and galvanised steels at 2×10^3 years causes a drop in the rate of production of the Fe_3O_4 corrosion product and a drop in the amount of FeCO_3 being produced through enhanced carbon dioxide corrosion (Figure 5-8). However, the amount of FeCO_3 being produced increases again when higher CO_2 partial pressures occur and ceases once the stainless steel and Nickel based alloys, which are the only other metals capable of enhanced CO_2 corrosion, are completely corroded at 3×10^4 years.

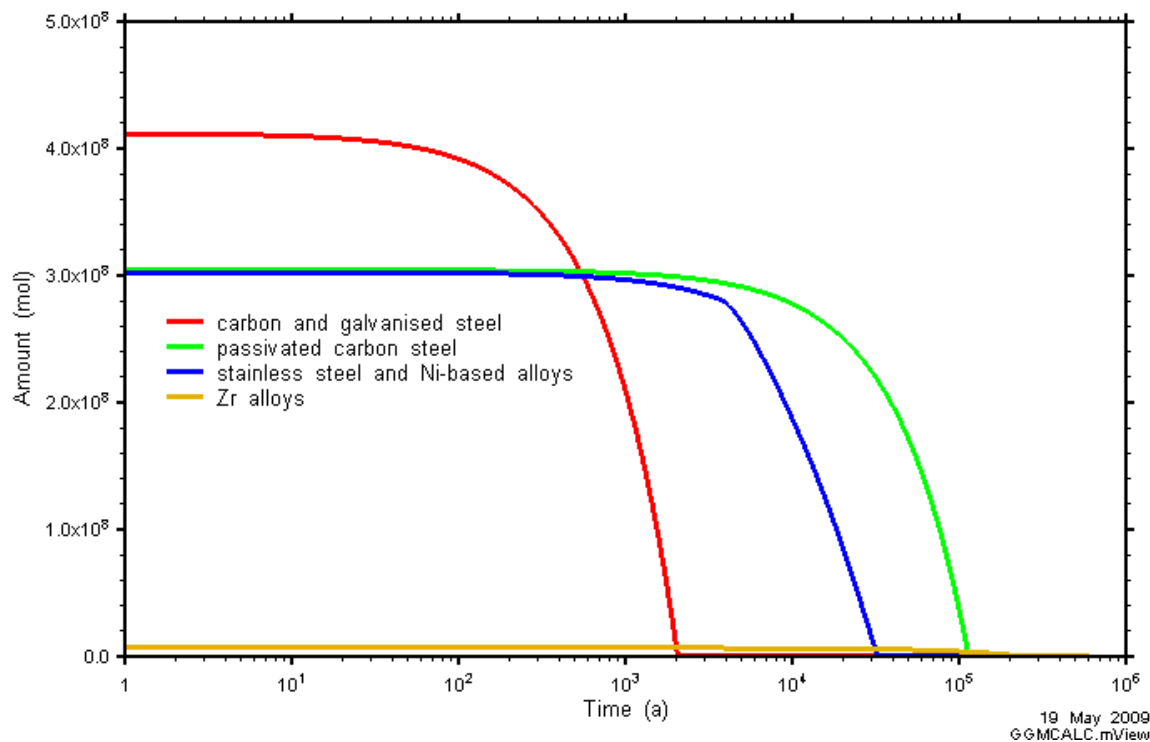


Figure 5-7: NE-BC: Amounts of Metallic Waste

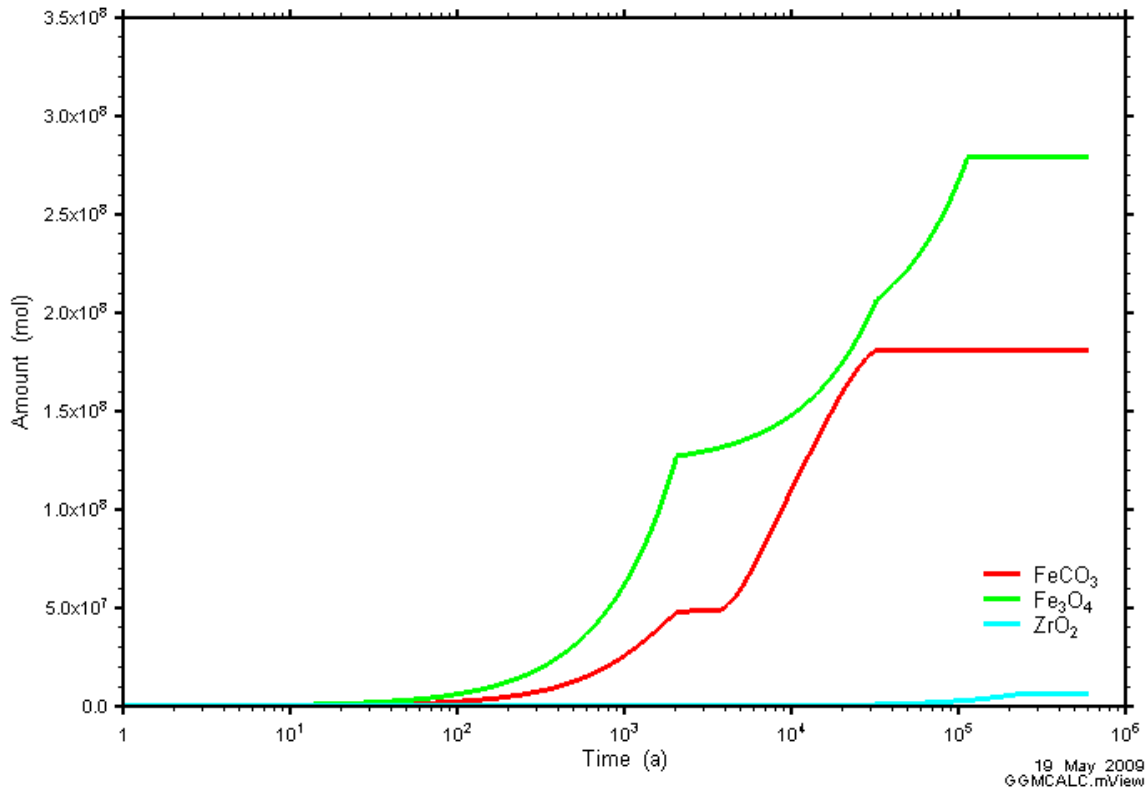


Figure 5-8: NE-BC: Amounts of Corrosion Products

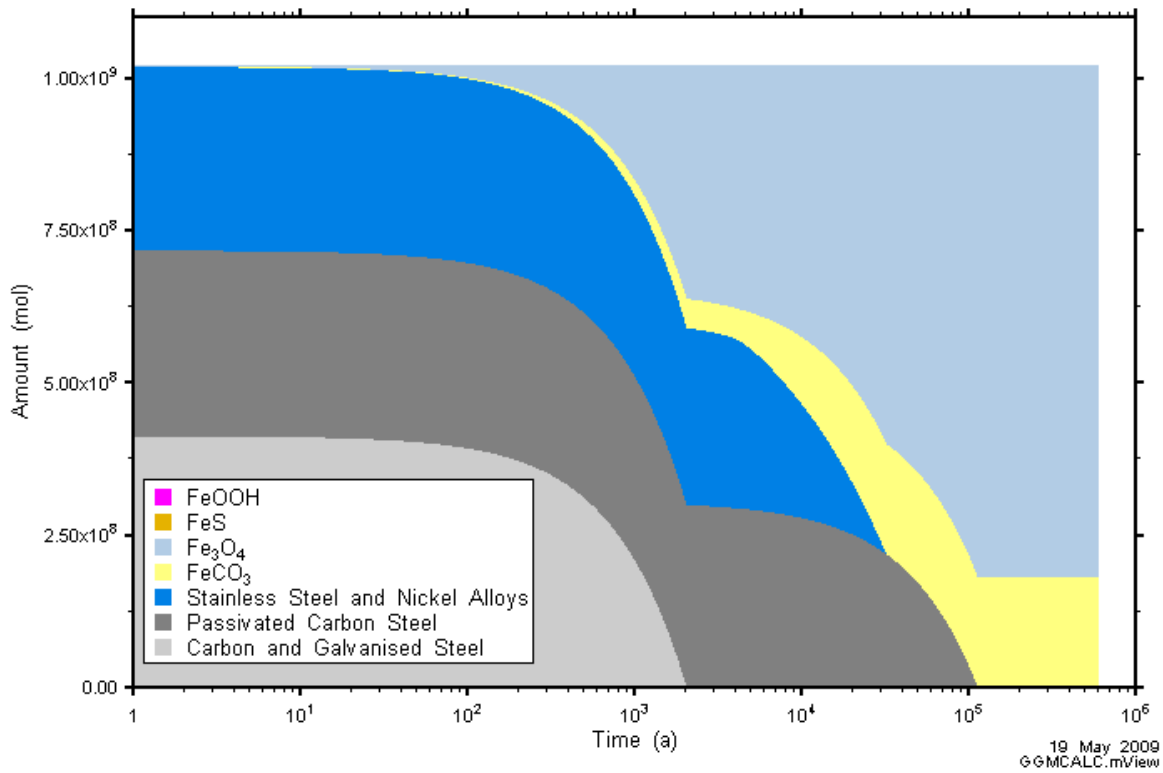


Figure 5-9: NE-BC: Iron Atom Stack Plot

5.1.1.4 Organic Wastes

The degradation of the organic wastes is shown in Figure 5-10. Complete degradation of each of the waste streams occurs by 4×10^5 years. Figure 5-11 shows the complete balance of carbon atoms. It can be seen that approximately 80% of carbon in the organic wastes ends up as CH_4 in the repository, 5% as CH_4 that has left the repository, and 15% as FeCO_3 .

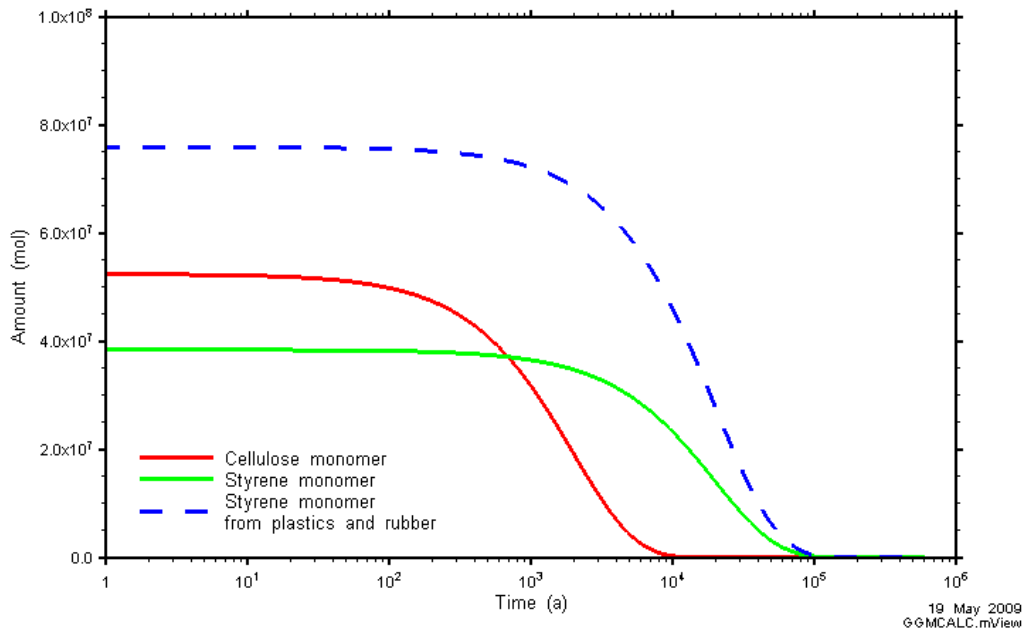


Figure 5-10: NE-BC: Amounts of Organic Waste

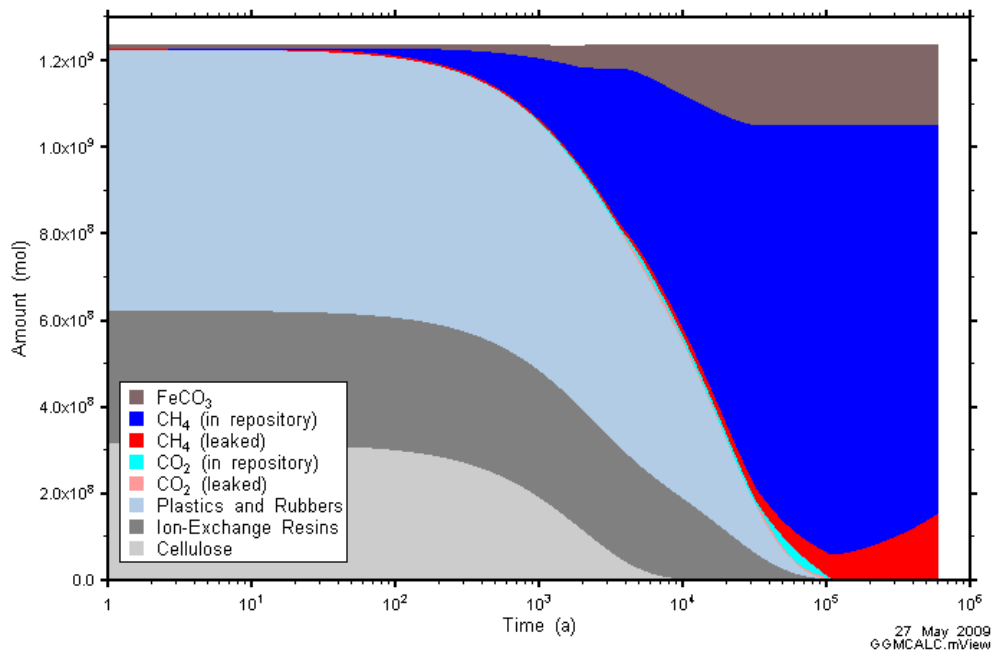


Figure 5-11: NE-BC: Carbon Atom Stack Plot

5.1.1.5 Relative Humidity

The relative humidity is calculated by TOUGH2 as the partial pressure of vapour divided by the saturated vapour pressure (at 20 deg C, this is 2340 Pa). Figure 5-12 shows that the relative humidity remains at 100% for the entire simulation. Since this is higher than the threshold relative humidity of 60% it means that microbial activity and corrosion proceed in the vapour phase of the repository throughout the simulation.

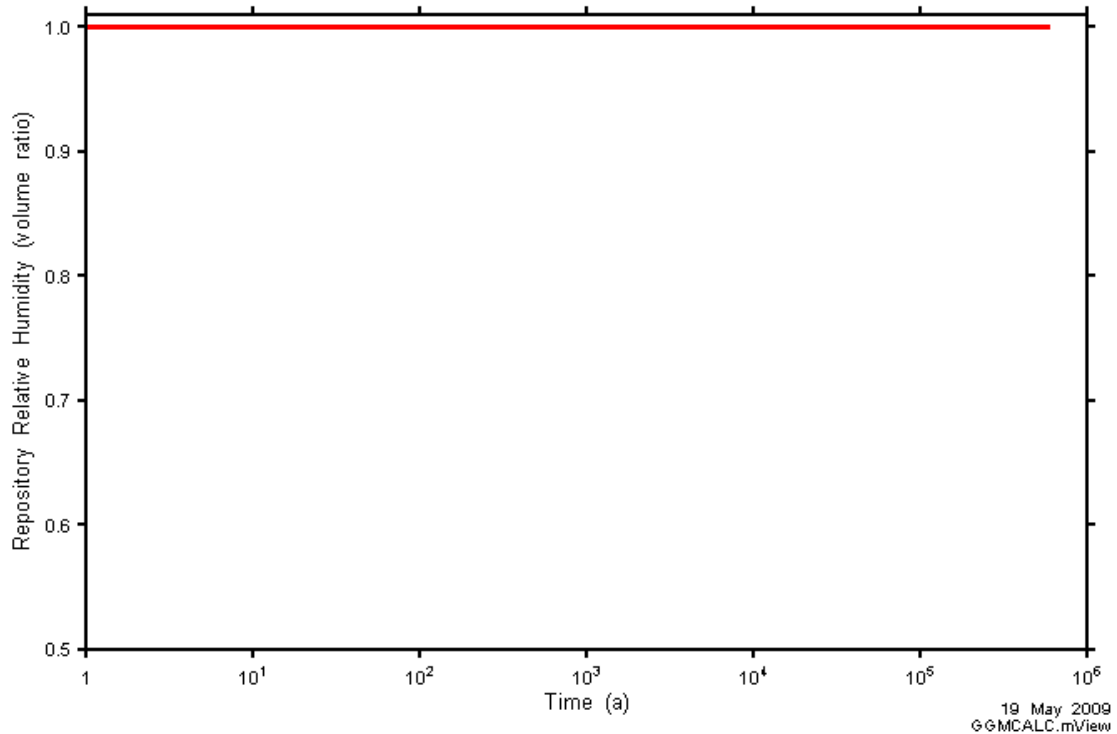


Figure 5-12: NE-BC: Relative Humidity

5.1.1.6 Gas and Water Generation

The rates of gas and water generation (or consumption) due to the various corrosion and microbial processes occurring within the repository are given in Figure 5-13. It can be seen that the sustained and more rapid production of gas during the first 2000 years gives rise to the peak pressure. This is primarily due to the production of hydrogen due to the corrosion of the carbon and galvanised steels.

The gas generation rate becomes negative as the microbial methane generation reaction takes over, consuming the remaining hydrogen and carbon dioxide and producing water and methane until approximately 4000 years. At this time the system becomes hydrogen limited and so the organic degradation reactions take over as the dominant gas producing reactions, producing carbon dioxide that is reduced by the microbial methane generating reaction dependent on the availability of hydrogen until approximately 10^5 years. Most of the waste has corroded or degraded by this time and the gas generation rates tail off.

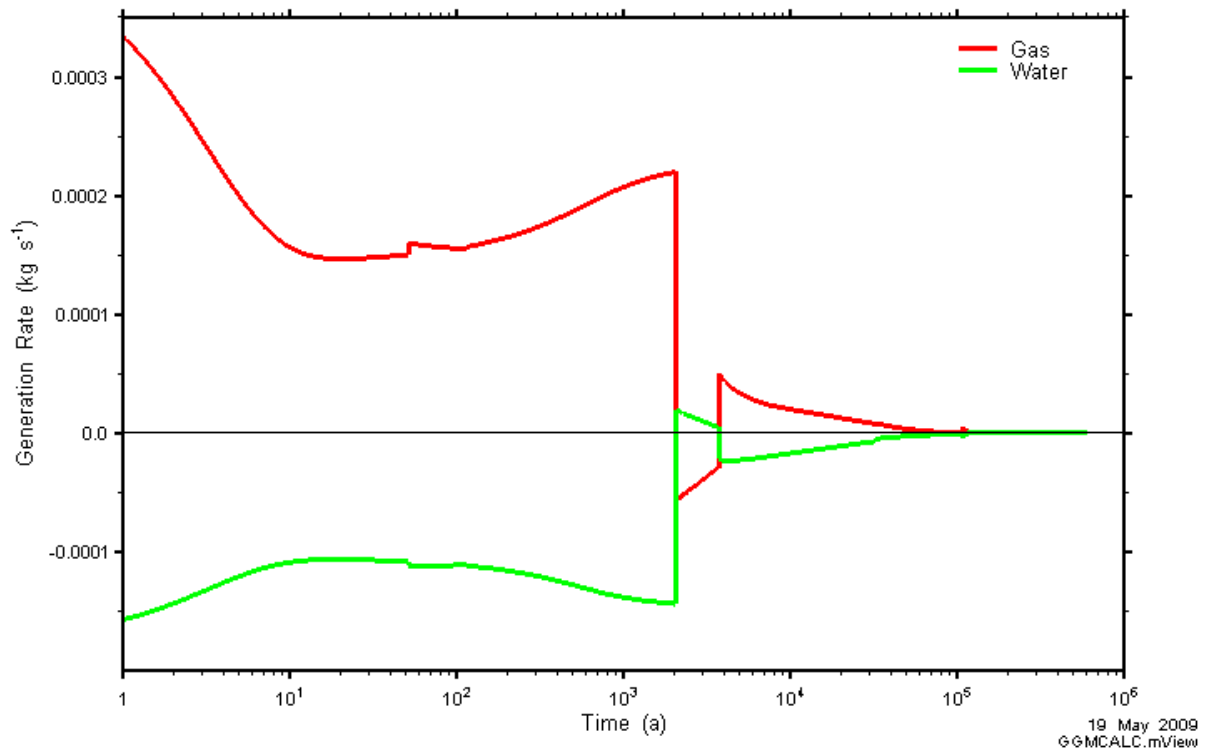


Figure 5-13: NE-BC: Gas and Water Generation Rates

5.1.2 Gas and Water Flows

The transport of gas and water is described chronologically. Figure 5-14 and Figure 5-15 show dissolved gas flow rates and dissolved gas mass transported through the ORD and SALF planes. As discussed in detail below, gas is not transported above the ORD plane. Early (small) peaks of dissolved gas flow rates (before 3000 years) across the shaft/EDZ of the ORD and SALF planes are composed of dissolved initial gases in the shaft. Cumulative dissolved gas crossing the ORD and SALF planes in the rock is greater than in the shaft/EDZ, showing that while the shaft/EDZ provides a slightly faster pathway for groundwater, this effect is small compared to the large area over which dissolved gas is transported in the rock mass.

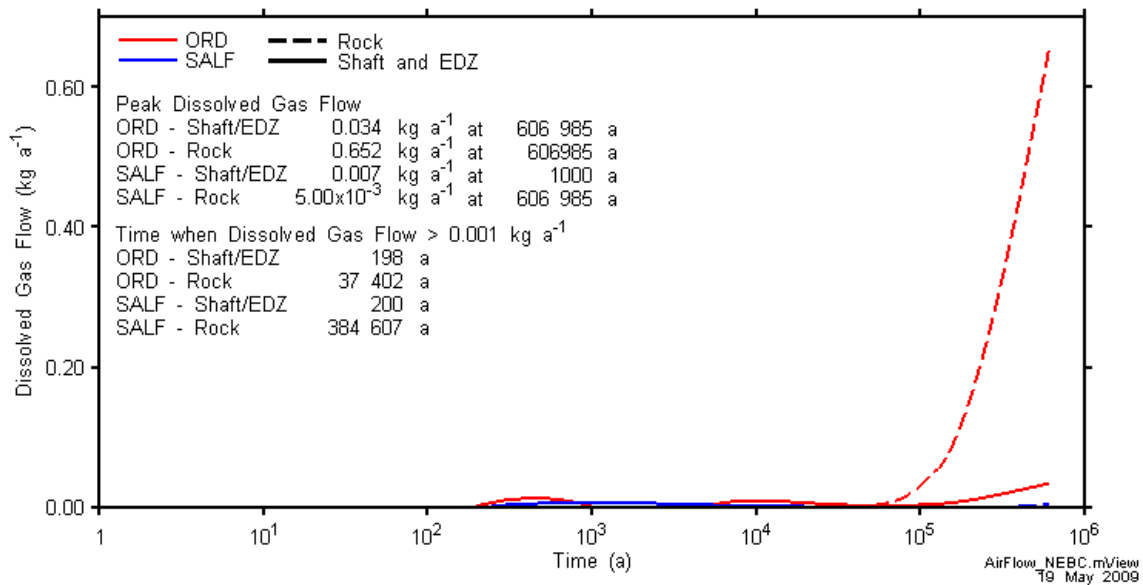


Figure 5-14: NE-BC: Dissolved gas flow rates across the ORD and SALF planes

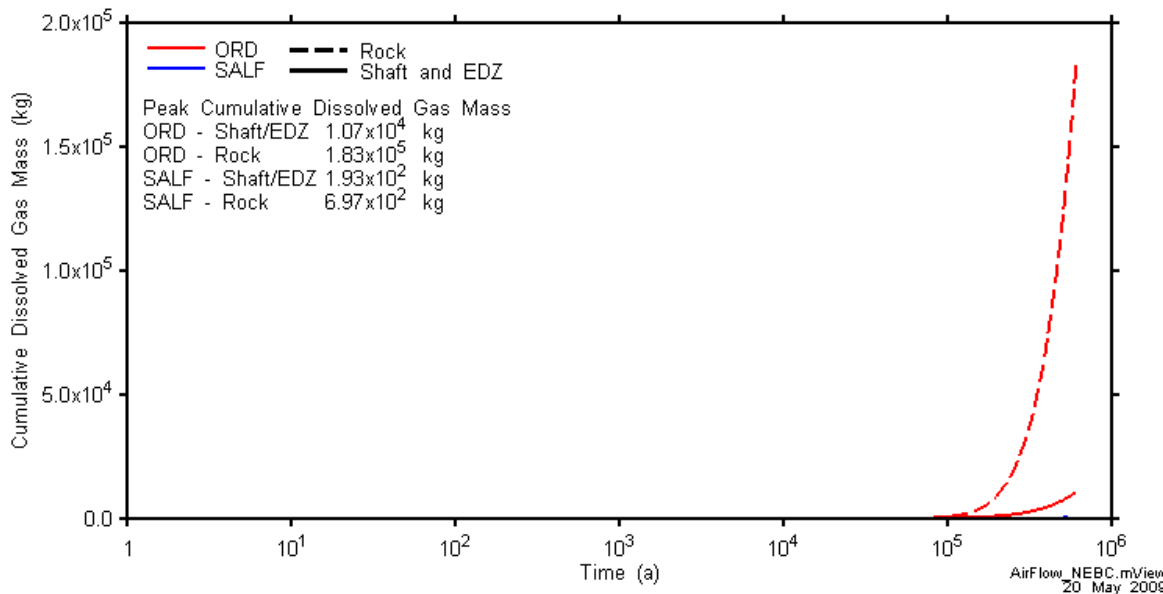


Figure 5-15: NE-BC: Cumulative dissolved gas mass crossing the ORD and SALF planes

5.1.2.1 Detailed Description of Gas and Water Transport

At the start of the simulation, the repository and shaft are at atmospheric pressure. The repository is mostly saturated with gas, with a small amount of water initially present in the waste. Shafts are initially 50% saturated with gas. See Figure 5-16 for gas saturations and gas and water flow at the transition between the repository, ring tunnel and shaft, as well as pressure and repository water saturations at the start of the simulation and several key times early in the simulation.

Initially, pressures in the repository and shaft are increasing, as the repository and geosphere move towards equilibrium pressures. Water is also flowing into the repository, ring tunnels and shaft. Most of the initial gas in the shaft dissolves in the water resaturating the shaft; however, a very small amount of these initial gases (4%), travels into the repository in the first 500 years, corresponding to the gas vectors shown in Figure 5-16 at time zero, which show downwards flowing gas towards the repository. This small amount of gas is due to shaft gas pressure increasing more quickly than repository gas pressure, due to capillary pressure effects in the shaft. As there is no capillary pressure in the repository, as liquid pressure increase relatively uniformly in the shaft and repository, gas pressure will be slightly greater in the shaft than the repository. A small amount of gas travels into the EDZ above the repository and into the rock mass at the sides of the repository (note that model does not currently define EDZ at the sides of the repository). By 800 years, the shaft at the repository horizon is fully saturated with water, and consequently, no gas saturations or gas flows are shown in the shaft in Figure 5-16 after time zero. Small amounts of gas (gas saturation less than 10^{-3}) are still present in the shaft above -50 mASL, with the shaft becoming fully saturated with water by 3000 years.

By approximately 1200 years, the repository has reached a maximum water saturation of 0.72. Water begins to be pushed out of the repository at this time, primarily into the rock mass below the repository, as pressures in the repository from generated gases become greater than pressures in the surrounding geosphere. See Figure 5-16 for gas saturations, repository water saturation, pressure and gas and water flows at 800 and 1200 years; and Figure 5-2: NE-BC: for the average repository water saturation.

Peak gas pressure occurs at 2000 years. Gas pressures drop sharply after 2000 years, due to a sharp change from gas generation to gas consumption, as well as water consumption to water generation, as explained in 5.1.1.6 and shown in Figure 5-13. As gas pressures in the repository drop below pressures in the geosphere, water begins to flow into the repository once again. Once gas generation and water consumption resume, at 3700 years, repository gas pressure begins to increase again and water saturation in the repository begins to decrease once repository gas pressures are greater than the surrounding geosphere. See Figure 5-17 for gas saturations, repository water saturation, pressure and gas and water flows at 2000 and 3000 years.

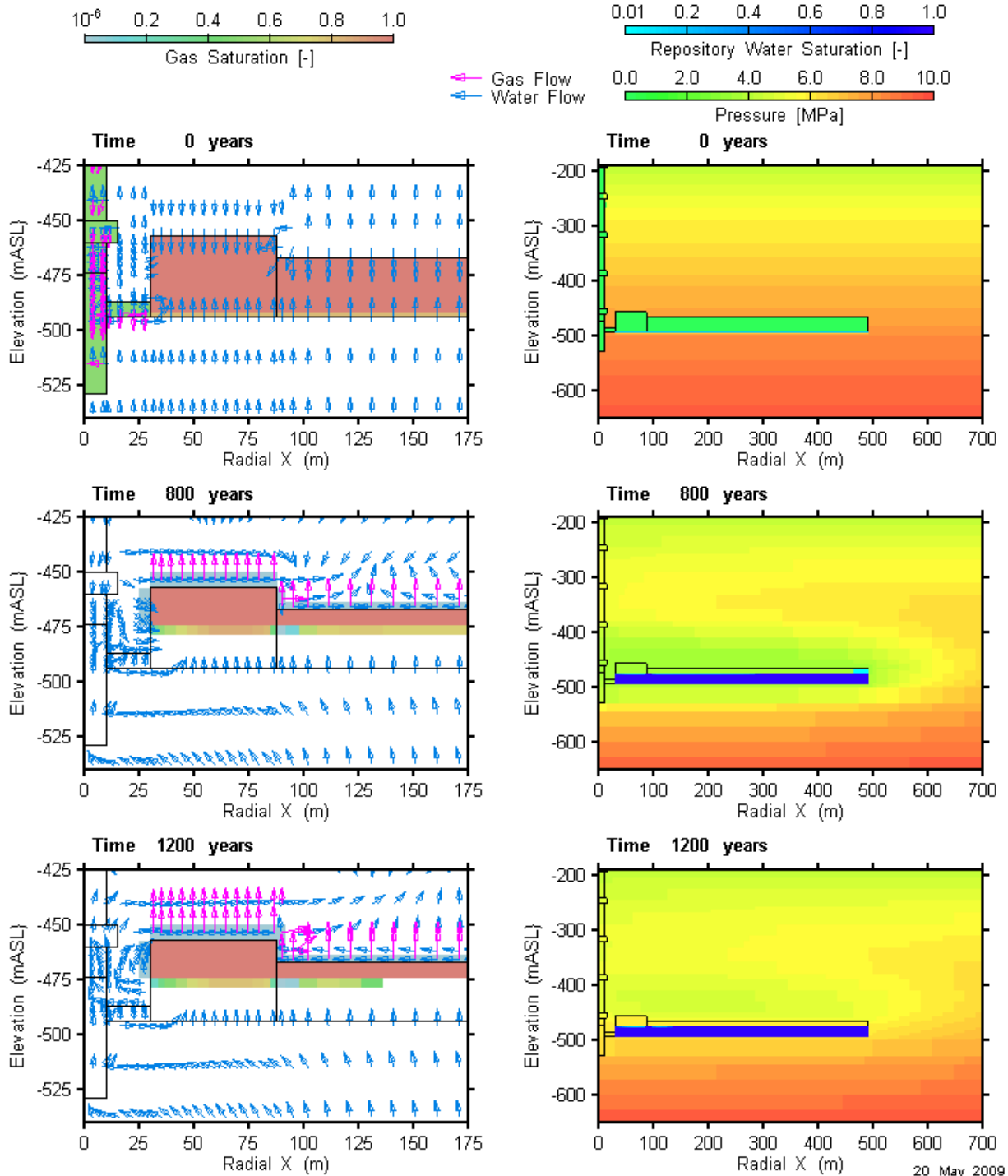


Figure 5-16: Evolution of conditions for the NE-BC at the start of the simulation (0 years), 800 years, and 1200 years. Gas saturation, and gas and water flow (outside repository) are shown in the figures on the left, and pressure and repository water saturation in the figures on the right.

Repository gas pressures begin to approach a steady-state value of 8 MPa around 6000 years. Gas generation is still occurring, however, the volume available for gas increases as water is pushed out of the repository. The repository EDZ and rock mass within a few meters of the repository still only contain very small amounts of gas, with gas saturations greater than 10^{-6} but less than 10^{-3} . See Figure 5-17 for gas saturations, repository water saturation, pressure and gas and water flows at 6000 years.

At 110 000 years, the gas generation rate and water consumption rate decrease to very small values, resulting in a maintenance of the repository gas pressure at 8 MPa, close to the initial steady-state pressure for the repository. Repository water saturation is at 0.18, and does not decrease any further. Note that the gas pressure is actually decreasing very slowly, and at approximately 125 000 years, the gas pressure in the repository decreases below the water pressure in the host rock below the repository, causing water to begin to saturate the repository again from the bottom of the repository. Gas continues to slowly leak out of the top of the repository, as repository pressures are slightly greater than water pressure in the host rock above the repository. Note that water pressure in the host rock is close to the initial steady-state pressure.

Both the host rock and the concrete monolith and shaft are effective barriers to gas migration. Over the one million time period of the simulation, gas saturations in the rock mass adjacent to the repository remain at saturations greater than 10^{-6} only within a few metres of the repository, indicating the effectiveness of the host rock as a barrier for gas migration.

Figure 5-18 shows gas saturation, repository water saturation, pressure and gas and water flows at the end of the simulation at 600 000 years. Over the course of the simulation, mainly gas leaves the repository, rather than dissolved gas, with approximately 12% of generated gases leaving the repository (1.08×10^9 mol of gas generated and 1.35×10^8 mol gas leaving the repository).

Note that most of the gas leaving the repository enters the host rock, with approximately 0.05% of the gas leaving the repository through the concrete monolith and shaft, indicating the effectiveness of the concrete monolith and shaft seals for preventing gas transport. Only a small amount of dissolved gas leaves the repository, approximately 0.5% of the gas generated (5.45×10^6 mol). The amount of dissolved gas observed at the ORD and SALF planes is greater than the amount leaving the repository (see Figure 5-15), as gas leaving the repository also dissolves into the groundwater, contributing to the amount of dissolved gas. In fact, ninety-nine percent of the gas leaving the repository has dissolved by the end of the simulation, leaving only 5.79×10^5 mol of gas in the host rock.

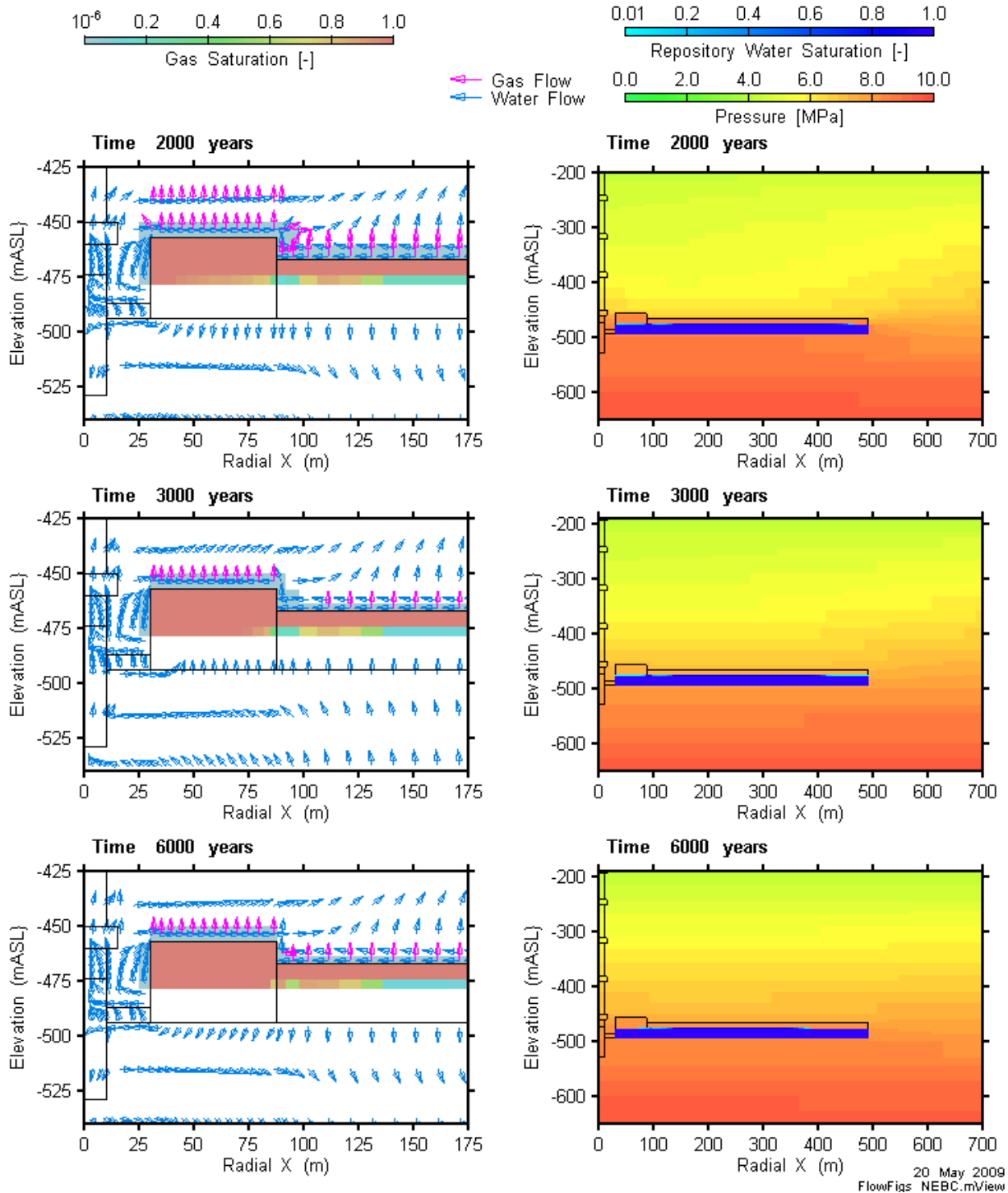


Figure 5-17: Evolution of conditions for the NE-BC simulation at 2000 years, 3000 years, and 6000 years. Gas saturation, and gas and water flow (outside repository) are shown in the figures on the left, and pressure and repository water saturation in the figures on the right.

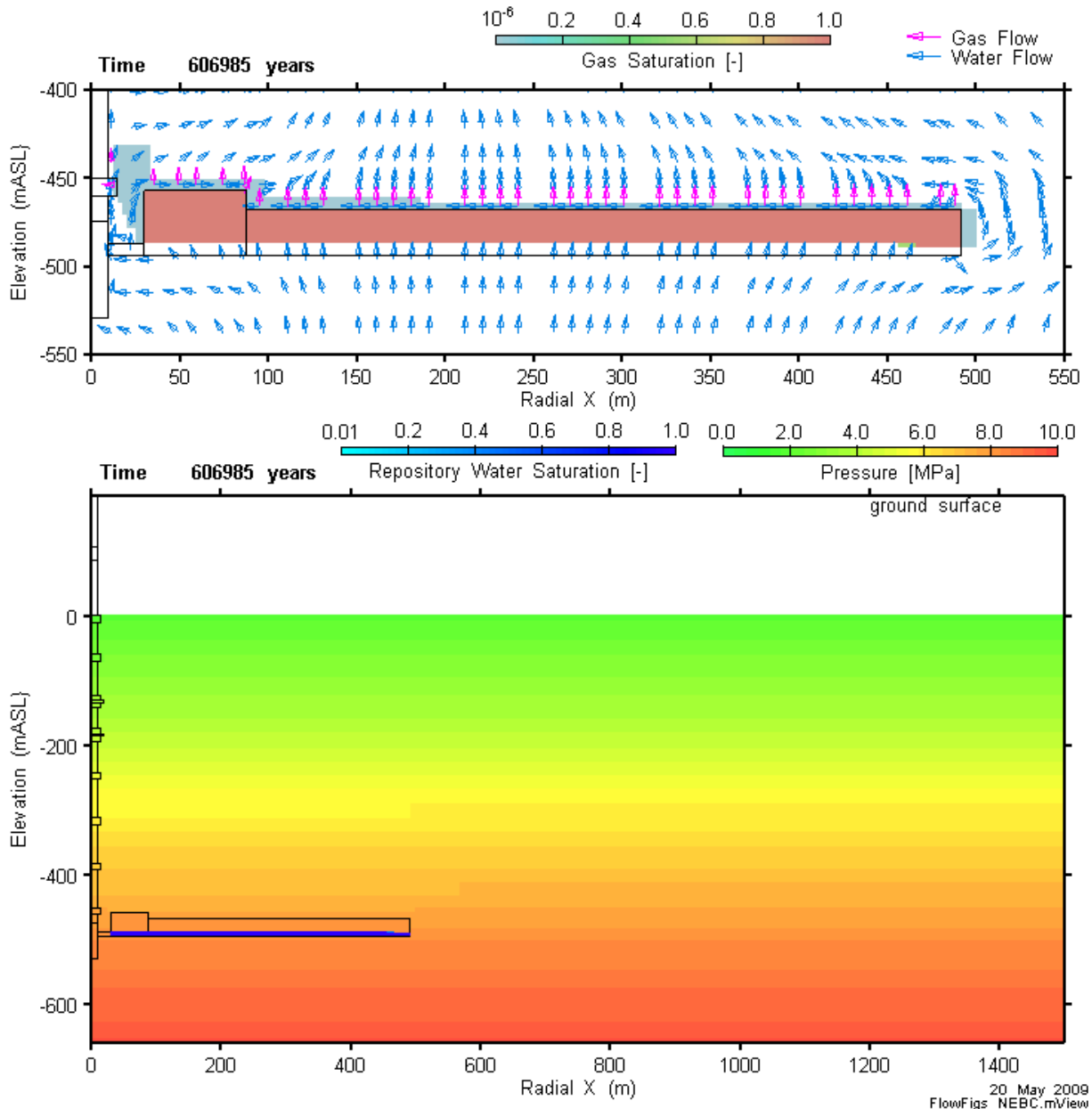


Figure 5-18: Evolution of conditions for NE-BC simulation at 600 000 years. Gas saturation and gas and water flows (outside repository) are shown in the figure above, and pressure and repository water saturation in the figure below.

5.1.2.2 Detailed Description of Dissolved Gas Transport

Initially, dissolved gas is present in the shaft, repository and ring tunnel. Initial dissolved gas concentrations are calculated from the initial gas pressure and the solubility of the gas using Henry’s law. Initial gas saturations were assumed 50% in the shaft, and 98.4% in the repository and ring tunnel (with single phase gas in all repository and ring tunnel elements except the bottom layer of the repository and ring tunnel, which contains the residual water from the waste packages). Consequently, where there is initially a single phase of gas (in the repository and

ring tunnels at time zero, except the bottom layer of the repository and ring tunnel), or a single phase of water (in the rock mass), the initial concentration of dissolved gas is zero; and where there is initially two phases (gas and water, in the bottom layer of the repository and ring tunnels and in the shaft), the concentration of dissolved gas is greater than zero.

As the shafts and repository re-saturate with water, gas dissolves into the water and the dissolved gas diffuses out into the rock. Dissolved initial gases in the shaft travels upwards and out of the system before dissolved gases originating from the repository travel up the shaft, explaining the small early peaks in dissolved gas flow rates in Figure 5-14.

Figure 5-19 shows dissolved gas concentrations at 0, 2000, 100 000 and 600 000 years. Note that at time 0, the repository and ring tunnel shows a small amount of dissolved gas in the top layer, as the results are actually at 100 seconds and a small amount of water has entered the top of the repository from the rock mass. The repository and ring tunnels show a dissolved concentration at late times, due to the small residual amount of water present. The distinct line changes apparent at 100 000 years and 600 000 years are due to transitions in geologic units.

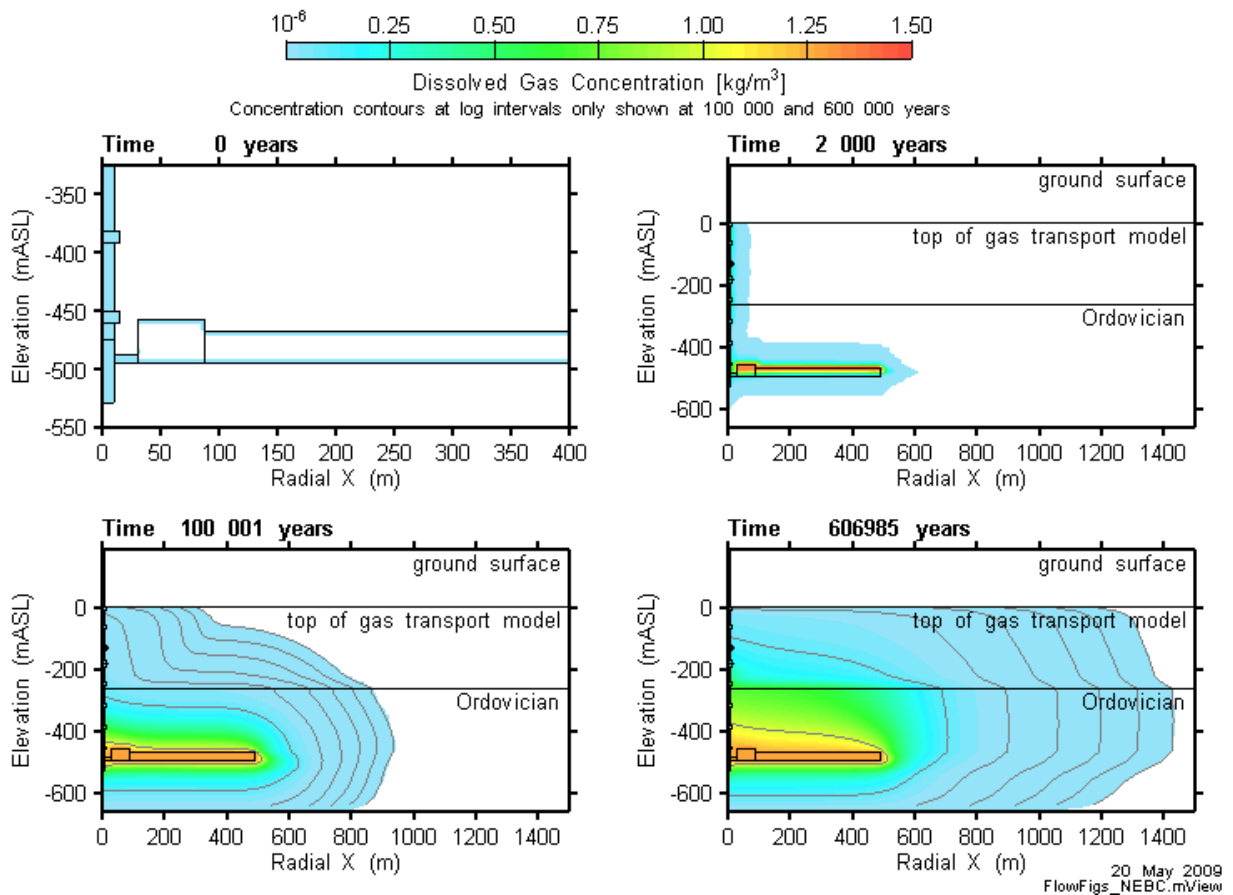


Figure 5-19: Dissolved gas concentrations at 0, 2000, 100 000 and 600 000 years for the NE-BC. Note the different radial X and elevation scale at 0 years.

5.2 CASE NE-GG1 – INCREASED RATES AND METAL INVENTORIES

The NE-GG2 case is only complete to 378 000 years, due to the same numeric issues with the TOUGH2 model encountered in the NE-BC.

5.2.1 Gas Generation

Case NE-GG1 differs from the base case in that higher metallic inventories and corresponding surface areas are used, and higher organic degradation and corrosion rates are used. The metal mass is increased by approx 27% compared to the base case to 7.3×10^7 kg and most corrosion rates are increased by an order of magnitude. The results show that more gas is produced more rapidly. The gas generation (and water consumption) rates are both an order of magnitude higher than the base case in the initial 1000 years (see Figure 5-20).

A higher peak gas pressure was observed, but this was only marginally higher (by 0.1 MPa) than the base case. (Figure 5-21). The reason for this is that the pressure was offset by two effects. The first is an increased flux of gas into the geosphere – particularly in the first 1000 years (see Figure 5-22). The second is the higher rate of water consumption and reduced ingress of water from the geosphere which together result in a lower peak saturation of approximately 0.25 (see Figure 5-23 and Figure 5-24).

There is a major qualitative difference between this case and the base case caused primarily by the rapid degradation of organic waste, and, in particular, the cellulosic wastes, which are degraded by approximately 3×10^3 years (see Figure 5-25). At this time, production of CO_2 ceases, and, since the CO_2 is being rapidly consumed by the microbial hydrogen mechanism it too is also exhausted. See the gas pressure plot, Figure 5-21. The microbial hydrogen mechanism is then limited by the amount of carbon dioxide being produced through organic degradation until such time all organic wastes are consumed. Since the initial organic waste inventory is small compared to the metallic waste inventory, the CO_2 is completely consumed first, leaving the final repository gas composition much richer in hydrogen than the base case.

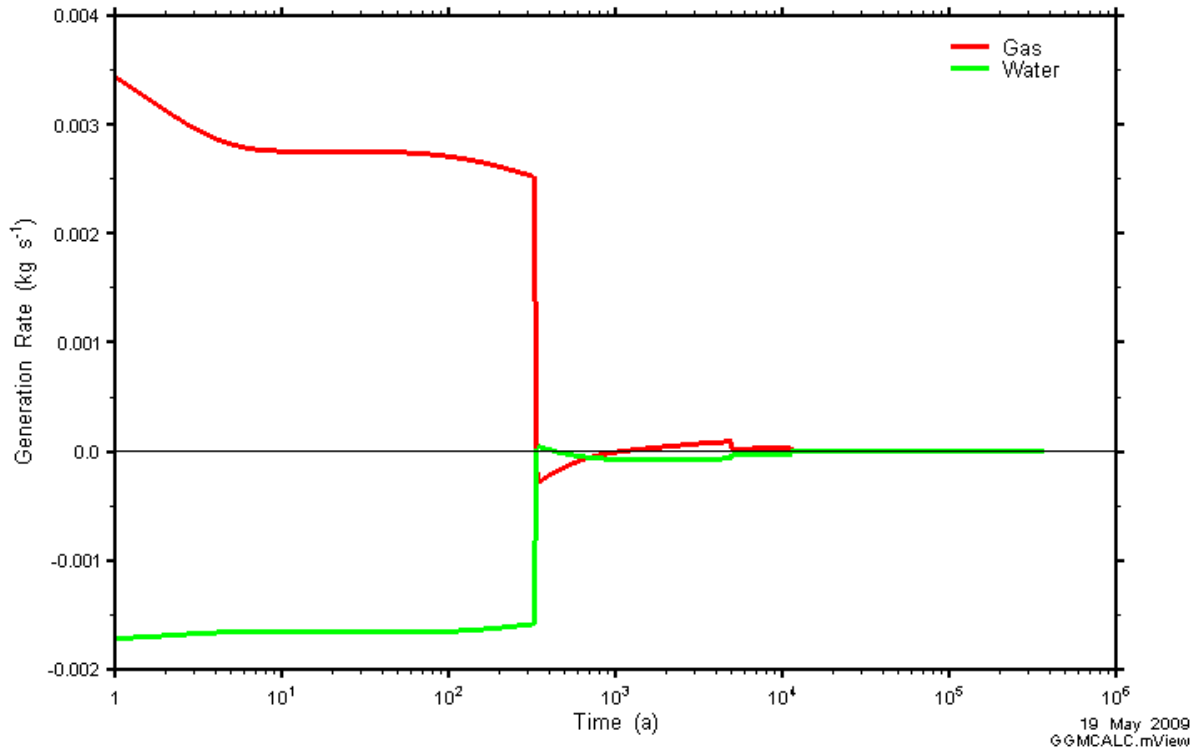


Figure 5-20: NE-GG1: Gas and Water Generation Rates

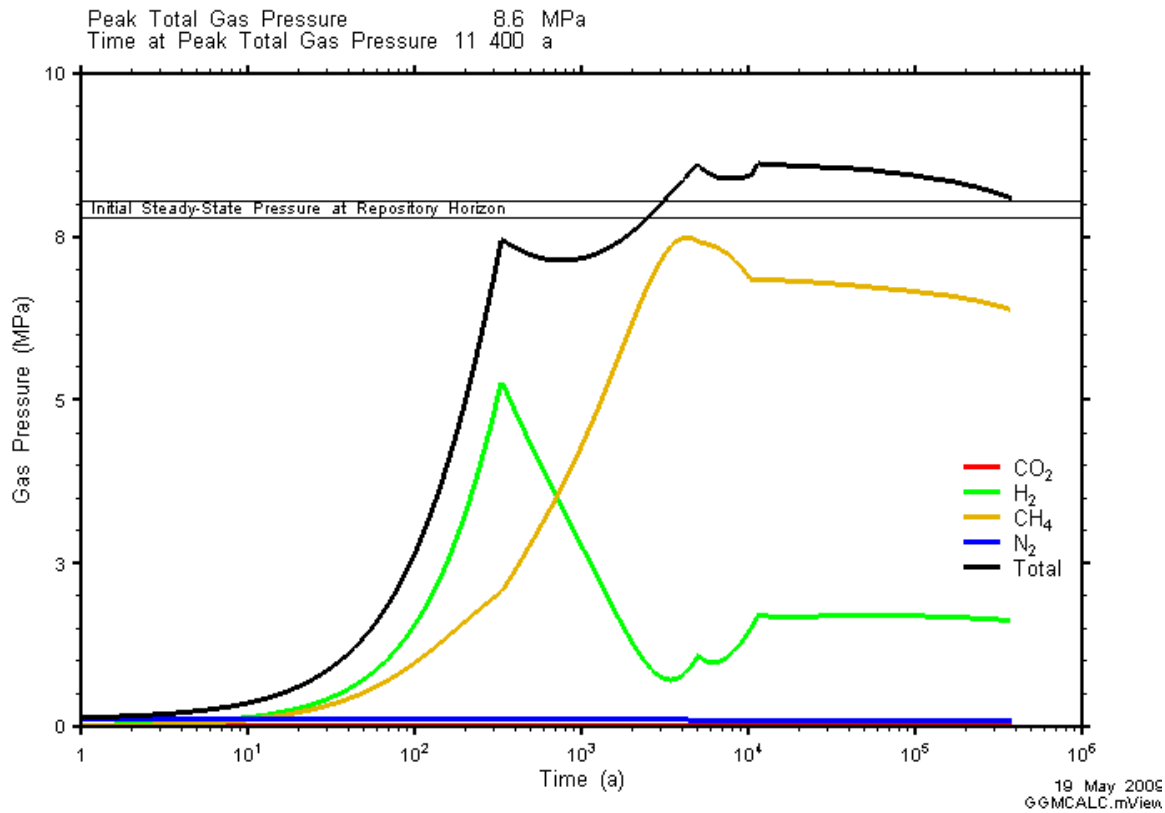


Figure 5-21: NE-GG1: Total and Partial Gas Pressures with the Repository

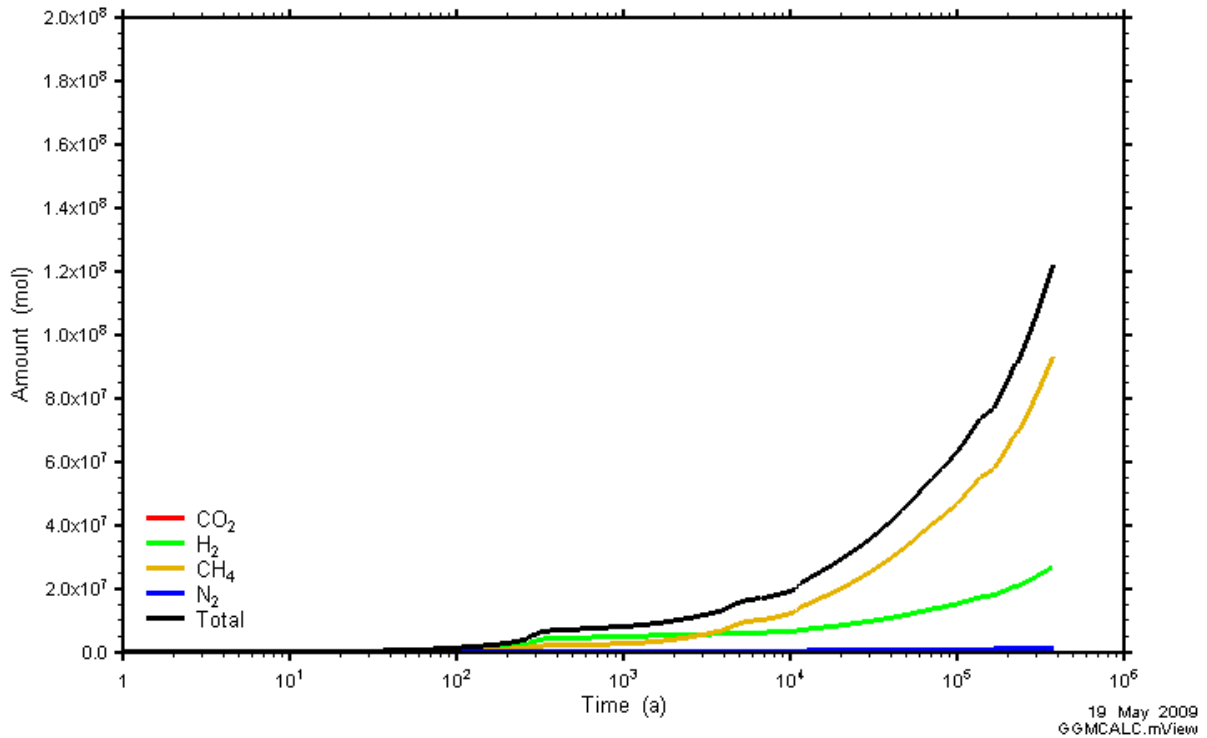


Figure 5-22: NE-GG1: Amounts of Gases which have Left the Repository

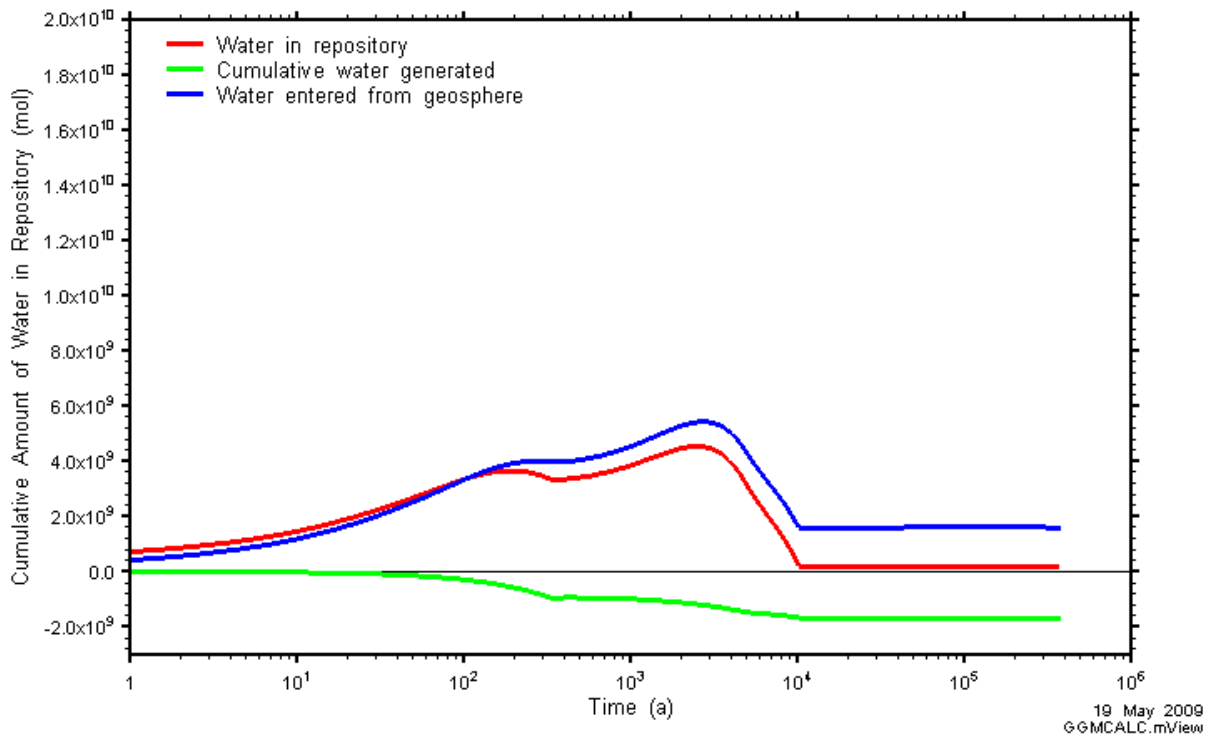


Figure 5-23: NE-GG1: Water Balance

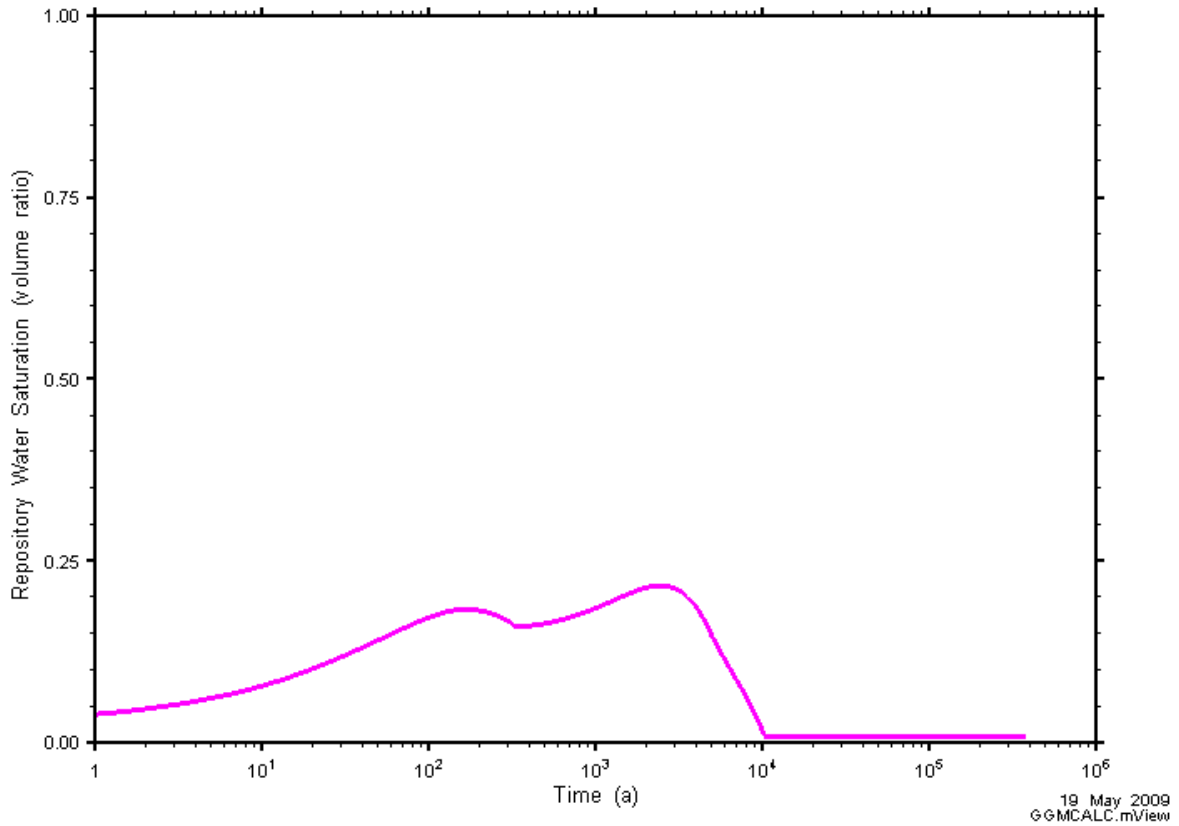


Figure 5-24: NE-GG1: Water Saturation

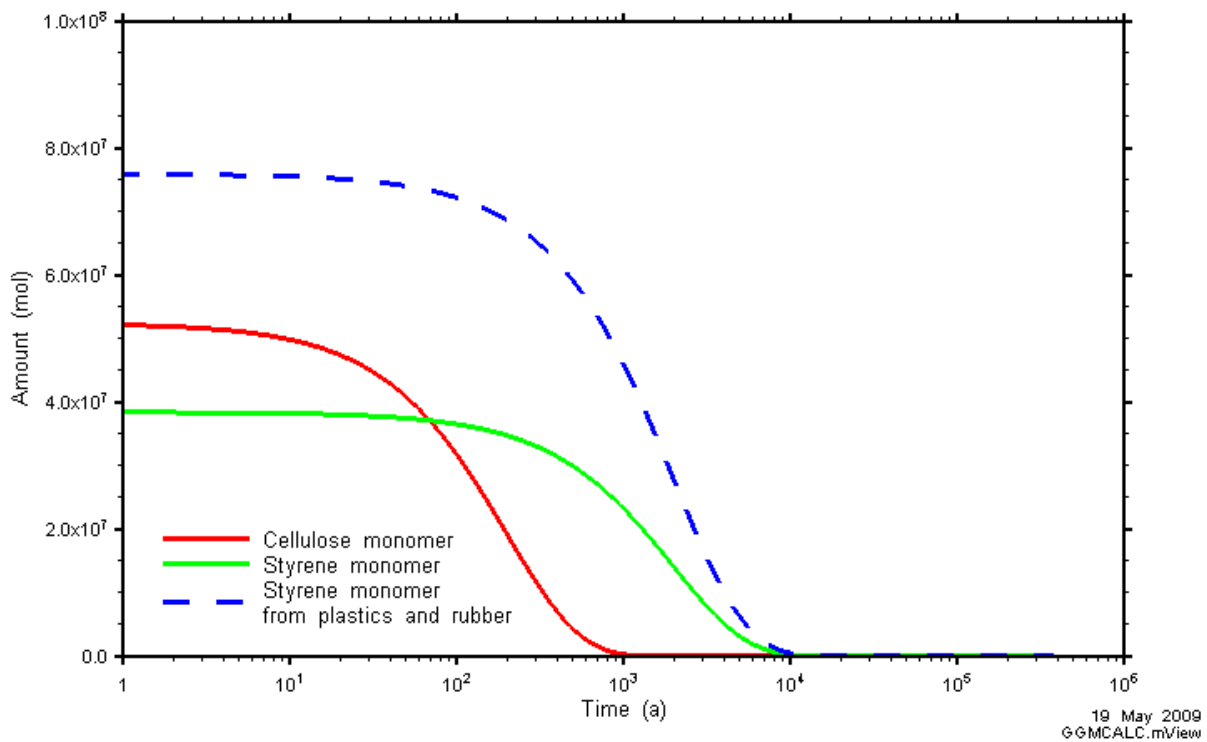


Figure 5-25: NE-GG1: Amounts of Organic Waste

5.2.2 Gas and Water Flows

The NE-GG1 case is based on the NE-BC, with increased metal inventory (specifically unpassivated carbon steel is increased to 3.8×10^7 kg from the NE-BC 2.8×10^7 kg) to study the effect of increasing gas generation. As in the NE-BC, no gas travels upwards through the ORD or SALF planes (except small amounts of initial gas in the shaft). The profiles of dissolved gas through the planes is similar to the NE-BC, except that dissolved gas flow rates and cumulative mass are greater, see Figure 5-26 and Figure 5-27.

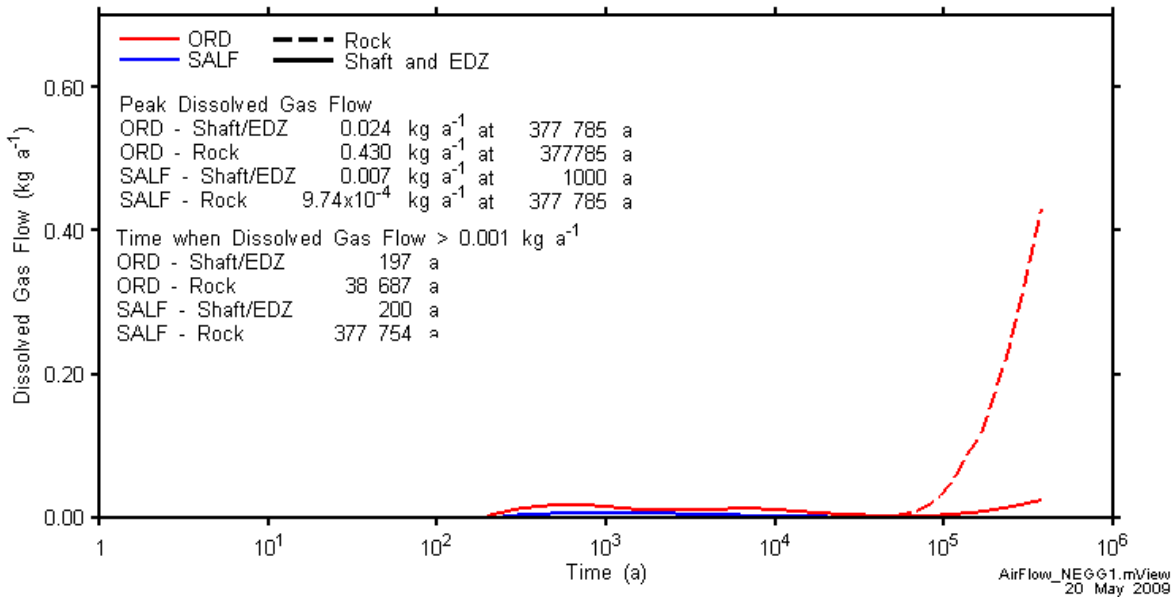


Figure 5-26: Dissolved gas flow rates across the ORD and SALF planes for the NE-GG1 case. Note different y-axis scale in comparison to the NE-BC.

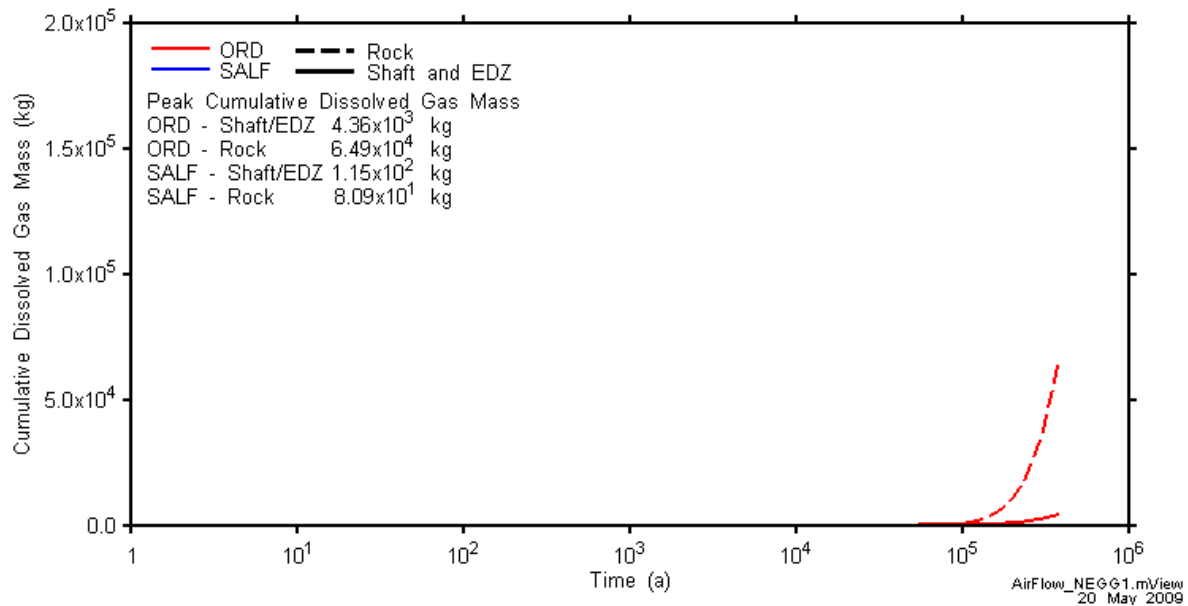


Figure 5-27: Cumulative dissolved gas mass crossing the ORD and SALF planes for the NE-GG1 case. Note different y-axis scale in comparison to the NE-BC.

5.2.2.1 Detailed Description of Gas and Water Transport

The different repository gas pressure profile is entirely attributed to the different gas generation rates. The greater repository gas pressure at earlier times prevents water from entering the repository in comparison to the NE-BC.

With less water saturation of the repository, the initial gas in shaft is slower to dissolve. In fact, early high pressures in the repository push gas out into the shaft, maintaining gas saturations in the shaft for a longer period of time in comparison to the NE-BC. Note that gas saturations in the shaft are limited to the repository horizon. At 1500 years, the connection of gas between the repository and shaft is broken, due to both a drop in repository gas pressure reducing gas migrating out into the shaft, and increased water saturation in the repository decreasing the area of connection between the ring tunnel and the monolith for gas migration towards the shaft. Gas saturations in the shaft dissolve by 3000 years, and as for the NE-BC, early peaks in dissolved gas flow across the ORD plane is the result of dissolved initial gases (see Figure 5-26). See Figure 5-28 and Figure 5-29 for gas saturations, repository water saturations, pressure and gas and water flows at the start of the simulation, 800 years, 1500 years and 3000 years.

Peak water saturation in the repository of 0.22 occurs at approximately 2500 years (see Figure 5-24). After this time, increasing repository pressures are greater than water pressure in the geosphere, causing water to be pushed out of the repository. By 11 000 years, no water is left in the repository, except for a small residual amount of water (water in the repository that is not mobile, less than 0.01 water saturation).

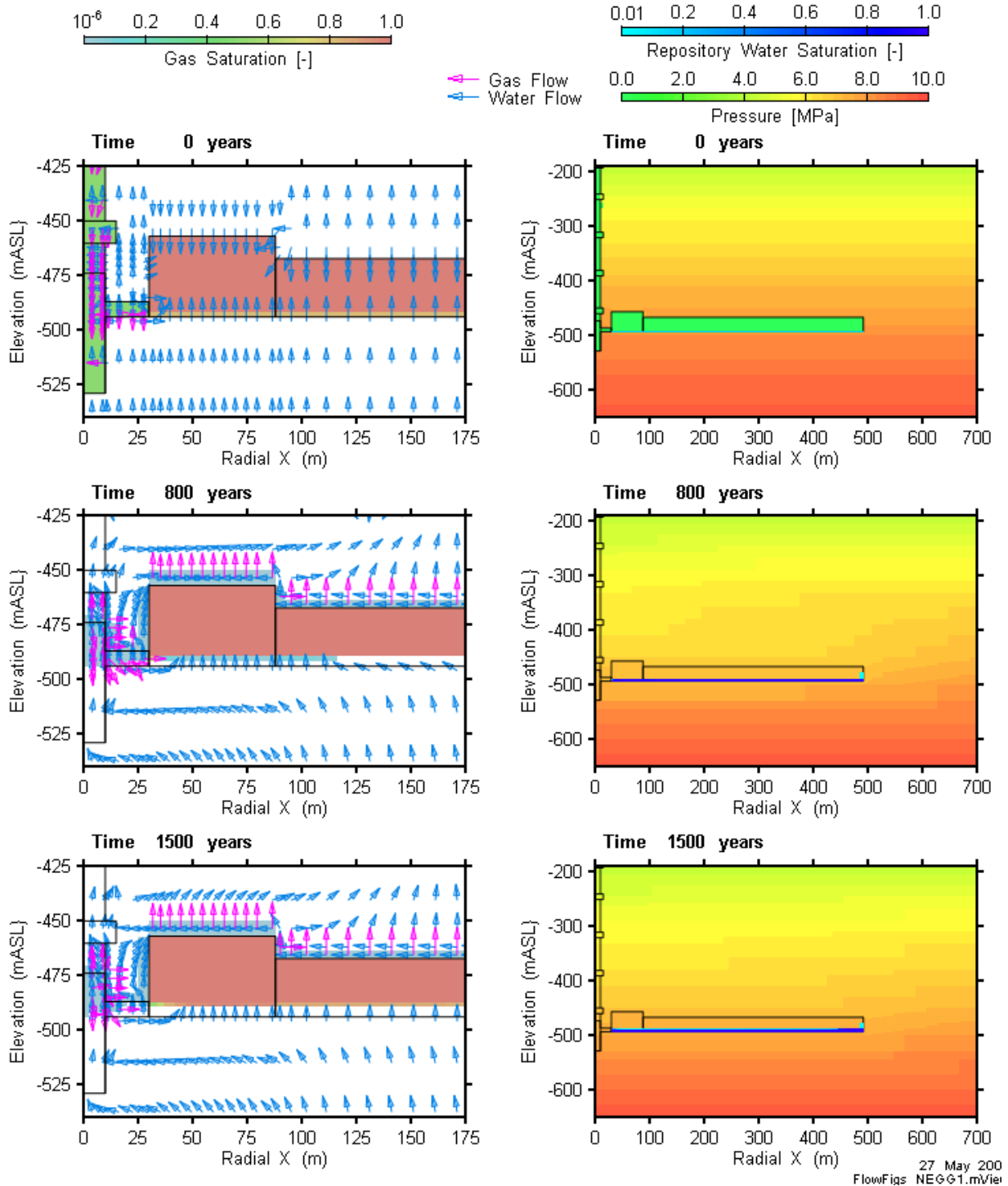


Figure 5-28: Evolution of conditions for the NE-GG1 case at the start of the simulation (0 years), 800 years, and 1500 years. Gas saturation, and gas and water flow (outside repository) are shown in the figures on the left, and pressure and repository water saturation in the figures on the right.

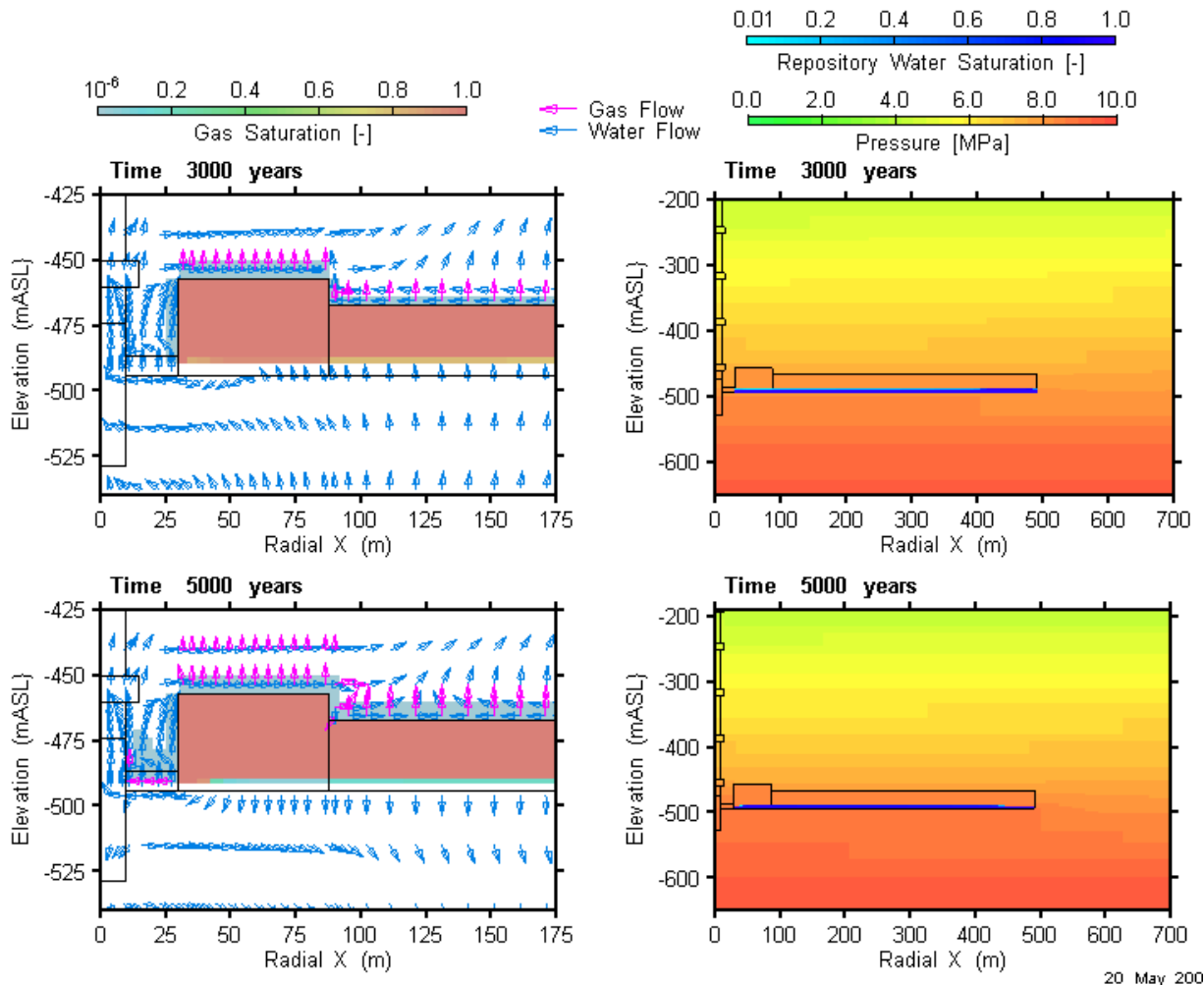


Figure 5-29: Evolution of conditions for the NE-GG1 case at 3000 years and 5000 years. Gas saturation, and gas and water flow (outside repository) are shown in the figures on the left, and pressure and repository water saturation in the figures on the right.

Gas begins to migrate towards the shaft at about 5000 years, when there are high repository gas pressures (only slightly less than peak pressure). Repository pressures decrease after 5000 years, due to reduced gas generation rates, before building to a peak repository pressure of 8.6 MPa at 11 000 years, the same time at which the repository is completely dry. Figure 5-29 shows gas saturations, repository water saturation, pressure and gas and water flows at 5000 years.

At 11 000 years, once the repository is completely dry, gas begins to migrate into the repository EDZ below the repository, and the rock mass farthest away from the shaft. Gas also migrates further into the shaft. Figure 5-30 shows gas saturations at 15 000 years, shortly after gas begins migrating into the rock mass.

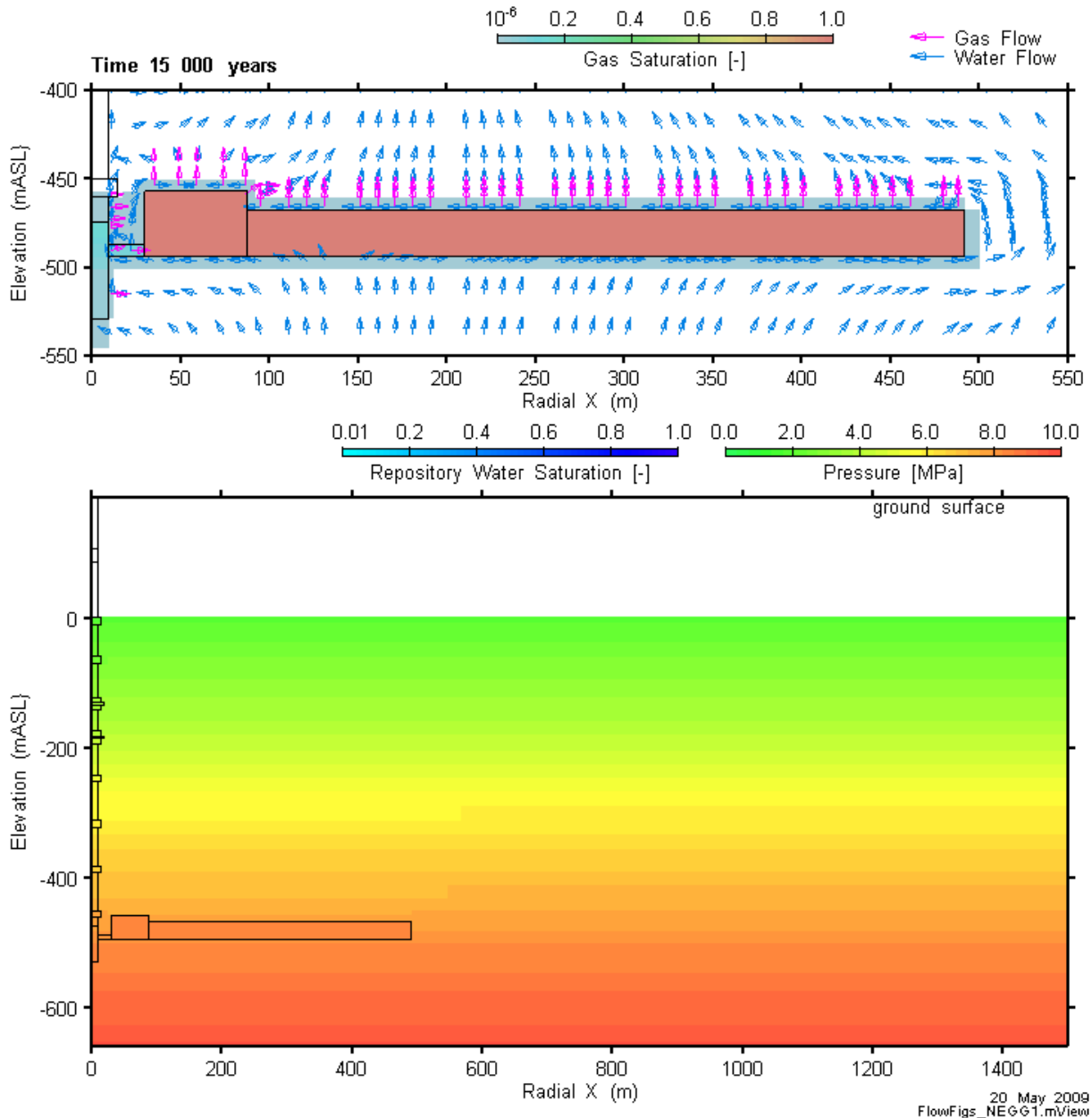
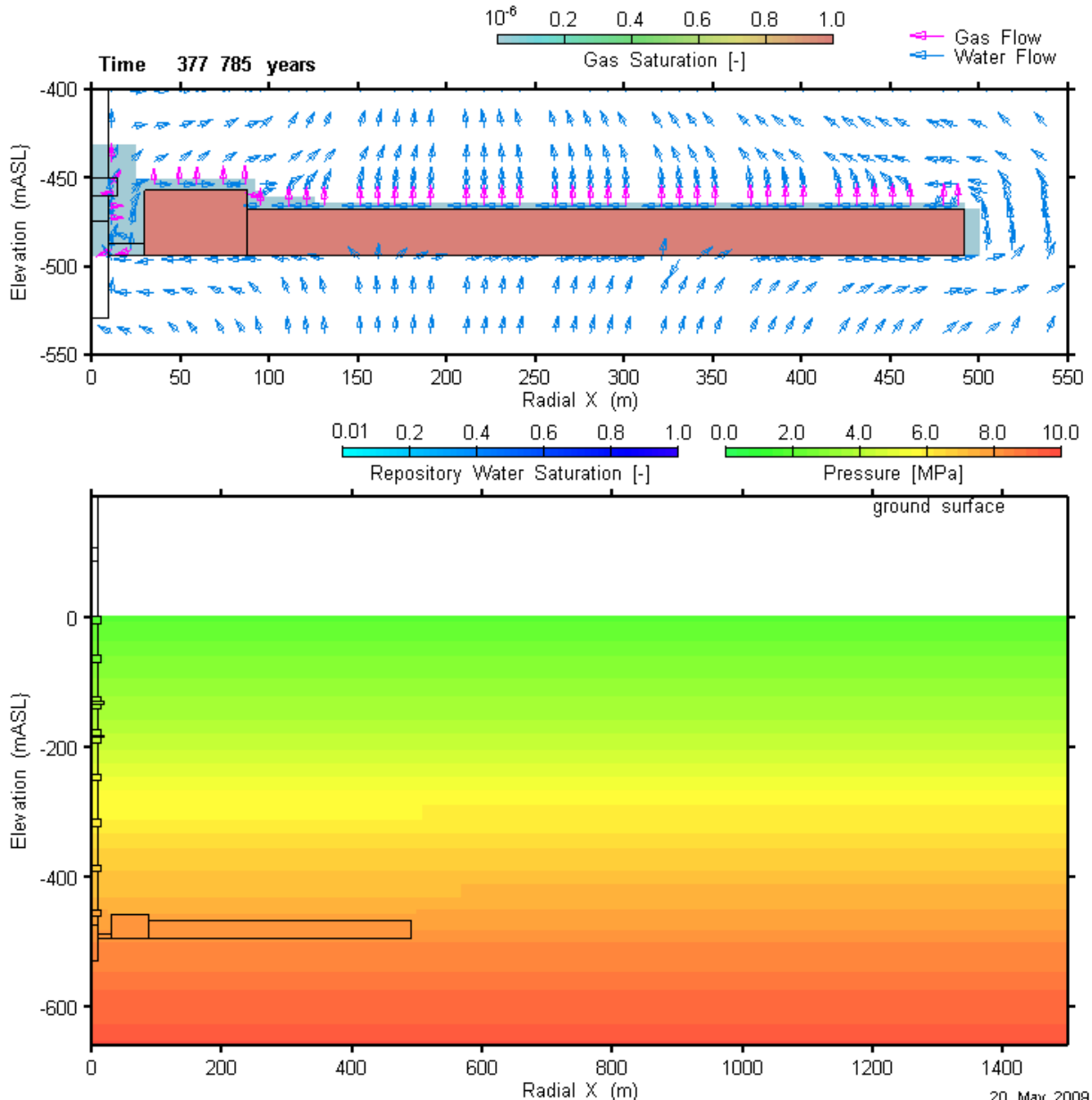


Figure 5-30: Evolution of conditions for the NE-GG1 case at 15 000 years. Gas saturation, and gas and water flows (outside repository) are shown in the figure above, and pressure saturation in the figure below. Note that there is no water saturation in the repository at this time.

Gas pressures begin to decrease after peak pressure, reaching 8 MPa at approximately 300 000 years. By the end of the simulation (378 000 years), only a small amount of gas migrates into the rock mass and shaft. Gas saturations greater than 10^{-6} do not occur in the shaft above -425 mASL by 300 000 years, and gas saturations in the rock above 10^{-6} only occur within a few metres from the repository. Figure 5-31 shows gas saturations and pressures at the end of the simulation, 378 000 years.



20 May 2009
FlowFigs_NE-GG1.mView

Figure 5-31: Evolution of conditions for NE-GG1 simulation at 500 000 years. Gas saturation, and gas and water flows (outside repository) are shown in the figure above, and pressure and repository water saturation in the figure below.

5.2.2.2 Detailed Description of Dissolved Gas Transport

Figure 5-32 shows the dissolved concentrations for the NE-GG1 case at 0, 2000, 100 000 and 378 000 years. Similar times as shown for the NE-BC were selected for comparison purposes only.

Dissolved gas concentrations are very similar to the NE-BC, which confirm the similar dissolved gas mass flow rates and cumulative mass.

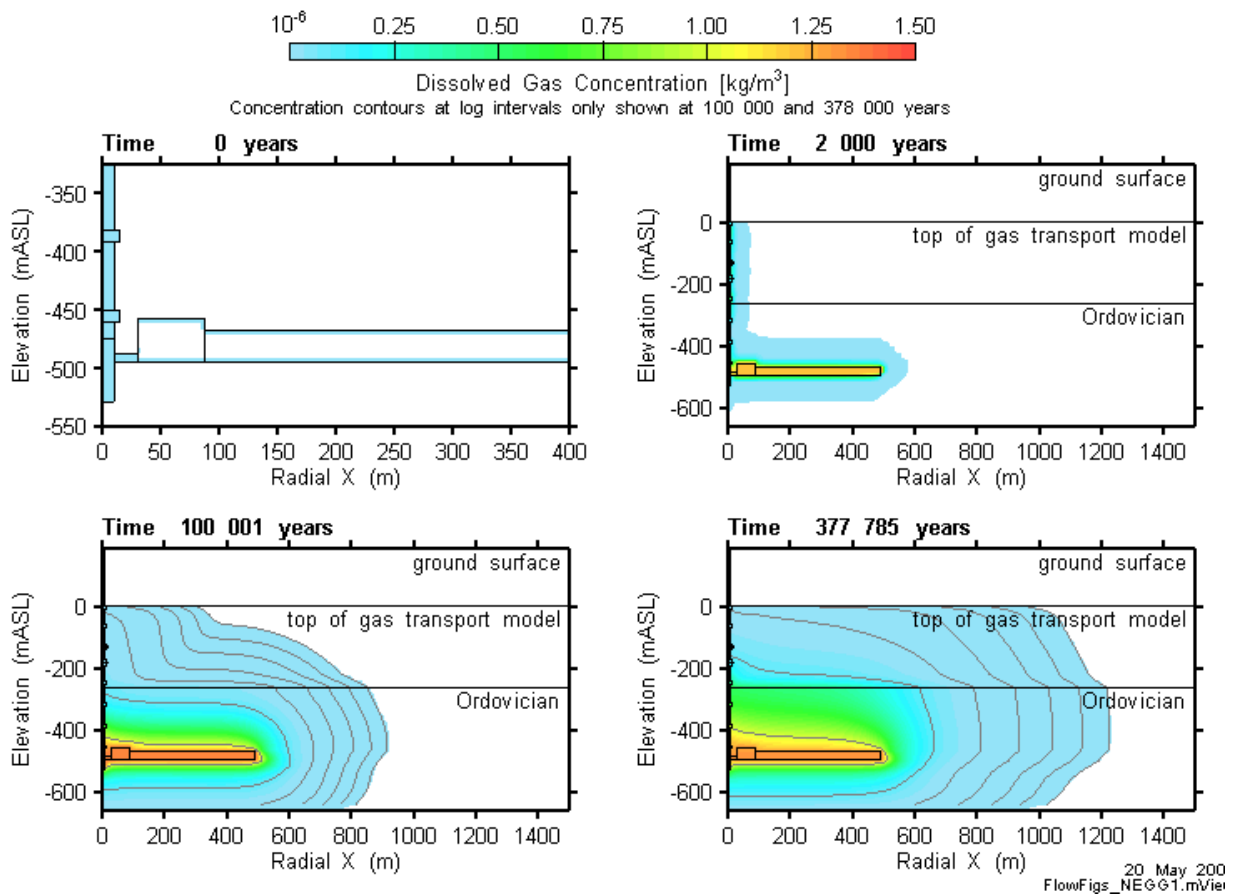


Figure 5-32: Dissolved gas concentrations at 0, 800, 45 000 and 378 000 years for the NE-GG1 case. Note the different radial X and elevation scale at 0 years.

5.3 CASE NE-GG2 – REDUCED ORGANIC DEGRADATION AND HYDROGEN CONSUMPTION RATES

The NE-GG2 case is only complete to 585 000 years, due to the same numeric issues with the TOUGH2 model encountered in the NE-BC.

5.3.1 Gas Generation

Case NE-GG2 differs from the base case in that lower organic degradation and hydrogen consumption rates are used. This corresponds to a scenario in which methanogens are present but not as active within the repository as in the base case – for example, due to the high salinity of the groundwaters. The results are qualitatively quite different to the base case. There is a higher peak gas pressure and the dominant gas is different throughout the simulation as described below.

The complete degradation of the organic wastes can be seen to take a factor of 10 longer than for the base case (see Figure 5-33). The slower degradation results in slower production of CO₂. Thus there is less CO₂ available for the hydrogen consuming methane generation reaction, which is also proceeding at a slower rate than for the base case. This results in hydrogen, rather than methane being the dominant gas in the repository until it is completely consumed at approximately 3 x 10⁵ years. This coincides with the time that the metallic wastes are completely corroded. At this point there is no mechanism for the production of hydrogen, but organic degradation continues to produce carbon dioxide.

The slower microbial hydrogen consuming reaction also results in a larger total number of moles of gas in the system until such time that this reaction has converted all available hydrogen and carbon dioxide to methane, explaining the larger peak pressure of 8.8 MPa at 2 x 10³ years compared to the NE-UG-BC case.

Another effect of the slower degradation rates and slower production of CO₂ is that the partial pressure of CO₂ is lower during the first 10⁵ years when both the carbon and galvanised steels and stainless steels and nickel based alloys are present. As a result, enhanced carbon dioxide corrosion has a weaker effect and less iron ultimately ends up in the form of siderite (see Figure 5-34).

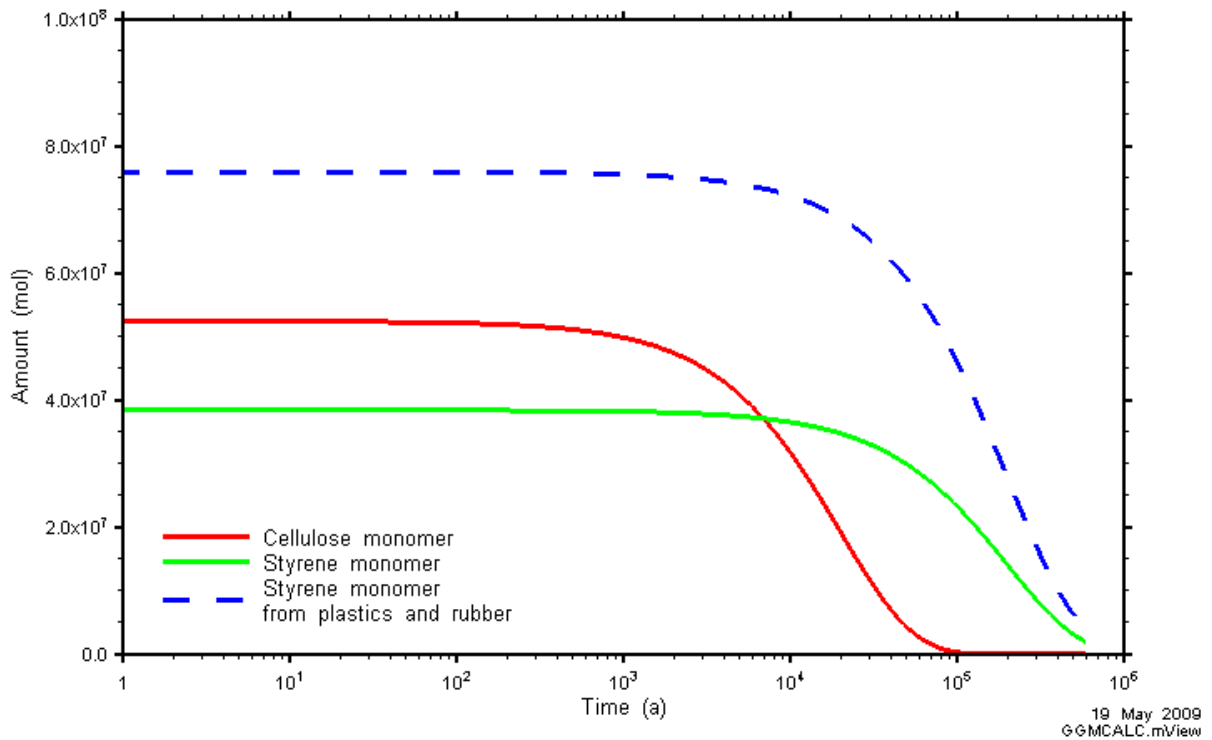


Figure 5-33: NE-GG2: Amounts of Organic Waste

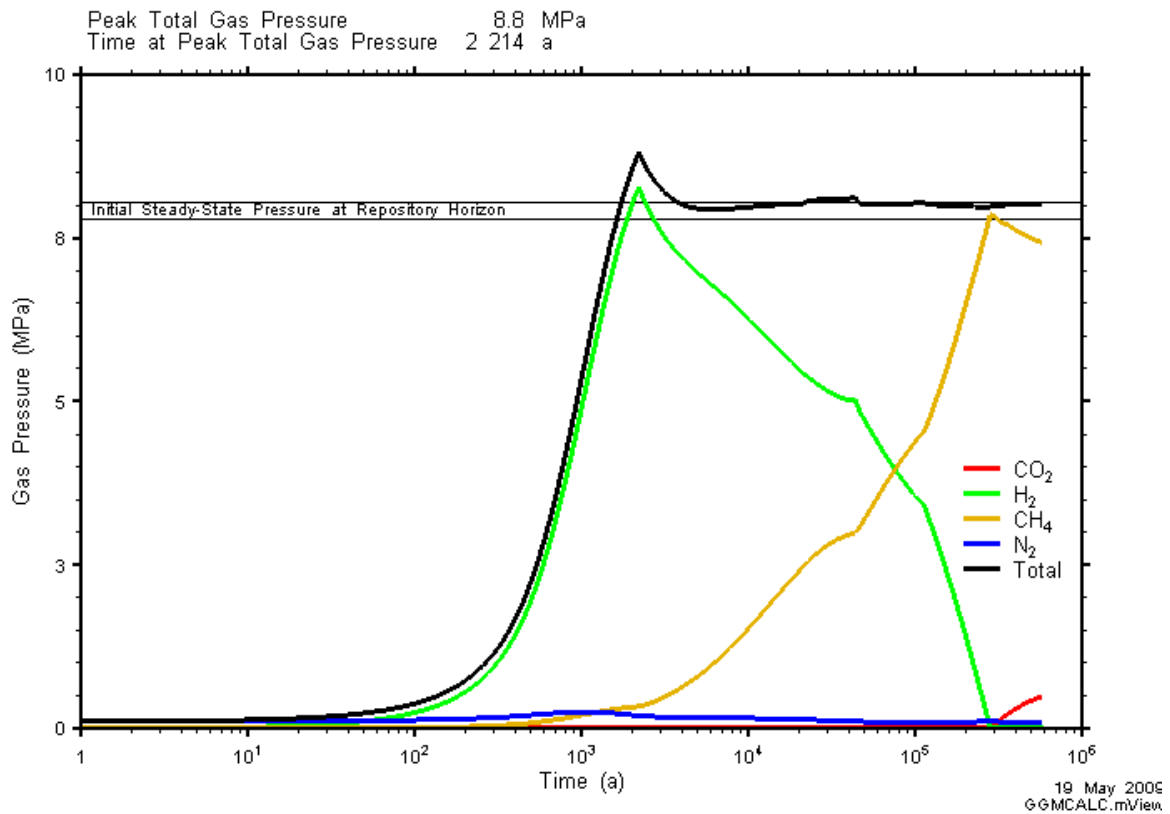


Figure 5-34: NE-GG2: Total and Partial Gas Pressures with the Repository

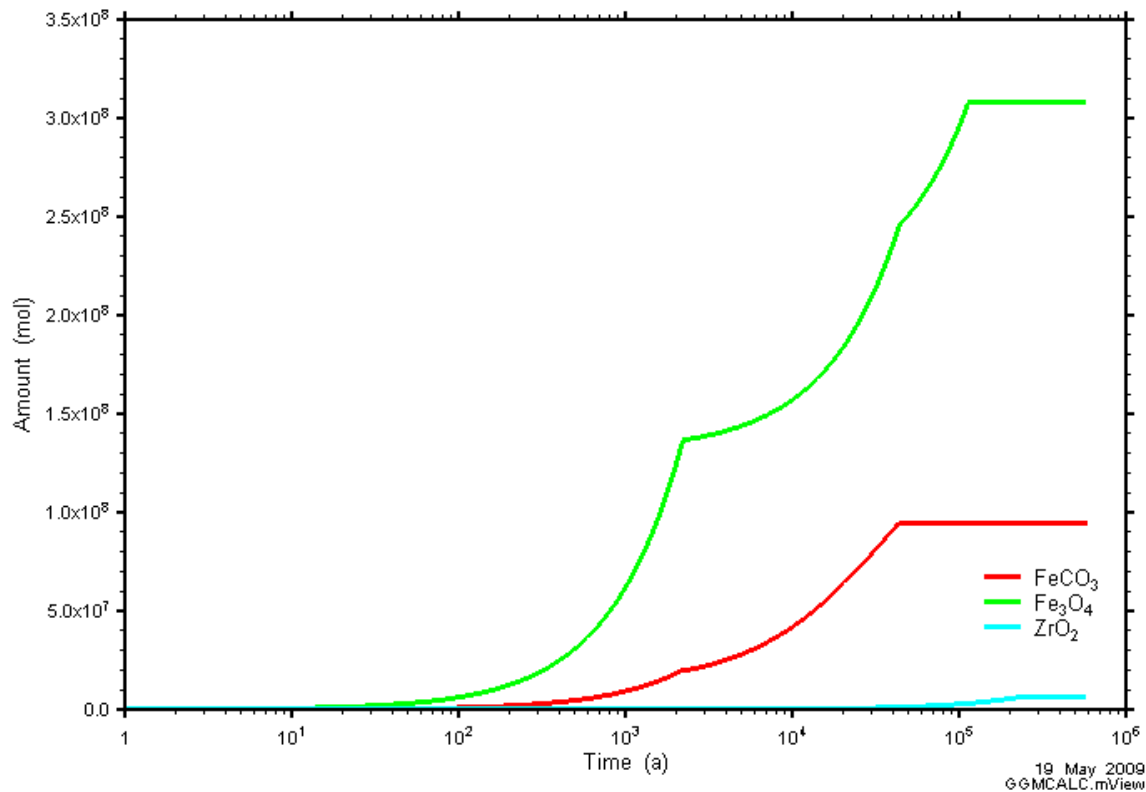


Figure 5-35: NE-GG2: Amounts of Corrosion Products

5.3.2 Gas and Water Flows

The NE-GG2 case is based on the NE-BC, with decreased degradation rates and a lower hydrogen consumption rate, consistent with (for example) reduced microbial activity. Low degradation rates provided different gas generation rates, which are more uniform and without any gas consumption or water generation (due to less CO₂ available for the hydrogen consuming methane generation) after the peak repository pressure. These differences have some minor impact on results:

- A slightly greater peak repository pressure of 8.8 MPa at a slightly later time of 2200 years (see Figure 5-34), and a smaller decrease in repository pressure after the peak, in comparison to the NE-BC.
- Compared to the NE-BC, slightly less repository water saturation of 0.66 at 1200 years.
- Dissolved gas flow rates and cumulative gas mass across the ORD and SALF planes are very similar as shown in Figure 5-36 and Figure 5-37. As for the NE-BC, early peaks in dissolved gas flow across the ORD plane is the result of dissolved initial gases.

Overall, the differences of the NE-GG2 case compared to the NE-BC have minimal impact on the flow of gas and water in the geosphere. As results are very similar to the NE-BC, further description of the flow of gas and water is not provided.

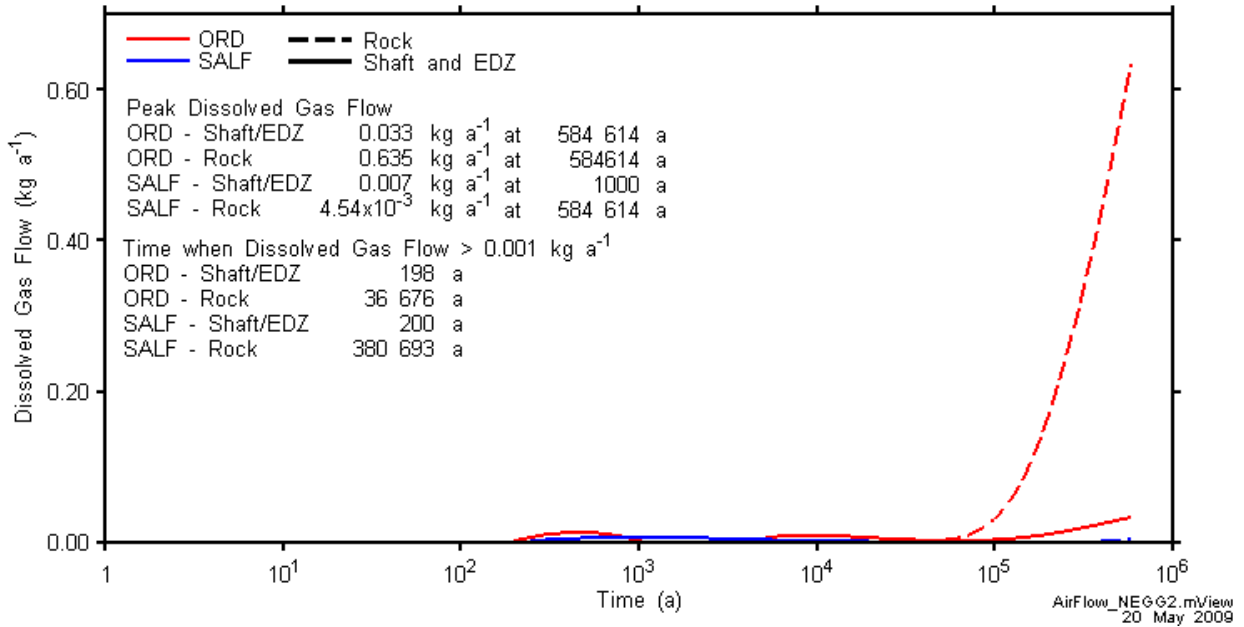


Figure 5-36: Dissolved gas flow rates across the ORD and SALF planes for the GG2 case.

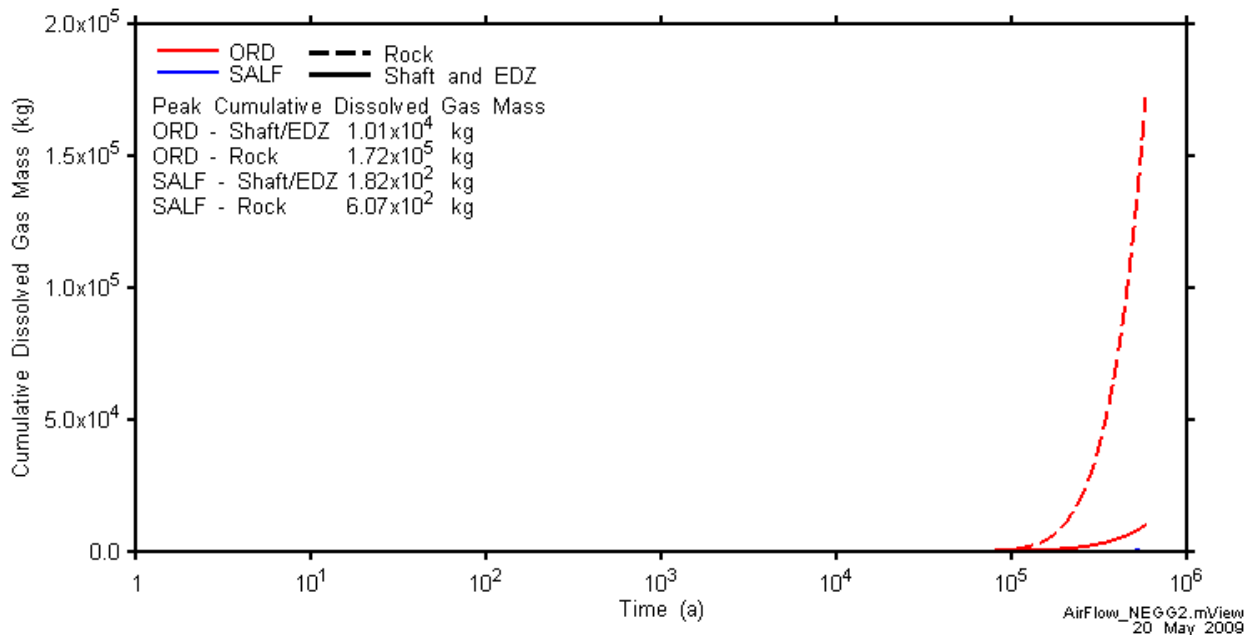


Figure 5-37: Cumulative dissolved gas mass crossing the ORD and SALF planes for the GG2 case.

5.4 CASE NE-EDZ – HIGH PERMEABILITY EDZ

5.4.1 Gas Generation

The NE-EDZ case considers base case gas generation but high permeabilities in the shaft EDZ. As a result, we might expect more rapid water ingress and expulsion within the repository. This is broadly what is observed.

Figure 5-38, Figure 5-39, and Figure 5-40, and show the water balance and saturation for this case. The main differences compared to the base case are: a higher initial peak in saturation, (under 0.75 for the base case and over 0.75 for this case); the plateauing of the saturation profile at approx 2×10^4 years and the onset of resaturation at 10^5 years. Water resaturates slowly from 10^5 years to the end of assessment period of 1 million years (note the log time scale).

While the overall water saturation of the repository is slow, a large amount of water enters the repository from the rock mass below the repository, and is pushed out of the repository into the permeable EDZ. By the end of the simulation, the total cumulative mass of water that has entered through the rock and exited through the permeable EDZ is approximately 2×10^{11} mol. Figure 5-39 shows the breakdown of these inflows and outflows.

The plateauing of the saturation profile at 2×10^4 years coincides with a sudden increase in the flux of gas out of the repository (Figure 5-41). This is caused by the creation of a connection between the repository and the EDZ above the concrete monolith, which relieves the repository gas pressure and halts water expulsion. Despite the larger saturation at the time of the peak pressure, the peak gas pressure within the repository is actually slightly lower than for the base case (8.3 MPa) due to the extra flux of gas out of the repository (Figure 5-42).

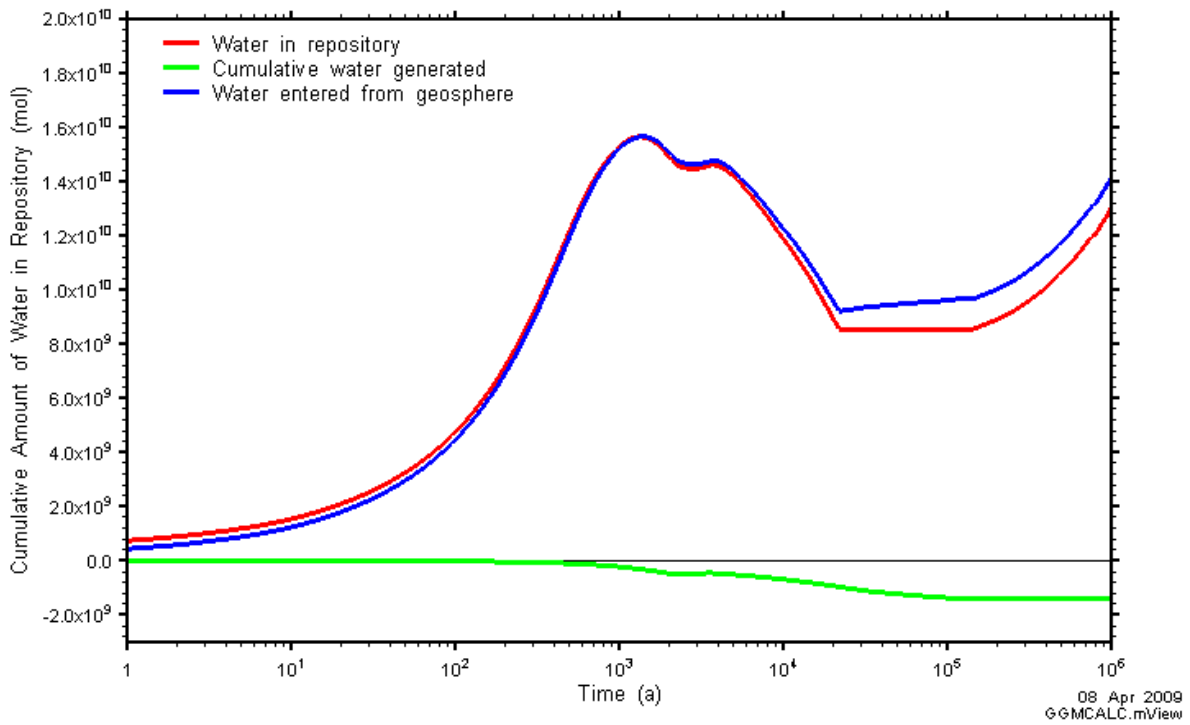


Figure 5-38: NE-EDZ: Water Balance

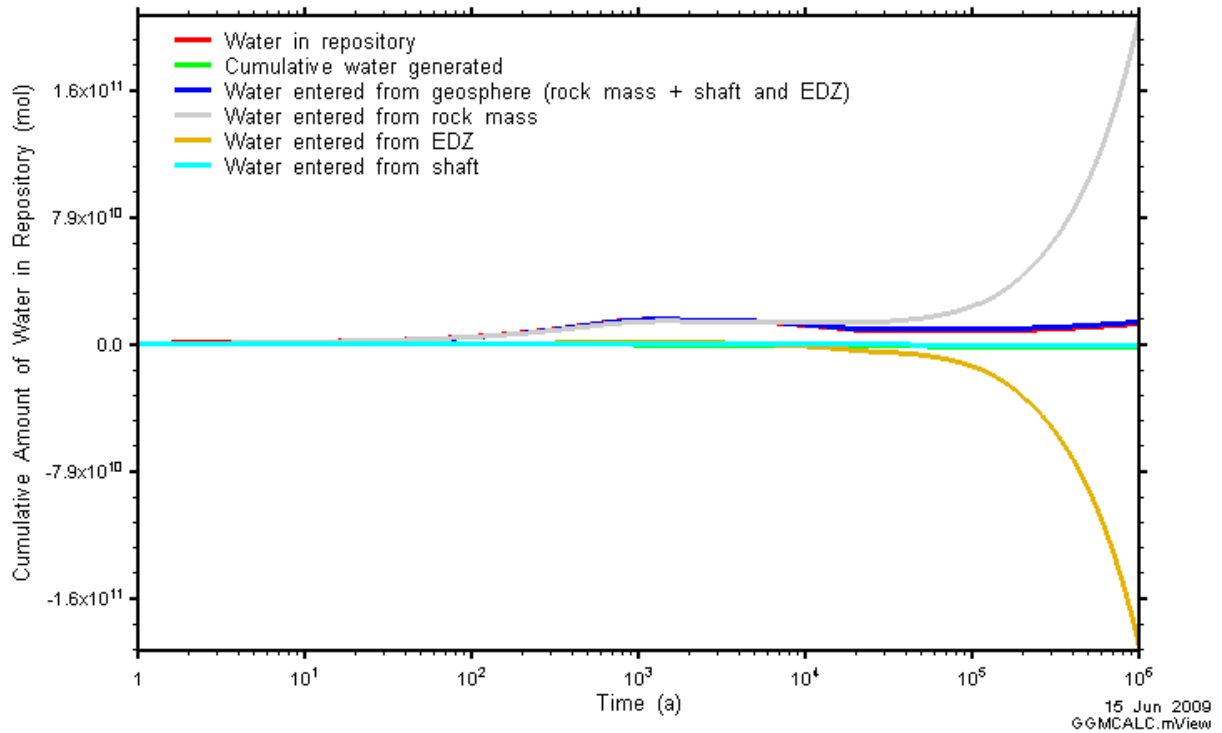


Figure 5-39: NE-EDZ: Water Balance - separate shaft/EDZ and rock mass flows.

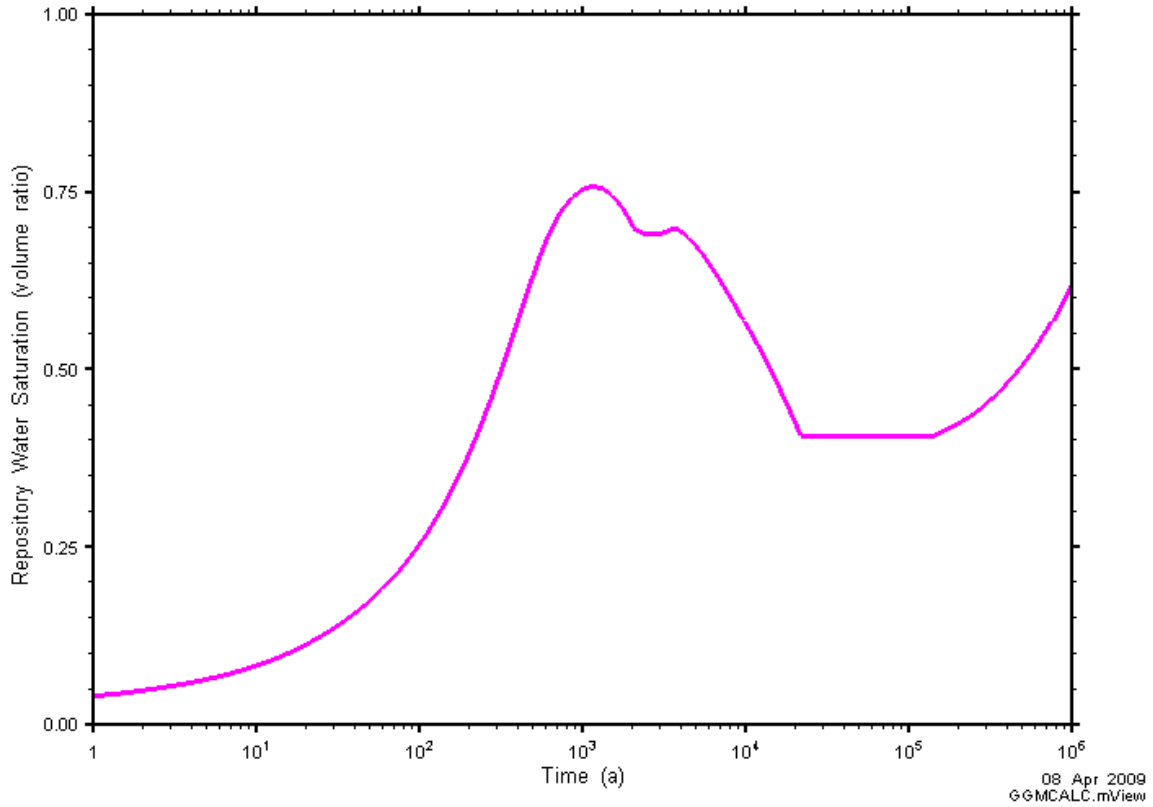


Figure 5-40: NE-EDZ: Water saturation

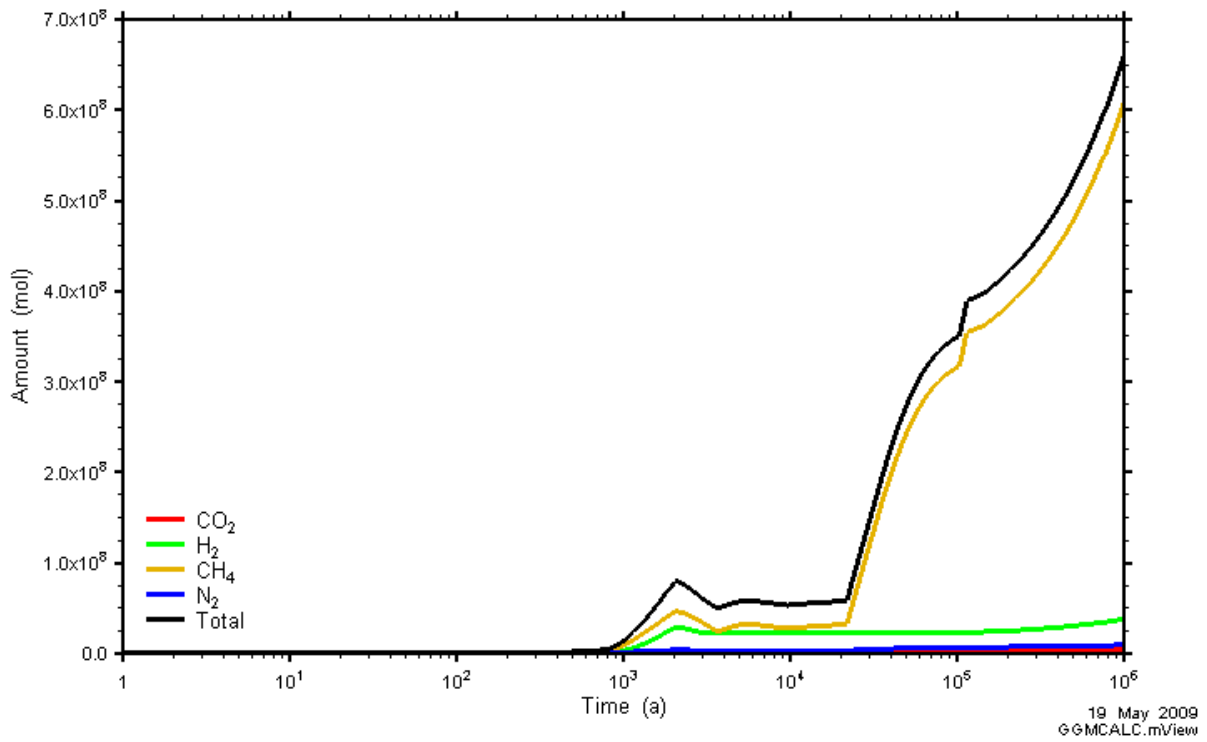


Figure 5-41: NE-EDZ: Amounts of Gases which have Left the Repository

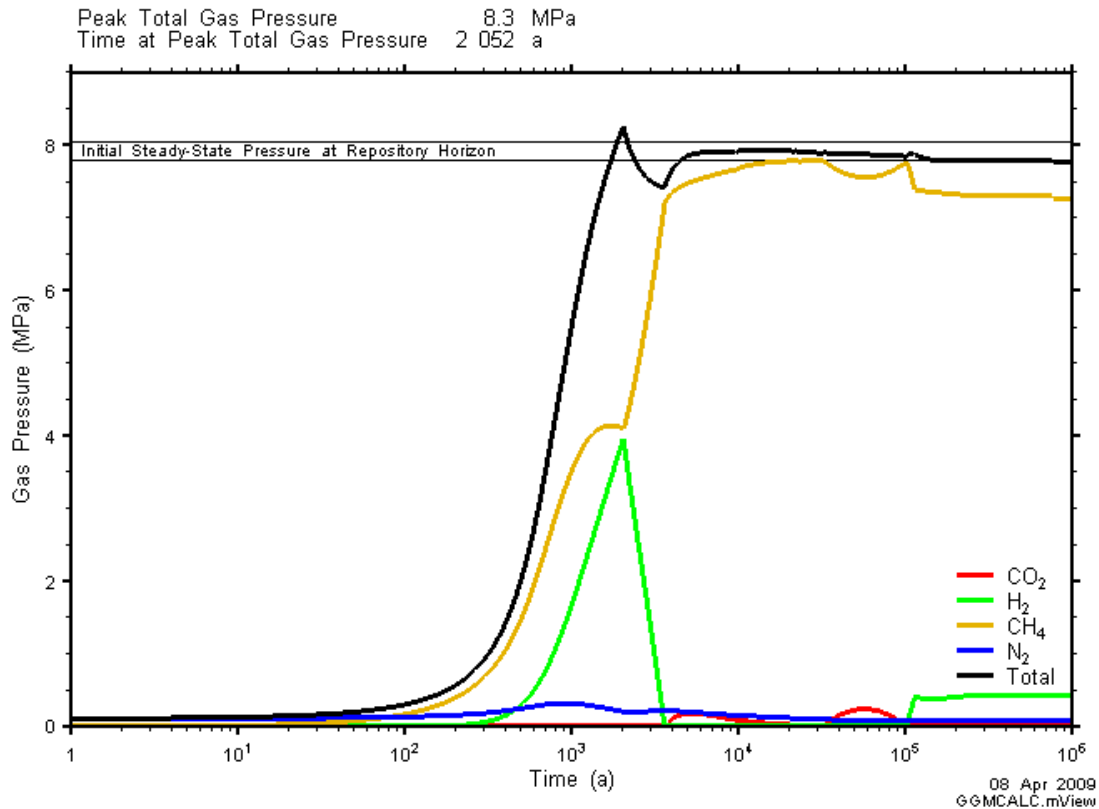


Figure 5-42: NE-EDZ: Total and Partial Gas Pressures with the Repository

5.4.2 Gas and Water Flows

The NE-EDZ case simulates a relatively (in comparison to the NE-BC) permeable shaft, due to higher permeabilities in the inner and outer shaft EDZ. Also, concrete bulkheads and asphalt waterstops do not intersect the shaft EDZ, to simulate the generation of EDZ around these features. Inner EDZ permeabilities are four orders of magnitude greater than the rock mass, and outer EDZ permeabilities are two orders of magnitude greater than the rock mass. Air-entry pressures in the EDZ are decreased consistent with the increased EDZ permeability.

Unlike the NE-BC, gas flows across the ORD and SALF planes within the shaft. As well, dissolved gas flow rates and cumulative mass across both planes are much greater than in the NE-BC. Figure 5-43 and Figure 5-44 show the gas flow rates and cumulative gas mass, respectively. All of the gas release from the repository is via the shaft/EDZ and most of dissolved gas is also released via the shaft/EDZ. Note that the total gas mass crossing the SALF plane is greater than the total gas mass crossing the ORD plane. While this seems intuitively incorrect, it is due to the dissolution of gas in the shaft, where gas that has dissolved in groundwater at depth (below the ORD plane) comes out of solution as gas within the shaft above the ORD plane (see discussion below). The mass balance of gas is correct, as the total amount of gas and dissolved gas crossing the ORD plane is greater than the total amount crossing the SALF plane.

The flow of gas and water will be discussed in detail in the sections below.

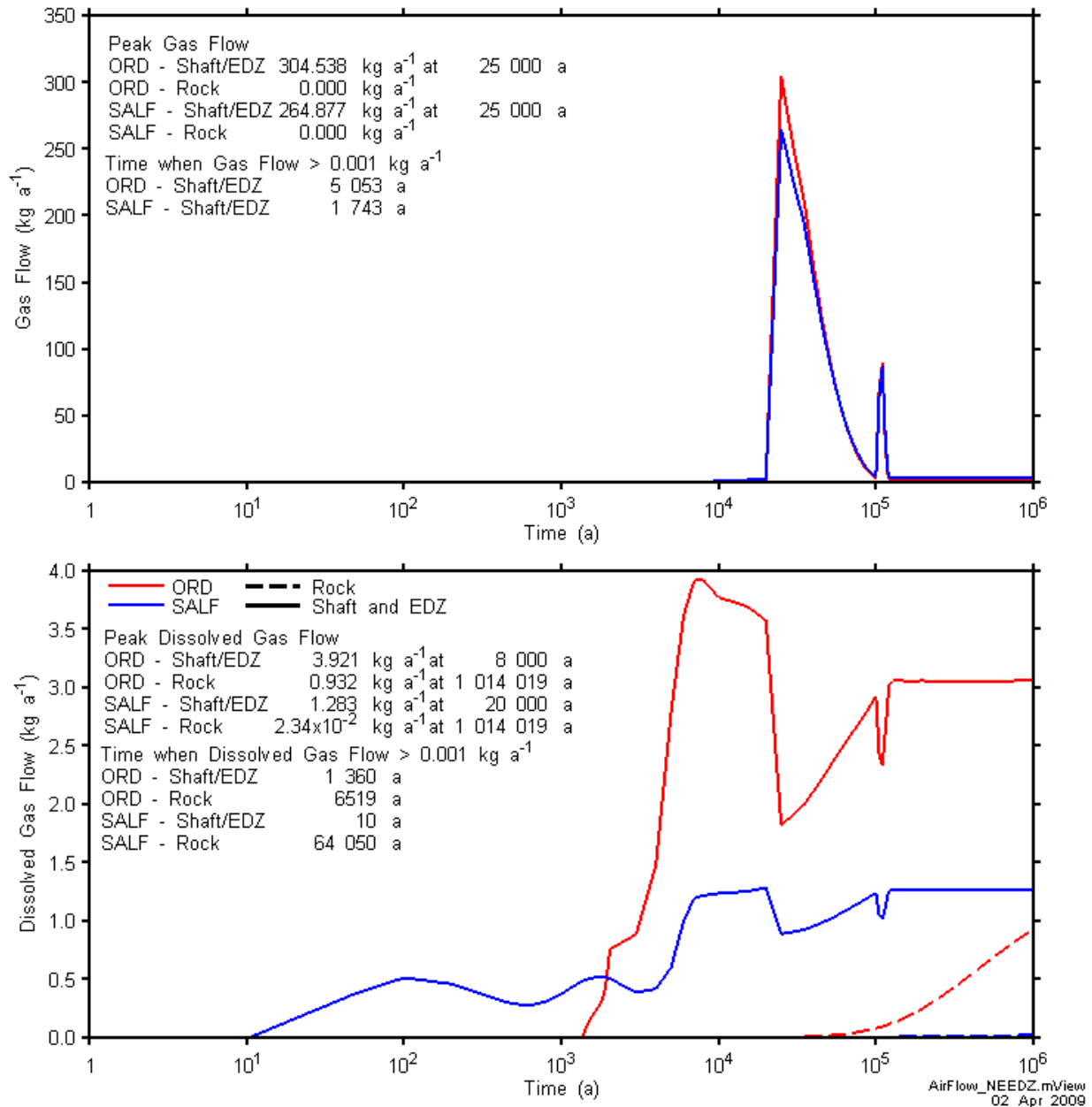


Figure 5-43: Gas flow rates across the ORD and SALF planes for the NE-EDZ case (top: gas, bottom: dissolved gas).

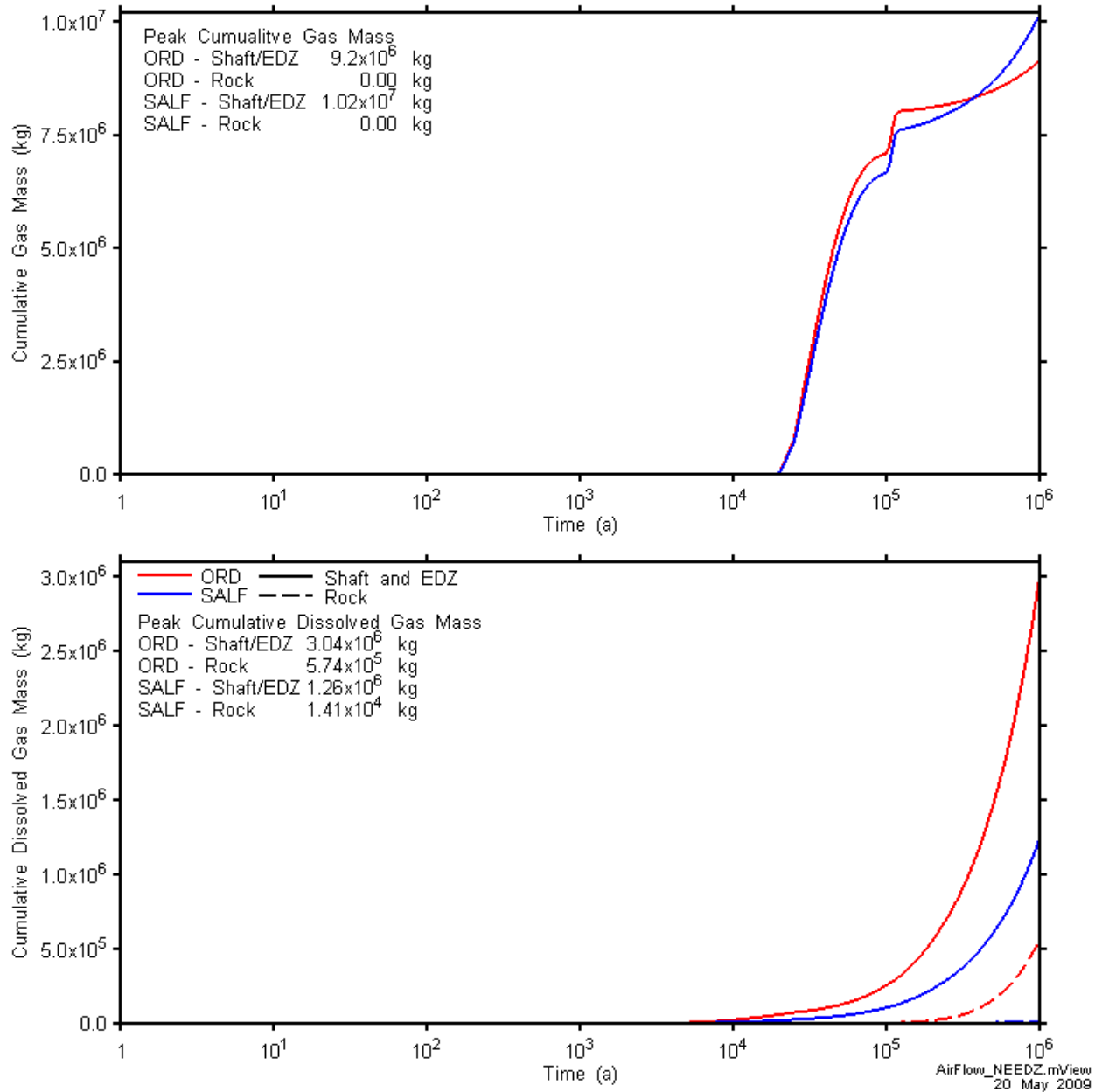


Figure 5-44: Cumulative gas mass crossing the ORD and SALF planes for the NE-EDZ case (top: gas, bottom: dissolved gas)

5.4.2.1 Detailed Description of Gas and Water Transport

While repository performance is nearly identical between the NE-EDZ case and NE-BC for the first 22 000 years, the high permeabilities of the EDZ impact transport of gas within the shaft and the rock mass:

- Resaturation of the shaft occurs more quickly than in the NE-BC, with the shaft in the vicinity of the repository fully saturated with water by 500 years, and the complete shaft fully saturated with water by 1700 years.
- Gas migrates into the rock above the repository EDZ by 1000 years.
- As shown in Figure 5-40, the initial water saturation profile (before 22 000 years) is very similar to the NE-BC, with a peak water saturation of 0.76 at 1200 years.
- As pressure in the repository builds, water is expelled out the repository. Unlike the NE-BC, where water is primarily expelled into the rock below the repository, in this case, water is expelled primarily out into the highly permeable shaft EDZ.
- Peak gas pressure is slightly less, at 8.3 MPa, at roughly the same time of 2100 years, see Figure 5-42.
- At 6 000 years, dissolved gas comes out of solution within the shaft EDZ. Dissolved gas from the repository is transported up the shaft, and as the dissolved gas reaches sufficient concentration at the lower pressures at the top of the shaft, gas comes out of solution. Gas comes out of solution according to Henry's law, i.e., after the partial pressure of gas ($=$ dissolved gas molar concentration / Henry's constant), is greater than the water pressure, a gas phase is created. Dissolution of dissolved gases in the NE-EDZ case is due to the greater dissolved gas concentrations in the EDZ near the top of the shaft, compared to the NE-BC, which is a result of the high permeabilities of the shaft EDZ.
- By 15 000 years, the gas saturations at the top of the repository connect to the gas saturations in the shaft, providing a pathway for gas to travel from the repository up the shaft and up to the top of the model.

Figure 5-45 and Figure 5-46 show the gas saturation, gas and water flows, repository water saturation and pressure at 0, 500, 1000, 10 000 and 15 000 years.

At 22 000 years, sufficient water has been pushed out of the repository to allow gas to migrate through the repository EDZ above the concrete monolith and into the shaft EDZ. This creates a permeable pathway along the EDZ from the repository, due to the high permeabilities of the EDZ in this case, to the top of the model, with the following effects:

- A pulse of gas migrating through the shaft EDZ, as evidenced by the peak gas flow rates through the ORD and SALF plane peak at this point (see Figure 5-43).
- As the pulse of gas migrates up through the shaft EDZ, gas is pushed out into the rock mass of the permeable SDB2R (Guelph and Salina A0) unit, see Figure 5-47. This is encouraged by the high permeabilities of the SDB2 rock, relative to the low EDZ permeabilities of the SA1R above the SDB2.
- Water is prevented from being pushed out of the repository, as gas pressure is relieved through gas migration into the shaft EDZ. This results in an unchanging water saturation profile (see Figure 5-40) from 22 000 years to 120 000 years.

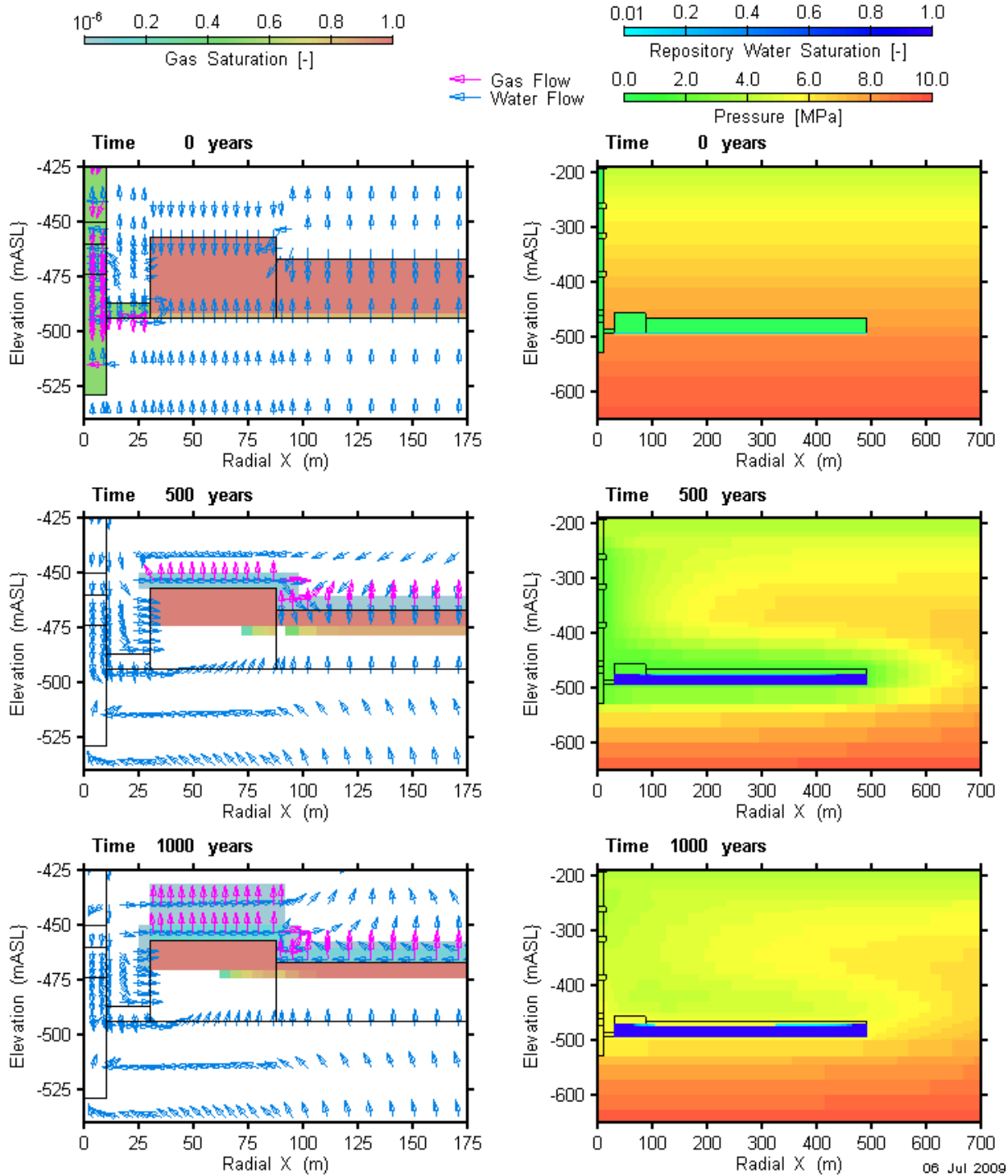


Figure 5-45: Evolution of conditions for the NE-EDZ case at the start of the simulation (0 years), 500 years, and 1000 years. Gas saturation, and gas and water flow (outside repository) are shown in the figures on the left, and pressure and repository water saturation in the figures on the right.

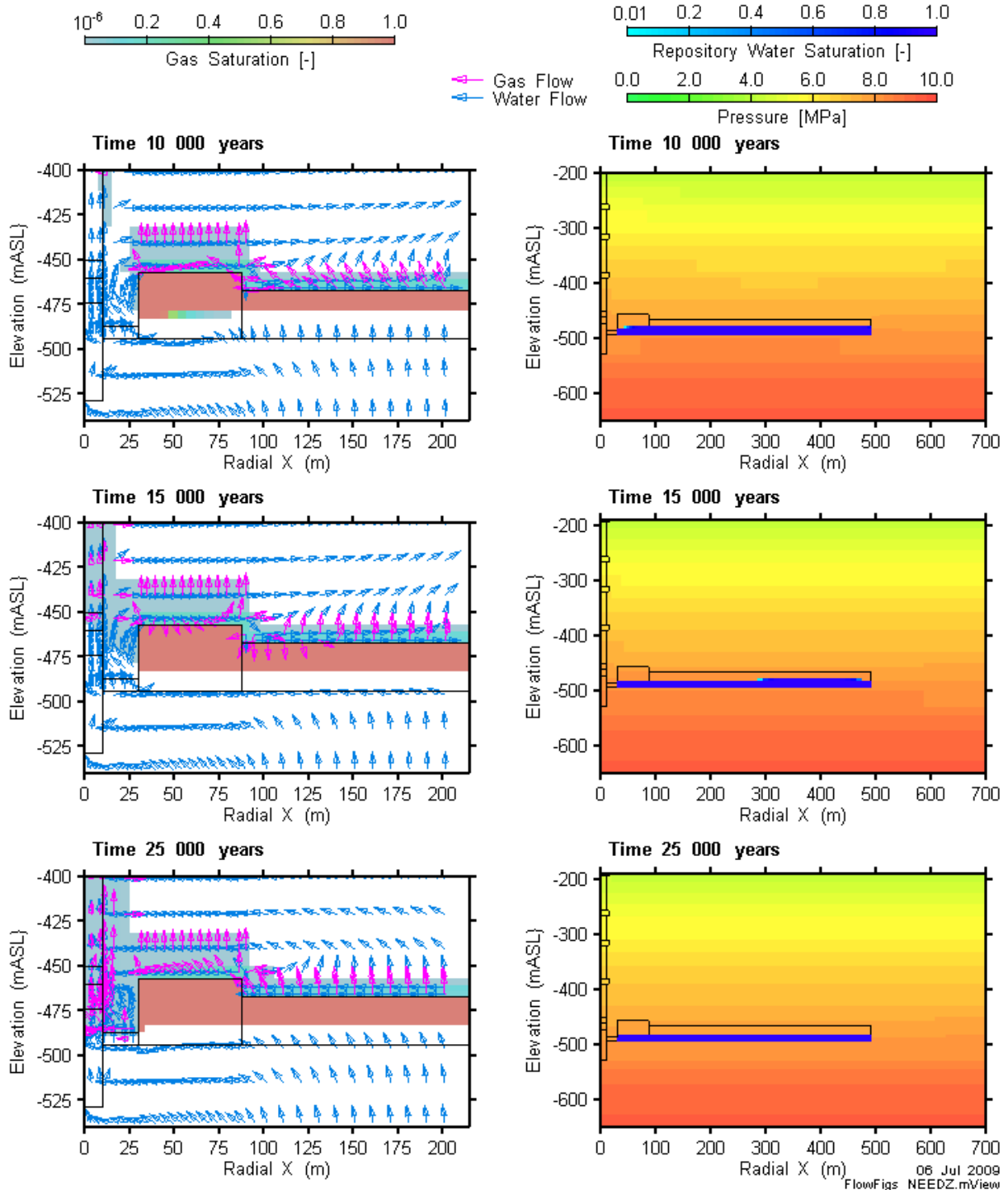


Figure 5-46: Evolution of conditions for the NE-EDZ case at 10 000 years, 15 000 years, and 1000 years. Gas saturation, and gas and water flow (outside repository) are shown in the figures on the left, and pressure and repository water saturation in the figures on the right.

Figure 5-46 and Figure 5-47 show gas saturation, gas and water flows, repository water saturation and pressure at 25 000 years, shortly after the pathway along the EDZ is created. After the initial pulse of gas along the EDZ, gas pressures along the EDZ begin to equilibrate, reducing the pressure gradient along the EDZ and consequently the flow of gas along the EDZ decreases. Gas is no longer pushed into the SDB2R unit, and gas within this unit dissolves.

At approximately 100 000 years, there is an increase in the gas generation rate, causing a small increase in pressure, and the second pulse of gas up the EDZ as shown in Figure 5-43. This second pulse of gas is also accompanied by a pulse of gas into the SDB2R unit. The gas in the SDB2R unit begins to dissolve once the gas generation rate decreases again.

Once repository gas pressures decrease below the geosphere pressure at 142 000 years, water begins to resaturate the repository. As the repository resaturates, the connection of gas between the repository and shaft EDZ along the monolith EDZ is broken. Gas continues to go into the shaft EDZ, but by travelling through the rock between the ring tunnel and the shaft. As well, once water begins to resaturate the repository, gas also begins to penetrate more rock above the repository. By the end of the simulation, water saturation in the repository is 0.62 and gas has travelled through the rock up to the Cabot Head formation, which for the NE-BC, is the lowest permeability unit in the model. Figure 5-48 shows gas saturations, repository water saturation, pressure and gas and water flows at 1 000 000 years.

The highly permeable EDZ pathway results in a greater amount of gas and dissolved gas leaving the repository, compared to the NE-BC. Approximately half of all generated gas leaves the repository by one million years (1.10×10^9 mol of gas are generated and 5.33×10^8 mol of gas leaves the repository), with half of these gases leaving the repository through the shaft and EDZ. Approximately 13% of generated gas leaves the repository as dissolved gas and enters the shaft EDZ.

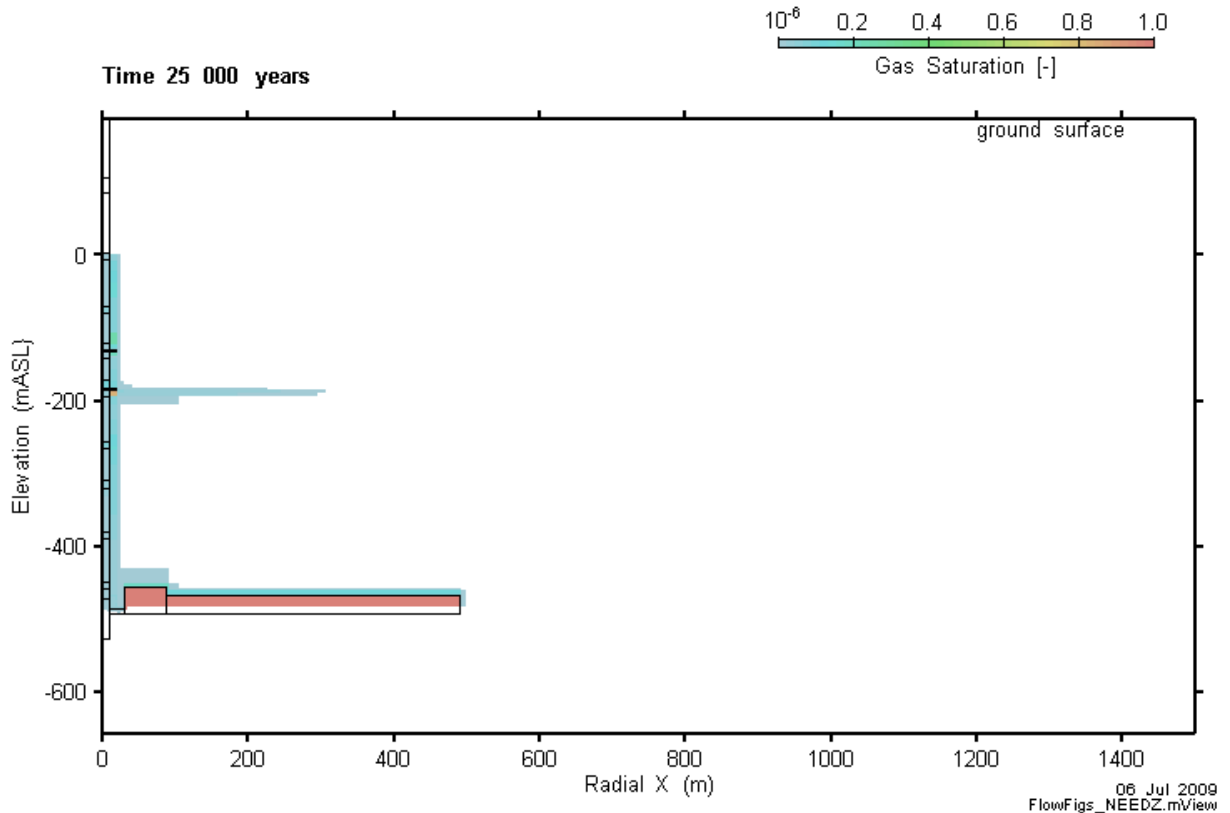
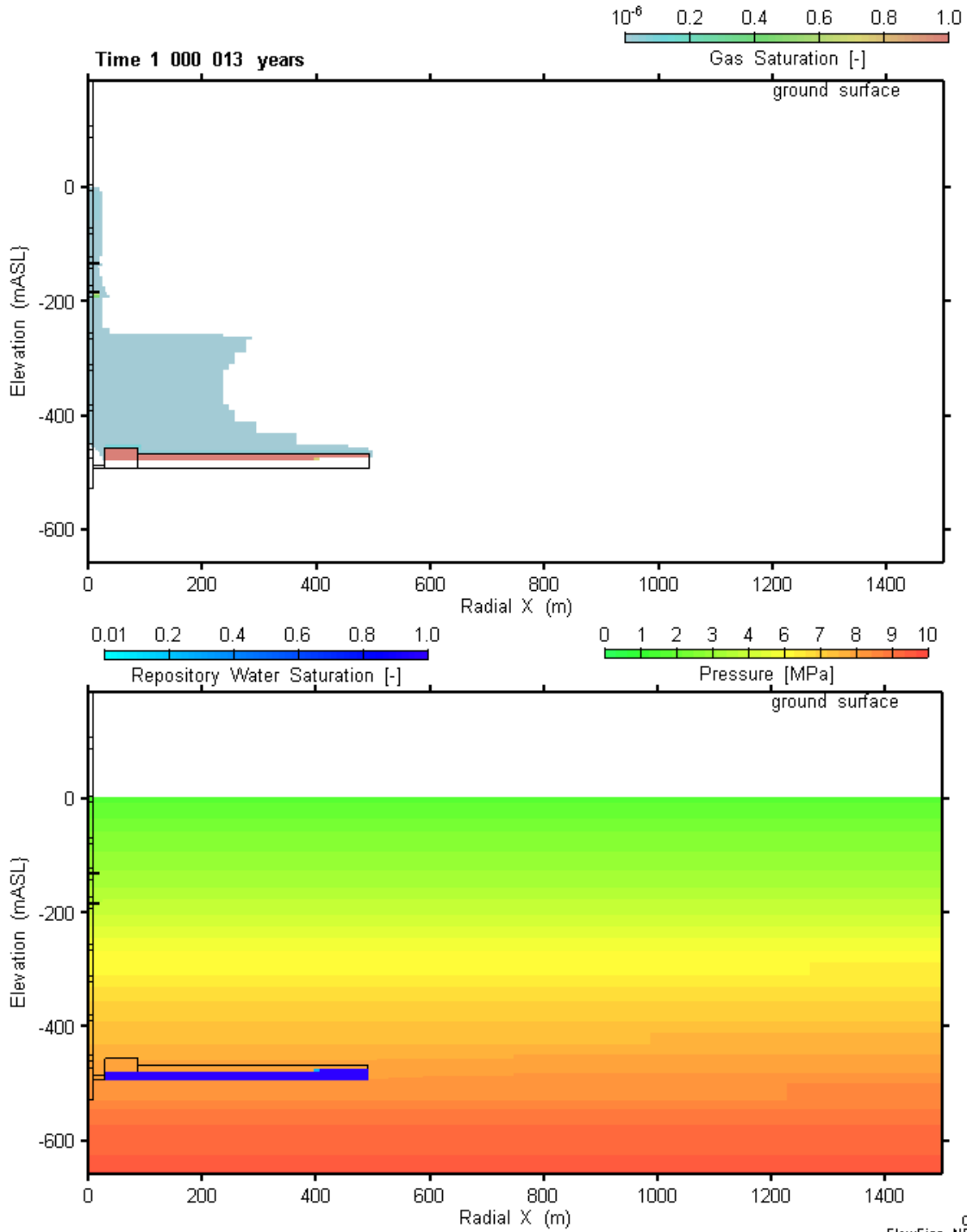


Figure 5-47: Gas saturation for the NE-EDZ case at 25 000 years.



06 Jul 2009
FlowFigs_NEEDZ.mView

Figure 5-48: Evolution of conditions for the NE-EDZ simulation at 1 000 000 years. Gas saturation is shown in the figure above, and pressure and repository water saturation in the figure below.

5.4.2.2 Detailed Description of Dissolved Gas Transport

Figure 5-49 shows the dissolved concentrations for the NE-EDZ case at 0, 2000, 100 000 and 1 000 000 years. The same times as shown for the NE-BC were selected for comparison purposes. Dissolved gas concentrations follow the pathway of gas; high dissolved gas concentrations are present where gas is present in the geosphere. For example, at 100 000 years, dissolved concentrations are greatest in the Ordovician above the repository and in the permeable SDB2R unit.

Note that dissolved gas concentrations are also present at greater distances than the gas. For example, dissolved gas originating from the repository are transported up the shaft before bulk gas (see Figure 5-43), with peak dissolved gas mass flow occurring at 8000 years, driven by the pressure gradient resulting from increased repository gas pressures, with the peak repository gas pressure occurring at 2100 years, and the water, laden with dissolved gases, expelled from the repository and into the permeable EDZ after peak pressure. Approximately 1.47×10^8 mol of dissolved gas leaves the repository and enters the permeable EDZ.

Within the shaft/EDZ, dissolved gas flow rates decreases at the same time gas flow rates peak (see Figure 5-43); this is a result of a decrease in the amount of water available for transport of dissolved gas, and represents a decrease in the flow rate of both water and dissolved gas crossing the plane, but not a decrease in the concentration or amount of dissolved gas in the shaft/EDZ (i.e., no drop in cumulative amount of dissolved gas, as shown in Figure 5-44).

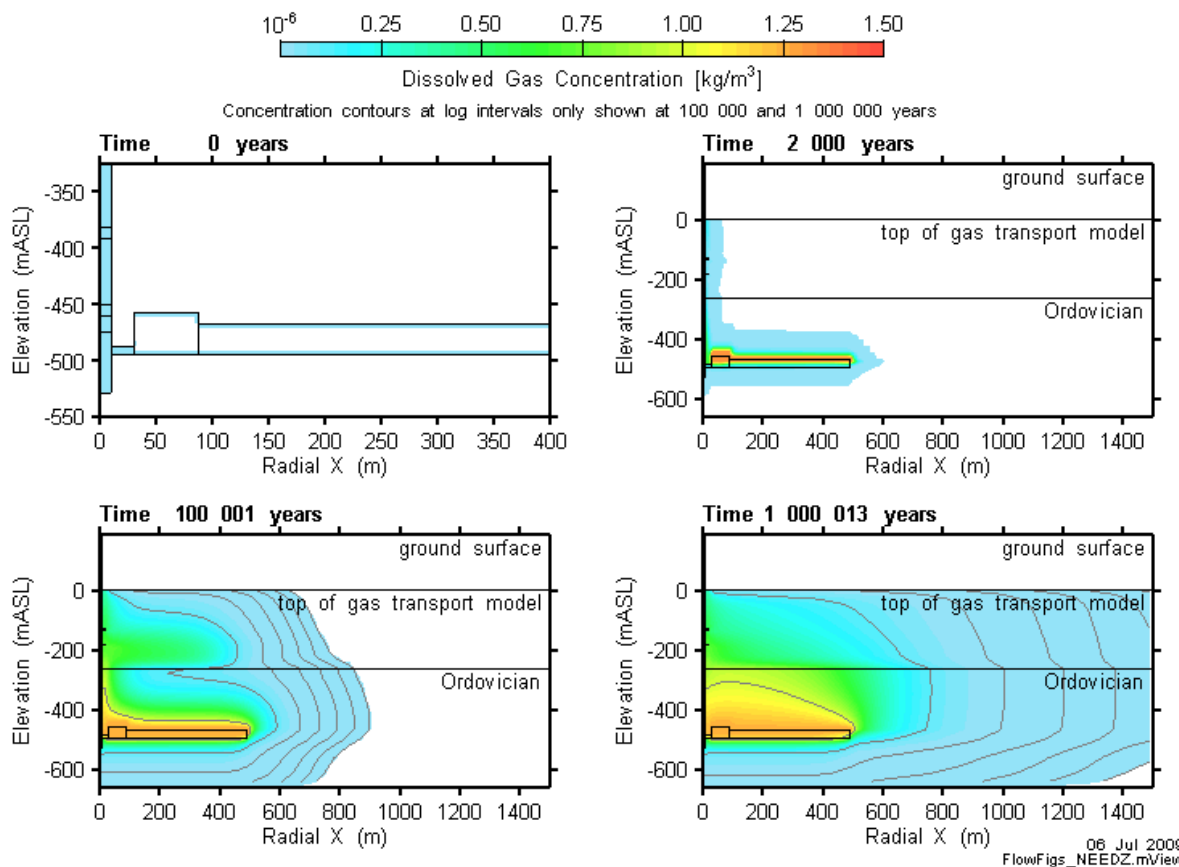


Figure 5-49: Dissolved gas concentrations at 0, 2000, 100 000 and 1 000 000 years for the NE-EDZ case. Note the different radial X and elevation scale at 0 years.

5.5 CASE NE-UG-BC – UPDATED GEOSPHERE PERMEABILITIES

5.5.1 Gas Generation

Normal evolution case NE-UG-BC differs from the base case in that it uses updated geosphere data based on preliminary information from boreholes DGR-3 and DGR-4. The UG cases are intended to look at permeabilities in the Silurian and Ordovician sediments which are significantly lower than the BC. As a result of the lower permeabilities we might expect that water is transported into and out of the repository at a slower rate.

This is what is observed. Figure 5-50 shows that while the amount of water consumed through gas generation reactions was the same as for the base case (i.e., Figure 5-1), significant amounts of water only start to enter the repository after 10^5 years. For the base case however (Figure 5-1), significant amounts of water entered the repository before the peak pressure at 10^3 years and were subsequently expelled. Figure 5-51 shows the effect in terms of water saturation.

The main consequence of the lower saturation over the first million years is that the gas pressures are lower than initial steady state pressure throughout the simulation. The results show that the number of moles of gas in the repository throughout the simulation is very similar to the BC. Using the ideal gas law and taking this into consideration, the pressure for this case should approximately be given by $P_{NE-BC} (1-S_{NE-BC})/(1-S_{NE-UG-BC})$, where S and P are the water saturation and pressure respectively. Checking this at 100,000 years, we have $P_{NE-BC} = 8$ MPa from Figure 5-6, $S_{NE-BC} = 0.18$ from Figure 5-2: NE-BC: and $S_{NE-UG-BC} = 0.02$ from Figure 5-51, giving a pressure of 6.7 MPa, which is approximately equal to the value of 6.9 MPa observed in Figure 5-52.

Figure 5-52 shows that the pressure has almost reached the initial steady state value by 10^6 years. For the base case there was a peak in saturation and gas pressure at around 10^3 years. This is no longer the main peak for either saturation or gas pressure.

The consequence of the lower gas pressures and lower permeabilities is that, compared to the base case, less gas leaves the repository. Compare Figure 5-53 and Figure 5-4.

There are no other major differences resulting from the updated geosphere data.

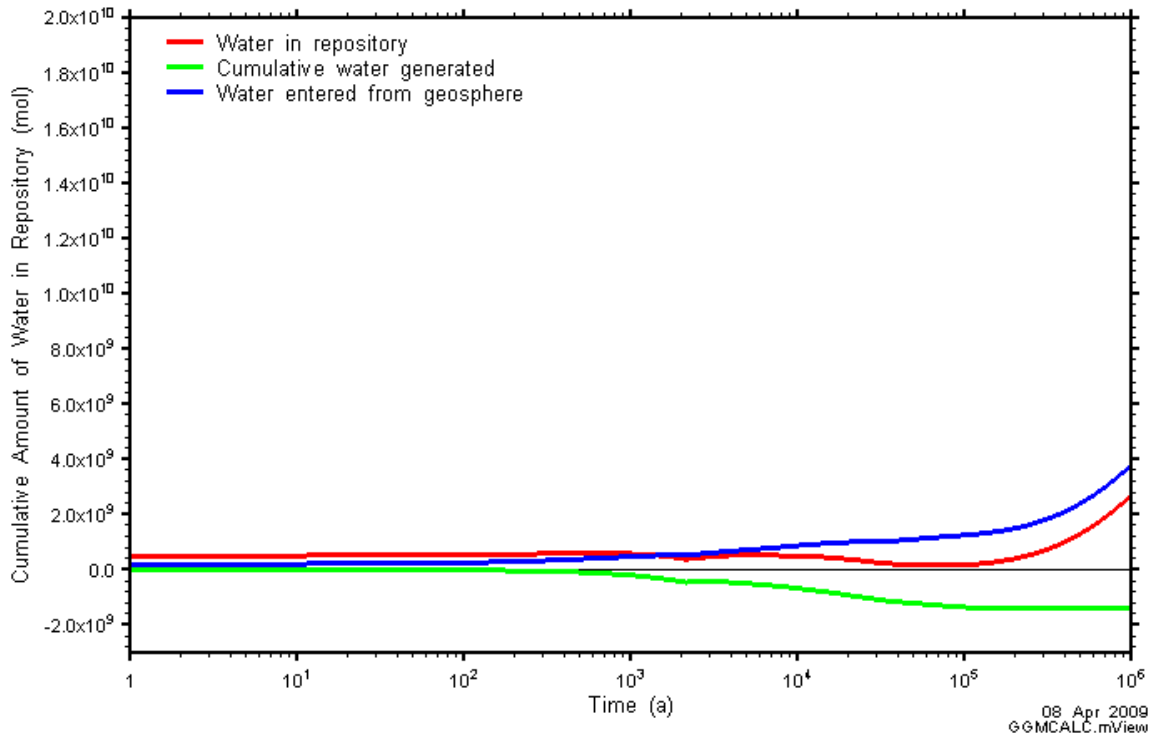


Figure 5-50: NE-UG-BC: Water Balance

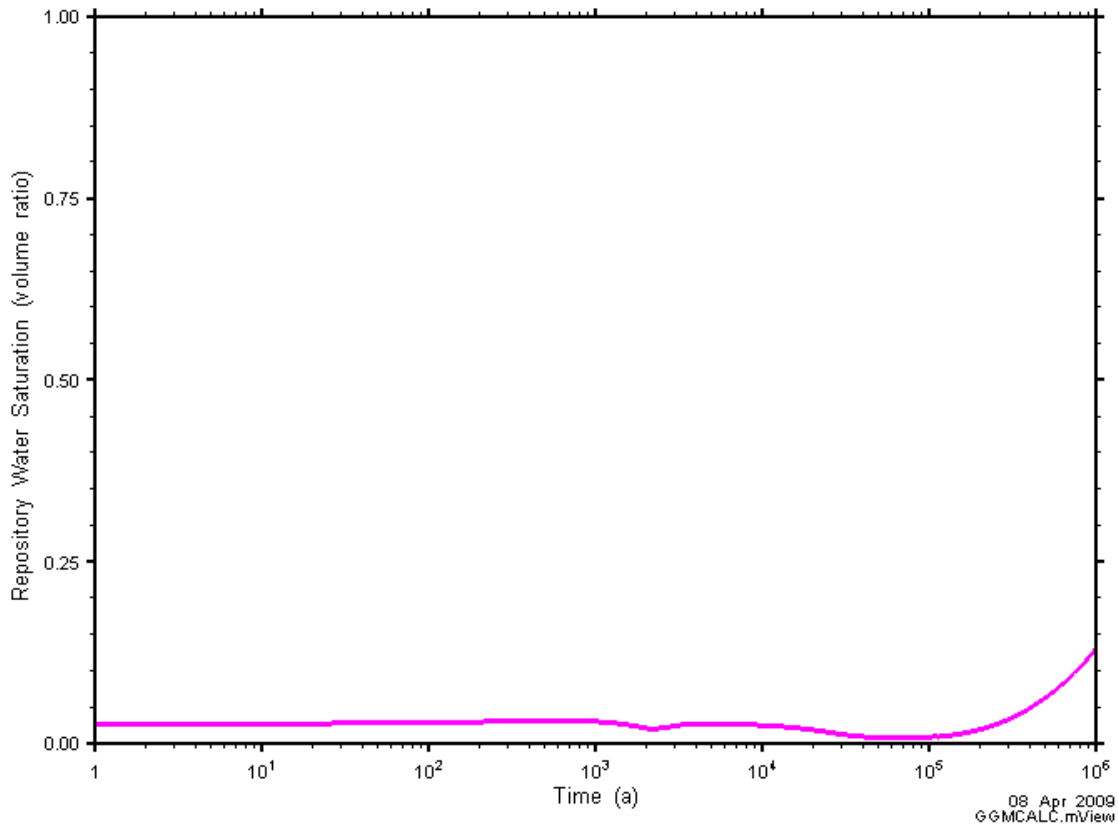


Figure 5-51: NE-UG-BC: Water saturation

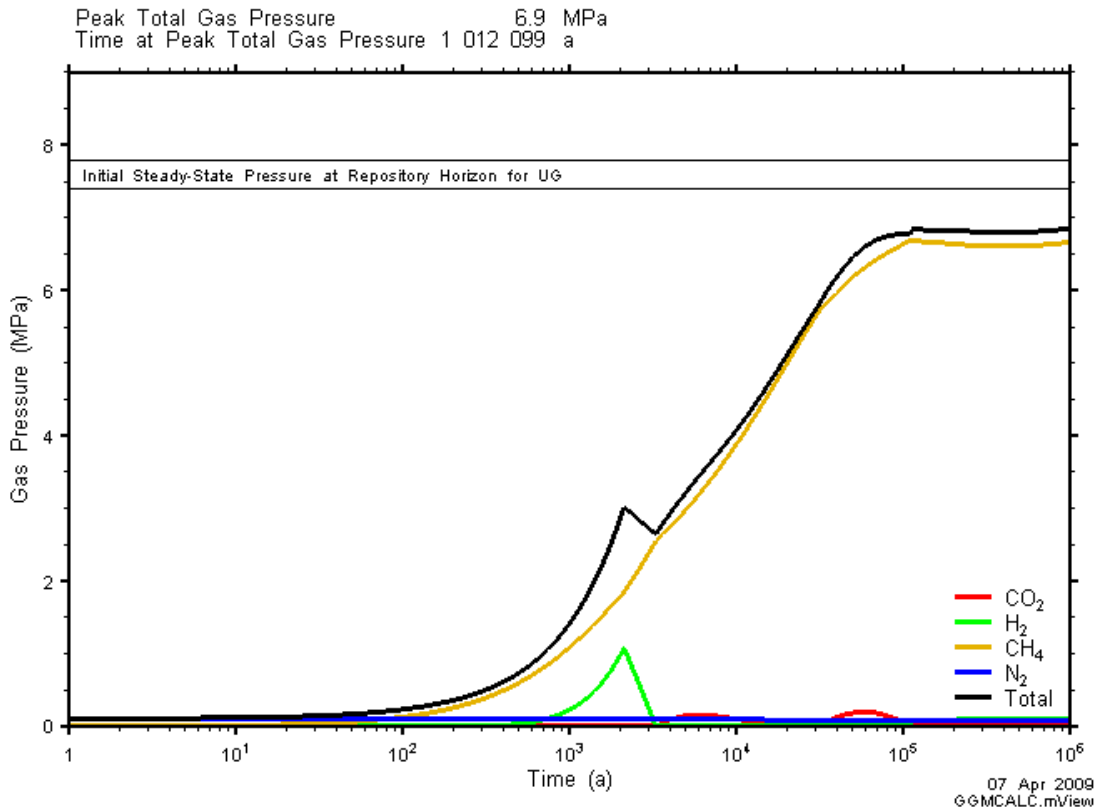


Figure 5-52: NE-UG-BC: Total and Partial Gas Pressures with the Repository

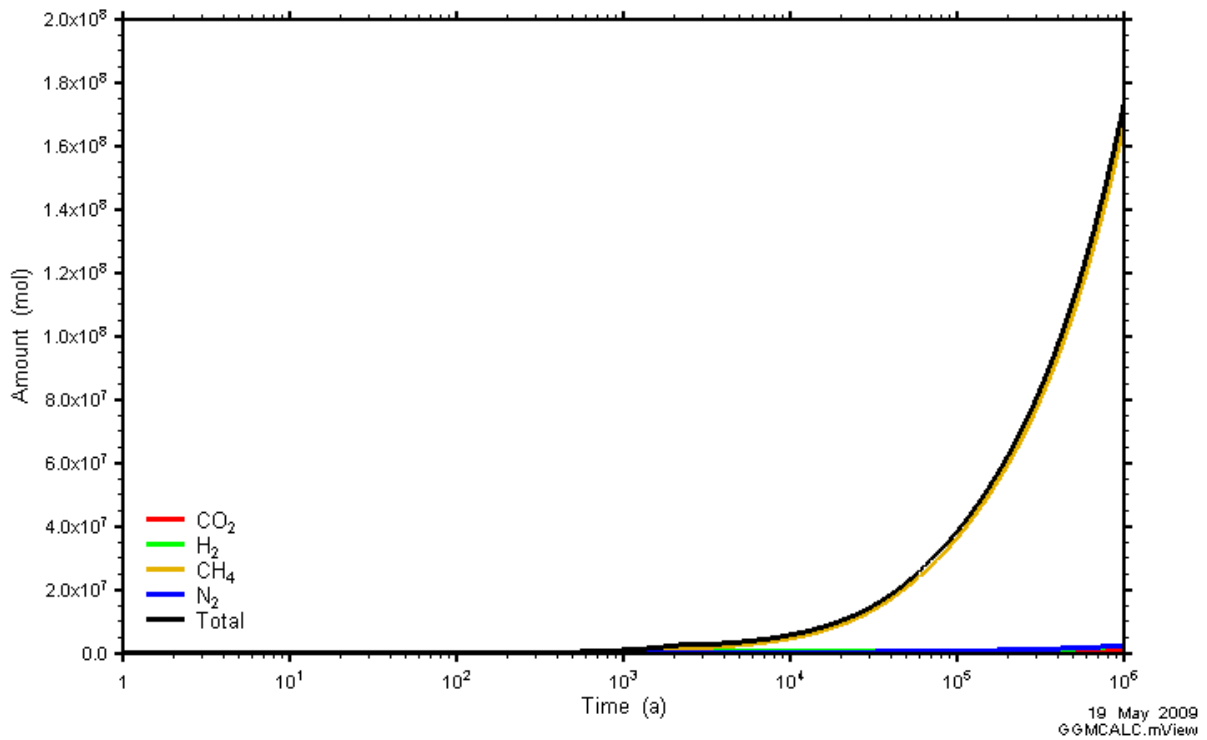


Figure 5-53: NE-UG-BC: Amounts of Gases which have Left the Repository

5.5.2 Gas and Water Flows

The NE-UG-BC uses updated permeabilities in comparison to the NE-BC, with NE-UG-BC permeabilities significantly lower than NE-BC within the Ordovician sequence. These lower permeabilities result in significant different key results in comparison to the NE-BC:

- Repository gas pressures remain below the initial steady-state pressure at the repository, with the maximum pressure of 6.9 MPa occurring at the end of the one million year simulation (see Figure 5-52). As will be described below, the NE-UG-BC has lower repository gas pressures compared to the NE-BC due to the greater void volume available in the repository resulting from minimal water saturation of the repository. As well, pressures at 1 000 000 years are below the initial steady-state pressure at the repository horizon as pressures are still equilibrating due to the low permeabilities in the geosphere. Consequently, it is expected that the repository pressure will continue to increase slowly after 1 000 000 years, until pressures reach an equilibrium pressure with the surrounding host rock, which is expected to be near the initial steady-state pressure.
- Little dissolved gas crosses the ORD and SALF planes, due to the low permeability of the rocks, as evidenced by the dissolved gas flow rates and cumulative dissolved gas mass shown in Figure 5-54 and Figure 5-55. Note that the dissolved gas flow rates for the shaft and EDZ across the SALF plane do not appear to correspond to cumulative dissolved gas mass, due to dissolved gas flow occurring downwards across the plane (essentially a negative cumulative mass). As with the NE-BC, no gas travels upwards across the ORD and SALF planes, with the exception of some initial gas from the shaft.

The results for the NE-UG-BC will be discussed in detail below.

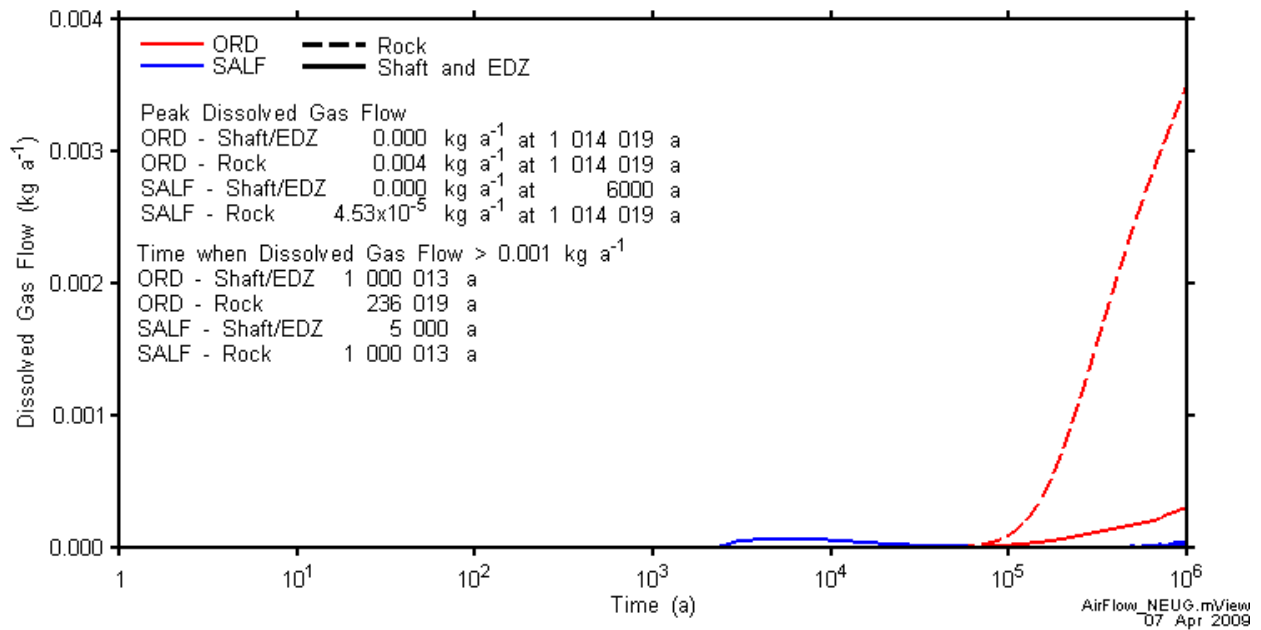


Figure 5-54: Dissolved gas flow rates across the ORD and SALF planes for the NE-UG-BC. Note different y-axis scale in comparison to the NE-BC.

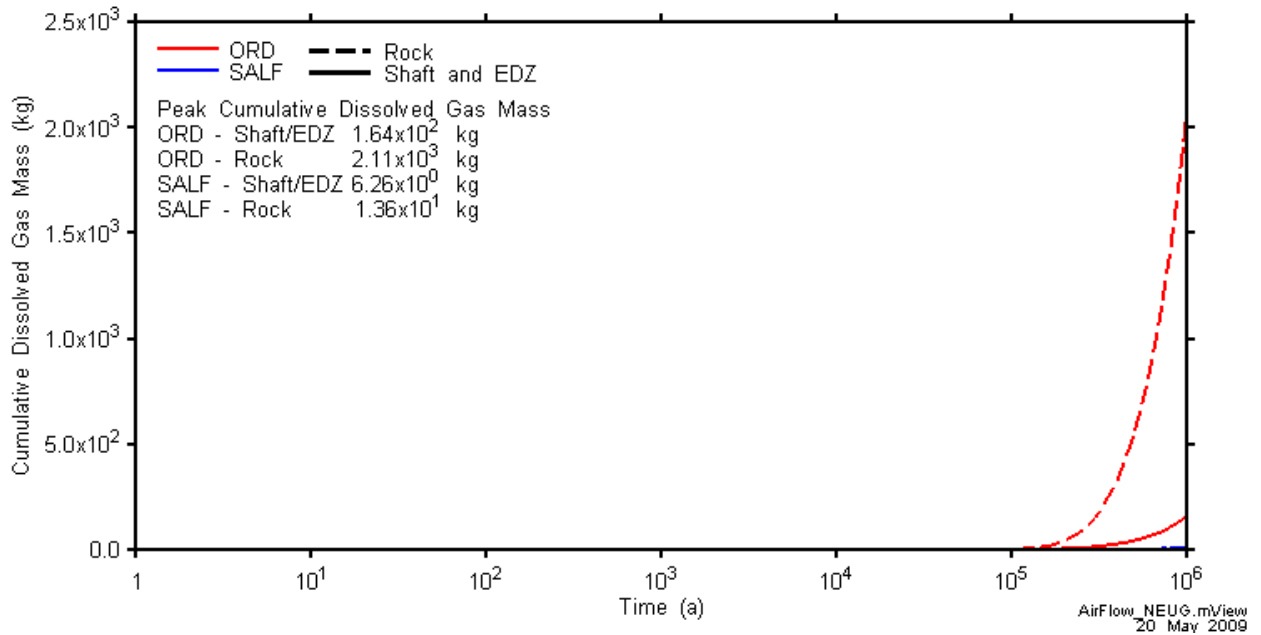


Figure 5-55: Cumulative dissolved gas mass crossing the ORD and SALF planes for the NE-UG-BC. Note different y-axis scale in comparison to the NE-BC.

5.5.2.1 Detailed Description of Gas and Water Transport

As in the NE-BC, pressures in the repository and shaft are increasing, as the repository and geosphere move towards equilibrium pressures. Small amounts of gas travel into the repository EDZ above the repository and water is flowing into the repository, ring tunnels and shaft, causing re-saturation of the repository, ring tunnels and shaft.

However, due to the low permeabilities in the Ordovician rocks and the consumption of water in the repository by corrosion reactions, the water saturation of the shaft and repository is very slow. Figure 5-56 shows gas saturations and pressures in the shaft in the vicinity of the repository at 0, 2000 and 10 000 years. Gas flows out of the repository and into the shaft and rock, except between 2000 and 10 000 years, when gas flows from the shaft and into the repository. This corresponds with the repository gas generation rates and gas consumption rates shown in Figure 5-13, with gas flowing into the repository when gas is consumed by microbial methane generation. The shaft at the repository horizon is not fully saturated with water (gas is dissipated through dissolution) until 25 000 years. At this point, the entire shaft is fully saturated with water. Water saturation in the repository does not begin to increase until after 100 000 years, once corrosion water consumption rates are very low. Figure 5-57 shows gas saturations and pressures in the shaft in the vicinity of the repository at 25 000 and 100 000 years.

With low permeabilities in the rock limiting flow of water and gas into and out of the repository, intuitively, one might expect repository gas pressures to be greater than the NE-BC; however, the repository pressures increase at a slower rate than the NE-BC, and the peak repository pressure is less than for the NE-BC at a much later time (end of the one million year simulation period). The lower repository pressure in the NE-UG-BC is a result of the greater void volume available in the repository, due to the slow water saturation of the repository. At the time of peak repository pressure in the NE-BC (approximately 2000 years), the NE-UG-BC void volume is 2.7 times greater than the NE-BC ($3.43 \times 10^5 \text{ m}^3$) and the NE-UG-BC repository pressure is 2.9 MPa. A simple ideal gas law check confirms that the greater void volume accounts for the lower pressures (note that the NE-UG-BC has a slightly smaller amount of gas in the repository at 2000 years of $4.11 \times 10^8 \text{ mol}$).

The small dip in repository pressure at approximately 2000 years occurs for the same reasons as the NE-BC, due to a sharp change from gas generation to gas consumption (as well as water consumption to water generation).

Figure 5-58 shows the gas saturation and pressures at the end of the simulation. As in the NE-BC, both the host rock and the concrete monolith and shaft are effective barriers to gas migration. Gas saturation greater than 10^{-6} is reached in the shaft at approximately 900 000 years (through the rock mass, rather than travelling through the concrete monolith and up the shaft), but otherwise, small gas saturations only remain within a few metres of the repository, as in the NE-BC. Pressures near the repository and shaft have not yet equilibrated with the rest of the geosphere, and consequently repository gas pressures are expected to continue to climb towards a pressure near the initial steady-state pressure of the surrounding host rock. As well, the low pressures near the shaft explain the small amount of gas which has migrated through the rock mass and into the shaft. As pressures in and near the shaft equilibrate towards initial steady-state pressures, this pathway towards the shaft will likely be removed.

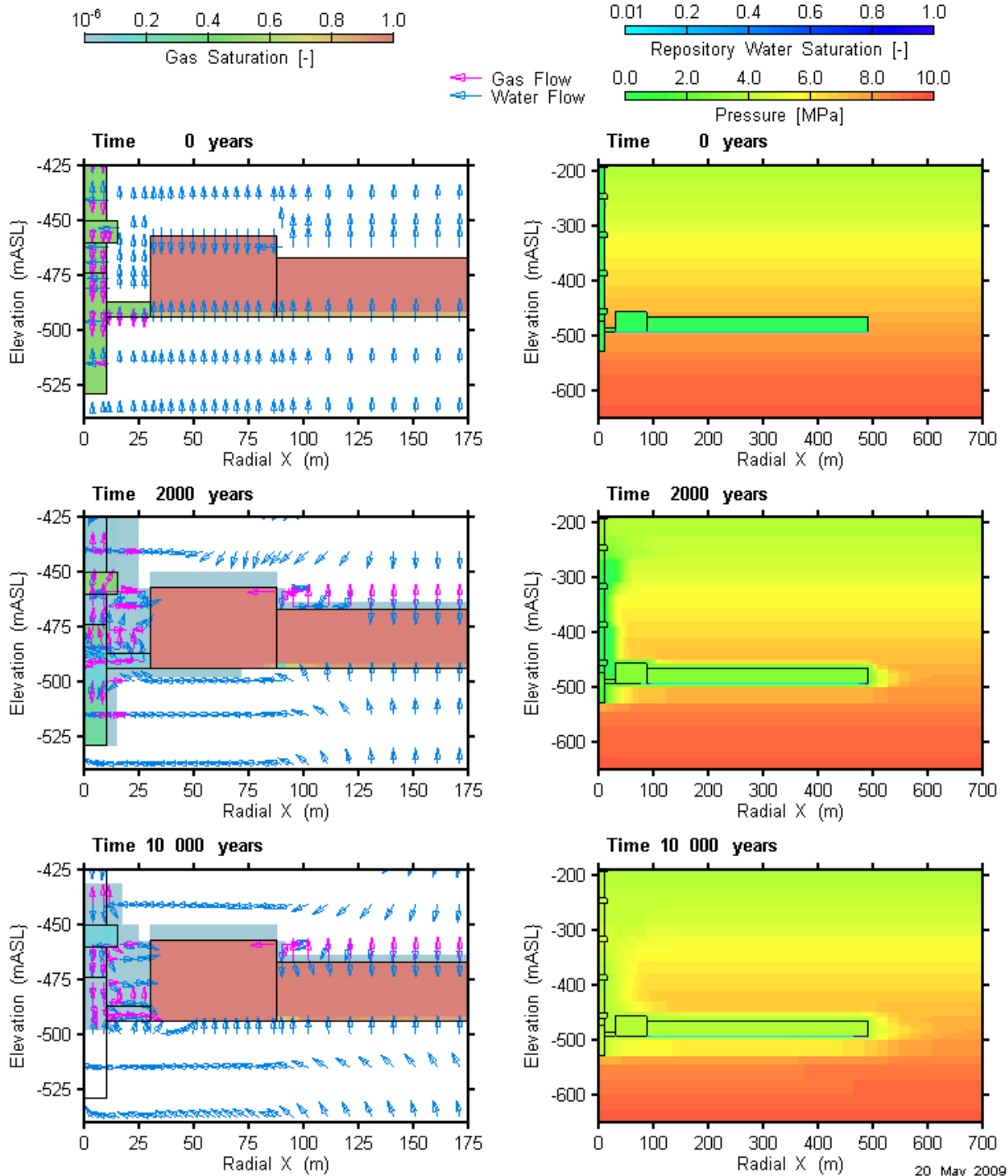


Figure 5-56: Evolution of conditions for the NE-UG-BC at the start of the simulation (0 years), 2000 years, and 10 000 years. Gas saturation, and gas and water flow (outside repository) are shown in the figures on the left, and pressure and repository water saturation in the figures on the right.

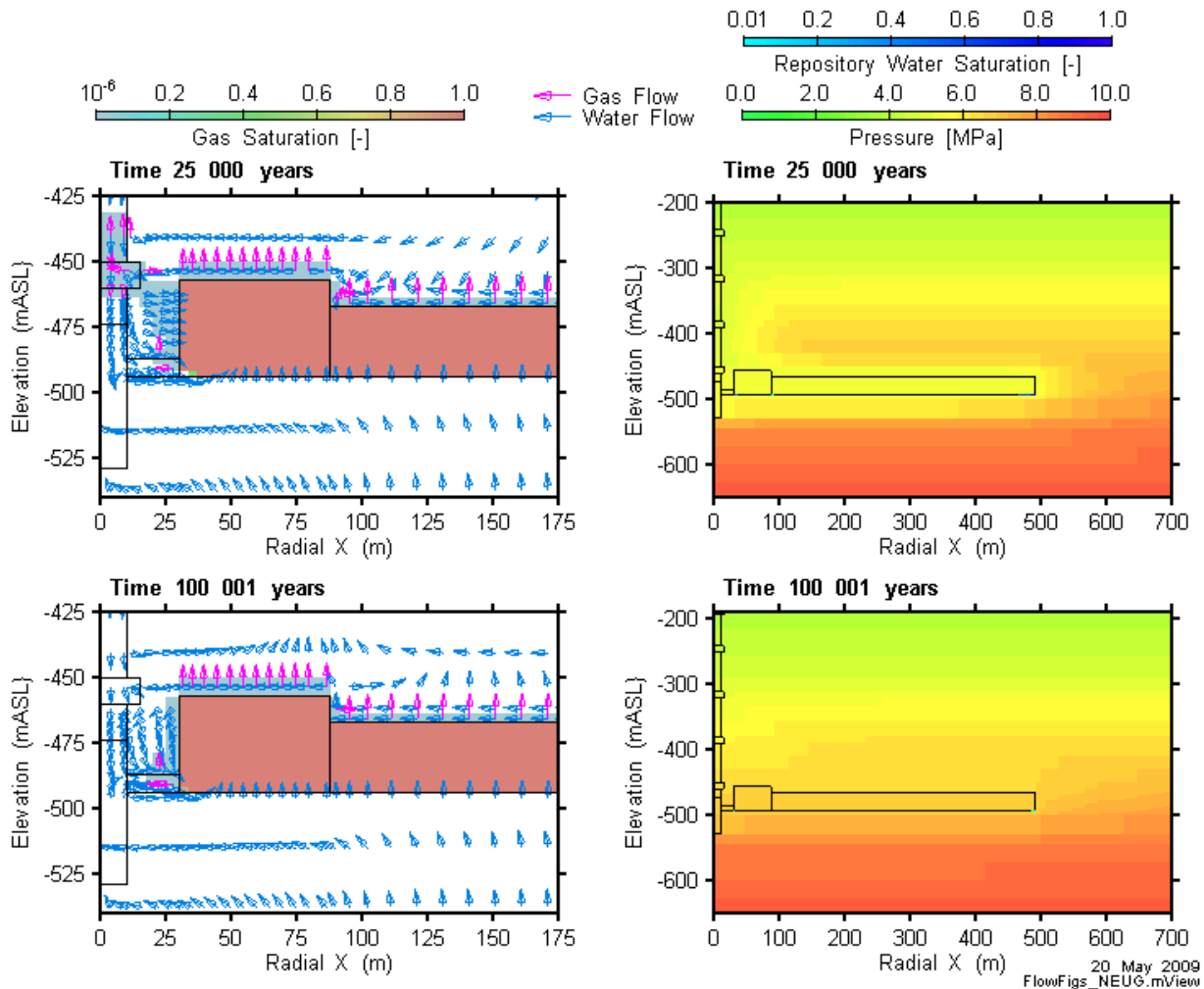


Figure 5-57: Evolution of conditions for the NE-UG-BC at 25 000 years and 100 000 years. Gas saturation, and gas and water flow (outside repository) are shown in the figures on the left, and pressure and repository water saturation in the figures on the right.

Over the course of the simulation, mainly gas leaves the repository, rather than dissolved gas, with approximately 14% of generated gases leaving the repository (1.07×10^9 mol of gas generated and 1.48×10^8 mol gas leaving the repository). Note that most of the gas leaving the repository enters the host rock, with approximately 0.2% of the gas leaving the repository through the concrete monolith and shaft, confirming the effectiveness of the concrete monolith and shaft seals for preventing gas transport.

As previously mentioned, some gas enters the repository through the shaft between 2000 and 10 000 years, although this amount is small relative to the amount that leaves before 2000 years and after 10 000 years (4.70×10^5 mol leaves the repository and enters the shaft, 1.55×10^5 mol enters the repository from the shaft) Dissolved gas actually only enters the repository, as water only enters the repository (see Figure 5-50) and is never pushed out of the repository (dissolved gas can only leave the repository with water). Approximately 0.2 % of the gas generated (2.07×10^6 mol or 6.00×10^4 kg) enters the repository as dissolved gas and the amount of dissolved gas observed at the ORD and SALF planes is entirely a result of the

dissolution of gas leaving the repository. 98% of the gas leaving the repository has dissolved by the end of the simulation, leaving only 2.53×10^4 mol of gas in the host rock and EDZ at one million years.

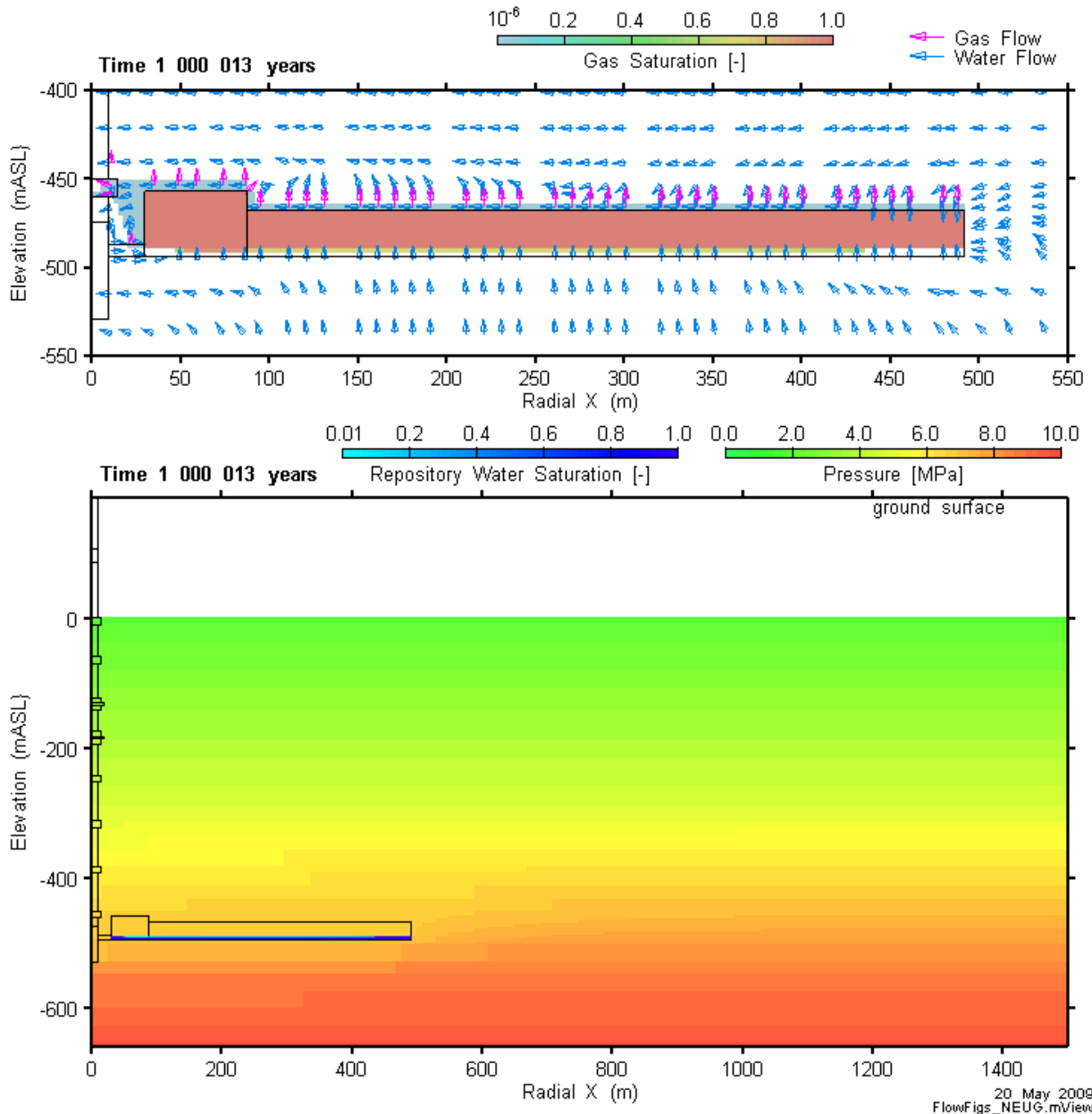


Figure 5-58: Evolution of conditions for NE-UG-BC simulation at 1 000 000 years. Gas saturation, and gas and water flows (outside repository) are shown in the figure above, and pressure and repository water saturation in the figure below.

20 May 2009
FlowFigs_NEUG.mview

5.5.2.2 Detailed Description of Dissolved Gas Transport

Figure 5-59 shows the dissolved concentrations for the NE-UG-BC case at 0, 2000, 100 000 and 1 000 000 years. The same times as shown for the NE-BC were selected for comparison purposes only. Dissolved gas concentrations follow a similar pattern to the NE-BC, with smaller concentrations in the rock, as might be expected given the lower rock permeabilities.

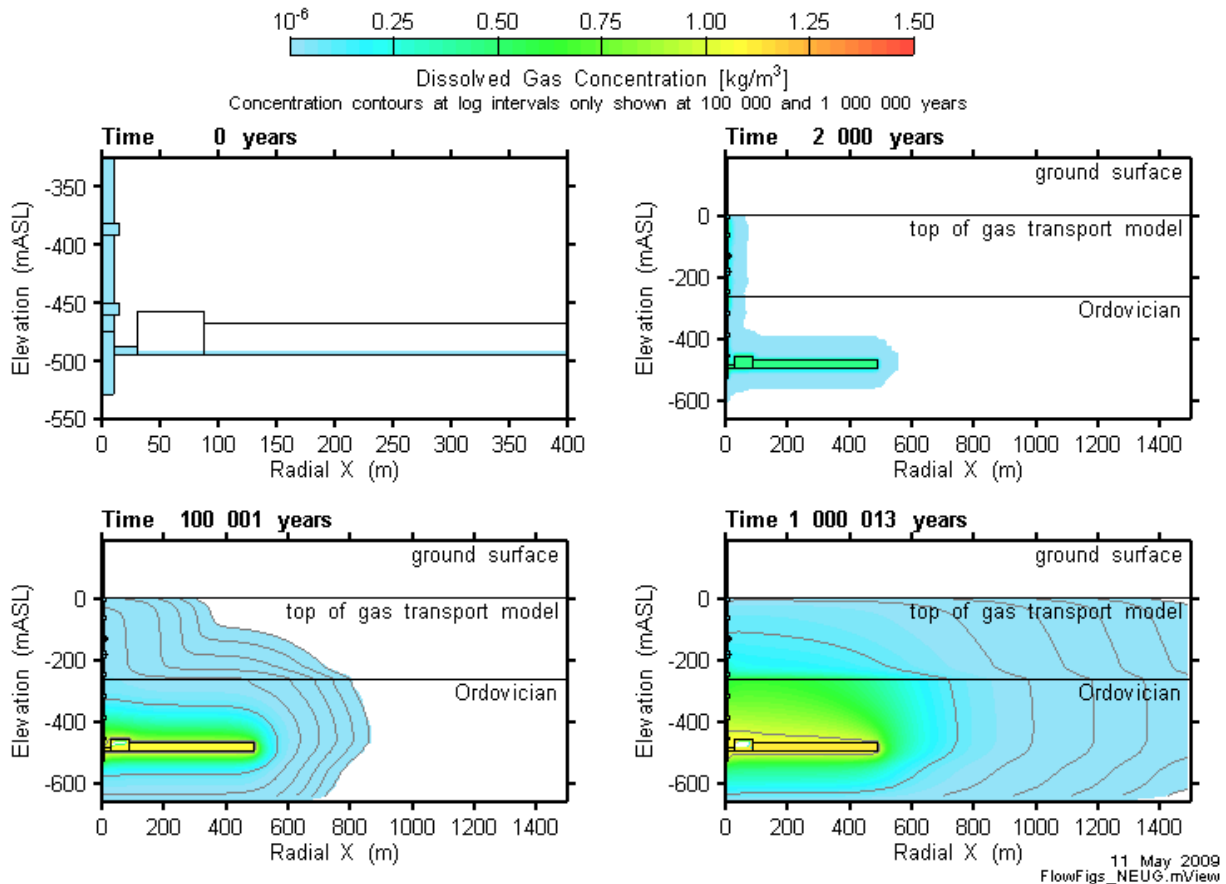


Figure 5-59: Dissolved gas concentrations at 0, 2000, 100 000 and 1 000 000 years for the NE-UG-BC. Note the different radial X and elevation scale at 0 years.

5.6 CASE NE-UG-EDZ – UPDATED GEOSPHERE PERMEABILITIES AND HIGH PERMEABILITY EDZ

5.6.1 Gas Generation

This case considers updated geosphere data, which includes lower permeabilities in the Silurian and Ordovician sediments, and the effects of a high permeability EDZ.

There are no significant differences in terms of gas generation between the results for this case and the results for NE-UG-BC. The higher permeability EDZ has made very little difference to the amounts of gas and water flowing into and out of the repository, and only results in a drop in the peak pressure of 0.1 MPa from the NE-UG-BC case (see Figure 5-60).

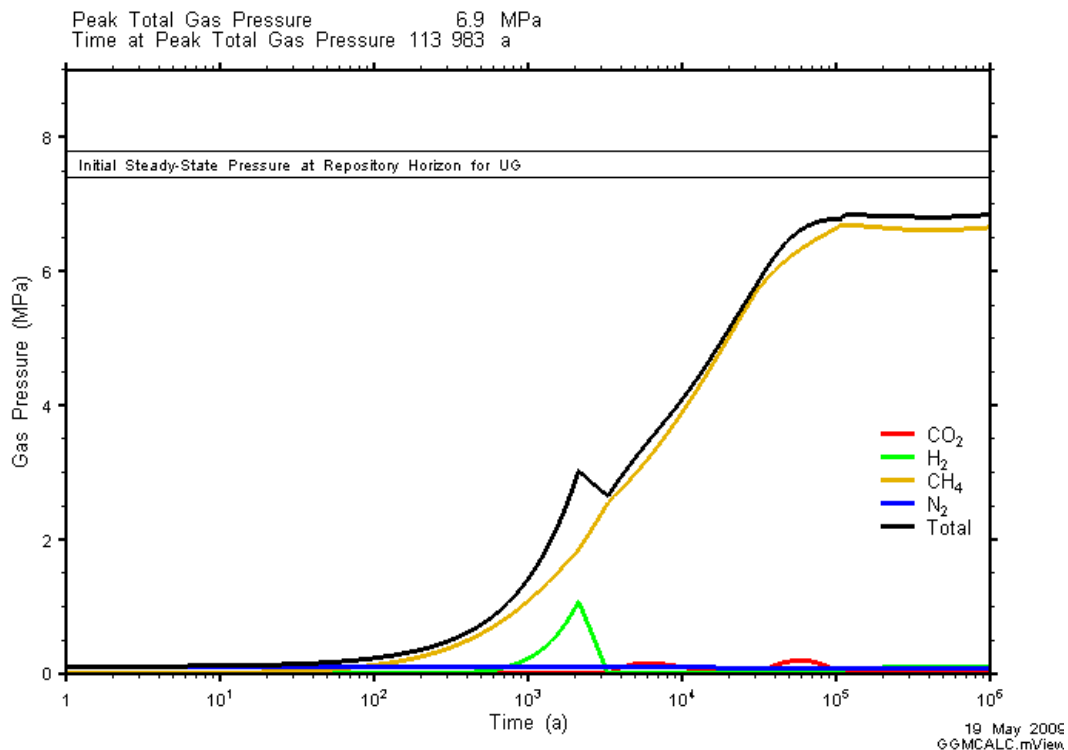


Figure 5-60: NE-UG-EDZ: Total and Partial Gas Pressures with the Repository

5.6.2 Gas and Water Flows

This case considers a permeable pathway along the shaft and EDZ, as in the NE-EDZ case, but with the lower permeabilities defined for the UG case.

Figure 5-61 and Figure 5-62 show dissolved gas flow rates and cumulate mass through the ORD and SALF planes. No gas travels up as far as the top of the Ordovician. Dissolved gas mass reaching the ORD and SALF planes is similar to the NE-UG-BC, with greater cumulative amounts in the shaft and EDZ (4.5 times more at the ORD plane and 2 times more at the SALF plane). Note that the small peak of dissolved gas up the shaft/EDZ at early times is the result of dissolved initial gases in the shaft.

In the base case geosphere, the high-permeability EDZ case (NE-EDZ) performs very differently from the base case (NE-BC), a result of a connection between the repository at high gas pressure to the permeable EDZ above the concrete monolith. In comparison, in the updated geosphere, the repository gas pressure in both the NE-UG-BC and NE-UG-EDZ cases stays below the initial steady-state pressure in the rock mass, providing little gradient for gas to leave the repository. Details of gas and water flow are presented below.

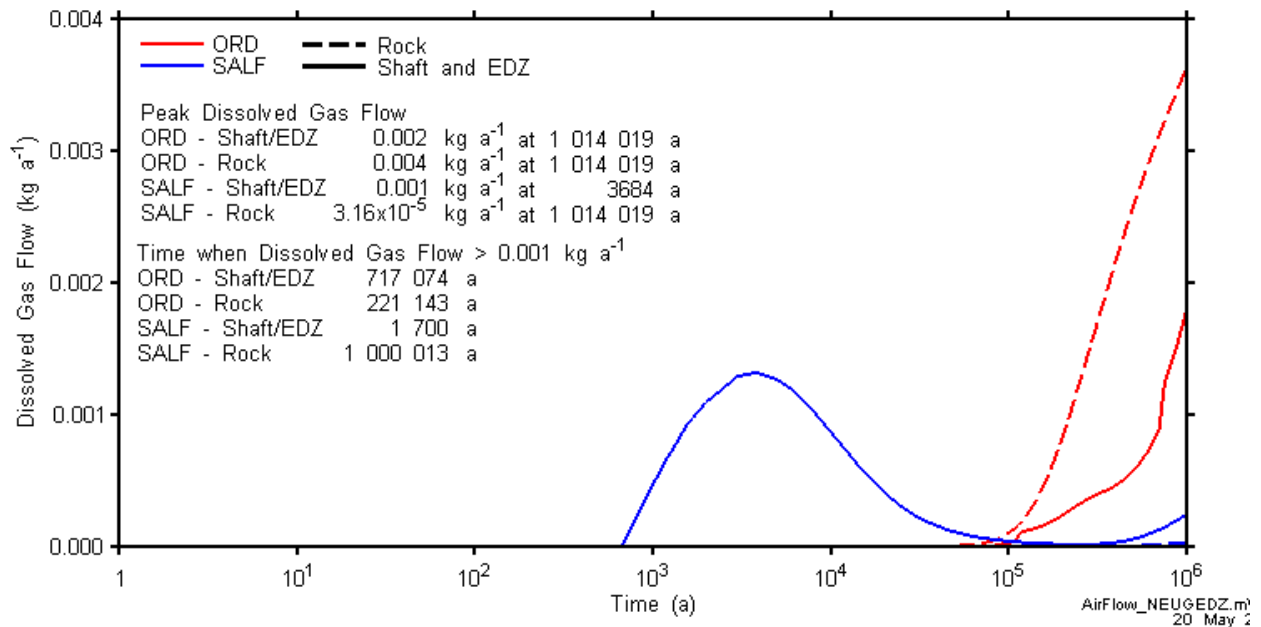


Figure 5-61: Dissolved gas flow rates across the ORD and SALF planes for the NE-UG-EDZ. Note different y-axis scale in comparison to the NE-UG-BC.

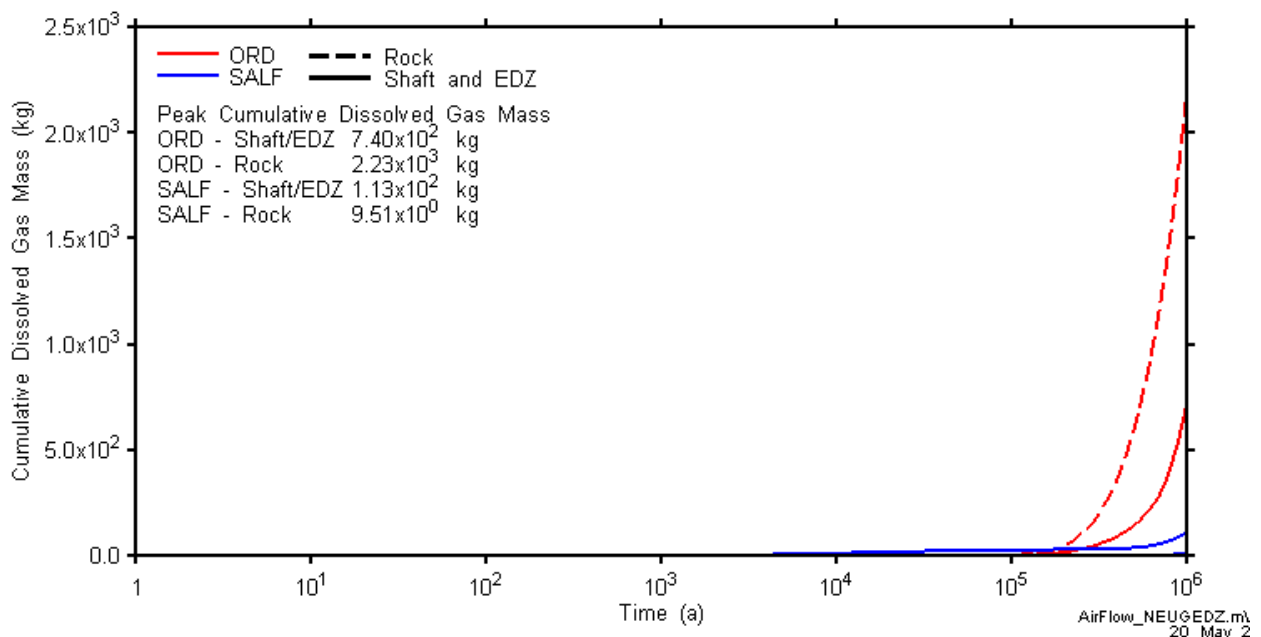


Figure 5-62: Cumulative dissolved gas mass crossing the ORD and SALF planes for the NE-UG-EDZ. Note different y-axis scale in comparison to the NE-UG-BC.

5.6.2.1 Detailed Description of Gas and Water Transport

The main difference in gas and water transport between the NE-UG-EDZ and NE-UG-BC cases is related to the water saturation of the shaft:

- The shaft becomes fully saturated with water by 5000 years, considerably earlier than in the NE-UG-BC (25 000 years). In the NE-UG-BC, some gas from the shaft enters the repository after 2000 years (during repository gas consumption) and continues until 10 000 years. Obviously, this contribution to gas in the repository is cut short at 5 000 years for the NE-UG-EDZ case. Figure 5-63 shows the gas saturations, pressures and repository water saturations at 0, 2000 and 5000 years.
- Water flows from the repository from shaft, starting at 2000 years as in NE-UG-BC, due to gas consumption in the repository. Water continues to flow in from shaft after 10 000 years (once gas consumption has reversed to gas generation), but as evidenced from the very slight increase in repository water saturation after 2000 years, the water flowing into the repository from the shaft is minimal (see Figure 5-64).

Other than these differences in shaft saturation, there is little difference in the NE-UG-EDZ and NE-UG-BC cases, due to the relatively small repository pressure compared to the pressures in the surrounding rock. Since results are so similar, further gas and water results for the NE-UG-EDZ case are not presented.

5.6.2.2 Detailed Description of Dissolved Gas Transport

Figure 5-65 shows the dissolved concentrations for the NE-UG-EDZ case at 0, 2000, 100 000 and 1 000 000 years. Dissolved gas concentrations follow a similar pattern to the NE-UG-BC, however, it is noticeable by the shape of the concentration contours near the shaft that dissolved concentrations travel up the permeable EDZ slightly faster. This corresponds with the slightly greater masses of dissolved gas reaching the ORD and SALF plane as previously discussed.

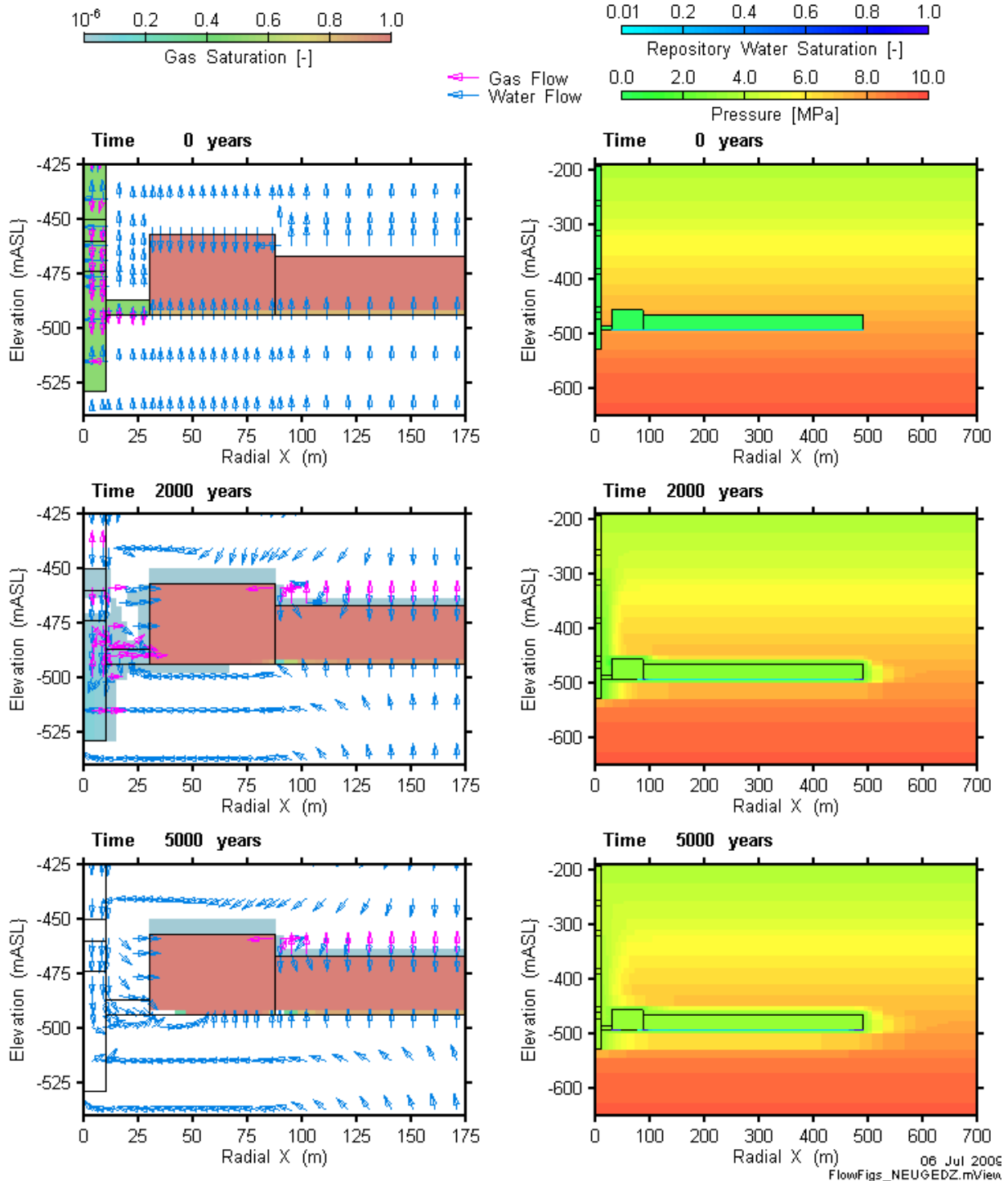


Figure 5-63: Evolution of conditions for the NE-UG-EDZ at the start of the simulation (0 years), 2000 years, and 5000 years. Gas saturation, and gas and water flow (outside repository) are shown in the figures on the left, and pressure and repository water saturation in the figures on the right.

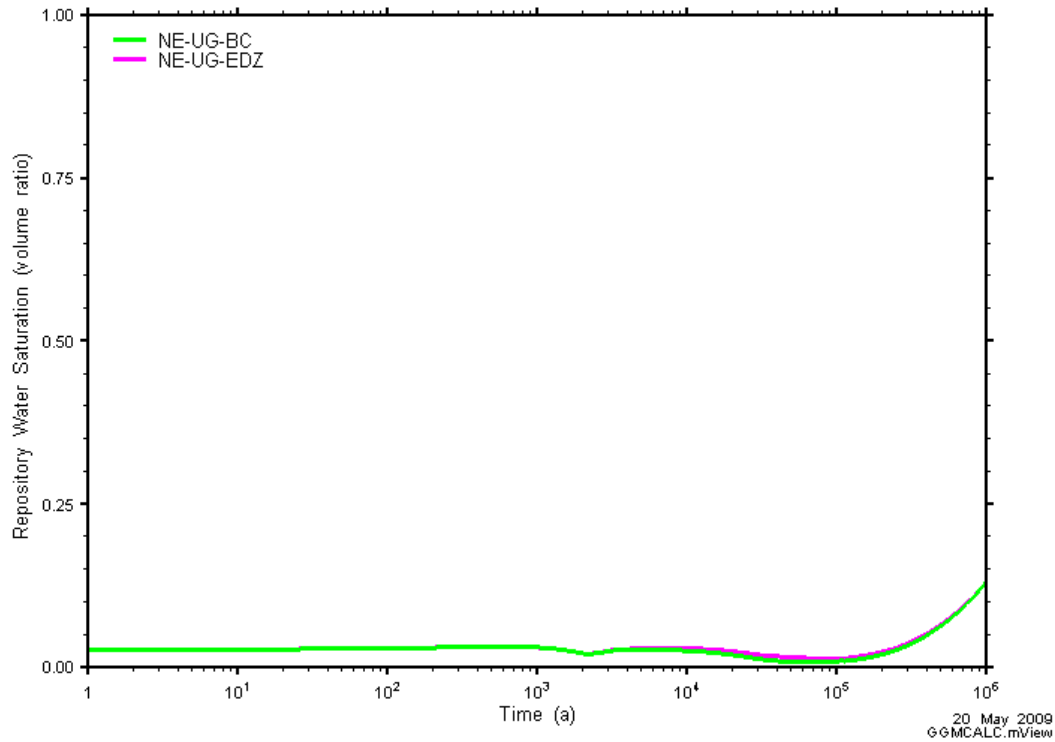


Figure 5-64: Repository water saturation for the NE-UG-EDZ case compared to the NE-UG-BC.

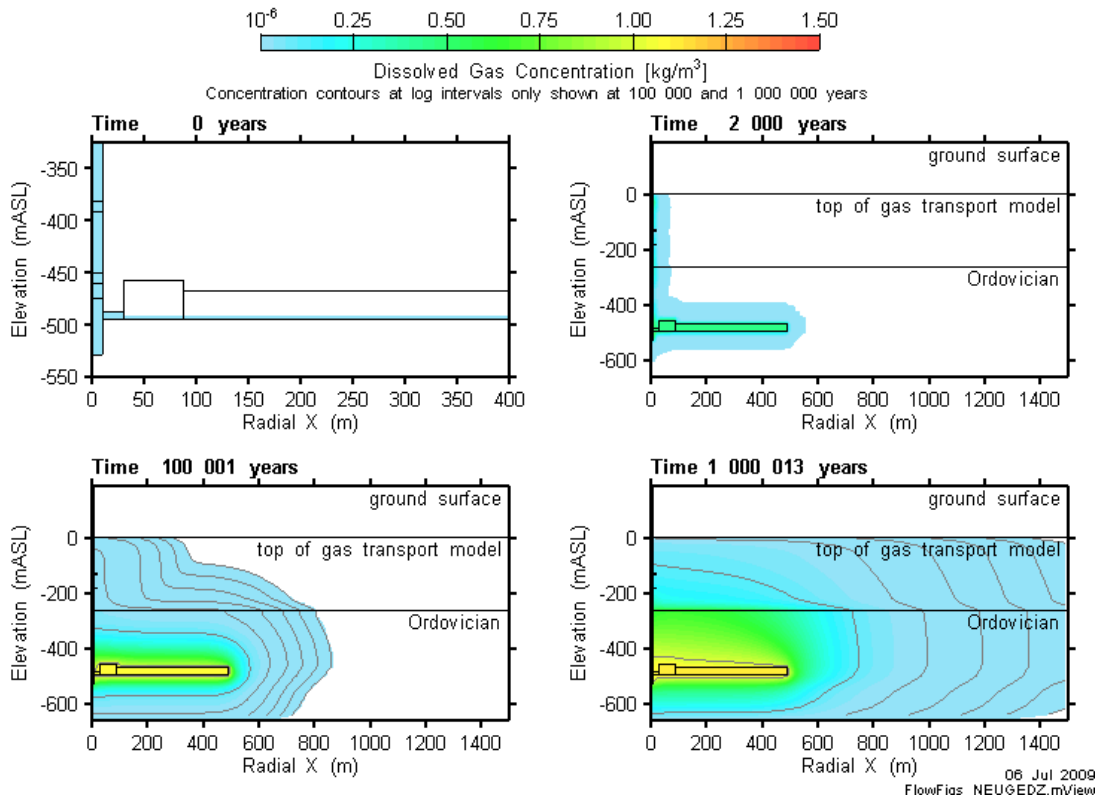


Figure 5-65: Dissolved gas concentrations at 0, 2000, 100 000 and 1 000 000 years for the NE-UG-EDZ case. Note the different radial X and elevation scale at 0 years.

5.7 CASE NE-UG-RD1 – UPDATED GEOSPHERE PERMEABILITIES AND BACKFILLING OF TUNNELS

5.7.1 Gas Generation

In addition to the updated geosphere data used for NE-UG-BC, this case includes additional modifications to the geosphere model that improve the sealing of the repository. Backfill access tunnels and ring tunnels are filled with concrete and bentonite seals have been added through the access tunnel EDZ. The initial repository void volume is $3.07 \times 10^5 \text{ m}^3$ compared to $3.37 \times 10^5 \text{ m}^3$ for the base case.

The results show that the additional sealing has little effect in general. There is a minor increase in peak pressure reported of approximately 0.5MPa over the duration of the simulation compared to NE-UG-BC. However, the peak is still low compared to the base case NE-BC and it is expected that both NE-UG-BC and NE-UG-RD1 will continue to tend to the initial steady state pressure at the repository horizon (see Figure 5-66). Over the period of 10^6 years very little water enters the repository compared to the base case, but the amount which enters for NE-UG-RD1 is slightly less than the amount which enters for NE-UG-BC in the final stages. See Figure 5-67 and Figure 5-68 for the total water balance and saturation.

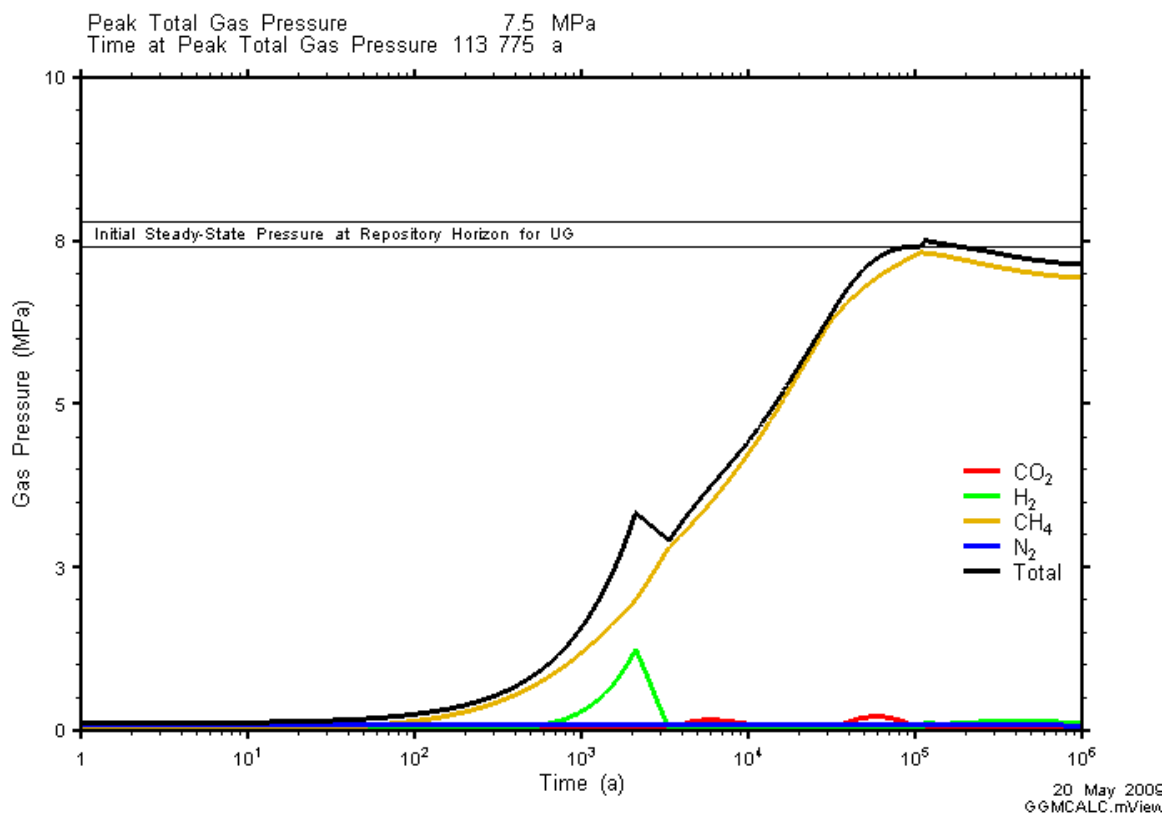


Figure 5-66: NE-UG-RD1: Total and Partial Gas Pressures with the Repository

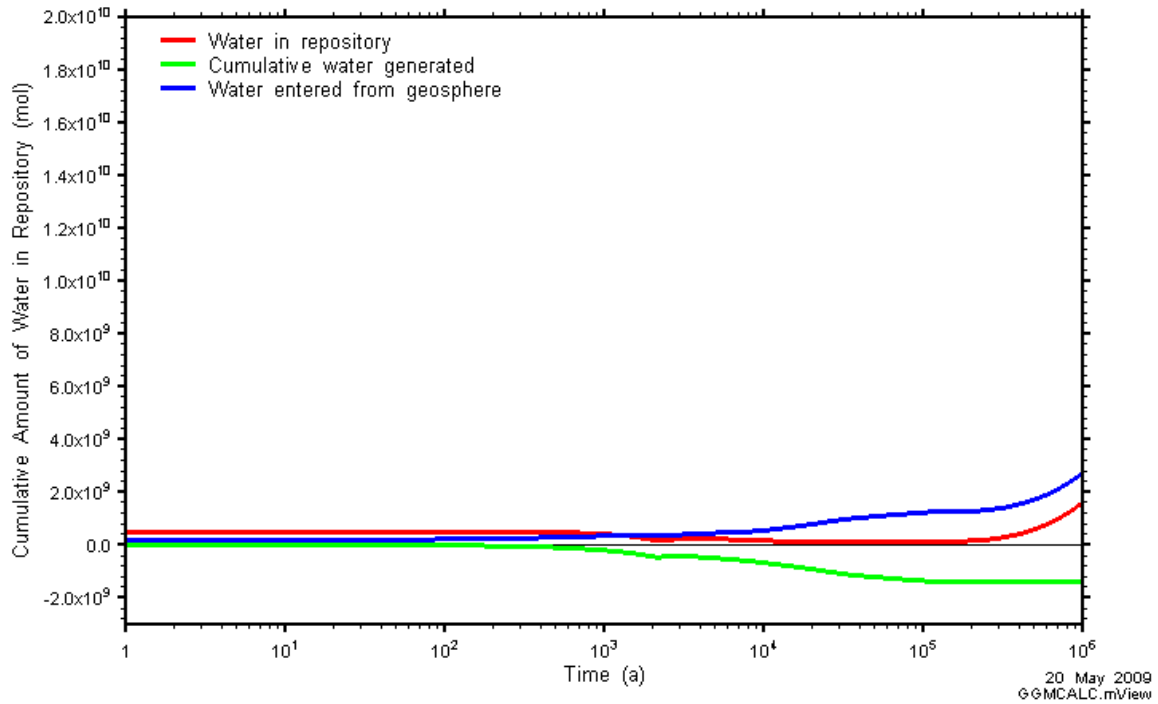


Figure 5-67: NE-UG-RD1: Water Balance

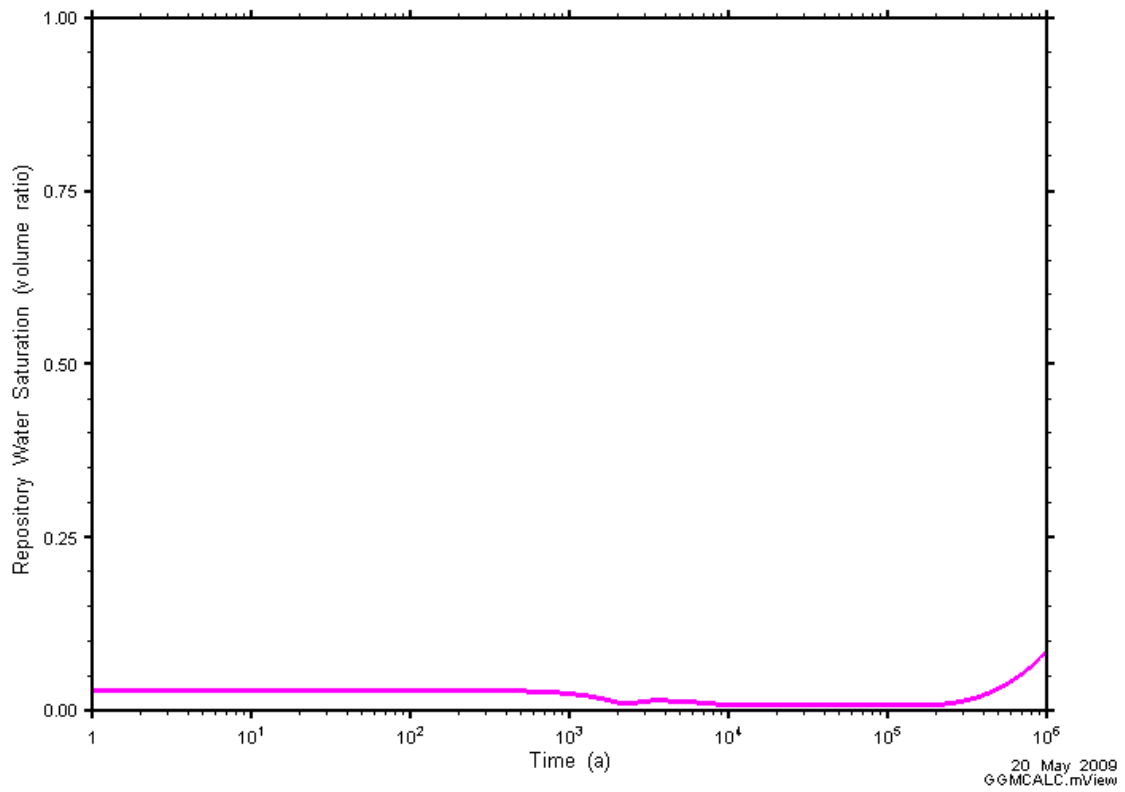


Figure 5-68: NE-UG-RD1: Water saturation

5.7.2 Gas and Water Flows

The NE-UG-RD1 case simulated a ring tunnel backfilled with concrete, effectively extending the monolith out to the repository and eliminating rockfall above the ring tunnel. The updated geosphere is used, and consequently, comparisons are made to the NE-UG-BC rather than the NE-BC.

Dissolved gas flow rates and cumulative mass are very slightly greater than the NE-UG-BC, see Figure 5-69 and Figure 5-70. As with the NE-UG-BC, no gas travels across the ORD or SALF planes, except for small amounts of initial gas from the shaft.

The small difference between the NE-UG-BC and the NE-UG-RD1 case highlights the general effectiveness of the UG base case at containing gas and dissolved gas. Backfilling the ring tunnel had the minor effect of decreasing the repository void volume, resulting in a small increase in repository pressure and a consequent slight increase in the amount of gas leaving the repository. As in the NE-UG-BC, the gas primarily leaves the repository through the rock mass: of the 16% of generated gases leaving the repository, approximately 0.2 % leaves through the ring tunnel (and into the concrete monolith and shaft).

A detailed description of results is presented below.

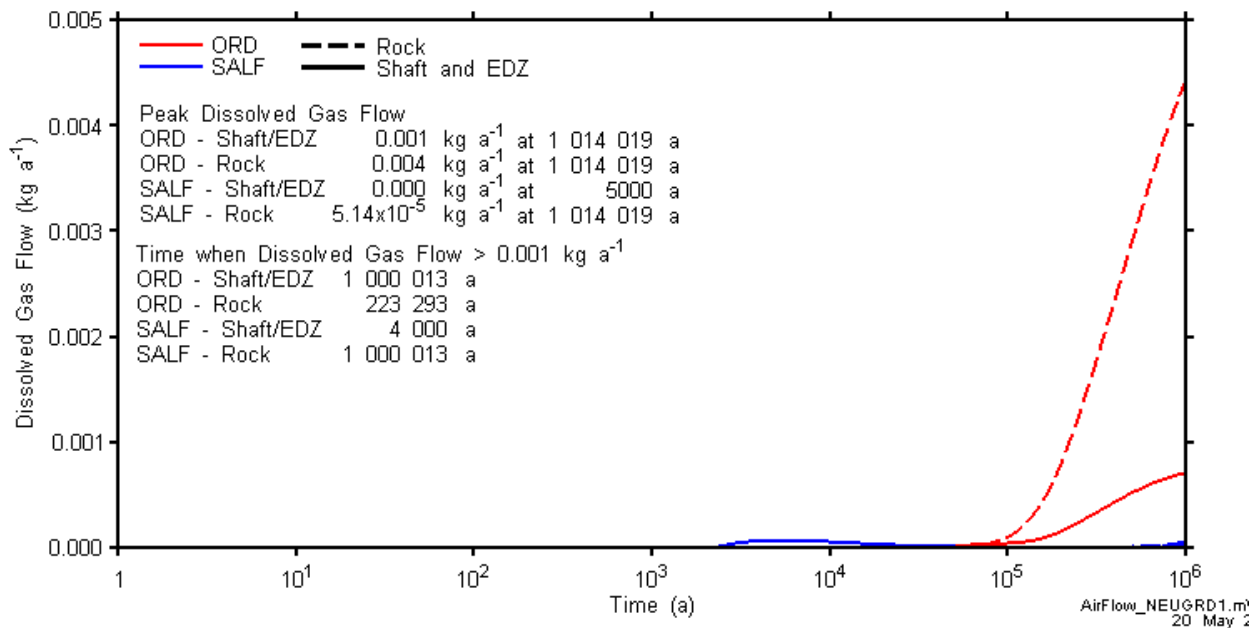


Figure 5-69: Dissolved gas flow rates across the ORD and SALF planes for the NE-UG-RD1 case. Note different y-axis scale in comparison to the NE-UG-BC.

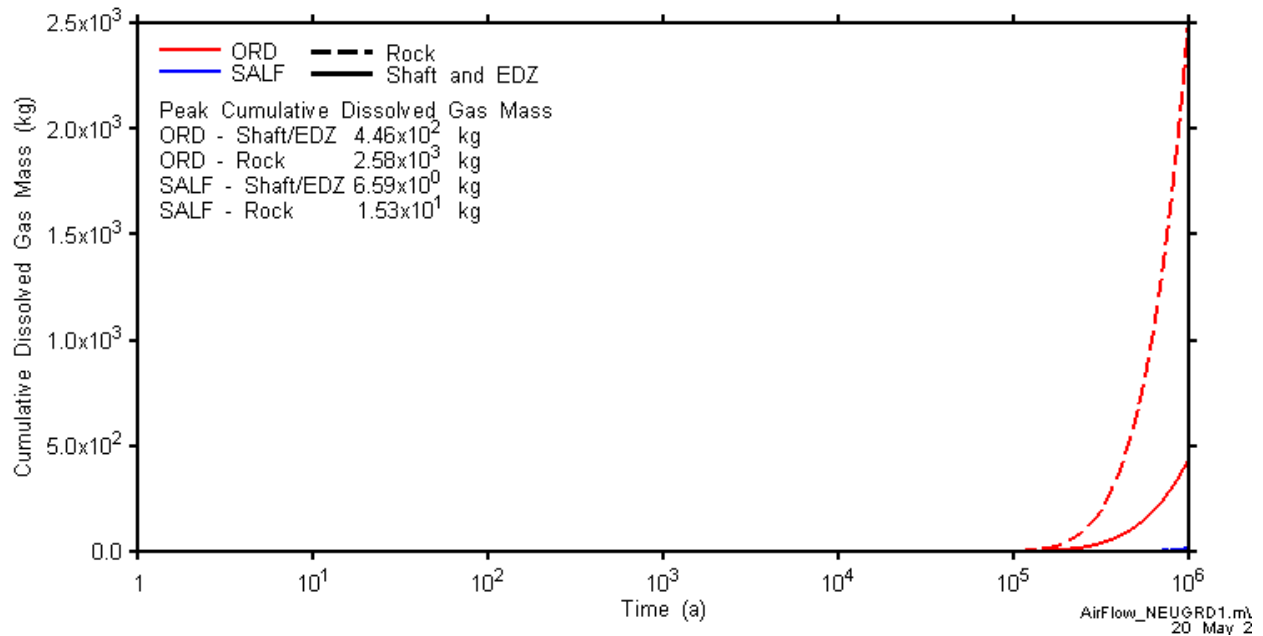


Figure 5-70: Cumulative dissolved gas mass crossing the ORD and SALF planes for the NE-UG-RD1 case. Note different y-axis scale in comparison to the NE-UG-BC.

5.7.2.1 Detailed Description of Gas, Dissolved Gas and Water Transport

As might be expected based on the key parameters, the flow of gas and water is very similar to the NE-UG-BC, with a few differences.

- With less void volume in the ring tunnel, generated gas is pushed down into the repository EDZ below the ring tunnel and the repository close to the ring tunnel. See Figure 5-71 for gas saturations, gas and water flows, repository water saturation and pressure at early times.

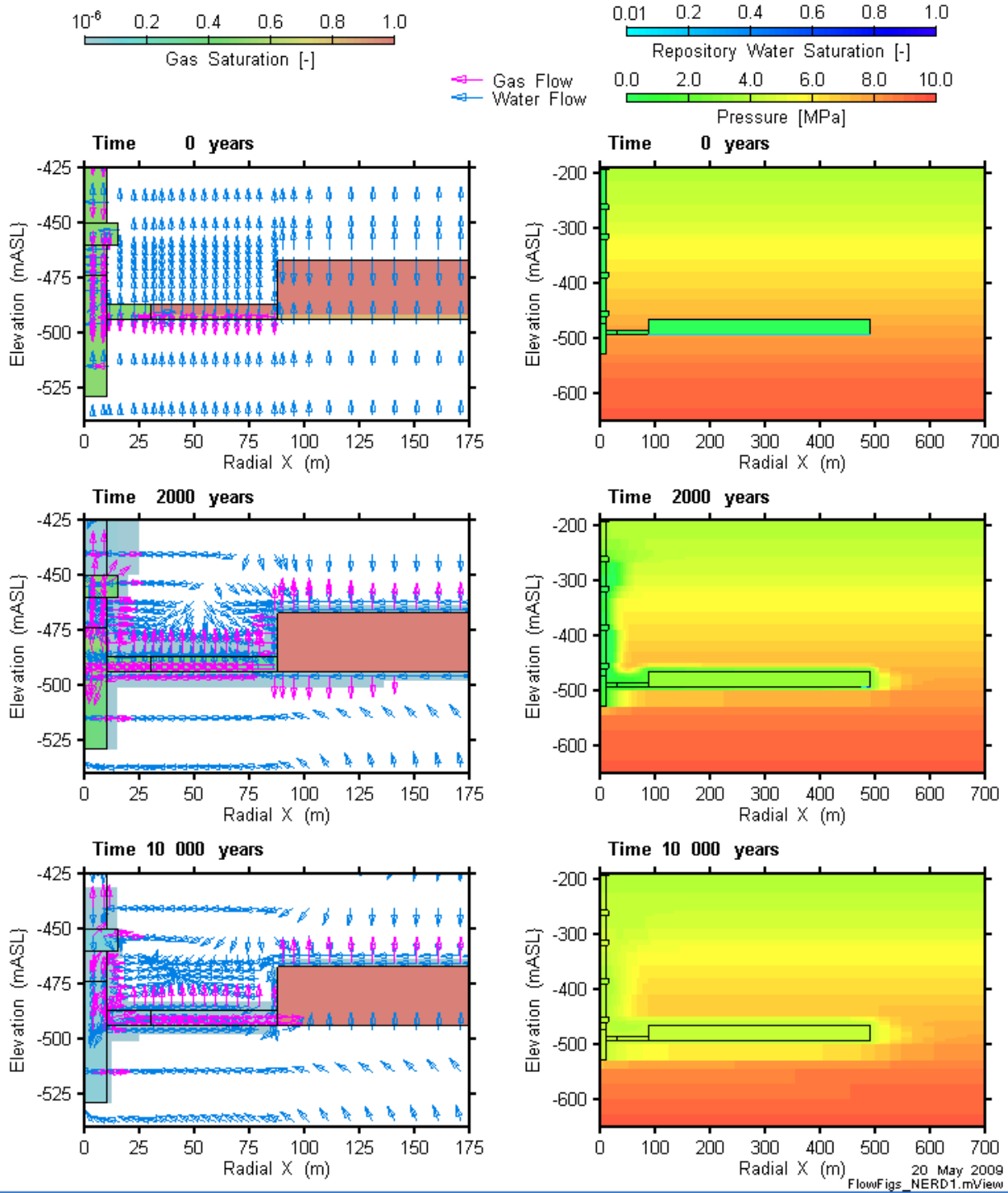


Figure 5-71: Evolution of conditions for the NE-UG-RD1 case at the start of the simulation (0 years), 2000 years, and 10 000 years. Gas saturation, and gas and water flow (outside repository) are shown in the figures on the left, and pressure and repository water saturation in the figures on the right.

- As well, by the end of the simulation, gas has not penetrated as far into the rock mass (slightly), due to the greater distance of the repository from the relatively permeable shaft EDZ. Gas saturations greater than 10^{-6} are still confined to a few meters from the repository, see Figure 5-72.

With the exception of detail at the ring tunnel, dissolved gases are indistinguishable from the NE-UG-BC.

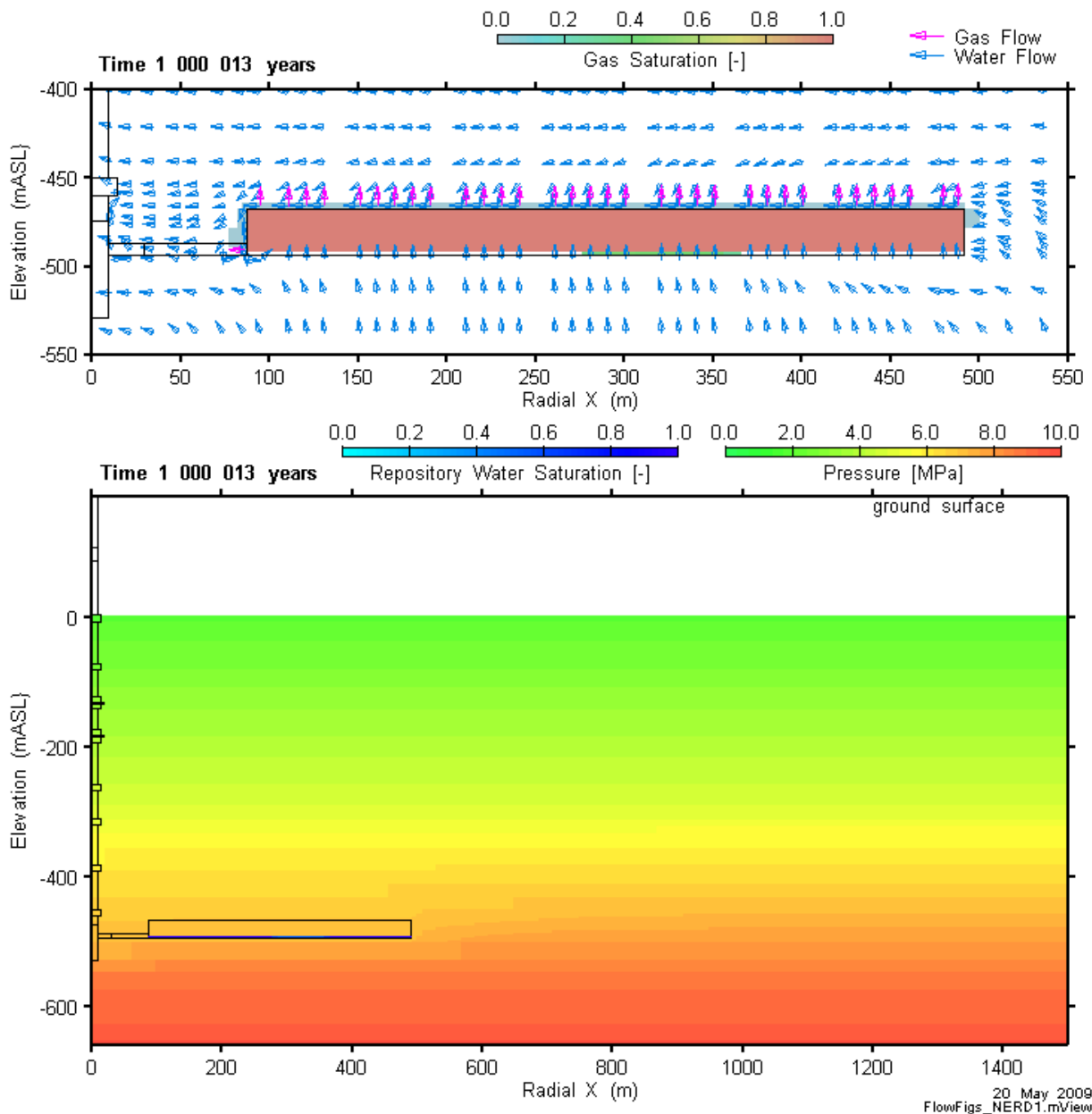


Figure 5-72: Evolution of conditions for NE-UG-RD1 simulation at 1 000 000 years. Gas saturation, and gas and water flows (outside repository) are shown in the figure above, and pressure and repository water saturation in the figure below.

5.8 CASE NE-UG-GT – UPDATED GEOSPHERE PERMEABILITIES AND INITIAL GAS SATURATION IN THE ORDOVICIAN

5.8.1 Gas Generation

Compared to the base case, this includes lower permeabilities in the Silurian and Ordovician sediments, and some initial gas within the Ordovician rocks (10% gas, compared to 0% in the base case).

The initial gas pressures within the geosphere are sufficiently high that gas enters the repository for the duration of the simulation, as shown in Figure 5-73 . The amounts of gases within the repository are shown in Figure 5-74. Current site characterization data suggests that the gas in the geosphere is mainly methane, with some CO₂. Approximately 3.8×10^8 moles of natural methane gas enters the repository, with the remaining inventory at the end of the simulation having been generated within the repository.

Another feature of this case is that the water saturation effectively reaches zero at approximately 1000 years (see Figure 5-75). This is accompanied by a sudden drop in the relative humidity (Figure 5-76). In the present calculation, microbial reactions were assumed to proceed at their normal rate even at low humidity and saturation, consuming water and producing gases. The additional water consumed is effectively drawn in from the geosphere, and the relative humidity is allowed to increase back up to its original value near 100%. Test simulations have shown that the recovery of the relative humidity is an artefact of the water being drawn in from the geosphere, and relative humidity is likely to remain very low beyond 1000 years for this case.

Allowing the degradation reactions to proceed at their normal rate once the system is water limited is believed to be conservative with respect to gas generation. A more realistic model would limit the rate at which water is consumed by gas generation reactions to balance the rate at which it enters the repository from the geosphere. This may consequently cause the relative humidity within the repository to drop and remain below the threshold for microbial activity. It would slow degradation and corrosion significantly until such time that the relative humidity and saturation recovered.

The continued gas generation and influx of gas from the geosphere results in a peak gas pressure of 9.8 MPa at approximately 10^6 years. Repository gas pressures are shown in Figure 5-77.

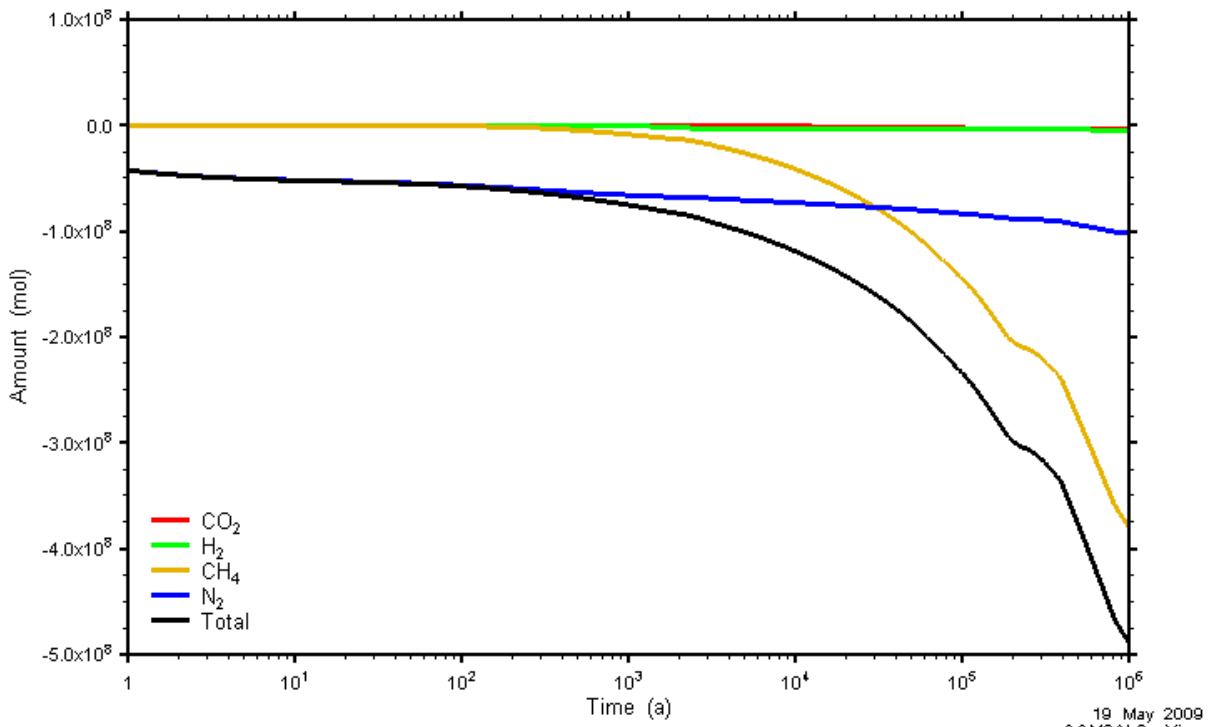


Figure 5-73: NE-UG-GT: Amounts of Gases which have Left the Repository. (Negative values indicate that gas has entered the repository.)

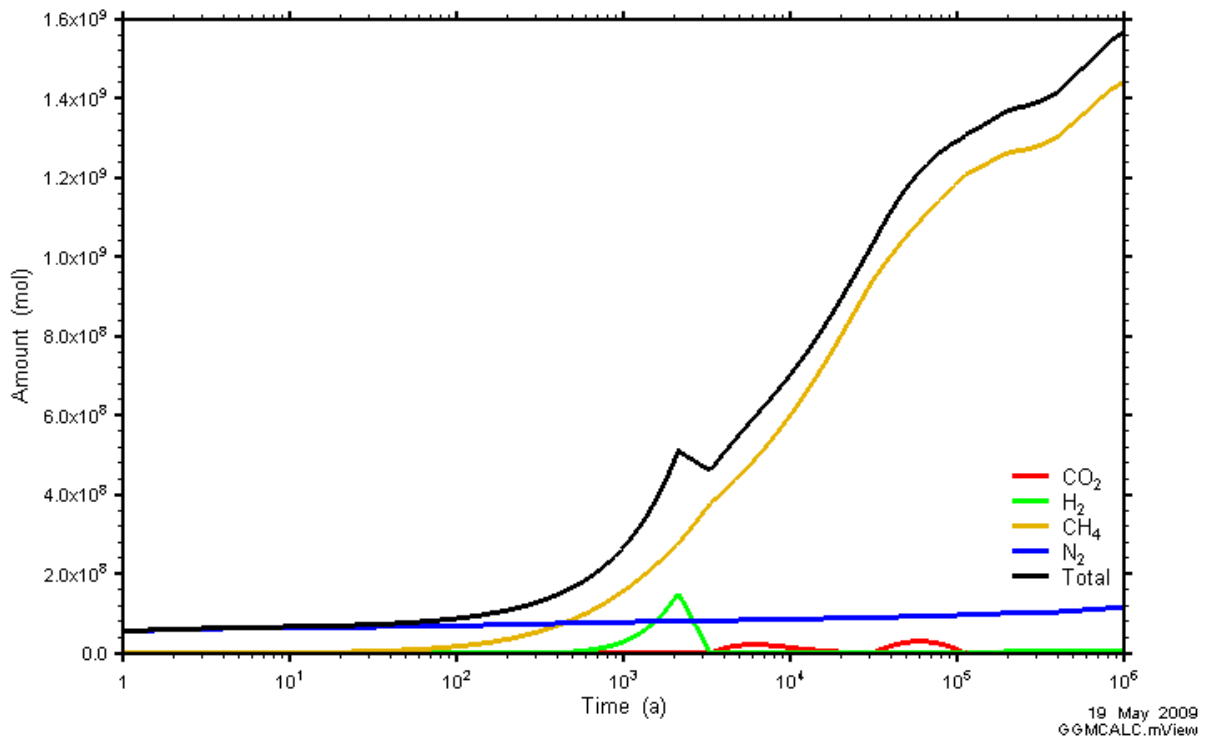


Figure 5-74: NE-UG-GT: Amounts of Gases within the Repository

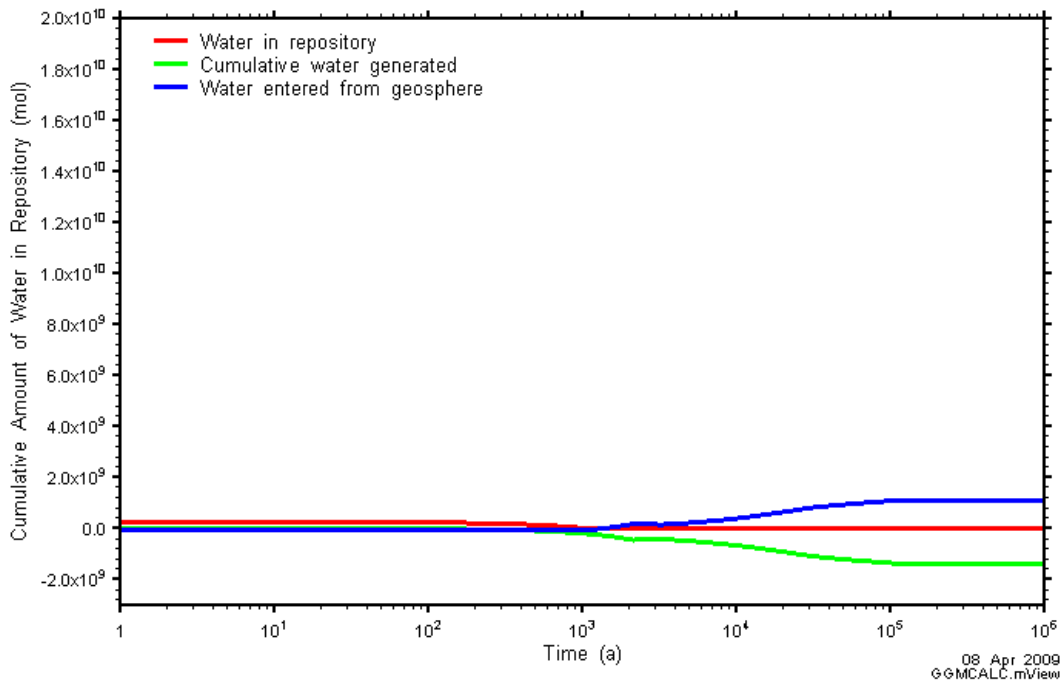


Figure 5-75: NE-UG-GT: Water Balance

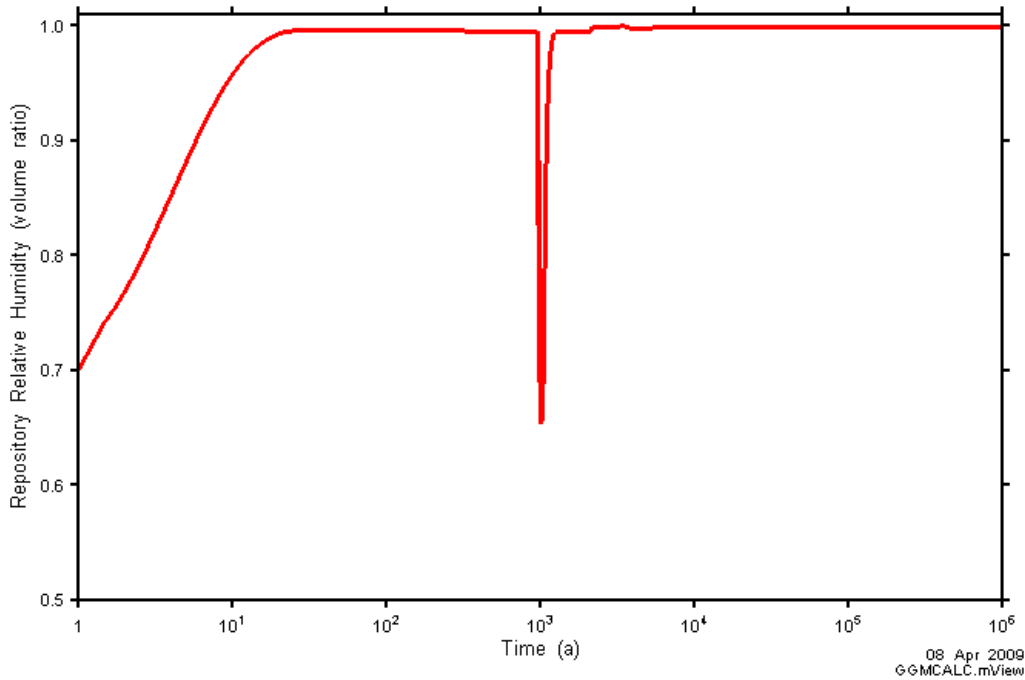


Figure 5-76: NE-UG-GT: Relative Humidity

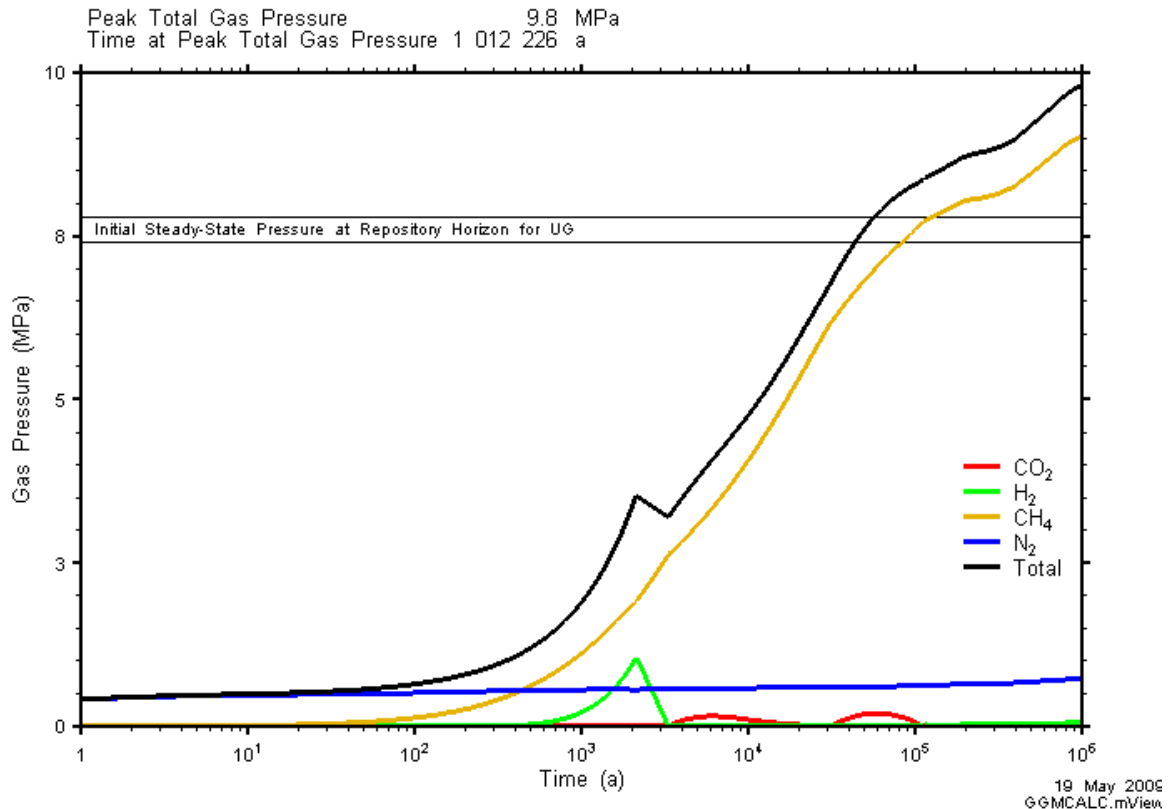


Figure 5-77: NE-UG-GT: Total and Partial Gas Pressures with the Repository

5.8.2 Gas and Water Flows

The NE-UG-GT case is identical to the NE-UG-BC, except initial gas saturations in the Ordovician sediments are set to 10% compared to 0% for the NE-UG-BC.

The initial pressures in the geosphere for a case with initial gas saturations are uncertain. Site characterization data does not provide any in-situ gas pressures, only water pressures. All previous cases assume initial water pressures at steady-state pressure (and no gas saturation), site characterization data suggests under-pressures in the Ordovician sediments (see Figure 2-3).

Two options are possible for initial pressures for the NE-UG-GT case:

- (1) Assume water pressures in the Ordovician sediments are hydrostatic, as in the NE-UG-BC. With this assumption, gas pressures will be very high due to the high capillary pressures of the Ordovician units. For example, in the Cobourg unit at the repository horizon, the initial water pressure in the rock mass at -480 mASL is 7.6 MPa and with a capillary pressure of 14.7 MPa for a gas saturation of 10 % (calculated from equation 4-1), the initial gas pressure in the rock mass would be 22.3 MPa (gas pressure = water pressure plus capillary pressure, with gas pressures always greater than water pressures).
- (2) Assume gas pressures in the Ordovician sediments are equal to the hydrostatic water pressures. Since the high capillary pressures of the Ordovician rocks for a gas saturation of 10 % would result in large negative water pressures (e.g., based on the

above example, the Cobourg unit would have an initial gas pressure of 7.6 MPa and initial water pressure of -7 MPa), which is conceptually and physically incorrect, the initial pressures, both gas and water, would need to be corrected to ensure the minimum water pressure is 0 MPa. Consequently, water pressures are assumed equal to 0 MPa or the difference between the hydrostatic water pressure and the capillary pressure, whichever is greater, and gas pressures are calculated by adding the capillary pressure to the water pressure. For the Cobourg unit at -480 mASL, initial water pressure is 0 MPa, and initial gas pressure is 14.7 MPa. Whereas for the Sherman Falls unit at -525 mASL, with hydrostatic water pressures of 8.2 MPa and capillary pressures at 10 % gas saturation of 7.6 MPa, initial water pressure is 0.6 MPa and initial gas pressure is 8.2 MPa.

The second option was chosen for analysis of the NE-UG-GT case for two reasons: (a) a good conceptual explanation is not available for the high gas pressures in option (1), which are greater than lithostatic pressure (17 MPa) with the potential to cause fracturing of the rock mass; (b) the low water pressures provided in option (2) are consistent with the underpressures observed during site characterization, and consequently, this case may provide insight into the reasons behind the underpressures in the Ordovician sediments.

These initial gas saturations, as well as initial pressures, equilibrate within the geosphere over the course of the simulation. Gas will penetrate more pores of units with low air-entry pressures, and consequently, these units will have greater gas saturation than units with high air-entry pressure. As well, the model's fixed head bottom boundary condition at the bottom of the Ordovician Shadow Lake formation is fully saturated with water, which slowly begins to push all gas upwards. As the gas saturation changes, so does the capillary pressure, and consequently the difference between gas and water pressures. By the end of the simulation, at the repository horizon (-480 mASL), gas saturations are 4 %, gas pressures are 12.6 MPa and water pressures are 4.7 MPa. Figure 5-78 shows gas pressure, water pressure and gas saturation in the geosphere at the beginning and end of the simulation.

The low initial water pressures and high initial gas pressures in the Ordovician sediments at the repository horizon result in a gradient for water transport away from the repository, and for gas transport towards the repository, for the duration of the simulation. As shown in Figure 5-77 and Figure 5-75, this results in a slowly increasing repository pressure, which reaches 9.8 MPa by the end of the simulation, and water is expelled from the repository by 1000 years.

As previously described in Section 5.8.1, the T2GGM model assumes that if gas generation were to cease, the repository would begin to saturate with water, and consequently, there is always water available for consumption by the gas generation reactions. While this is true for all other cases, it is not true for the GT case due to the water pressure gradient out of the repository.

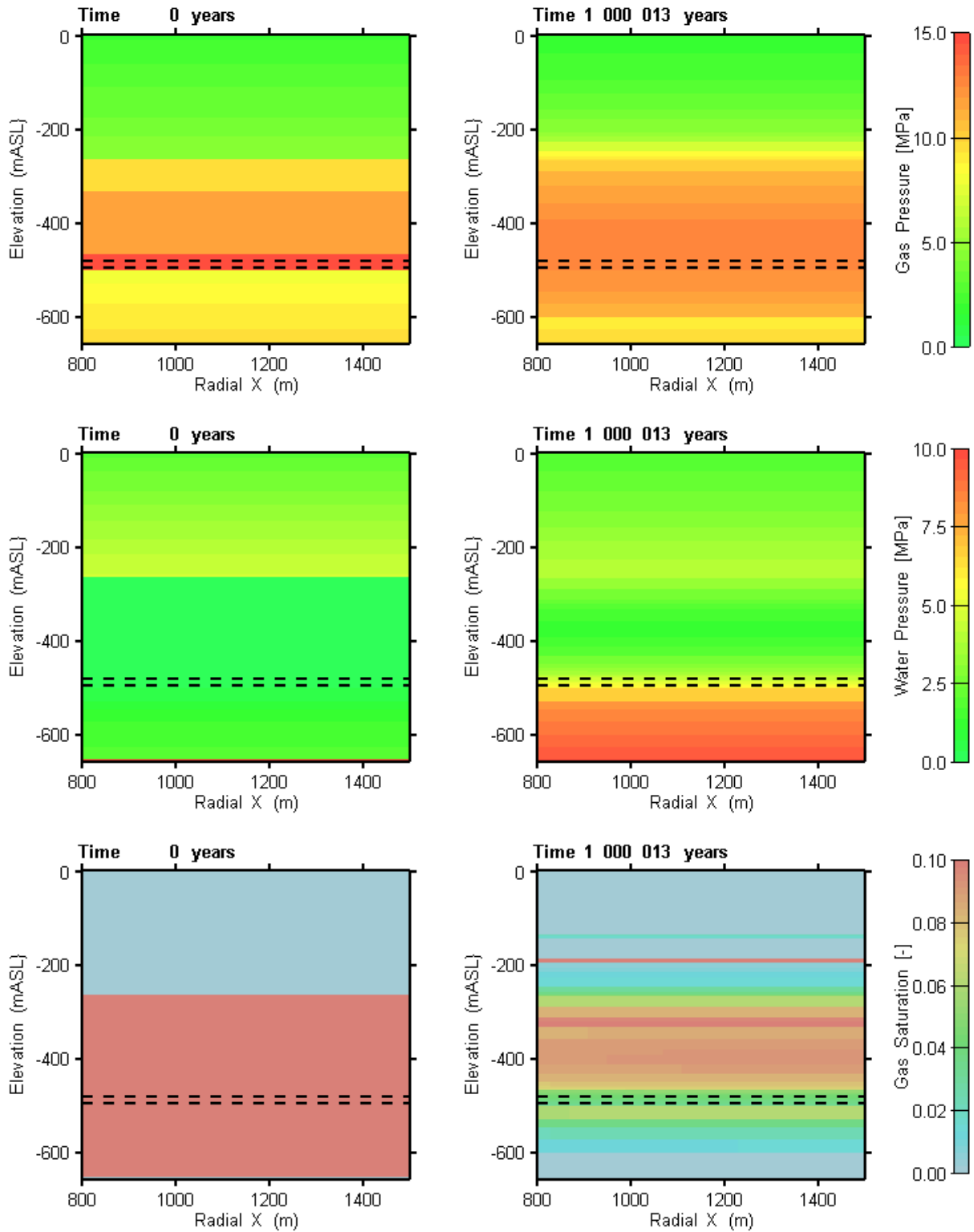


Figure 5-78: Conditions at the start and end of the simulation (0 and 1 000 000 years). Gas pressure is shown in the top two figures, water pressure in the middle two figures and gas saturation in the bottom two figures.

To determine whether the repository will remain dry without gas generation, the GT case was re-started at 1000 years, without any repository reactions. In this case, the repository was found to saturate with water after 50 000 years, and relative humidity recovered from the drop prior to 1000 years (see Figure 5-76), and was maintained close to 1 for the duration of the simulation. In this case, saturation of the repository occurs as water pressures in the geosphere exceed pressure in the repository. Repository pressures are only 3 MPa at 50 000 years (compared to 7.6 MPa at 50 000 years with gas generation), with the increase in pressure relatively slow due to the lack of gas generation.

As a consequence, the GT case presented here is conservative from a repository pressure perspective. Gas generation reactions continue as though there is always sufficient water available. In actuality, as the repository dries out, gas generation reactions requiring water will continue until any residual water is consumed, and then cease. Relative humidity might drop once residual water is consumed below a level required for microbial activity. At some point, if gas generation is slowed sufficiently, water will begin to saturate the repository, and all gas generation reactions will resume.

This case also has the limitation that is impossible to differentiate between initial gases present in the rock mass from gases generated. Consequently, gases crossing the ORD and SALF planes are not presented, as results are overwhelmed by initial gas flows. This limitation also impacts interpretation of gas migrating out of the repository. However, gas from the repository does not migrate into the rock mass, due to gas pressure gradients towards the repository. Gas from the repository does migrate out into the concrete monolith and up the shaft by 140 000 years. It should be noted that this gas will be a combination of initial and generated gases. While repository gas continues to migrate out through the shaft for the duration of the simulation, gas does not travel above -80 mASL in the shaft. Figure 5-79 and Figure 5-80 shows gas saturations, gas and water flows and pressures at 10 000 years, 140 000 years and 1 000 000 years. Gas saturations are greater in the concrete seals compared to the bentonite seals, due to the lower capillary pressure of the concrete compared to the bentonite, allowing more pores to be penetrated at a given pressure. Also note that at 1 000 000 years, gas has travelled slightly farther upwards in the rock than the shaft, due to the limitation of gas migration in the shaft and shaft EDZ by the asphalt waterstop and concrete bulkheads above the Salina A2 evaporite, and the gas migration into the permeable Salina A2 evaporite, which then migrates upwards through the rock mass.

Figure 5-80 also illustrates gas pressure, which is affected by the pressure gradient towards the repository, resulting in lower pressures near the repository. This is also reflected in the gas saturations surrounding the repository, although it is not evident in the figure as gas saturations in the rock mass are very small.

Figure 5-81 shows dissolved gases for the NE-UG-GT case, which shows dissolved gases to be greatest where gas is present. Dissolved gas concentrations are also smaller close to the repository, due to the lower gas pressures and gas saturations close to the repository.

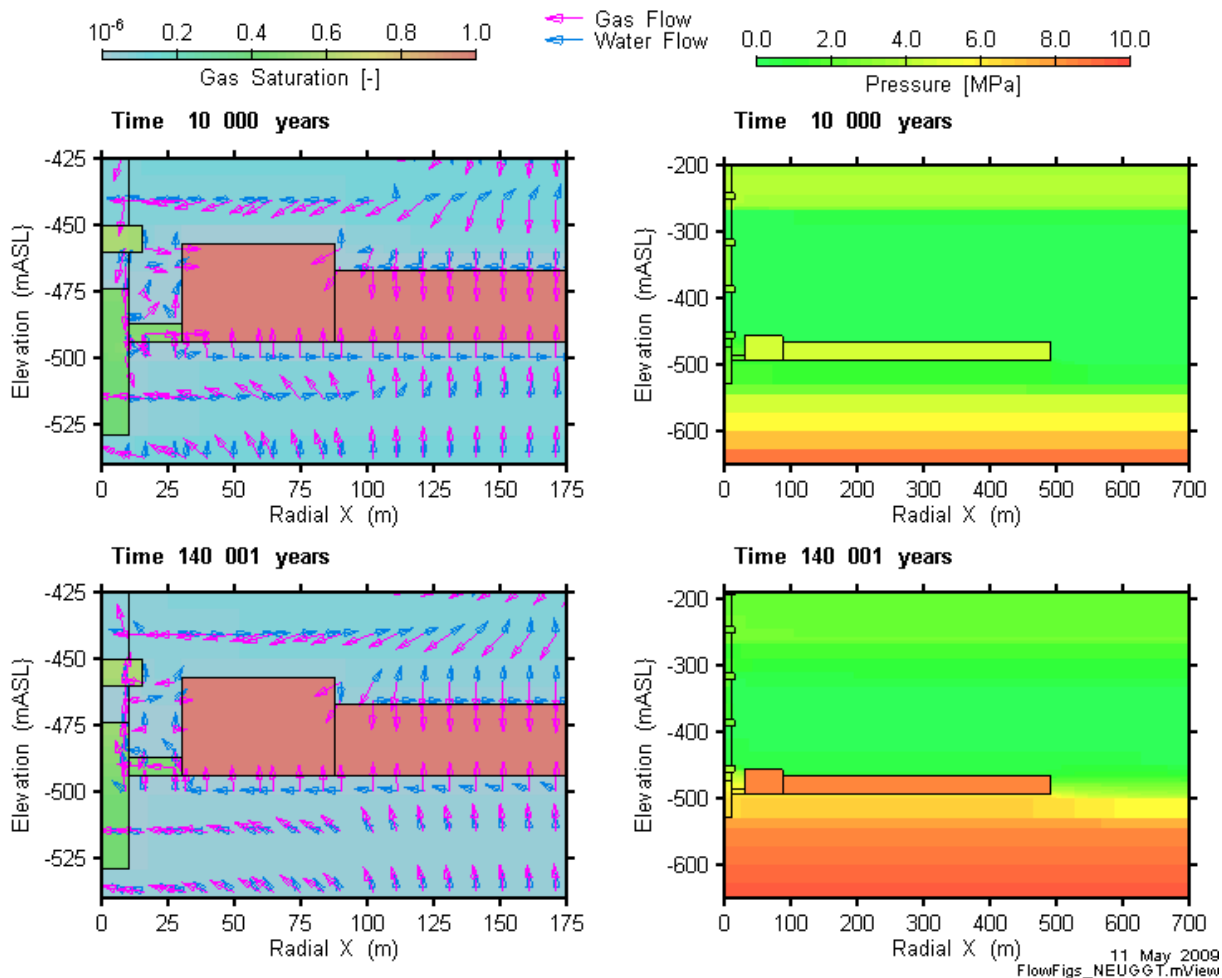
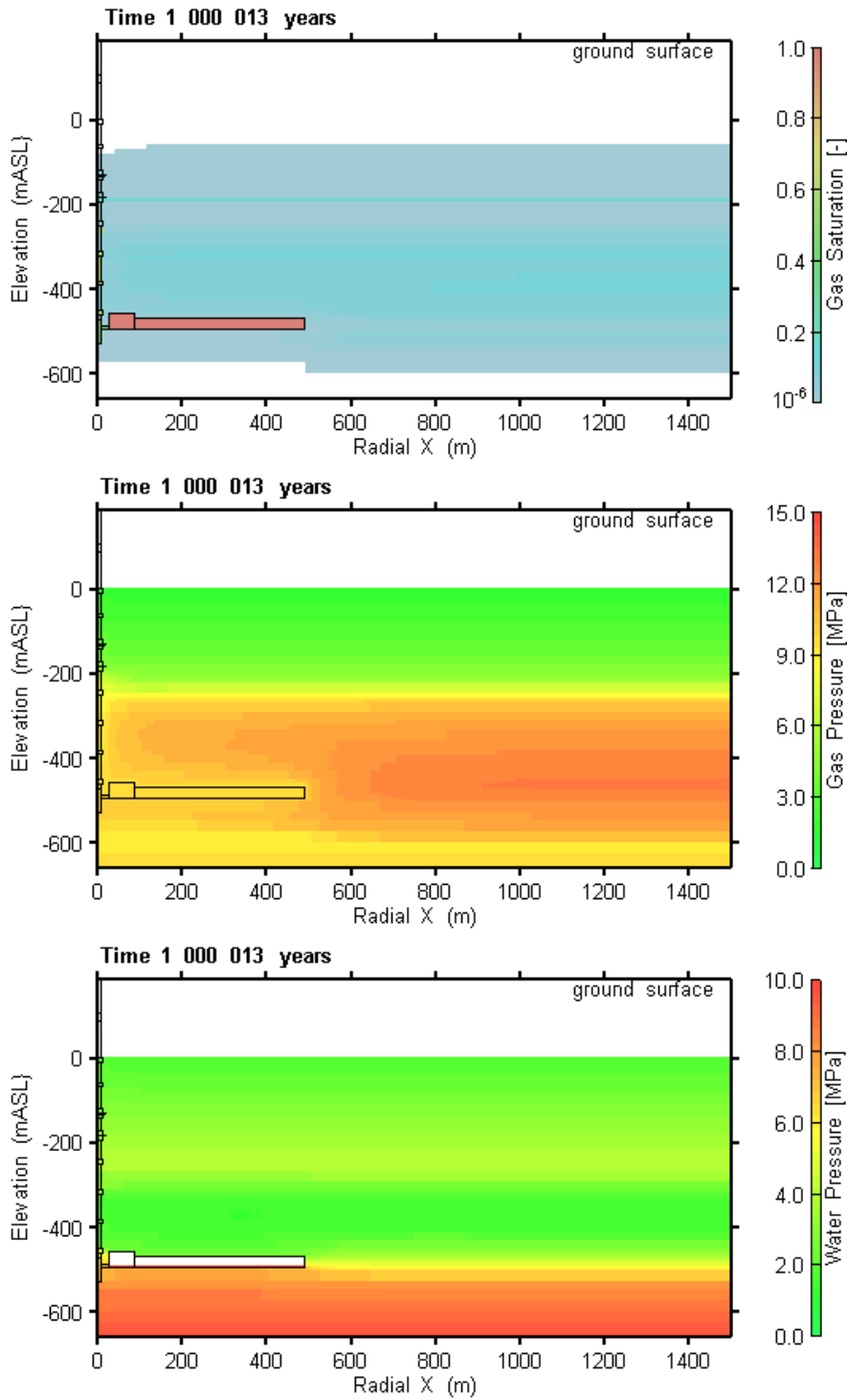


Figure 5-79: Evolution of conditions for the NE-UG-GT case at the 10 000 years, and 140 000 years. Gas saturation, and gas and water flow (outside repository) are shown in the figures on the left, and pressure in the figures on the right. Note that pressures are water pressures, except in the repository, where they are gas pressures.



11 May 2009
FlowFigs_NEUGGT.mView

Figure 5-80: Evolution of conditions for the NE-UG-GT case at 1 000 000 years. Gas saturation is shown in the figure above, and gas pressure in the middle figure and water pressure below.

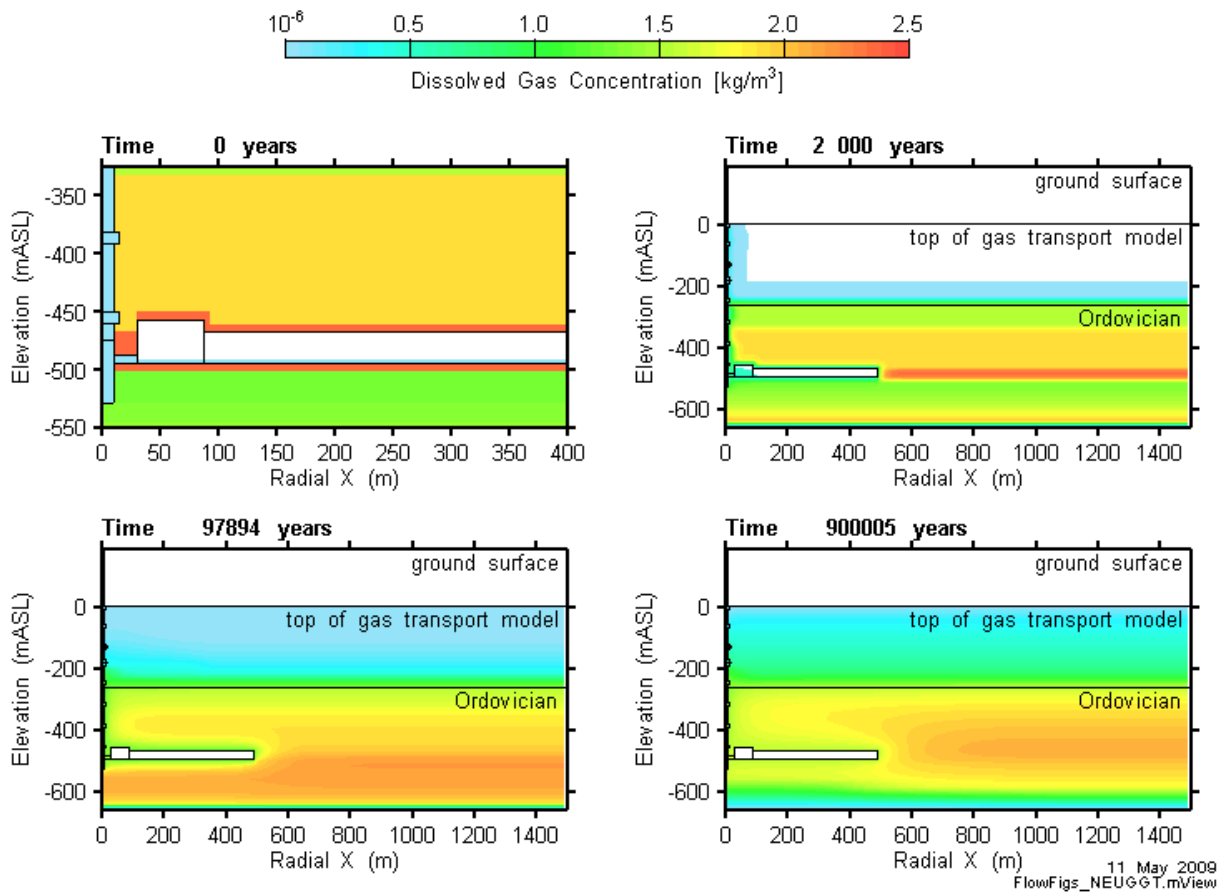


Figure 5-81: Dissolved gas concentrations at 0, 2000, 100 000 and 1 000 000 years for the NE-UG-GT case. Note the different radial X and elevation scale at 0 years.

6 RESULTS FOR THE DISRUPTIVE SCENARIOS

Only a single disruptive scenario was simulated; the Severe Shaft Seal Failure Scenario (SF).

The Severe Shaft Seal Failure Scenario (SF) assumes:

- very high permeabilities in the shaft and inner shaft EDZ; and
- the concrete bulkheads and asphalt waterstops do not intersect the inner EDZ, providing a continuous pathway up the inner EDZ.

Three calculation cases are considered for the SF scenario.

6.1 CASE SF-ES1: SEVERE SHAFT FAILURE

6.1.1 Gas Generation

This differs from the base case in that the hydraulic properties of all seals, backfill and inner EDZ have been set to extreme degraded values, and the seals are not keyed into EDZ. We would expect this to enable faster ingress and expulsion of water from the repository.

The peak in water entering the repository occurs earlier than for the base case (Figure 6-1). As a result, the gas pressure rises more rapidly from atmospheric, reaching a peak earlier. The peak pressure of 7.7 MPa is lower than for the base case since the degraded hydraulic properties allow water to leave sooner, reducing the pressure within the repository (Figure 6-2). Compared to the base case, less gas has been generated by the time the peak pressure is achieved.

In addition the repository starts to resaturate after 10^5 years, similar to the NE-EDZ high permeability case and more gas leaves the repository at late times (Figure 6-3). The results are otherwise similar to the base case.

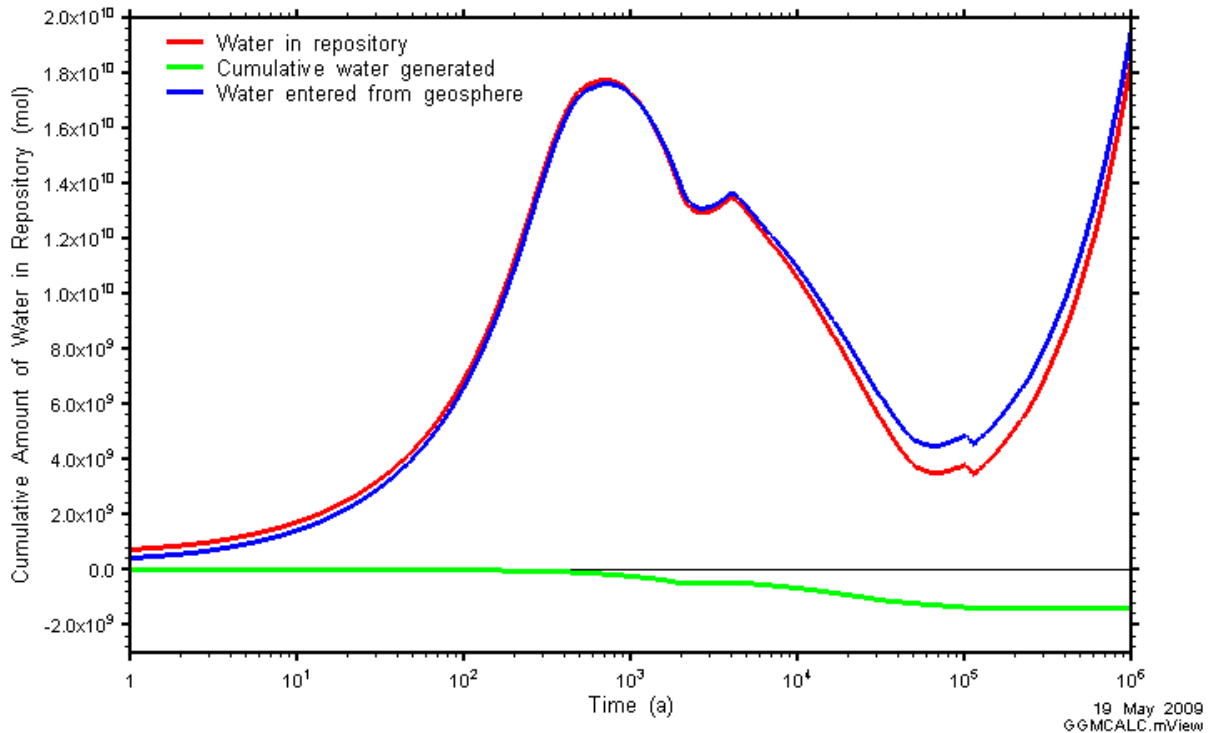


Figure 6-1: SF-ES1: Water balance

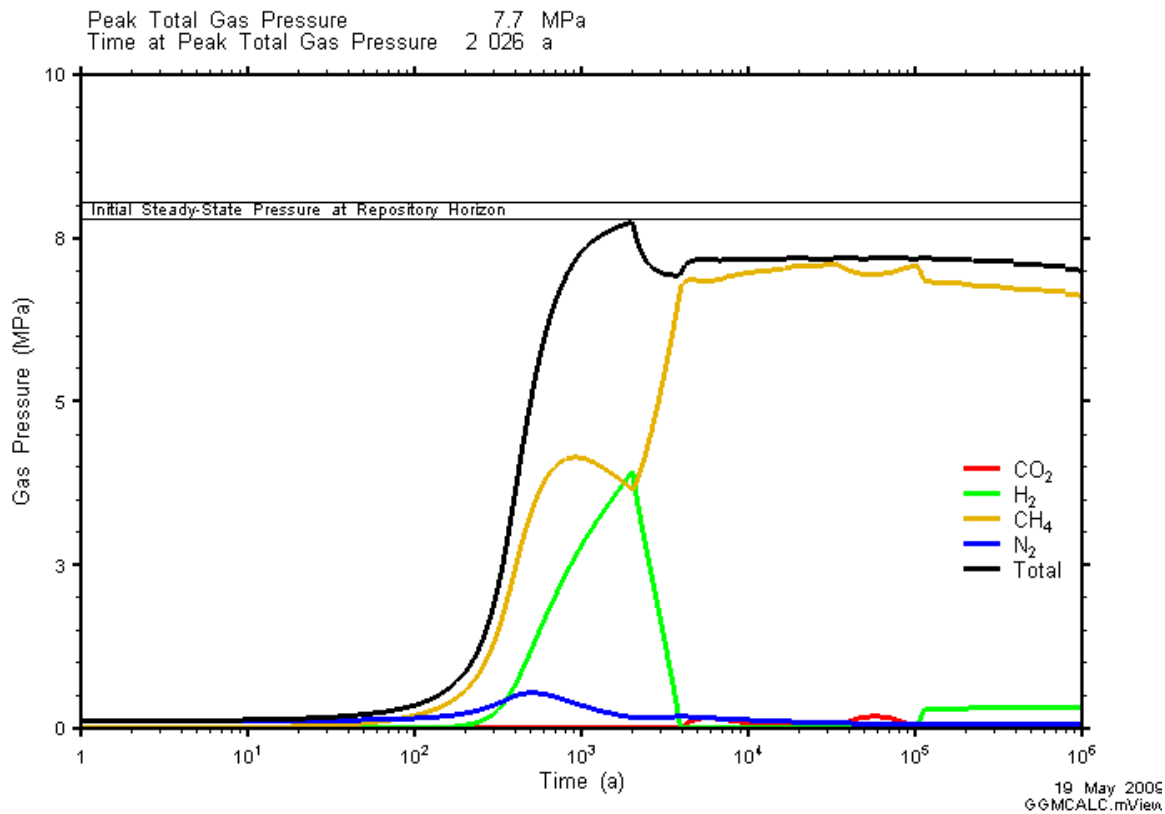


Figure 6-2: SF-ES1: Total and Partial Gas Pressures with the Repository

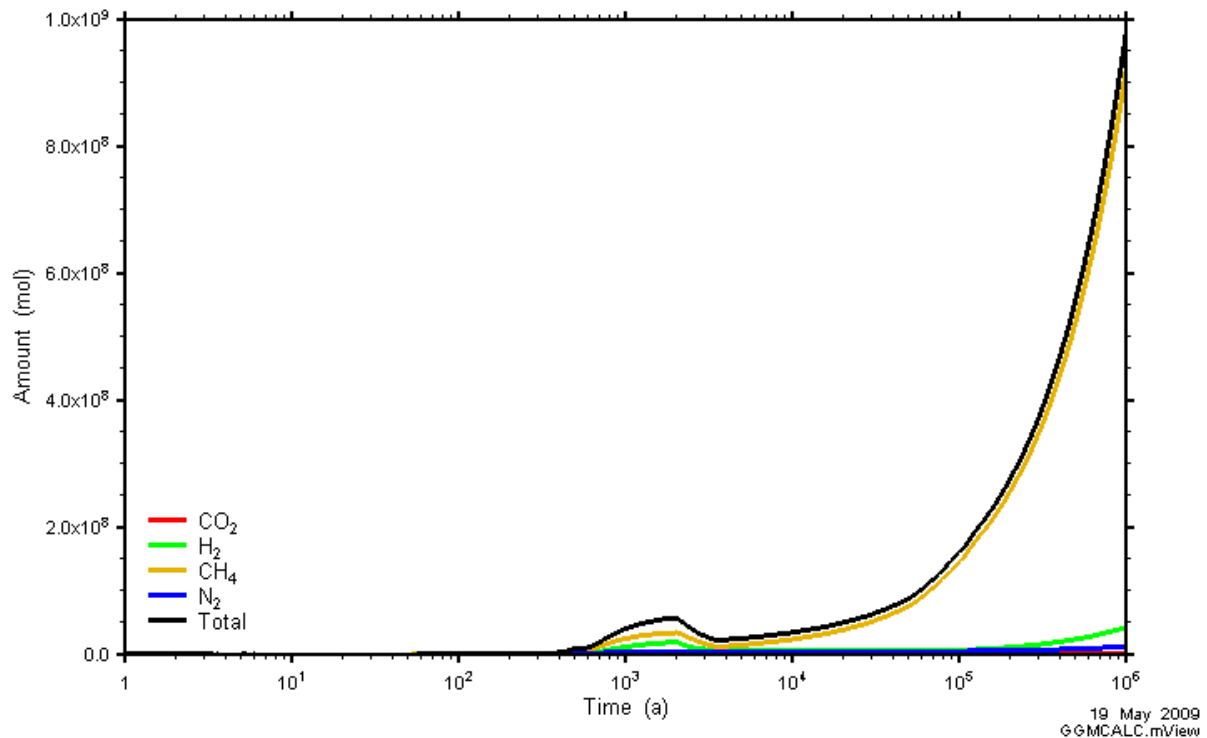


Figure 6-3: SF-ES1: Amounts of Gases which have Left the Repository

6.1.2 Gas and Water Flows

In the SF-ES1 case, all shaft and seal materials are assigned an extremely high hydraulic conductivity of 10^{-7} m/s, and the inner EDZ permeability is assumed to be four orders of magnitude greater than for rock mass. Concrete bulkheads, as well as the asphalt waterstops, are not keyed into the inner EDZ, to simulate the generation of new EDZ around these features, resulting in a continuous flow path up the inner EDZ. Failure of the seals is assumed to occur instantly for all three cases.

Results for key parameters are presented first, followed by a more detailed description of gas and water transport. Figure 6-4 provides the gas and dissolved gas flow rates and Figure 6-5 provides the gas and dissolved gas cumulative mass. No gas travels through the rock mass, although unlike the NE-BC, gas travels upwards through the shaft and EDZ through both the ORD and SALF planes. As might be expected given gas transport up the shaft and EDZ, dissolved gas transport is increased by 4 to 5 orders of magnitude in the shaft and EDZ, and one order of magnitude in the rock. Note that the cumulative mass of gas through the SALF plane is slightly greater than in the ORD plane; however, the total cumulative mass (gas and dissolved) across the SALF plane is equal to the total mass crossing the ORD plane. Consequently, the additional amount of gas crossing the SALF plane is due to dissolution of gas above the Ordovician.

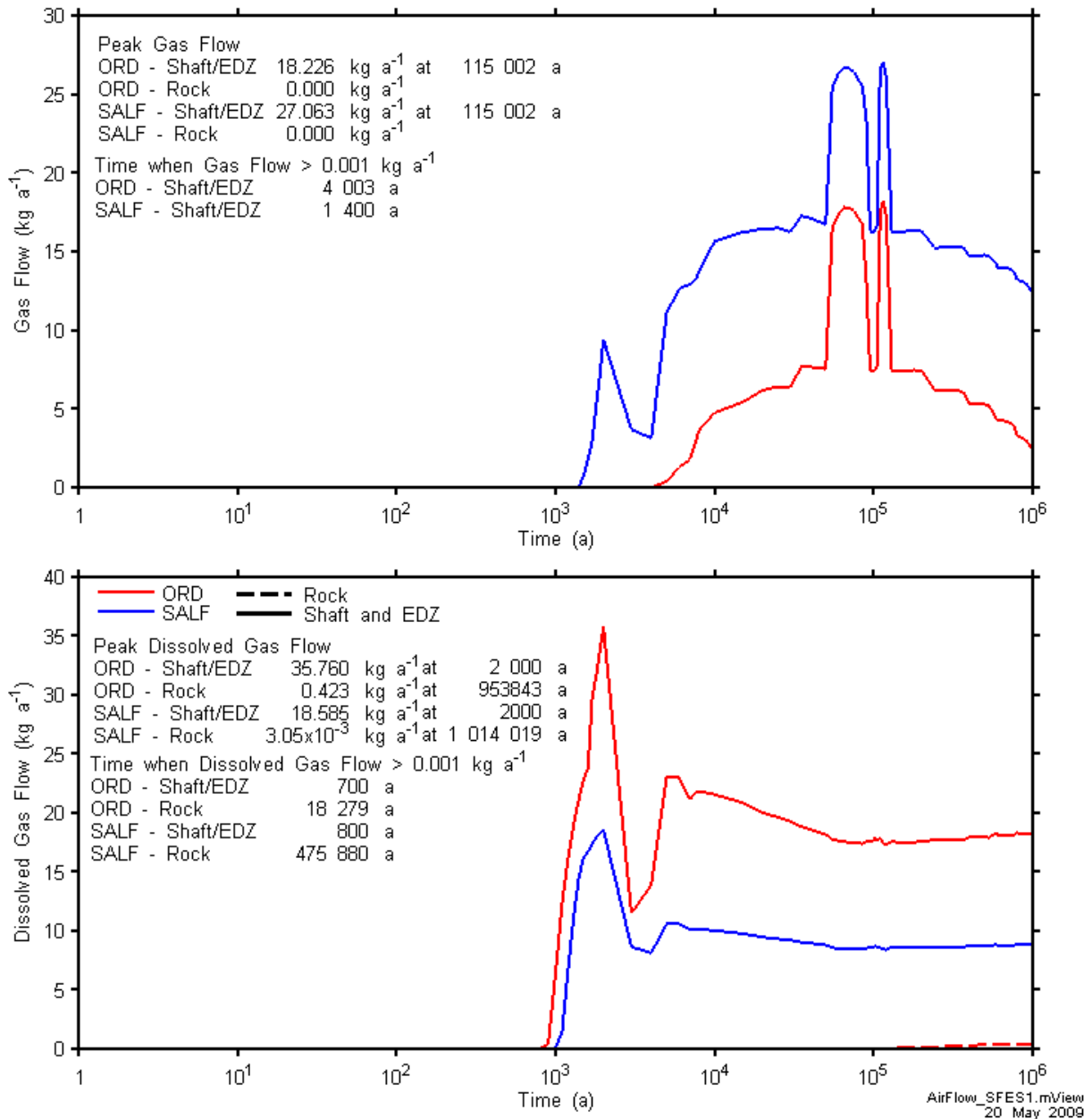


Figure 6-4: Gas flow rates across the ORD and SALF planes for the SF-ES1 case (top: gas, bottom: dissolved gas).

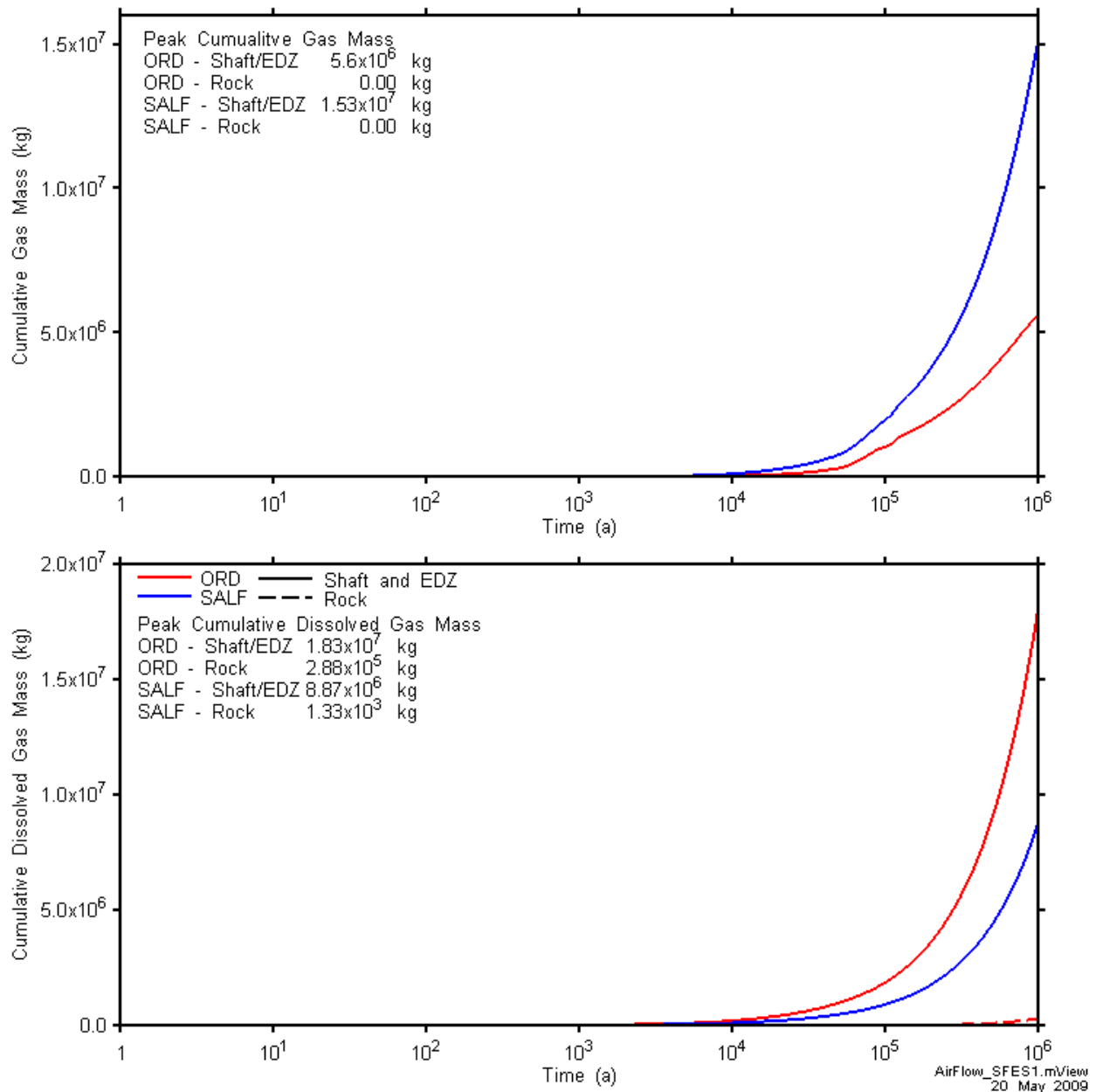


Figure 6-5: Cumulative gas mass crossing the ORD and SALF planes for the SF-ES1 case (top: gas, bottom: dissolved gas). Note different y-axis scales to comparable figures.

6.1.2.1 Detailed Description of Gas and Water Transport

While repository performance (mainly repository gas pressure and repository water saturation) is different from the NE-BC and the NE-EDZ case for the first 20 000 years, the processes of gas and water transport are very similar to the NE-EDZ case in which the shaft seal materials have their design values but the EDZ permeabilities are very high. In either case, the high permeabilities within the shaft/EDZ results in relatively quick resaturation of the shaft and repository, and minimizes transport into the rock mass. Figure 6-6 and Figure 6-7 show the gas saturation, gas and water flows, repository water saturation and pressure at 0, 200, 600, 1400 and 20 000 years. The resaturation process can be described as follows.

- Resaturation of the shaft occurs more quickly than in the NE-EDZ case, with the complete shaft fully saturated with water by 200 years.
- Repository water saturation peaks at 0.86 at 560 years.
- Gas migrates into the rock mass above the repository EDZ by 600 years.
- At 1400 years, dissolved gas comes out of solution within the shaft and shaft EDZ. Dissolved gas from the repository is transported up the shaft, and as the dissolved gas reaches sufficient concentration at the lower pressures at the top of the shaft, gas comes out of solution. Gas comes out of solution according to Henry's law, i.e., after the partial pressure of gas ($=$ dissolved gas molar concentration / Henry's constant) is greater than the water pressure, a gas phase is created.
- By 20 000 years, the gas saturations at the top of the repository connect to the gas saturations in the shaft, providing a pathway for gas to travel from the repository up the shaft and up to the top of the model.

At 35 000 years, sufficient water has been pushed out of the repository to allow gas to migrate through the repository EDZ above the concrete monolith and into the shaft EDZ. This creates a permeable pathway along the EDZ from the repository to the top of the model, see Figure 6-7.

Gas saturations in the EDZ above the concrete monolith are slow to increase, in comparison to the NE-EDZ case, due entirely to the presence of a permeable concrete monolith in the SF-ES1 case which is not present in the NE-EDZ case. In the NE-EDZ case, once a pathway between the repository gas and the EDZ above the concrete monolith is created, the repository water saturation remains constant with increasing gas pressures relieved through gas transport into the EDZ above the concrete monolith, until repository pressures have decreased sufficiently for water to begin to saturate the repository once again.

In the SF-ES1 case, the permeable pathway for water provided by the permeable concrete monolith allows increasing gas pressures to be relieved by both pushing gas into the EDZ above the concrete monolith, as in the NE-EDZ case, as well as pushing water out of the repository and into the permeable shaft. In fact, for the SF-ES1 case, water enters the repository from the rock below the repository, and leaves through the shaft, from the time of peak pressure until the end of the simulation. The tight concrete monolith in the NE-EDZ case ensures that it is more difficult to push water out of the repository, and consequently, the path of least resistance is to push gas out into the permeable pathway of the EDZ. This explanation corresponds with the difference in the repository gas pressure curves between the NE-EDZ and SF-ES1 cases; repository gas pressures are less in the SF-ES1 case, as the gas easily pushes water out of the repository and into the shaft.

Once gas saturations in the EDZ above the repository increase to gas saturations comparable to the shaft (0.01), at approximately 55 000 years, flow rates through the ORD and SALF plane peak (see Figure 6-4). Unlike the NE-EDZ case, gas remains in the shaft and EDZ, and does not penetrate rock mass adjacent to the shaft during these times of peak gas flow through the shaft (due to the greater permeabilities available in the shaft). As the repository gas pressures decrease slightly, gas flow into the shaft decreases.

At approximately 100 000 years, there is an increase in the gas generation rate, causing a small increase in repository gas pressure, and corresponding increase in the flow of gas up the EDZ as shown in Figure 6-4.

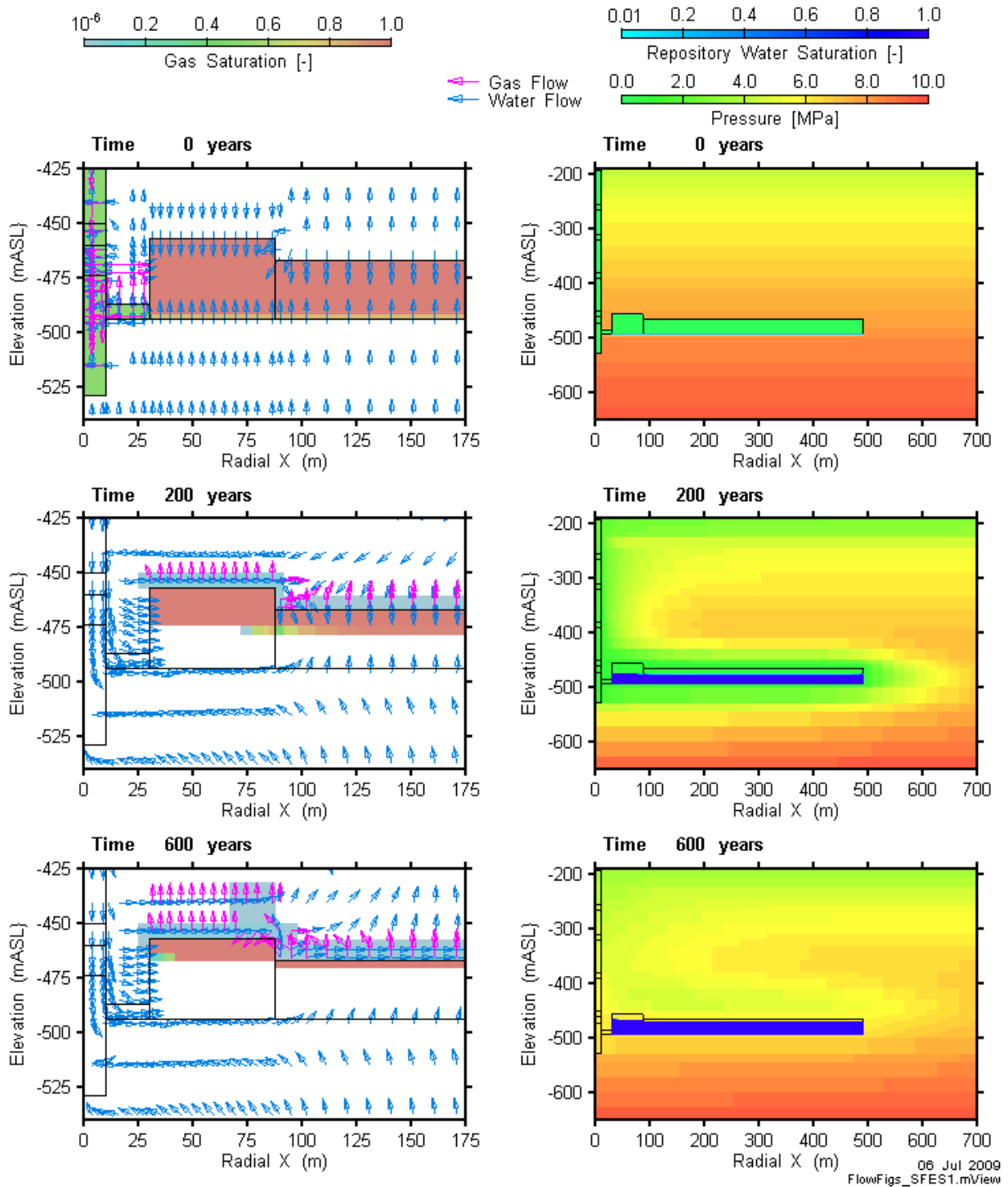


Figure 6-6: Evolution of conditions for the SF-ES1 case at the start of the simulation (0 years), 200 years, and 600 years. Gas saturation, and gas and water flow (outside repository) are shown in the figures on the left, and pressure and repository water saturation in the figures on the right.

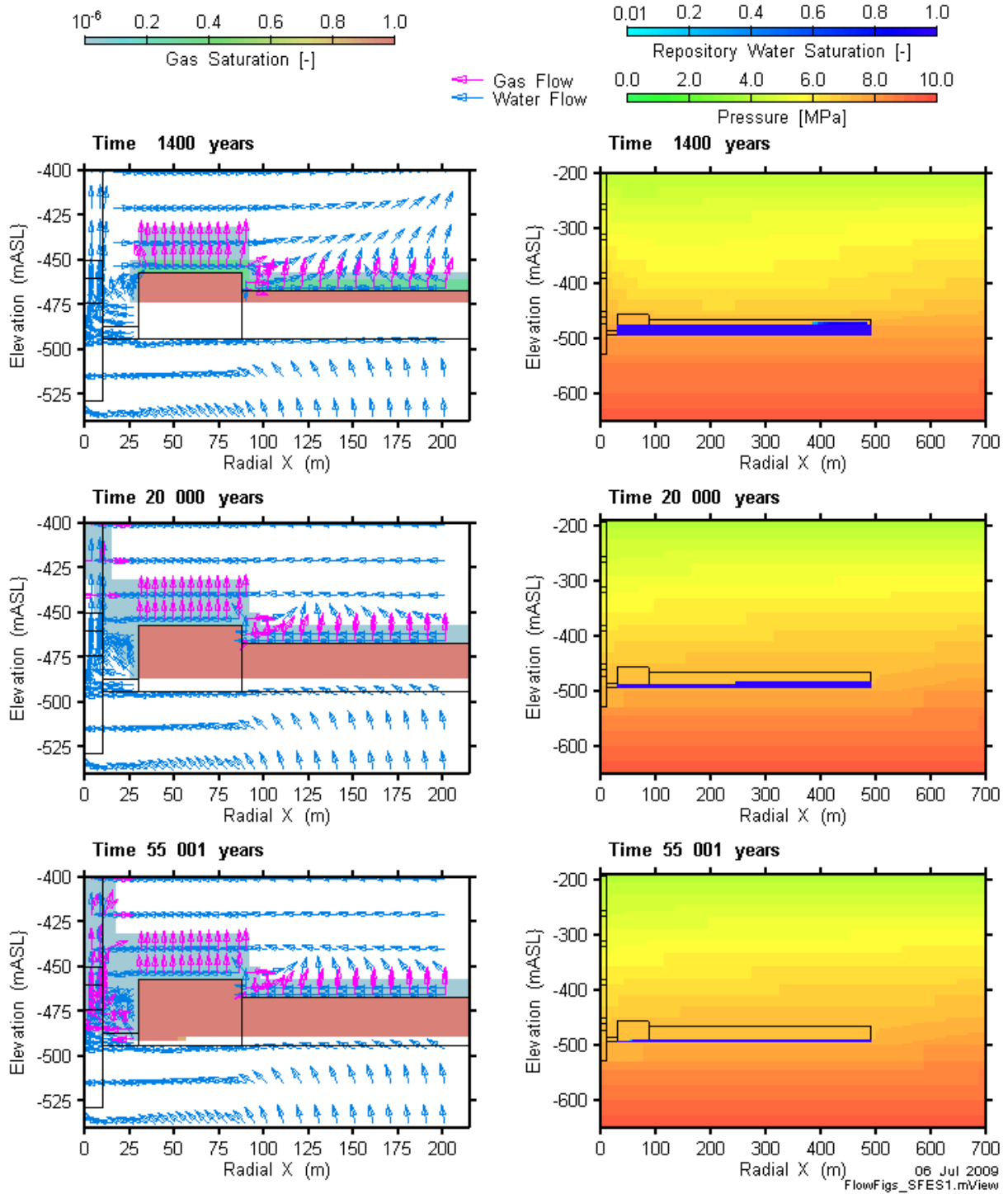
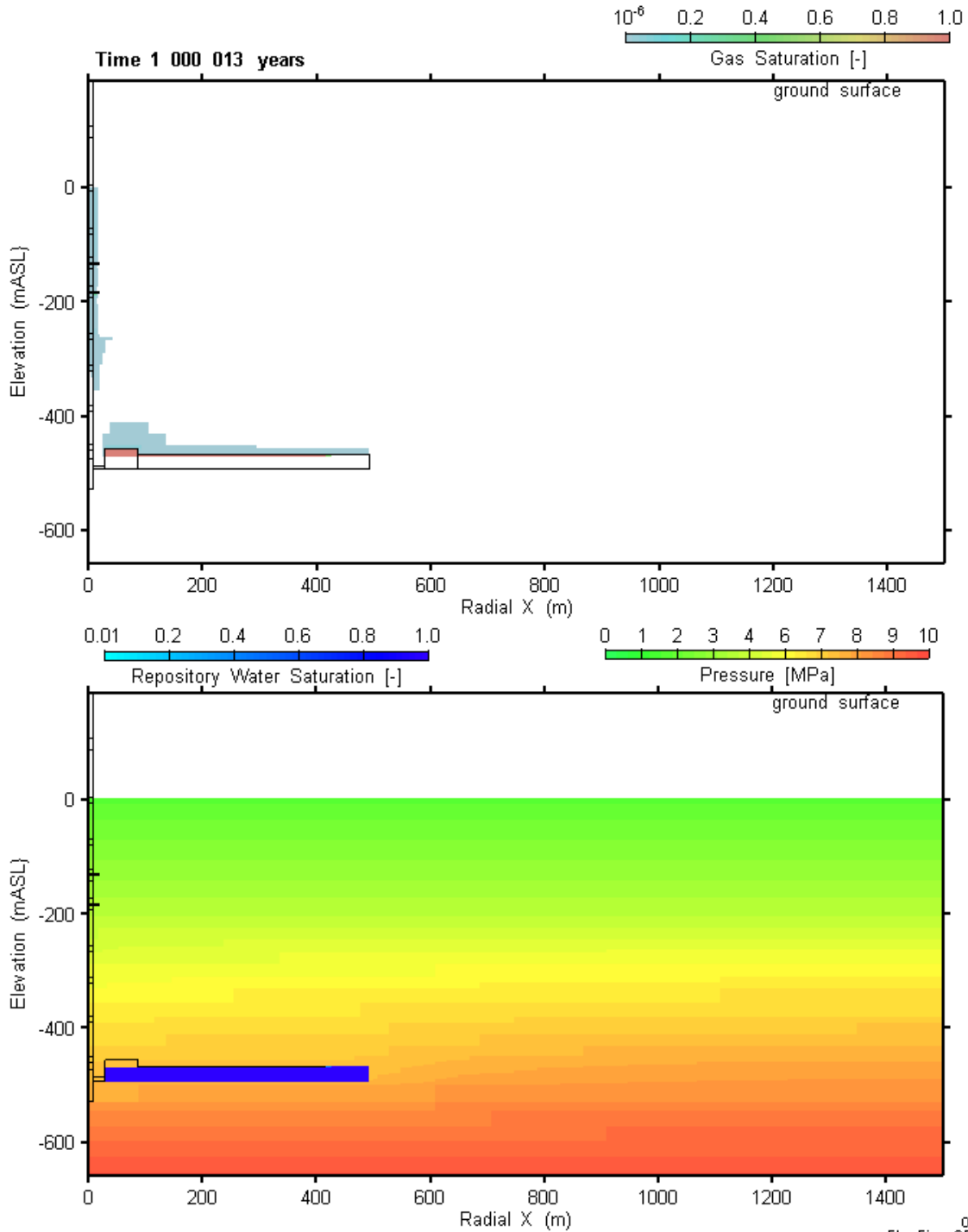


Figure 6-7: Evolution of conditions for the SF-ES1 case at 1400 years, 20 000 years, and 55 000 years. Gas saturation, and gas and water flow (outside repository) are shown in the figures on the left, and pressure and repository water saturation in the figures on the right.

After a decrease in water saturation to 0.16 at 114 000 years, the repository begins to resaturate, reaching a water saturation of 0.89 by the end of the simulation. As the repository resaturates, the connection of gas along the EDZ in the monolith is broken (at approximately 240 000 years), and the gas in the monolith dissolves. Gas continues to go up the shaft, but by way of the rock mass between the ring tunnel and the shaft. At approximately 500 000 years, the connection of gas saturation between the rock mass above the repository and the shaft breaks. Once this happens, small amounts of gas begin penetrating a small area of rock mass above the repository. Figure 6-8 shows gas saturations, repository water saturation, pressure and gas and water flows at 1 000 000 years (end of the simulation).

It is interesting to note the difference in response between the SF-ES1 and NE-EDZ cases (other than those previously noted). The SF-ES1 and NE-EDZ cases are very similar, except for the high permeabilities in the shaft in the SF1 case. The permeabilities in the shaft's inner EDZ, for both the NE-EDZ and SF-ES1 cases, range between 10^{-11} and 10^{-16} m². Permeabilities in the shaft for the SF-ES1 case are 10^{-14} m². Despite higher conductivities in some sections of the inner EDZ than the high permeabilities of the SF-ES1 shaft, transport up the inner EDZ in the NE-EDZ case is limited by the low conductivity in other sections of the inner EDZ.



06 Jul 2009
FlowFigs_SFES1.mView

Figure 6-8: Evolution of conditions for the SF-ES1 simulation at 1 000 000 years. Gas saturation is shown in the figure above, and pressure and repository water saturation in the figure below.

6.1.2.2 Detailed Description of Dissolved Gas Transport

Figure 6-9 shows the dissolved concentrations for the SF-ES1 case at 0, 2000, 100 000 and 1 000 000 years. Similar times as shown for the NE-BC were selected for comparison purposes only. Dissolved gas concentrations are greater in the permeable Silurian units at early times, compared to the NE-BC, due to the quick transport of dissolved gas from the repository up the shaft. The overall extents of dissolved gas are less than the NE-BC, due to preferential transport up the high permeability shaft.

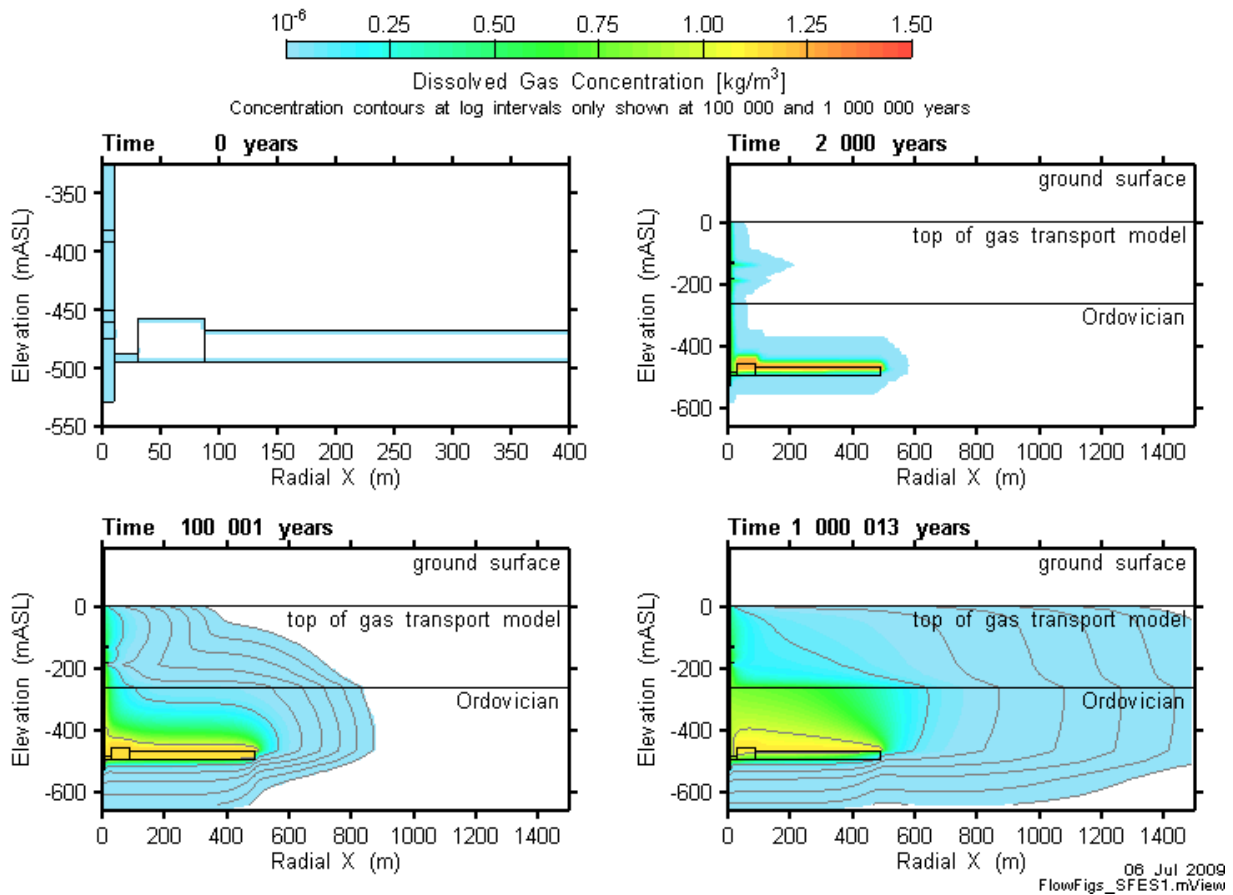


Figure 6-9: Dissolved gas concentrations at 0, 2000, 100 000 and 1 000 000 years for the SF-ES1 case. Note the different radial X and elevation scale at 0 years.

6.2 CASE SF-US: UPPER SHAFT FAILURE

The SF-US case is only complete to 435 000 years, due to the same numeric issues with the TOUGH2 model encountered in the NE-BC.

6.2.1 Gas Generation

This differs from the base case in that there is a failure of the upper seal system. Unlike case SF-ES1, hydraulic properties of the Ordovician seals, backfill and inner EDZ (including those at the Silurian-Ordovician boundary) are not set to highly degraded values, but remain the same as for the base case, NE-BC.

The difference between the results for this case and the base case are negligible, implying that the hydraulic properties of the Ordovician seals, backfill and inner EDZ have a much greater influence on gas and water evolution than failure of the upper shaft alone.

6.2.2 Gas and Water Flows

The SF-US case, in which shaft failure only occurs in the Silurian, is very similar to the NE-BC. This is likely due to the fact that gas transport does not extend above the Ordovician in the NE-BC. In terms of the key parameters:

- Repository gas pressure and repository gas saturation is almost indistinguishable between the NE-BC and SF-US cases.
- Figure 6-10 and Figure 6-11 shows dissolved gas mass flow rates and cumulative mass, respectively. As in the NE-BC, no gas travels through the ORD or SALF plane (except for early initial gases in the shaft). The scale on the dissolved gas mass flow rate figure ignores the mass flow rates through the shaft and EDZ of the SALF plane, as the early very large peak is a result of initial gases, rather than gas originating from the repository. Flow rates and cumulative mass are much greater than the NE-BC. Of particular note, cumulative mass through the SALF plane is primarily through the shaft and EDZ, whereas cumulative mass through the ORD plane is largely through the rock, indicating that dissolved gas in the rock above the ORD plane is directed towards the shaft.

As the results for the SF-US case are so similar to the NE-BC, particularly near the repository and within the Ordovician sediments, further results are not presented except for dissolved gas concentrations, in Figure 6-12. These are also very similar to the NE-BC, with the extents of dissolved gas slightly less farther out into the rock mass in the Silurian units, due to the high permeability pathway up the shaft in the Silurian.

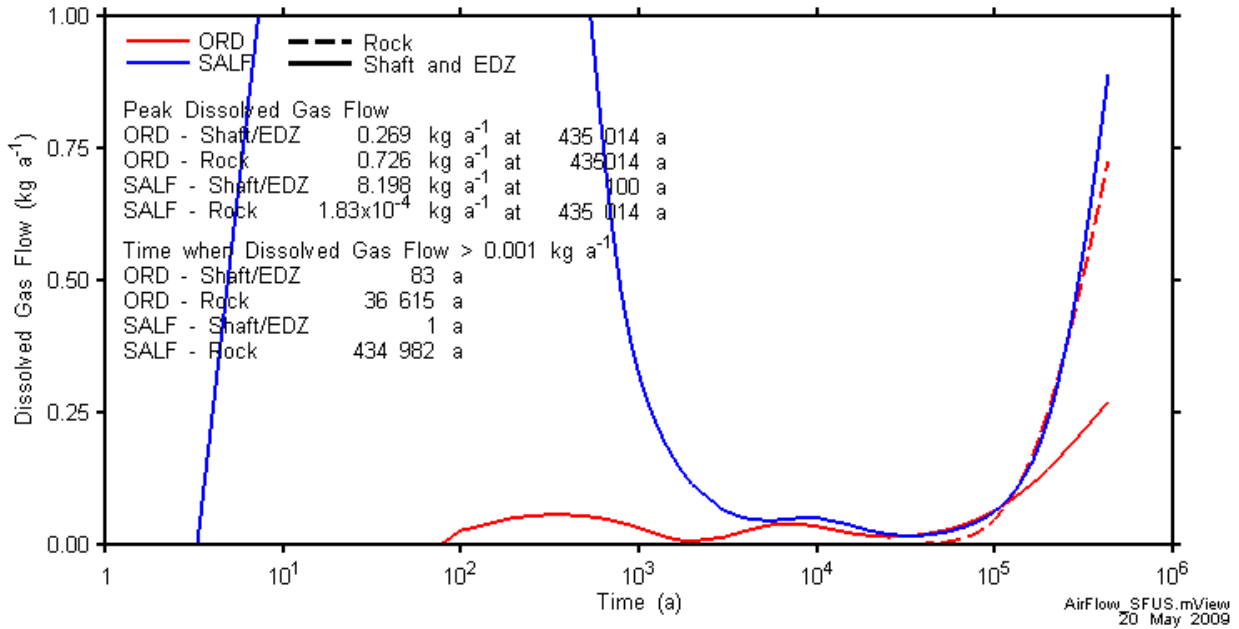


Figure 6-10: Dissolved gas flow rates across the ORD and SALF planes for the SF-US case.

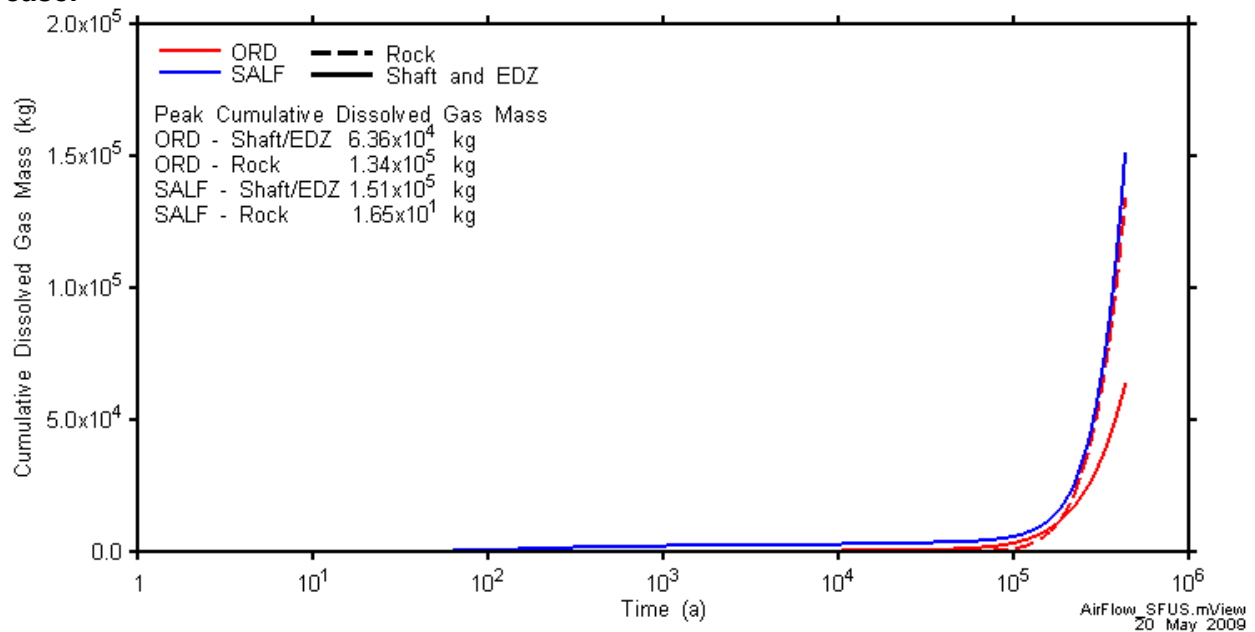


Figure 6-11: Cumulative dissolved gas mass crossing the ORD and SALF planes for the SF-US case.

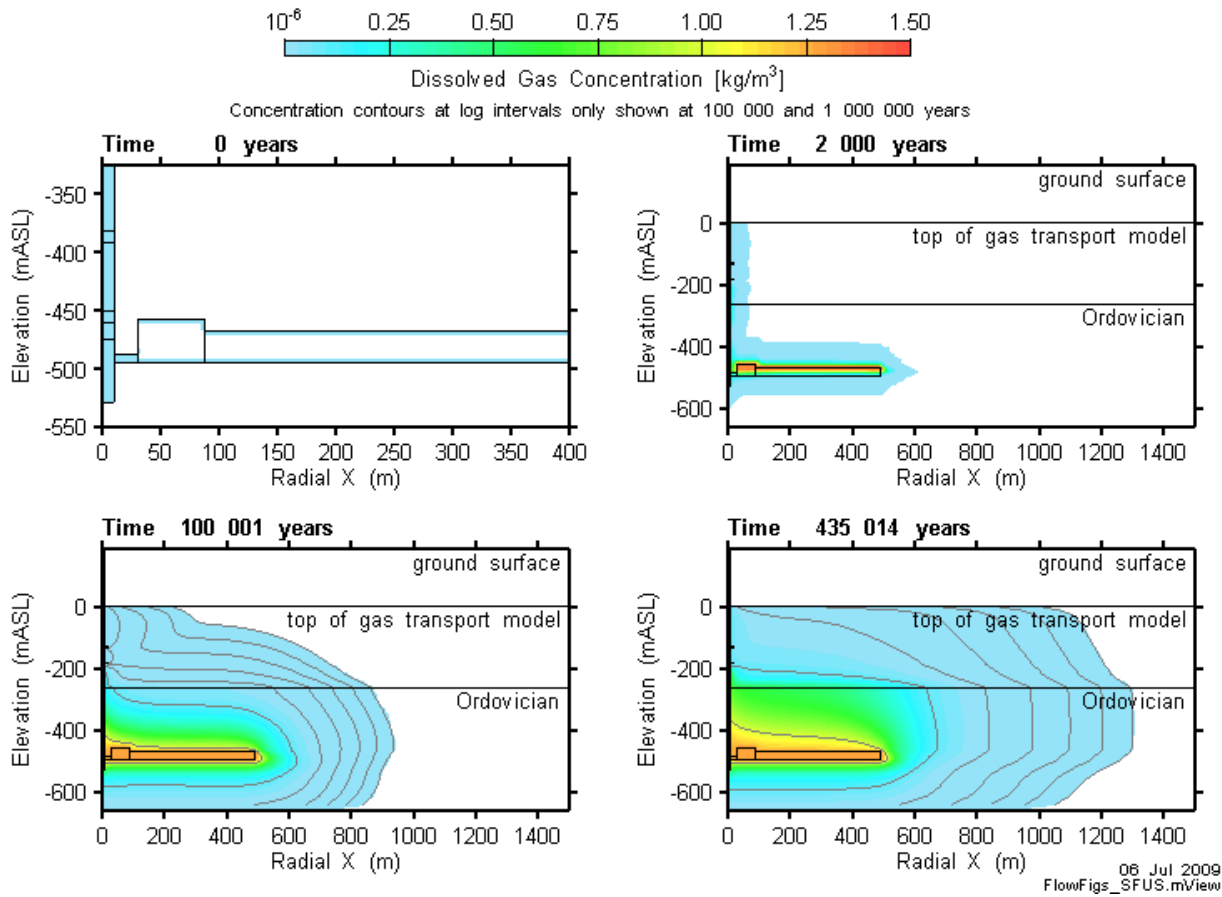


Figure 6-12: Dissolved gas concentrations at 0, 2000, 100 000 and 1 00 000 years for the SF-US case. Note the different radial X and elevation scale at 0 years.

6.3 CASE SF-UG-ES1: SEVERE SHAFT FAILURE AND UPDATED GEOSPHERE DATA

The SF-UG-ES1 case is only complete to 315 000 years, due to numeric issues with the TOUGH2 model. The TOUGH2 model stalls at this point due to very small timesteps; a numeric issue that will be resolved for future safety assessments.

6.3.1 Gas Generation

For this case, in addition to setting the hydraulic properties of all seals, backfill and inner EDZ to extreme degraded values and not keying the seals into the EDZ as was done for case SF-ES1, the updated geosphere data is considered, which includes lower permeabilities in the Silurian and Ordovician sediments.

From case NE-UG-BC we observe that the effect of the lower permeabilities is to slow transport of water into and out of the repository. We might expect this to act to counter the effect of the ineffective seals and the EDZ surrounding them.

The observed effect is as expected. The peak in water entering the repository occurs slightly later than for the SF-ES1 case and is slightly lower. The timing and magnitude of the peak saturation have been moved back much closer to the base case. However, the increase of saturation leading up to the peak pressure occurs more rapidly (Figure 6-13).

The lower permeabilities for this case compared to SF-ES1 have not influenced the peak pressure greatly (7.6 MPa compared to 7.7 MPa) (Figure 6-14).

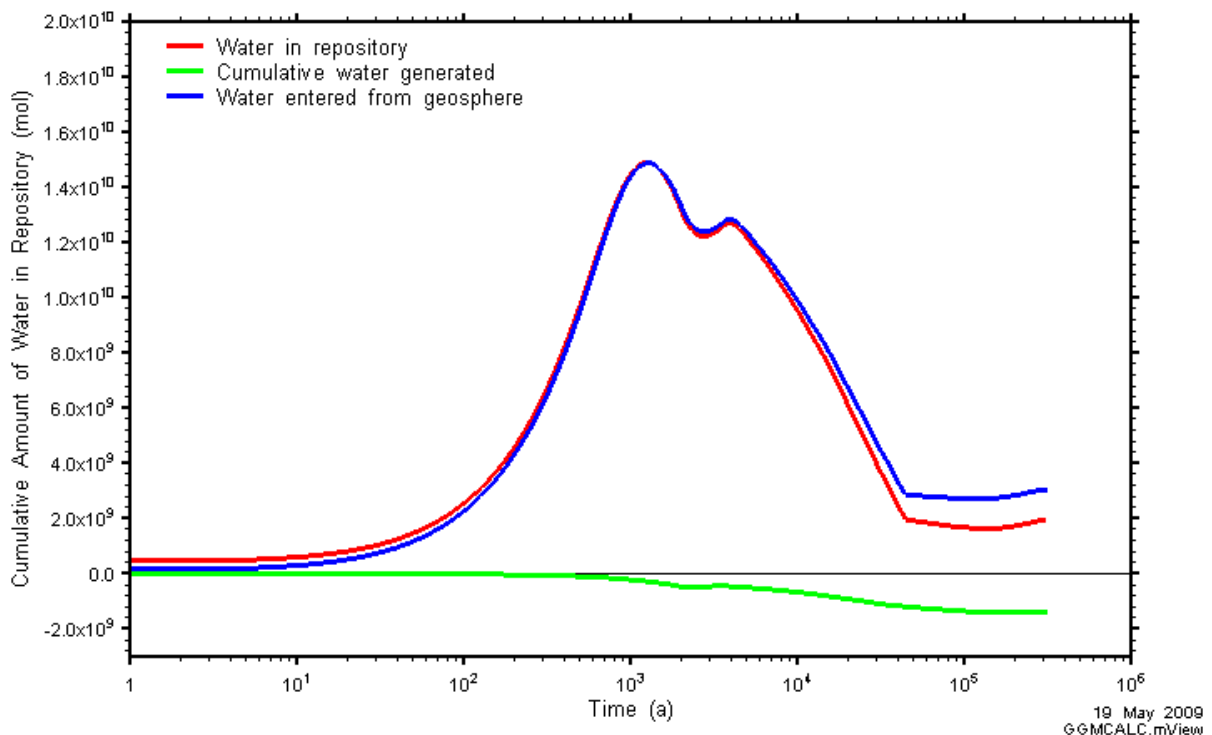


Figure 6-13: SF-UG-ES1: Water balance

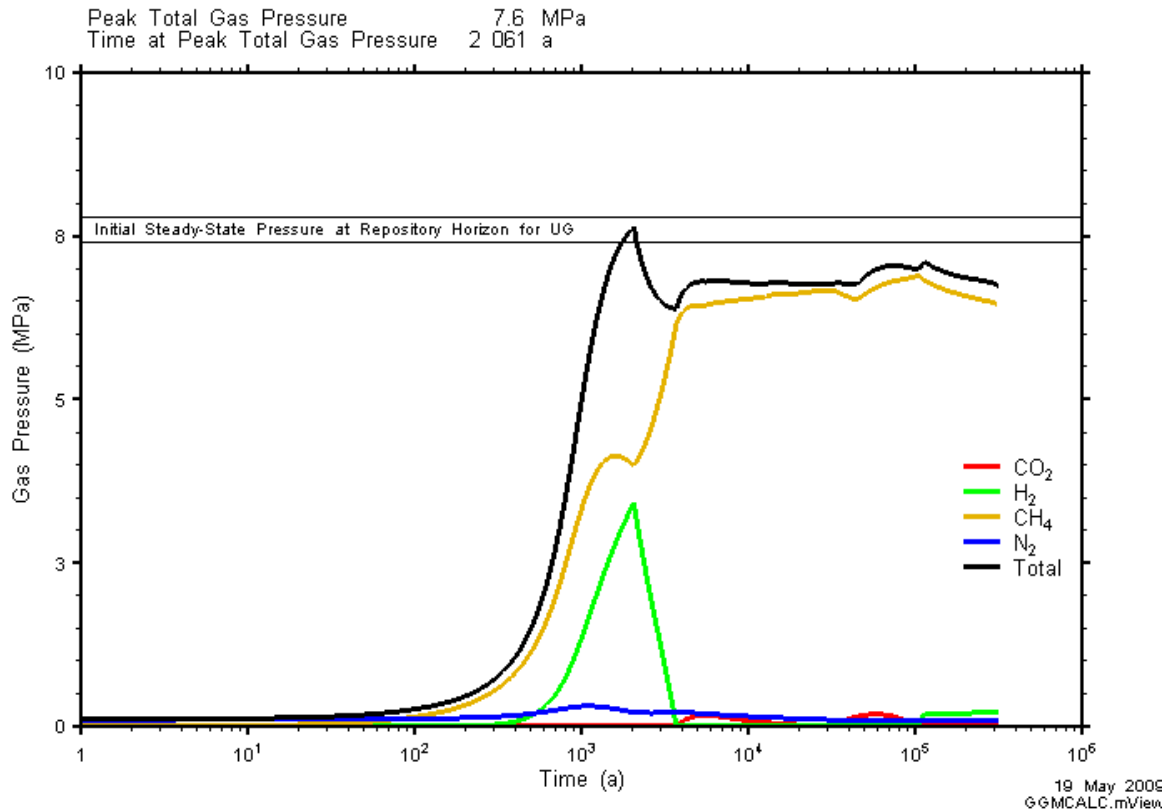


Figure 6-14: SF-UG-ES1: Total and Partial Gas Pressures with the Repository

6.3.2 Gas and Water Flows

The SF-UG-ES1 case is identical to the SF-ES1 case, but updated geosphere permeabilities are used. Due to the similarity of this case to the SF-ES1 case, this case is compared the SF-ES1 as well as the NE-UG-BC case. In terms of the key parameters:

- Peak repository gas pressure and time of peak is the same as the SF-ES1 case, although pressures are slower to increase, see Figure 6-15. Gas pressures also level out, but at a lower pressure than observed in the SF-ES1 case, approximately 6.8 MPa, due to the lower permeabilities and pressures in the UG geosphere. Repository pressures peak earlier than the NE-UG-BC due to the saturation of the repository (described below), and consequently a smaller void volume for gas.
- Water saturation of the repository follows a similar profile to the SF-ES1 case, although slower, see Figure 6-16. Peak water saturation is 0.73 at 1100 years. This is dissimilar to the NE-UG-BC, as water saturation is not limited by the low permeabilities of the rock mass but supplied from water flowing down the permeable shaft and into the repository.
- Gas and dissolved gas mass flow rates and cumulative mass are shown in Figure 6-17 and Figure 6-18. Similar to the SF-ES1 case, no gas travels up through the rock, only through the shaft and EDZ. Peak values are much less (approximately 1 order of magnitude) than the SF-ES1 case at a comparable time.

Detailed results are described below.

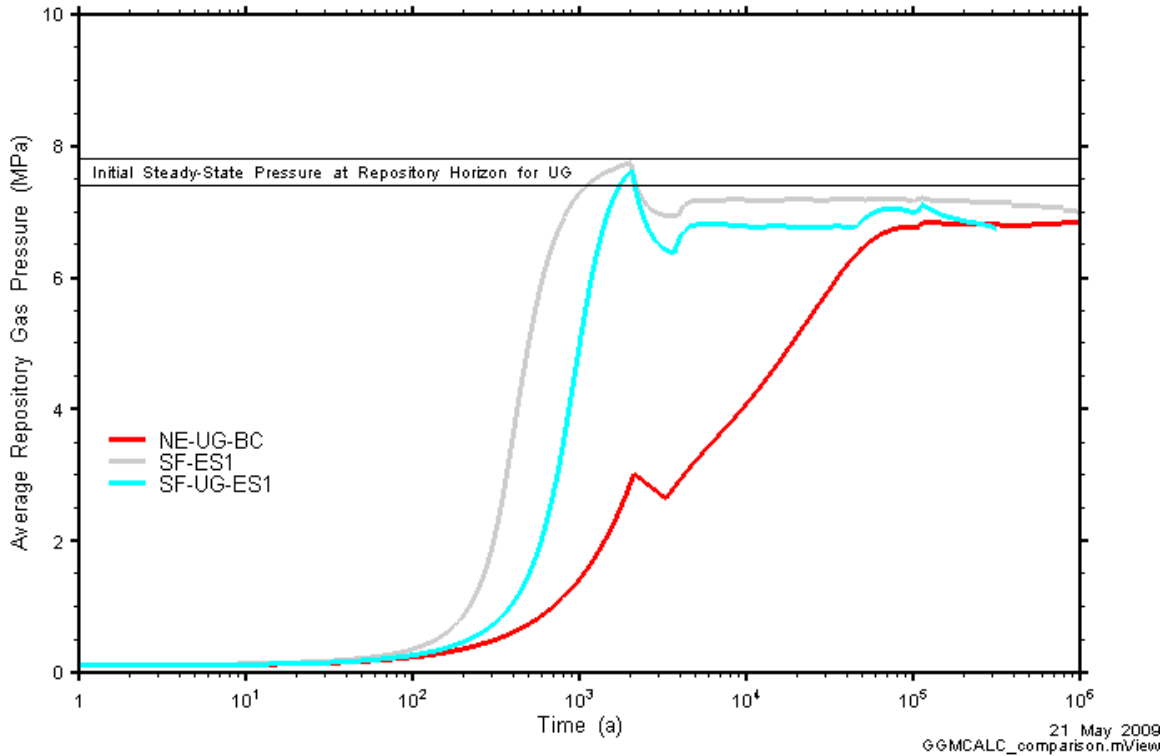


Figure 6-15: Repository gas pressures for the SF-UG-ES1 case, compared to the NE-UG-BC and SF-ES1 cases.

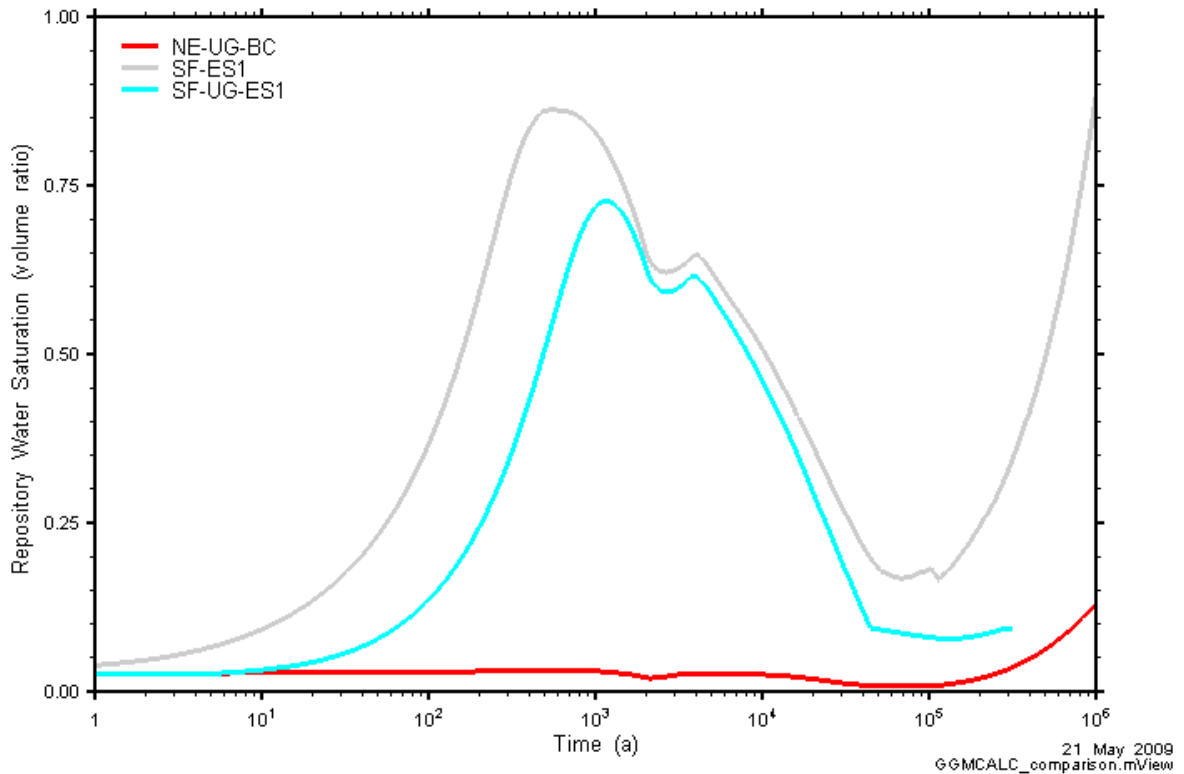


Figure 6-16: Repository water saturation for the SF-UG-ES1 case, compared to the NE-UG-BC and SF-ES1 cases.

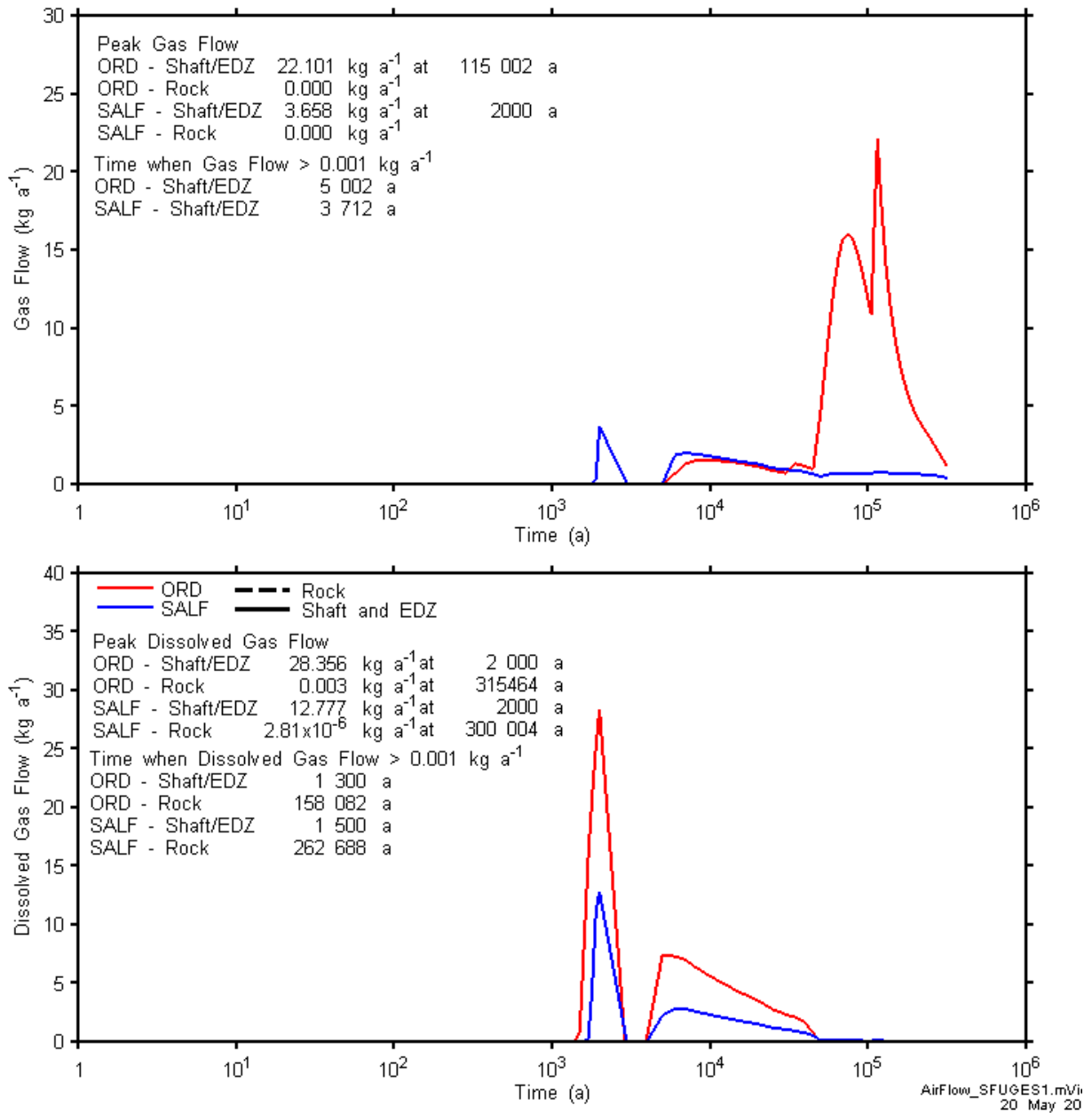


Figure 6-17: Gas flow rates across the ORD and SALF planes for the SF-UG-ES1 case (top: gas, bottom: dissolved gas).

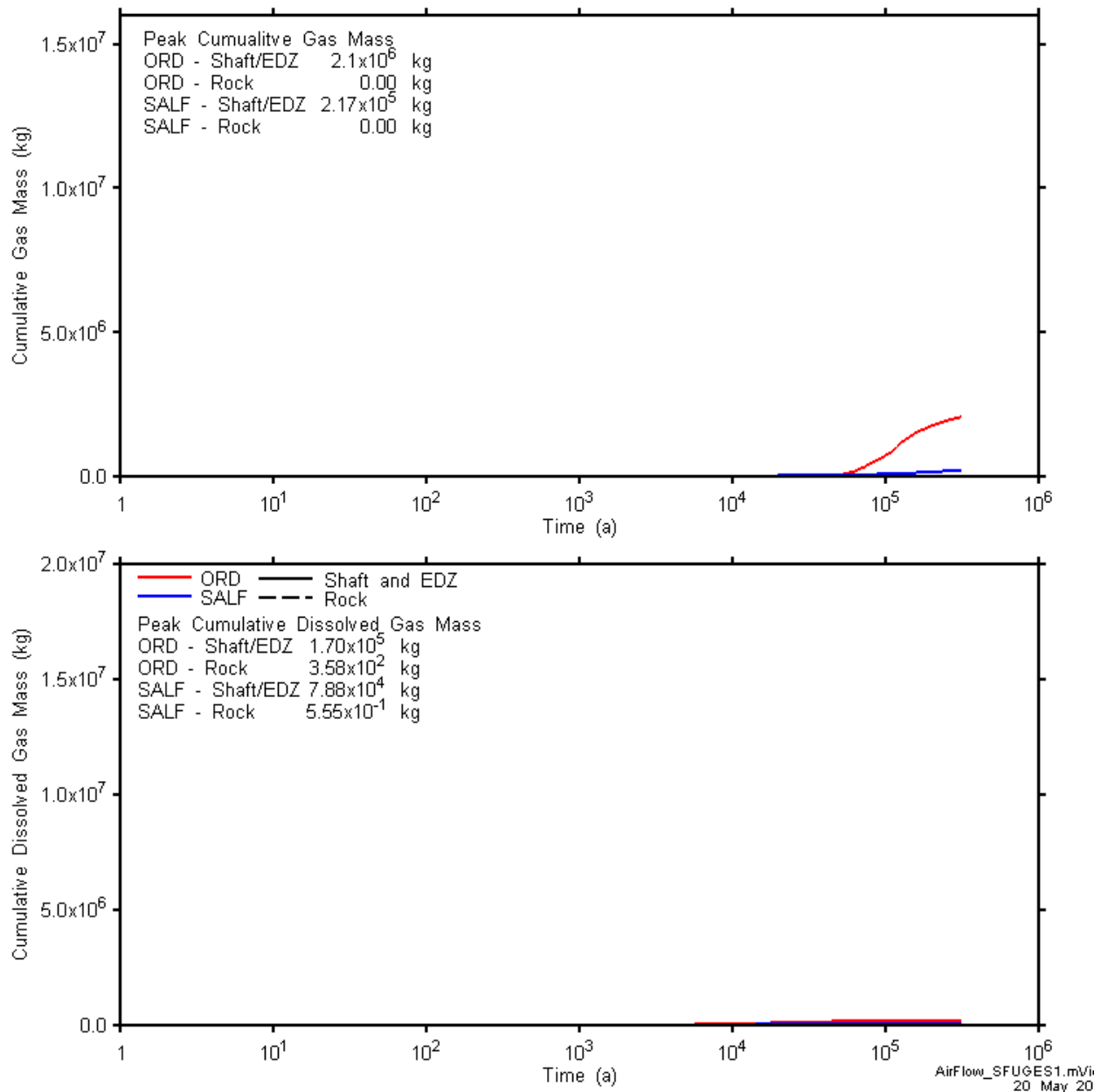


Figure 6-18: Cumulative gas mass crossing the ORD and SALF planes for the SF-UG-ES1 case (top: gas, bottom: dissolved gas).

6.3.2.1 Detailed Description of Gas and Water Transport

Flow of gas and transport is very similar to the SF-ES1 case, with differences as expected for the lower permeability of the rock mass, as well as the associated EDZ. Figure 6-19 and Figure 6-20 show the gas saturation, gas and water flows, repository water saturation and pressure at 0, 200, 8000, 15 000, 25 000 and 45 000 years:

- Resaturation of the shaft occurs around the same time as the SF-ES1 case, with the complete shaft fully saturated with water by 200 years.
- At 1900 years, dissolved gas comes out of solution at the top of the shaft, due to a slight increase in dissolved gases from the repository moving up the shaft, a result of

increasing gas pressures in the repository. This gas dissolves back into solution as pressures drop in the repository, and pressures in the shaft equilibrate. This small amount of gas dissolution is responsible for the first peak of gas mass flow across the SALF plane (see Figure 6-17).

- As in the NE-BC and SF-ES1 case, the pressure drop after peak pressure is a result of a switch to gas consumption and water generation in the repository, and the recovery of the repository pressure is a result of the resumption of gas generation and water consumption. The steady value at which repository pressures recover is lower than the initial steady-state pressure in the geosphere due to the pressure relief provided by the permeable shaft.
- Dissolved gas comes out of solution at 5500 years, as repository pressures increase and dissolved concentrations in the shaft increase, a little later than for the SF-ES1 case. Note that dissolved gas mainly comes out of solution in the shaft, rather than the shaft and EDZ. The second peak in gas mass flow rates, across the SALF plane (and the first across the ORD plane) occur at this time (see Figure 6-17). Figure 6-19 shows gas saturations at 8000 years, once dissolved gas has come out of solution close to the repository.
- As gas pressures propagate up the shaft, the repository gas pressure levels off to a relatively steady-state value.
- By 15 000 years, the gas saturations at the side of the repository connect to the gas saturations in the shaft, providing a pathway for gas to travel from the repository up the shaft and up to the top of the model. This is slightly earlier than the SF-ES1 case.
- At 25 000 years, sufficient water has been pushed out of the repository to allow gas to migrate through the repository EDZ above the concrete monolith, and into the shaft EDZ. This is slightly faster than the SF-ES1 case due to the smaller repository water saturations in the SF-UG-ES1 case (i.e., from peak water saturations, less water has to be pushed out to reach the critical level at which a connection is made between the repository and EDZ above the concrete monolith).
- At approximately 45 000 years, the amount of water in the repository begins to level off, as gas begins to saturate the concrete monolith, reducing the permeable pathway for water to be pushed out of the repository. This does not occur in the SF-ES1 case, as repository water saturations do not reach the low levels of the SF-UG-ES1 case. As mentioned above, lower repository water saturations are reached in the SF-UG-ES1 case as peak repository water saturations are less. Corresponding to this decreased rate of water desaturation is a small increase in repository gas pressure and the transport of gas into the permeable Silurian units.
- Water begins to saturate the repository once again at the same time as the SF-ES1 case, 114 000 years, although repository resaturation occurs much more slowly, due to the comparatively tight permeabilities in the rock. As with all other cases, this saturation of the repository occurs as repository pressures drop below those in the rock mass below the repository.
- The connection of gas along the monolith and the EDZ above it is not broken over the course of the simulation (up to 315 000 years). It is broken earlier in the SF-ES1 case, due to the faster water saturation of the repository. Figure 6-21 shows gas saturations and pressures at the end of the simulation.
- Gas does not migrate into the rock mass, except between the repository and shaft.

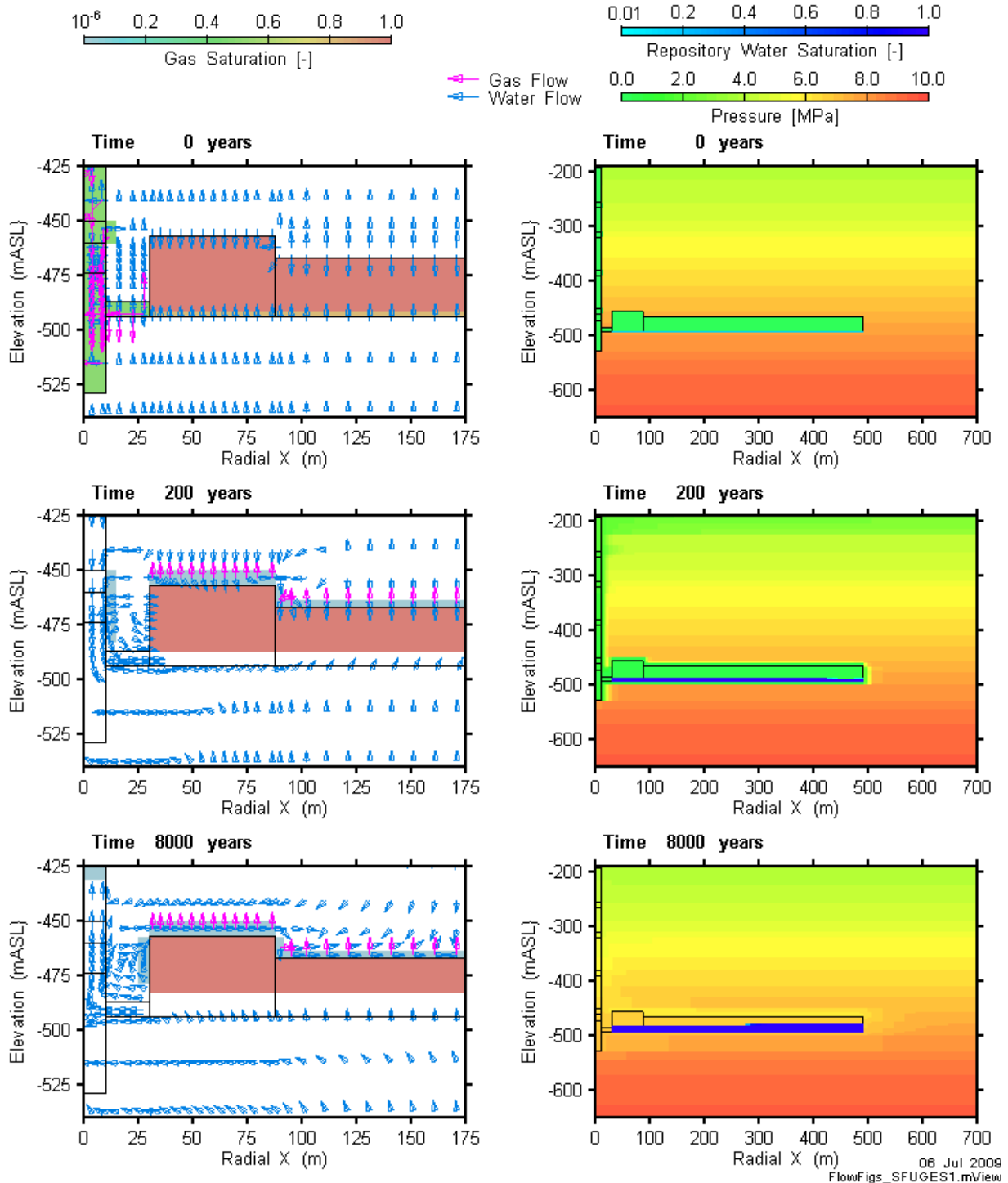


Figure 6-19: Evolution of conditions for the SF-UG-ES1 case at the start of the simulation (0 years), 200 years, and 600 years. Gas saturation and gas and water flow (outside repository) are shown in the figures on the left, and pressure and repository water saturation in the figures on the right.

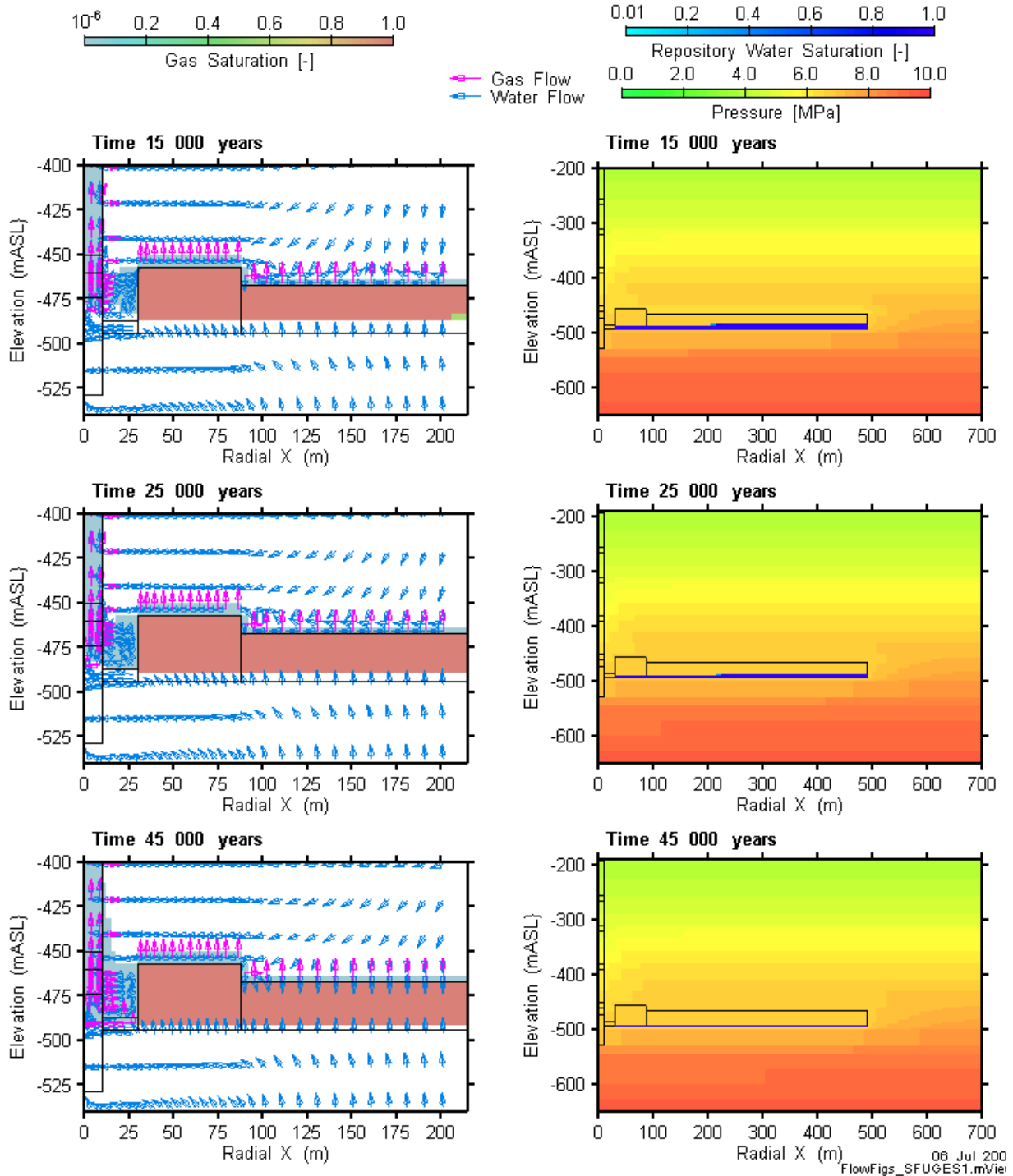
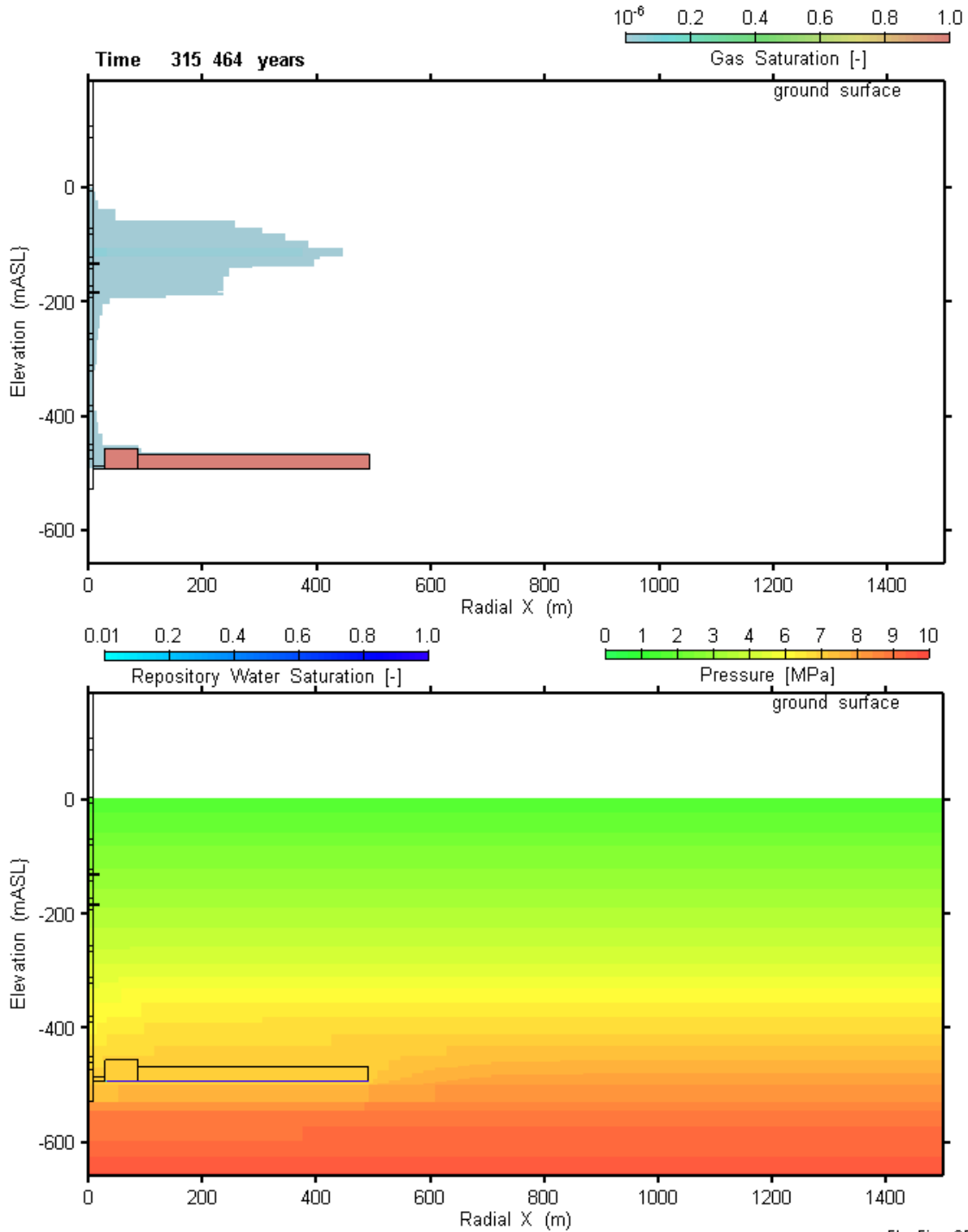


Figure 6-20: Evolution of conditions for the SF-UG-ES1 case at 15 000, 25 000 and 45 000 years. Gas saturation, and gas and water flow (outside repository) are shown in the figures on the left, and pressure and repository water saturation in the figures on the right.

06 Jul 2009
FlowFigs_SFUGES1.mView



06 Jul 200
FlowFigs_SFUGES1.mView

Figure 6-21: Evolution of conditions for the SF-UG-ES1 simulation at 315 000 years. Gas saturation is shown in the figure above, and pressure and repository water saturation in the figure below.

6.3.2.2 Detailed Description of Dissolved Gas Transport

Figure 6-22 shows the dissolved concentrations for the SF-UG-ES1 case at 0, 2000, 100 000 and 315 000 years. Similar times as shown for the NE-BC and SF-ES1 were selected for comparison purposes only. Compared to the SF-ES1 case, dissolved gas concentrations after 100 000 years are present in a broader area of the rock in both the Silurian and Ordovician units:

- Within the Silurian, due to the presence of gas in the permeable Silurian units.
- Below the repository in the Ordovician, as the downward transport of dissolved gases is less limited by flow of water through the bottom of the repository and up the shaft than in the SF-ES1 case. Flow of water through the bottom of the repository and up the shaft is less significant in the SF-UG-ES1 case due to lower rock permeabilities.

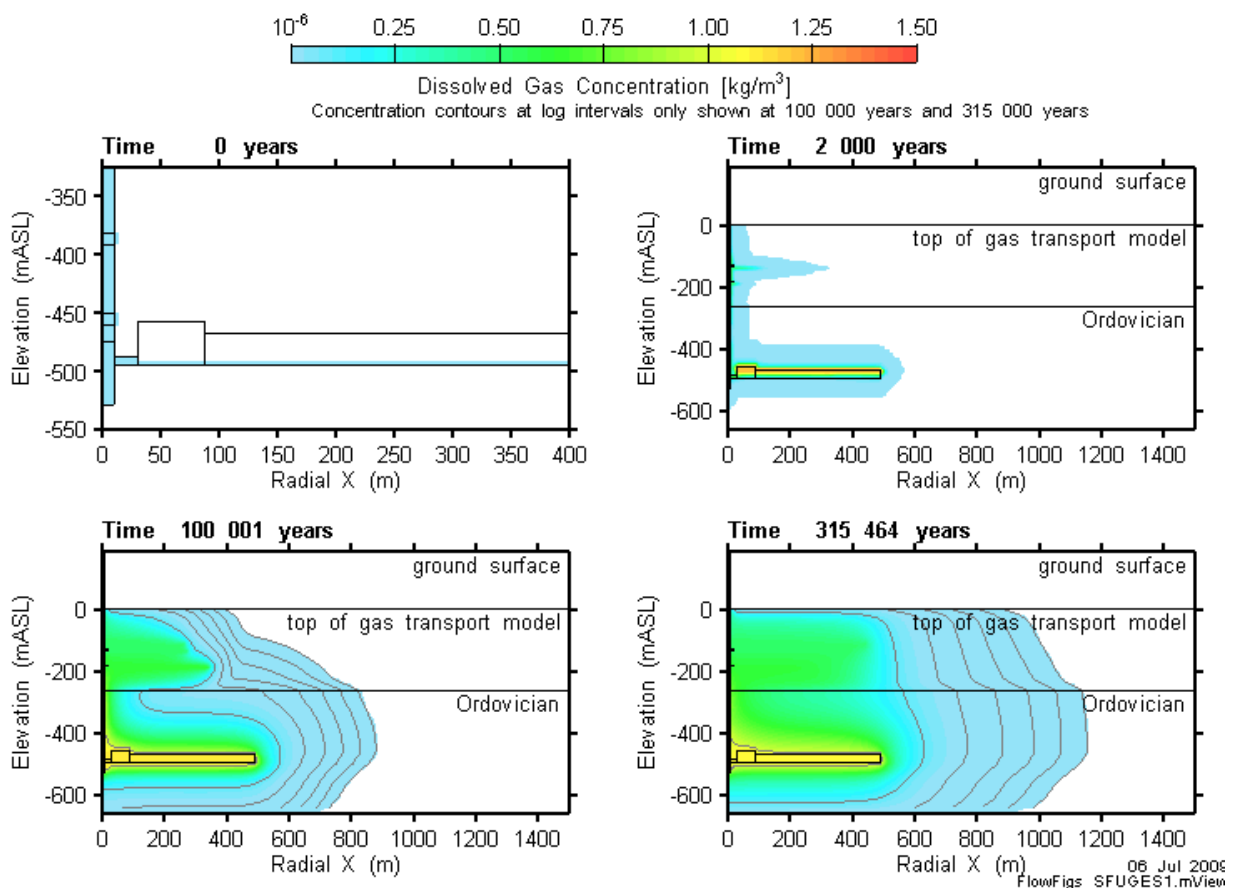


Figure 6-22: Dissolved gas concentrations at 0, 2000 and 25 000 for the SF-UG-ES1 case. Note the different radial X and elevation scale at 0 years.

7 RESULTS ASSESSMENT AND COMPARISON

This section provides graphical and tabular comparative summaries of gas and water flows for all calculation cases.

Figure 7-1 and Figure 7-2 shows repository pressure as a function of time for all cases. Points to note are as follows.

- Geosphere permeability had the greatest impact on repository pressure.
- Cases based on the NE-BC geosphere permeabilities generally have similar repository pressure profiles, whereas cases based on the NE-UG-BC geosphere permeabilities have generally similar repository pressure profiles. Due to the low geosphere permeabilities, and the consequential reduced inflow of water into the repository, NE-UG cases are much slower to reach a peak repository pressure than cases based on the NE-BC geosphere permeabilities. Low permeabilities in the NE-UG also result in slow water saturation of the repository, providing a relatively larger void volume for gases, resulting in repository peak pressures that are generally less than simulations with the NE-BC geosphere permeabilities.
- The NE-UG-GT case provides the greatest repository pressure. However, this case provides a conservative estimate of the repository peak pressure due to limitations in the T2GGM code, which allows gas generation while the repository dries out. Also this case starts with an assumed high gas pressure within the Ordovician rocks, due to the initial gas saturations and high capillary pressures in the Ordovician rocks. See the detailed description of results for this case for more detail (Section 5.8).
- Increasing gas generation (NE-GG1) had an impact on the repository pressure profile; however, peak pressures remain similar to the NE-BC.
- SF cases resulted in marginally lower peak pressures than the NE-BC. Repository pressures are decreased if a conductive pathway along the full length of the shaft is provided, as in the SF-ES1 and SF-UG-ES1 cases. The conductive pathway of the NE-EDZ case, which is less conductive than for the SF cases, only provides a small decrease in the repository gas pressure. The SF-US case, for which the conductive pathway is only above the Ordovician rock, is nearly identical to the NE-BC.

In all cases, the peak pressures are well below the estimated lithostatic pressures at the repository horizon (17 MPa).

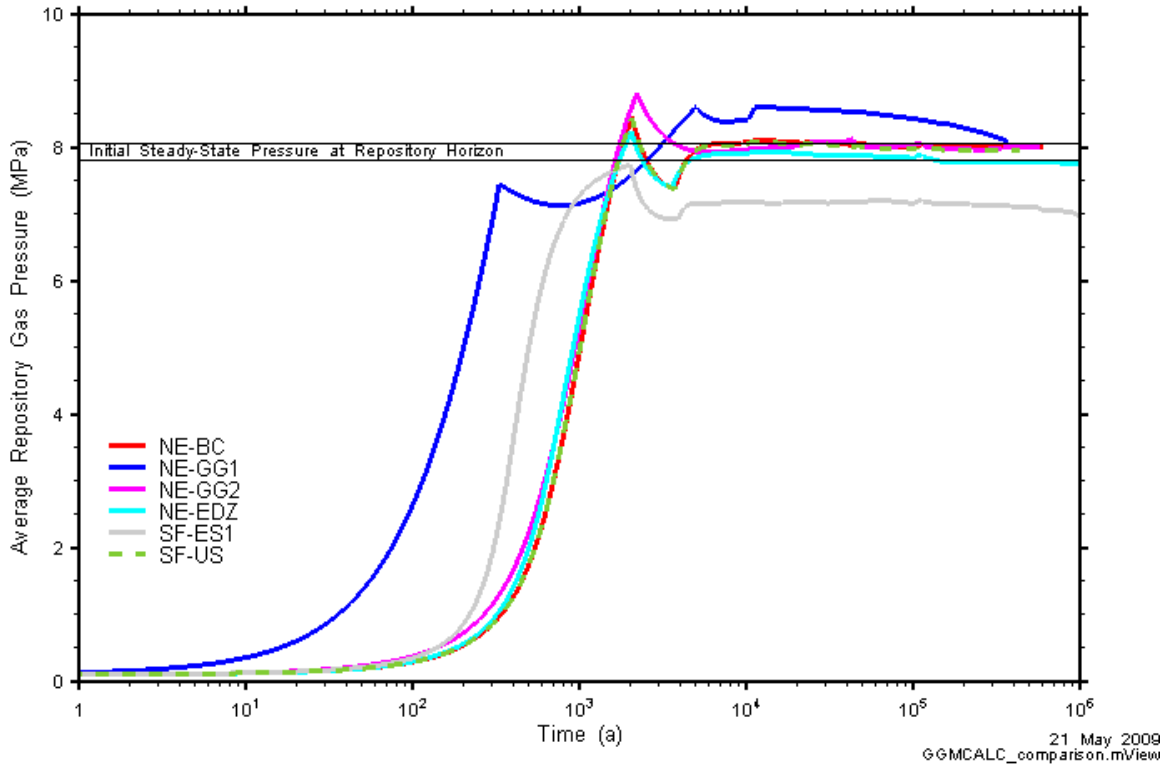


Figure 7-1: Average repository gas pressure for all cases based on the NE-BC geosphere.

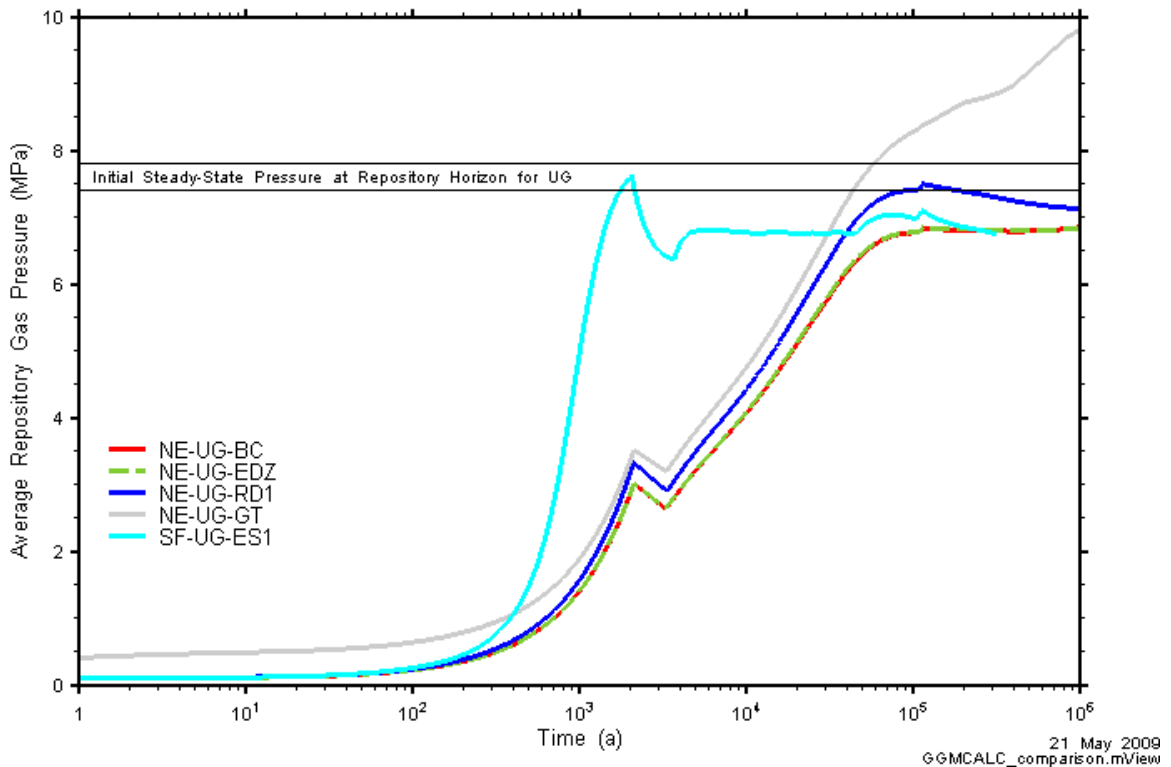


Figure 7-2: Average repository gas pressure for all cases based on the NE-UG-BC geosphere, as well as the NE-BC for comparison.

Figure 7-3 and Figure 7-4 displays the repository water saturation history for all cases. With the exception of the NE-UG cases, all cases undergo early water saturation, between 0.22 and 0.86, before gas pressures develop and water is pushed out of the repository. Only the NE-GG1 and NE-UG-GT cases result in repositories which are completely dry; all other cases begin water saturation at the point which the average repository pressure drops below the geosphere pressures in the rock mass.

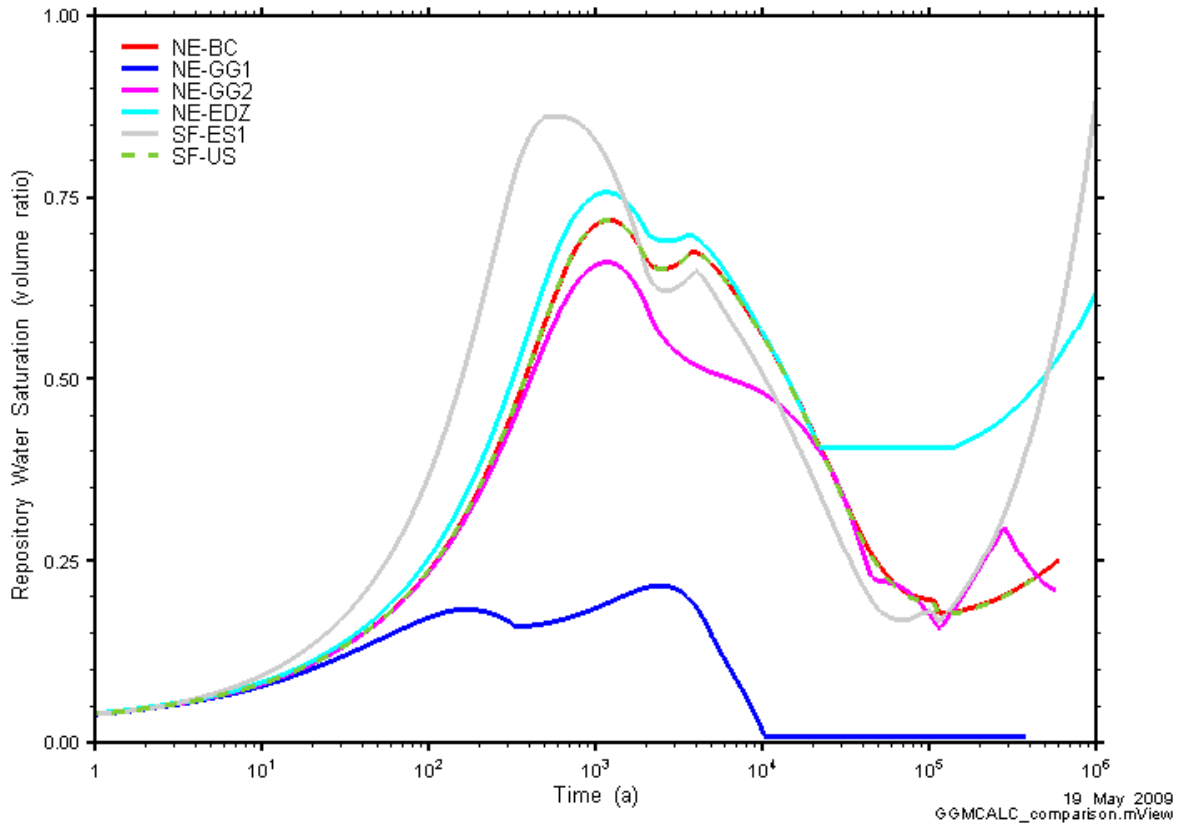


Figure 7-3: Average repository water saturation all cases based on the NE-BC geosphere.

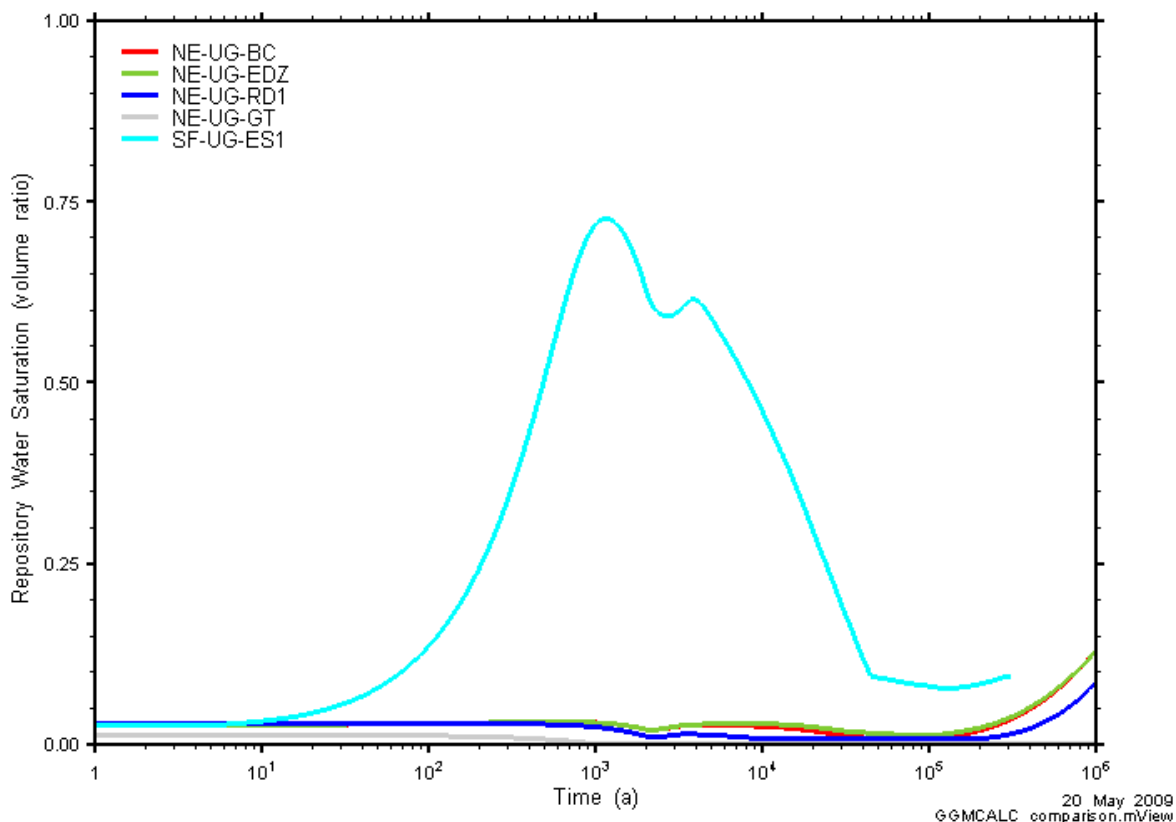


Figure 7-4: Average repository water saturation all cases based on the NE-UG-BC geosphere.

Data displayed on Figure 7-1, Figure 7-2, Figure 7-3 and Figure 7-4 are summarized in Table 7-1.

Table 7-1: Summary of Peak Repository Pressures and Water Saturations

Calculation Case	Peak Repository Gas Pressure (MPa)	Time of Peak Gas Pressure (a)	Peak Repository Water Saturation (-)	Time of Peak Water Saturation (a)
NE-BC	8.5	2 000	0.72	1 200
NE-GG1	8.6	11 000	0.22	2 500
NE-GG2	8.8	2 000	0.66	1 200
NE-EDZ	8.3	2 000	0.76	1 200
SF-ES1	7.7	2 000	0.89	1 000 000
SF-US	8.4	2 000	0.72	1 200
NE-UG-BC	6.9	1 000 000	0.13	1 000 000
NE-UG-EDZ	6.9	114 000	0.13	1 000 000
NE-UG-RD1	7.5	114 000	0.09	1 000 000
NE-UG-GT	9.8	1 000 000	0.02	0
SF-UG-ES1	7.7	2 000	0.73	1 100

Figure 7-5 and Figure 7-7 present gas and dissolved gas flow rates and cumulative mass through the SALF plane (the top of the Intermediate Bedrock Groundwater Zone) for all cases. The figures show the total response for the shaft/EDZ and rock mass. A numeric summary with separate shaft/EDZ and rock mass data are presented in Table 7-2. Early peaks that are clearly a result of initial gases in the shaft are ignored.

In the SF-US case and all NE cases except NE-EDZ, only dissolved gas reaches the top the Intermediate Bedrock Groundwater Zone in either the rock mass or the shaft. The amount of dissolved gas is small (< 100 kg over one million years) for the NE cases except NE-EDZ. For the SF-US and NE-EDZ cases most of the dissolved gas is via the shaft and EDZ. While not shown in these figures, no gas is transported above the Ordovician units for NE cases except NE-EDZ, cases in which only dissolved gas reached surface, and the presence of gas (at saturations greater than 10^{-6}) is limited to a few metres from the repository, once initial shaft gases have dissolved.

Only the NE-EDZ, SF-ES1 and SF-UG-ES1 cases result in gas reaching the top of the Intermediate Bedrock Groundwater Zone. All these cases provide permeable pathways to surface via the shaft and EDZ.

For the NE cases (except NE-EDZ), the dissolved gas released to the top of the Intermediate Bedrock Groundwater Zone over the assessment period of 1 million years is <0.01% of the total amount of generated gases (3.1×10^7 kg for the NE-BC and NE-UG-BC). No gas is released over the assessment period. For the SF and NE-EDZ cases, the total gas and dissolved gas released to the top of the Intermediate Bedrock Groundwater Zone over the assessment period of 1 million years is < 1 % for SF-US and SF-UG-ES1 cases, < 5 % for NE-EDZ case and < 30 % for the SF-ES1 case.

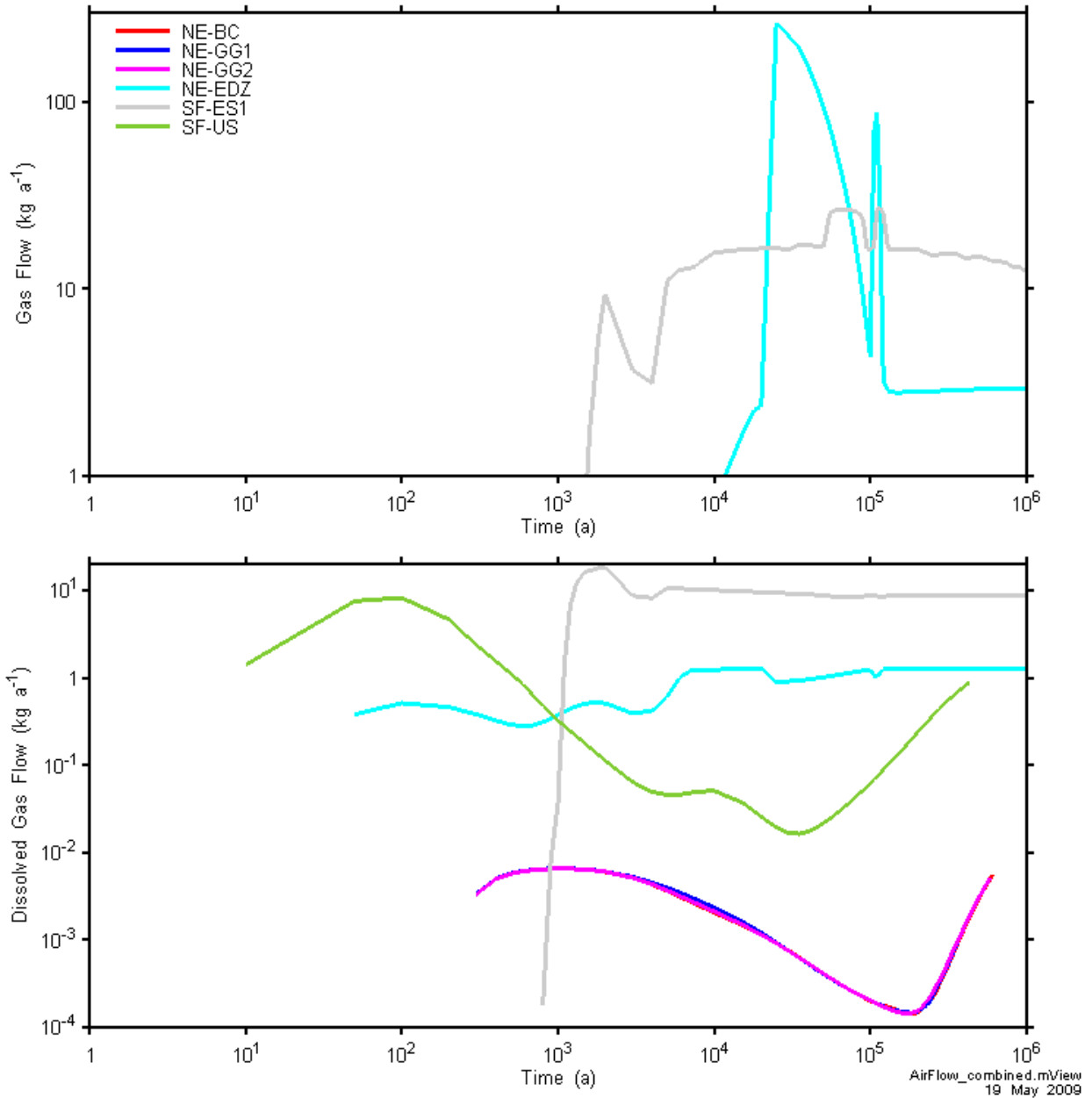


Figure 7-5: Gas and dissolved gas flow rates crossing the SALF plane for all cases based on the NE-BC geosphere.

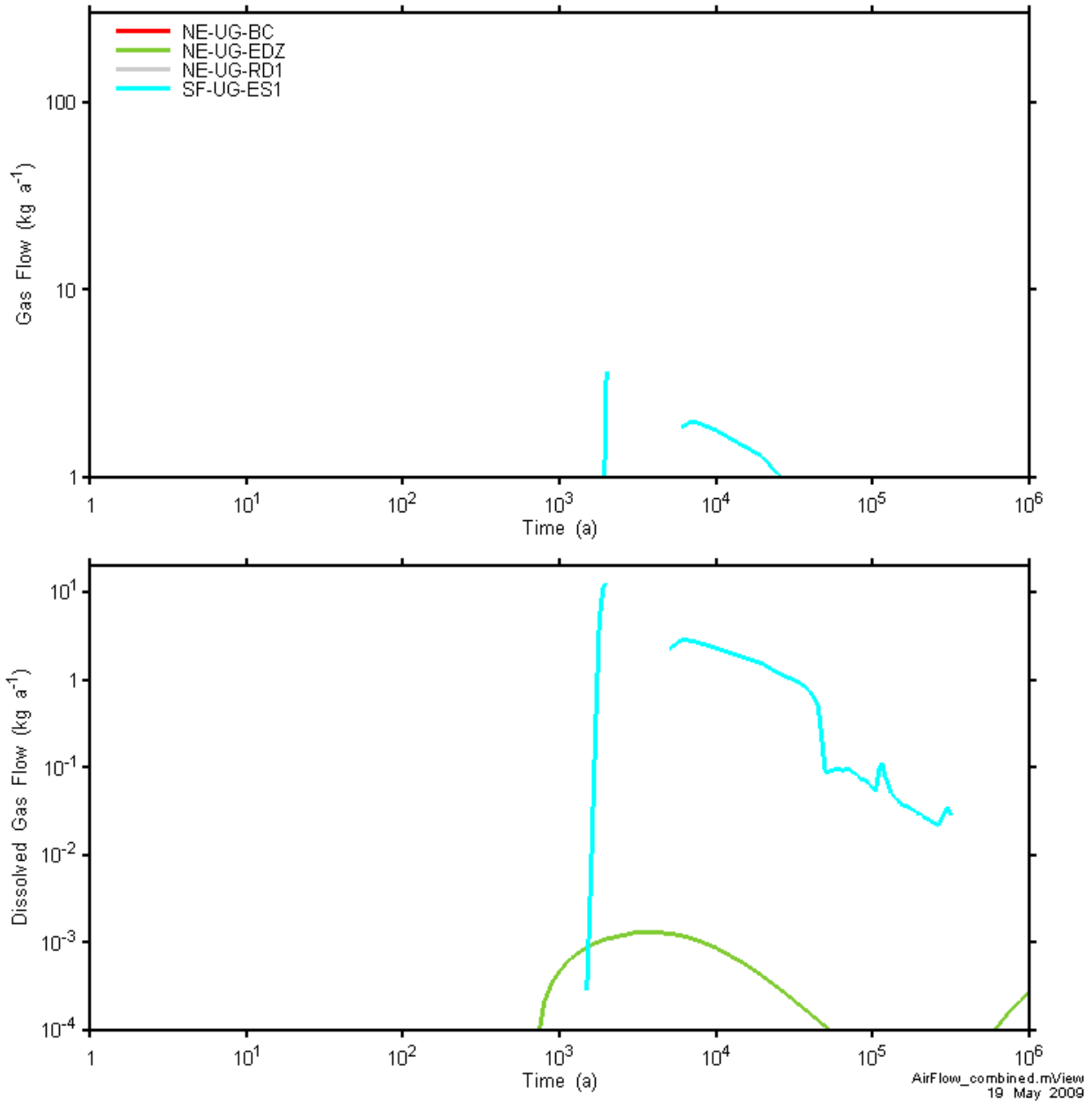


Figure 7-6: Gas and dissolved gas flow rates crossing the SALF plane for all cases based on the NE-UG-BC geosphere. Note that all NE-UG-BC and NE-UG-RD1 case results are below the lower limit of the Y-axis.

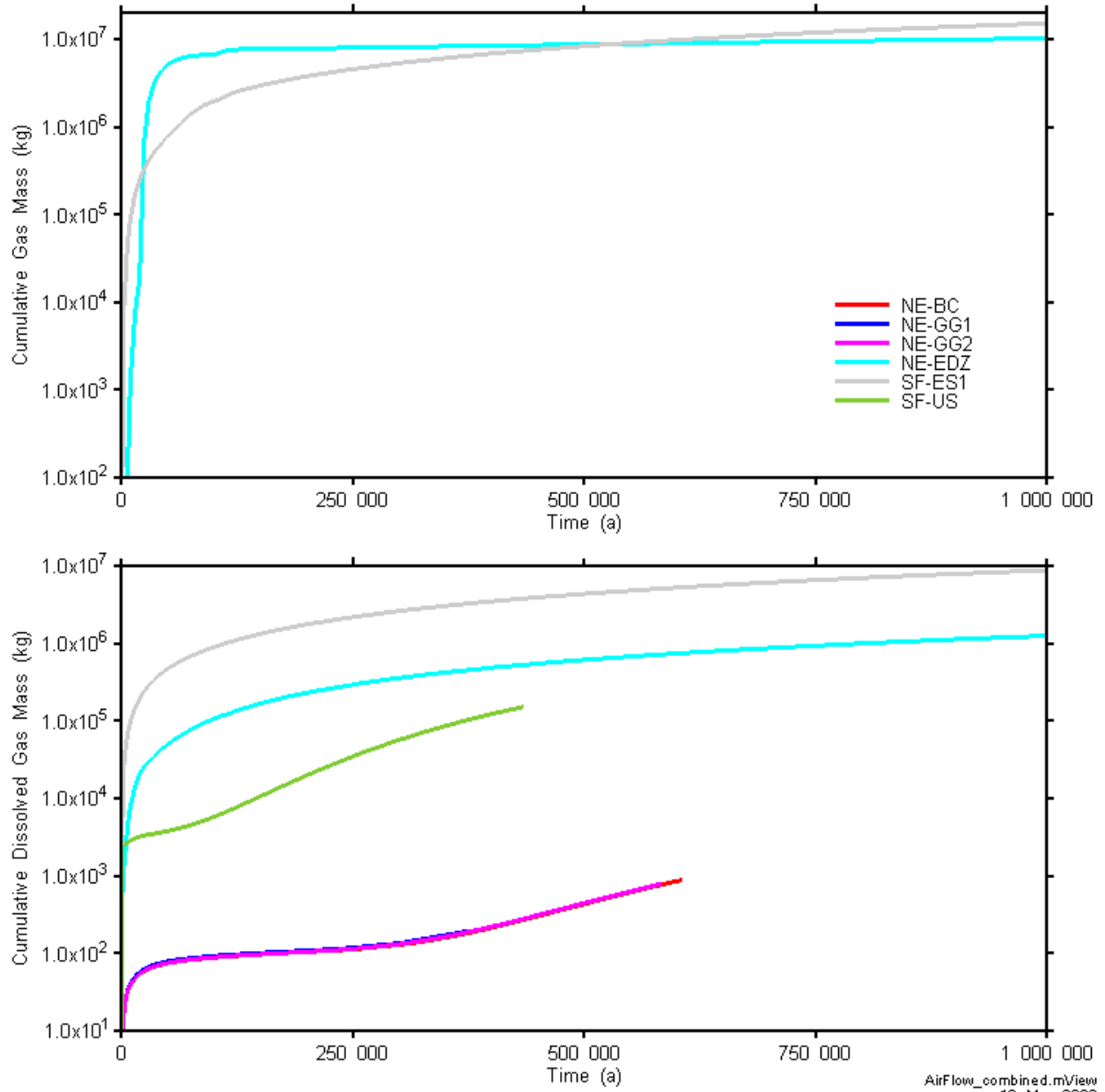


Figure 7-7: Gas and dissolved gas cumulative mass crossing the SALF plane for all cases based on the NE-BC geosphere.

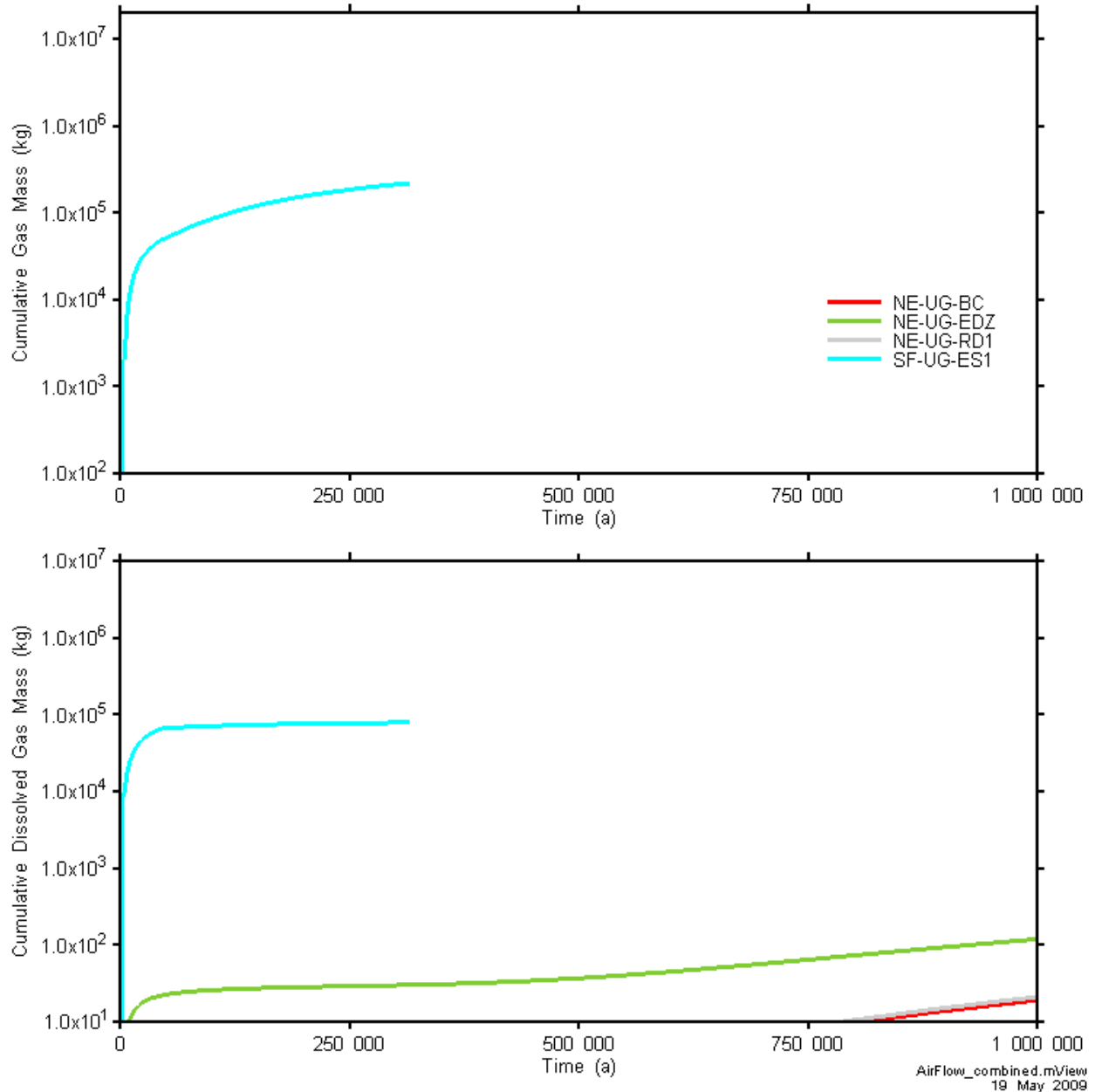


Figure 7-8: Gas and dissolved gas cumulative mass crossing the SALF plane for all cases based on the NE-UG-BC geosphere.

Table 7-2: Summary of cumulative gas mass (in kg) crossing the SALF transport plane at the top of the detailed gas model

Calculation Case	at 250 000 years		at 500 000 years		at 750 000 years		at 1 000 000 years	
	Shaft/EDZ	Rock	Shaft/EDZ	Rock	Shaft/EDZ	Rock	Shaft/EDZ	Rock
NE-BC	0.000	0.000	0.000	0.000	-	-	-	-
NE-GG1	0.000	0.000	-	-	-	-	-	-
NE-GG2	0.000	0.000	0.000	0.000	-	-	-	-
NE-EDZ	7.96×10^6	0.000	8.68×10^6	0.000	9.41×10^6	0.000	1.01×10^7	0.000
SF-ES1	4.54×10^6	0.000	8.29×10^6	0.000	1.18×10^7	0.000	1.51×10^7	0.000
SF-US	0.000	0.000	-	-	-	-	-	-
NE-UG-BC	0.000	0.000	0.000	0.000	0.000	0.000	0.000	0.000
NE-UG-EDZ	0.000	0.000	0.000	0.000	0.000	0.000	0.000	0.000
NE-UG-RD1	0.000	0.000	0.000	0.000	0.000	0.000	0.000	0.000
NE-UG-GT	-	-	-	-	-	-	-	-
SF-UG-ES1	1.84×10^5	0.000	-	-	-	-	-	-

Note:

Results for NE-UG-GT not presented, as they are obscured by the initial gas saturations in the Ordovician

Table 7-3: Summary of cumulative dissolved gas mass (in kg) crossing the SALF transport plane at the top of the detailed gas model

Calculation Case	at 250 000 years		at 500 000 years		at 750 000 years		at 1 000 000 years	
	Shaft/EDZ	Rock	Shaft/EDZ	Rock	Shaft/EDZ	Rock	Shaft/EDZ	Rock
NE-BC	95.7	17.3	142	289	-	-	-	-
NE-GG1	99.7	18.5	-	-	-	-	-	-
NE-GG2	95.8	18.5	144	300	-	-	-	-
NE-EDZ	2.92×10^5	1400	6.07×10^5	4680	9.23×10^5	8660	1.24×10^6	1.38×10^4
SF-ES1	2.18×10^6	67.6	4.35×10^6	240	6.54×10^6	643	8.74×10^6	1290
SF-US	3.50×10^4	0.94	-	-	-	-	-	-
NE-UG-BC	1.81	0.08	2.20	0.79	3.51	4.55	6.08	13.0
NE-UG-EDZ	28.9	0.05	36.2	0.56	61.1	3.18	110	9.07
NE-UG-RD1	1.80	0.08	2.20	0.86	3.60	5.08	6.39	14.6
NE-UG-GT	-	-	-	-	-	-	-	-
SF-UG-ES1	7.69×10^4	0.38	-	-	-	-	-	-

8 UNCERTAINTIES AND ISSUES FOR FURTHER WORK

Uncertainties and issues in model results presented in this report arise from a variety of sources, including: the modelling approach and the parameterization, for both the gas generation and gas transport models; and the conceptual model of the geosphere. The calculation cases presented in this report are intended to bound the uncertainty in key model results such as repository gas pressure and gas flux. Even so, the results are subject to additional uncertainty due to model implementations and modelling approaches, parameter uncertainty and conceptual model uncertainty. These sources of uncertainty and possible future approaches to reducing uncertainty and optimizing system and code behaviour are discussed in the following subsections.

8.1 GAS GENERATION MODEL

The gas generation model is a simple model of the gas generation processes within the repository, which is sufficiently detailed to consider the key processes that govern the fluxes of water and gases between the repository and the geosphere, and to estimate the repository gas pressure.

Analysis of the modelling results has identified several areas where the GGM model requires further development or could be improved to reduce conceptual model and parameter uncertainty. These issues are discussed below. Most of the issues identified have both conceptual model and parameter uncertainty components. For example, a more detailed consideration of variability will require updates to the underlying model to allow variability to be taken into consideration and may require additional data to support the degree of variability being modelled.

The GGM can be run as a standalone code, whereby TOUGH2 is replaced by a very simple model of the repository response. In standalone mode a simulation only takes several minutes to run. As well as being a useful tool for testing the gas generation model, it can be used to investigate model and parameter uncertainties rapidly before full T2GGM runs are undertaken.

1. **Variability:** The GGM allows heterogeneity of the wastes to be taken into account through their categorisation into the various waste streams, whose corrosion and degradation paths can be modelled independently. The heterogeneous nature of the environment in which the waste is situated is modelled by assigning different reaction rates to wastes in the saturated phase and in the vapour phase under high and low relative humidity conditions.

Gas generation results currently exhibit relatively sharp changes of behaviour at certain stages during the evolution of the repository. This is most evident at the moments when metallic or organic waste streams are completely corroded/degraded. To a certain extent, variability, whether that is spatial heterogeneity of the wastes within the repository, or of the chemical composition of the wastes, or of the environment in which the wastes are situated, will affect gas generation. It is anticipated that it would act to smooth the sharp transitions observed with the current model, which may impact on the magnitude and timing of the peak pressure. Possibilities for taking variability into consideration include: (a) moving to a detailed 3D description of the repository environment, (b) subdividing the repository into smaller regions and coupling a single GGM to each one, (c) subdividing the waste streams into bins which are assigned

surface areas and reaction rates from a distribution of rates chosen to reflect the anticipated variability. Option (c) is recommended as it is likely to be effective and have the least impact on run times and the stability of the coupling between TOUGH2 and the GGM. Additional data may be required to support the degree of variability in the system.

- 2. Water consumption at zero water saturation.** There is potential for improvement in the way the GGM models gas generation, once the repository has reached zero water saturation. Initially the relative humidity will be high and the water consuming reactions will proceed, thus reducing the relative humidity within the repository. This is likely to be a relatively fast process compared to the timescales of interest. Currently the GGM can modify its behaviour dependent on the relative humidity calculated by TOUGH2, shutting down microbial reactions when the relative humidity drops. However, the GGM does not model water vapour explicitly and does not supply any information to TOUGH2 about the amount of water vapour being consumed through microbial reactions. The GGM only supplies information to TOUGH2 about the amount of bulk water being consumed. The evidence from case NE-UG-GT is that the consumption of bulk water is sufficient to reduce the relative humidity and so this aspect of the model at zero saturation is sufficiently accurate.

From this point onwards, the saturated phase water consuming reactions should be limited to consume only water that enters the repository. This may be a slow diffusive process. Vapour phase reactions should continue provided there is sufficient humidity. Currently the water consuming saturated phase reactions are allowed to proceed at their full rate, which they can only do by drawing in water from the geosphere. It is recommended that the model be updated to take this into consideration. This may significantly affect the results for the NE-UG-GT case after 1000 years.

- 3. Limits of zero and complete water saturation:** Currently the GGM is structured such that it is reliant on the concept of both saturated and vapour phases, through, for example, use of Henry's Law. As a result it cannot make smooth transitions to the cases of complete or zero saturation. While complete saturation of the repository was not observed within 1 million years for any of the cases, it is anticipated that this state will eventually be reached. Zero saturation occurs for the NE-UG-GT case and this is currently handled by enforcing a minimum saturation of 10^{-10} . It is recommended that the model be modified to allow zero and complete saturation to be achieved smoothly.
- 4. The composition of gas entering the repository:** The difference in gas pressure between the geosphere and the repository for the case NE-UG-GT was such that gas originating in the geosphere entered the repository. However, the model which determines the composition of the gases entering the repository is the same as the model that determines the fluxes leaving the repository. This keeps the ratios of the partial pressures of the gases equal while the total gas pressure changes. This assumes therefore that the composition of the gases entering the repository is similar to the composition of gases existing within the repository. However, the repository atmosphere is dominated by hydrogen or methane and this may have a very different composition to the gas in the geosphere which is currently modelled as containing a single bulk gas with similar properties to air. It is recommended that the GGM inputs be updated to obtain information from TOUGH2 about the composition of the gases around the repository, and that the GGM is modified to use this information when gas enters the

repository. Current site characterization data suggests that the composition of gas in the geosphere is mainly CH₄, with some CO₂.

5. **Transport of gas via water:** The general pattern observed for water evolution is that it enters the repository up until such time that sufficient gas pressure builds up and then water starts to leave the repository, before, after some time, proceeding towards resaturation. Currently any gases dissolved within the water in the repository are assumed by GGM to remain within the repository rather than being transported out with the water when it leaves. GGM could be made more realistic by taking this effect into account.

While transport of the dissolved gas out of the repository with water is not modelled in GGM, diffusion of dissolved gas is taken into account by TOUGH2. This affects gas pressures in the geosphere which ultimately feeds back to the GGM and alters the fluxes of water and bulk gas between the repository and the geosphere.

6. **Salinity and microbial activity:** The water entering the repository is expected to be highly saline, which will affect the types of bacteria which operate. With the current model this can be taken into consideration by selecting appropriate microbial reactions rates. These need to be reviewed to ensure that they are compatible with highly saline conditions. The high salinity environment has the potential to affect methane generation to some extent, and there may be potential for improving the underlying gas generation model to more accurately represent microbial behaviour in highly saline environments. This is an area that may need some experimental support. Under highly saline environments there may be other competing microbial processes which operate rather than gas generation, and so this is expected to be conservative with respect to gas generation. There is some uncertainty over the microbial hydrogen consumption rates used and much of the data in the literature are expressed in units that are incompatible with the first order rate constants required by the GGM (Walke et al. 2009b). Some studies suggest rates as high as 1/hour. However, investigations have shown that gas evolution is not highly sensitive to this parameter provided it is sufficiently fast to cause periods of time where the system is hydrogen limited. A rate of 1/year has been assumed in this study, which meets this criterion. The slower rate chosen is deemed conservative, since it allows less hydrogen and carbon dioxide to be converted to methane, and this in turn acts to increase total gas pressures.
7. **Surface areas:** Currently, at a given moment in time, the surface areas of the metallic waste streams within the saturated phase of the repository are calculated as the initial surface areas of the wastes multiplied by the water saturation. In terms of gas generation, this is likely to be a conservative assumption at large times where the amount of metallic waste remaining is small and the saturation may be large. There may be some scope for improving the model for surface areas based on data from long term corrosion studies.

In addition to the way the surface areas will evolve as the metals are corroded, there is inherent uncertainty in the initial surface areas of the wastes. This can be mitigated to a certain extent by allowing for variability in surface areas as discussed in point 1.

There are three additional issues for potential consideration in further work that do not impact directly on the results presented here.

1. **Run times:** Currently the GGM and TOUGH2 take the same time steps. The GGM currently limits the time steps taken by TOUGH2 to ensure that detailed gas generation processes are resolved accurately. However, since TOUGH2 and the GGM are coupled by variables such as the total gas pressure and saturation, which are relatively smooth and are not strongly affected by the details of the gas generation processes, it should be possible to decouple them. This would allow TOUGH2 to take fewer and longer time steps, improving run times, and would allow the GGM to continue to take the time steps it required to accurately resolve the gas generation processes.
2. **Carbonation of concrete:** A potential sink for CO₂ in the repository is the carbonation of the cementitious material. This process could consume significant quantities of CO₂, especially if the repository is grouted. The evolution of the concrete pore-water chemistry is a complex process which is not currently included in the GGM, but this is considered conservative with respect to gas generation.
3. **Magnesium oxide:** The GGM is able to model the consumption of CO₂ via the precipitation of magnesium carbonate that could occur if magnesium oxide was added to the repository as a “gas scavenger”. This could be considered as an alternative normal evolution scenario.

8.2 GAS TRANSPORT MODEL

8.2.1 MODELLING APPROACH

Analysis of the modelling results raised several issues related to the modelling approach, which can be addressed by further developing the T2GGM model and/or increasing the level of detail currently considered in the modelling approach.

Issues which may have an impact on simulation results are as follows.

1. **Air as the bulk gas.** The current modelling assumes air as the bulk gas transported through the geosphere. Gas generation results show the composition of the bulk gas to be very different from that of air, comprised mainly of CH₄ and, at early times, H₂. As well, current site characterization data suggests initial gases in the geosphere are primarily CH₄, with some CO₂, which is relevant for cases such as the NE-UG-GT. The consequences of the differences between air and the actual composition of gases are not straightforward, due to the combination and different properties of these gases. Comparing air to methane, the primary gas generated and existing in the geosphere, air is expected to provide a reasonable approximation as methane has a solubility half that of air (other properties between air and methane are similar). The use of air as the bulk gas is currently hard-coded into the T2GGM model, as a result of air being hard-coded in the selected TOUGH2 EOS3 model. Modification of the bulk gas in the T2GGM to another gas, such as CH₄, requires modification of the molar mass, Henry’s solubility coefficient and viscosity calculation. TMVOC, another TOUGH2 family model using multiple gases could be used; however, it would require some effort to integrate this model with GGM and modify it to include appropriate gases (e.g., H₂ currently not included in available TMVOC gases). Modelling multiple gas species with TMVOC is considerably more complex and consequently will significantly increase model run times. TMVOC is therefore not likely to be practical for running multiple simulations; however a modified TMVOC would serve as a useful tool for verifying T2GGM NE-BC

performance. Modification of T2GGM to allow for user selection of a single gas and user input of gas properties would allow for relative effects of different single gases (CH₄, CO₂, and H₂) to be evaluated and is recommended.

2. **2D spatial representation.** A further cause of uncertainty relates to simplifications in spatial representation of the repository system and the geosphere. The 2D radial model is a simplified representation of the actual Hatch (2008) design, and does not allow for inclusion of horizontal gradients or open borehole or fracture features required to consider disruptive scenarios. A 3D model, similar to that described in Avis et al. (2009) for groundwater modelling, could improve repository system representation and incorporate these features; however, simplifications will still be required in order to keep this model tractable. The increased mesh size of a 3D model will ensure long run times, and as a consequence, a 3D model is only recommended as a sensitivity case to increase confidence in the 2D model.
3. **Constant density fluid.** Although some effects of variable-density flow are incorporated by using environmental head to calculate the Cambrian overpressure, other possible impacts are ignored by selection of the TOUGH2/EOS3 code to model groundwater and gas flow. However, from the perspective of gas transport, effects of variable density will have minimal impact on results.

Issues which impact model tractability and result interpretation are as follows.

4. **Uncontaminated gases.** The repository and shaft system contain initial uncontaminated gases, and in the NE-UG-GT case, the rock mass also contains initial uncontaminated gases. However, the current modelling approach is unable to differentiate between initial uncontaminated gases and gases potentially contaminated by waste degradation. Initial gas represents a small portion of the gases in the system; 3.94×10^5 kg of gas is initially present in the shaft and geosphere, whereas 3.14×10^7 kg of gas is generated in the NE-BC. In the cases where gas reaches the surface of the model, while most of the initial gas in the shafts dissolves, it is impossible to tell whether the gas reaching the surface is contaminated, uncontaminated or a mixture of the two. Several approaches are possible to resolve this issue: use of a multi-gas model such as TMVOC, and assume all initial gases are another gas different from those generated in the repository; use an alternate TOUGH2 module such as EOS7R to include radionuclides, modification would be required for GGM integration and use of appropriate bulk gas (currently uses air).
5. **Long model run times.** Long run times in the T2GGM model are partly related to the coupling of the GGM and TOUGH2 model, as described in Section 8.1. Long times are also seen as a result of TOUGH2 instabilities of rapidly evolving and disappearing gas phase within elements, particularly as the repository saturates with water for the second time (and gas is disappearing from below the repository). Efforts to minimize these instabilities, for example by smoothing out gridding to minimized large differences in element size, might significantly improve run times and allow simulations that stalled to complete (e.g., NE-BC). TOUGH2-MP, a multi-processor version of TOUGH2, may also be investigated to reduce run times by increasing the number of processors used by TOUGH2.

8.2.2 PARAMETER UNCERTAINTY

The base case and sensitivity cases for the Normal Evolution Scenario considered in this report were intended to illustrate possible or feasible conceptual models. Cases showing very different responses, such as the NE-UG-GT case, help define parameters requiring increased certainty.

The following list enumerates the major sources of parameter uncertainty.

1. **Geosphere permeabilities:** The UG cases resulted in the lowest repository gas pressures, due to limited water saturation of the repository as a result of the low permeabilities. Additional site characterization data and analyses to confirm permeabilities should be forthcoming in 2009.
2. **Sensitivity of the model to capillary pressure and relative permeability parameters** in rock mass, EDZ, and in engineered barriers was not examined in these cases. The capillary pressure curves are particularly important in defining conditions for cases with initial gas saturation, such as the NE-UG-GT case, as initial gas pressures in the rock cannot be measured directly, only inferred from liquid pressures and capillary pressures. For units above the Queenston, data to support the values for these parameters did not exist, and values were assumed or calculated based on the Davies relationship. Additional site characterization data and analyses should provide this data.

The sensitivity of the model to these two-phase flow parameters should be examined in future studies. Due to the number of parameters, ideally probabilistic modelling would be conducted to determine the sensitivity of the model to the Van Genuchten model; however, as previously noted, probabilistic modelling is currently not tractable due to the long run times of the T2GGM model.

3. **Shaft EDZ characterization and shaft seal effectiveness:** Effectiveness of the shaft seals and permeability of the shaft EDZ is clearly important, particularly with the assumed steady Cambrian overpressure and the base case geosphere. The shaft seal and EDZ uncertainties are less important in the updated geosphere; also shaft properties above the Ordovician have limited impact on performance. As described in Walke et al. (2009b), the EDZ characterization is largely based on international experience and expert opinion. The sensitivity cases provided in this report are conservative, and consequently provide bounding cases. The rationale for selection and justification of capillary pressure and relative permeability curves to represent EDZ properties requires further investigation.

8.3 GEOSPHERE CONCEPTUAL MODEL UNCERTAINTY

Our understanding of the geosphere history and future evolution is described in the Geosynthesis report (Gartner Lee 2008a), and the repository system evolution is summarized in the System and its Evolution report (Little et al. 2009). Specific areas of uncertainty that have significant impact on gas transport results are listed below, along with how they are current addressed in this study.

1. **Mechanism of Ordovician underpressures:** Transport of dissolved gas from the repository will be significantly reduced for as long as underpressures persist in the Ordovician units. During this period prevailing liquid gradients will be downward at all

points above the repository horizon, including the shaft and EDZ system. As the causal mechanism for underpressures measured at the Bruce site is not known with certainty, the long-term behaviour cannot be predicted. Therefore the current study makes the conservative assumption that the underpressures have been dissipated to steady state.

2. **Time dependence of Cambrian overpressure:** In the steady-state flow analyses presented in this report, the transport of dissolved gas through the shaft EDZ and rock mass is driven by high pressure in the Cambrian unit forming the lower boundary of the modelled system. The Cambrian lower boundary condition is also a sink for gas transported downwards from the repository. If steady-state flow is assumed, this gradient determines flow of water from the surrounding rocks into the repository and subsequently through the shaft/EDZ system. The impact of the gradient is mitigated substantially by reduced permeability in the UG geosphere cases. Although this pressure is proven present from site characterization results, its origin and therefore evolution is currently unknown. In the current study, the Cambrian pressure has been assumed constant.
3. **Initial gas saturations in the Ordovician:** The NE-UG-GT case demonstrates the importance of initial gas saturations and pressures on repository performance. Preliminary site characterization data suggest that gas saturations exist in the rock mass at the repository horizon. The existence of gas at these horizons is one possible explanation for the observed underpressures. Quantification of gas saturations is uncertain, as the permeability and porosity of the rock mass are at the threshold at which existing measurement techniques can be applied. Additionally, the source of the initial gas saturations has not been determined. Consequently, the long term behaviour cannot be predicted and the conservative assumption is used that gas will slowly be transported and dissolved into solution and water pressures will dissipate to a steady-state flow condition.
4. **Silurian flow system** - The conceptual model for groundwater flow in the Silurian formations at the Bruce site is currently under development. Measured vertical pressures at the DGR-1 borehole indicate that overpressures exist in the lower Silurian (below the Guelph Formation) with limited or nonexistent vertical gradients above the Guelph. Horizontal gradients are assumed to exist in the more permeable formations (Guelph and Salina A2 evaporite) and horizontal groundwater flow through these units will occur. These processes are not represented in the gas model, but may be expected to substantially reduce, if not eliminate, vertical transport of gas and dissolved gases above the permeable horizons. Site data describing gradient magnitudes and directions will be available from the Phase 2 site characterization activities. Incorporation of horizontal flow will require use of a 3D model as described in Section 8.2.1 above.
5. **Future glaciation events:** The impact of sequential future glaciation events on the repository system has not been evaluated in detail. The primary effects are expected to be transient overpressurization during glacial advances followed by dissipation during glacial retreats. The effects of overpressures on repository saturation are unclear, as it will depend on the corresponding increase in repository pressure caused by the overpressures. Glaciation may have mechanical impacts such as causing roof failure within the repository. However, calculations presented here all assumed complete roof failure from an early period.

6. **Porewater and rock mass interactions with gases.** There may be interactions of dissolved and free phase CO₂ with the carbonate rocks and porewaters that may impact CO₂ transport. The collection of porewater and rock geochemical data will assist in determining if these reactions are important.

Ideally, the sensitivity of the system to Cambrian overpressure evolution and the parameterization of Ordovician underpressures and initial gas saturations would be assessed using probabilistic analyses. However, due to the long run times of the T2GGM model, probabilistic analyses are currently intractable. Sensitivity cases examining Cambrian overpressure and Ordovician underpressures could be guided by probabilistic analyses conducted for the groundwater modelling. Further examination and sensitivity analysis of the capillary pressure curves will improve certainty in the initial gas saturations and gas and water pressures.

The inclusion of glaciation effects will require the development of more complex modelling approaches where transient boundary conditions representative of glacial loading are applied to the surface of the model. The current gas transport model cannot consider hydro-mechanical effects, and alternate modelling approaches would be required. Effects of overpressures from glaciation on repository saturation may be examined by applying a constant glacial loading at an appropriate time during the simulation (e.g., start glacial loading at 10 000 years).

9 SUMMARY AND CONCLUSIONS

The long-term performance of the proposed L&ILW repository at the Bruce site has been assessed with the use of numeric models of two-phase gas and groundwater flow. Base case and sensitivity analyses have been performed for the Normal Evolution Scenario and for a 'what if' disruptive scenario (Severe Shaft Seal Failure).

The modelling considered two primary conceptual models for the geosphere – a base case (BC) with low permeability rock, consistent with the Phase I Geosynthesis results, and an "updated geosphere" (UG) exploring a possible lower permeability rock as suggested by more recent site characterization results.

The modelling approach used is a dimensionally simplified two-dimensional radial model which incorporates aggregate properties of the repository and shaft in a computationally efficient model. The T2GGM model was employed, which couples the GGM gas generation model with the TOUGH2/EOS3 two-phase flow model. The GGM model component generates several different gas species, while the TOUGH2 model component approximates the total of these species as a single bulk gas of air.

The following general gas and water processes describe the main results for the Normal Evolution Scenario after closure and sealing of the shafts.

1. Oxygen within the repository is consumed and conditions become anaerobic.
2. Shaft becomes fully saturated with water, and initial gas in the shaft dissolves into the surrounding water.
3. Moisture initially present in the wastes, plus water that seeps into the repository from the surrounding rock and the shaft, support the anaerobic corrosion of metals and the degradation of organic wastes, resulting in generation of hydrogen, CO₂ and CH₄ gases. The gas pressure in the repository rises.
4. There is a pressure balance between the water seepage into the repository and the gas generation within the repository. For the base-case geosphere, the water inflow rate is enough to cause partial repository resaturation on a time scale of 1000 years. As gas generation continues and increases the repository pressures, water is pushed out of the repository, primarily into the rock mass below the repository. The repository becomes mostly unsaturated. Once repository gas pressures decrease such that they are less than the pressure in the geosphere, water begins to slowly saturate the repository once again. For the updated geosphere (UG), the very low permeability of the rock delays significant water saturation of the repository until after 200 000 years.
5. For most cases considered, with either base-case or updated-geosphere, the peak repository gas pressure is in the range 7 to 10 MPa, which is comparable to the environmental head at the repository horizon of around 7.5 MPa, and much less than the lithostatic pressure of 17 MPa. For the updated-geosphere, the gas pressures increase much more slowly than for the base-case geosphere.

6. As pressures in the repository develop, small amounts of gas are pushed out into the shaft and the rock mass. The high capillary pressures in the rock mass and bentonite seals ensure leakage of gas out of the repository is slow. Gas saturations in the rock remain very small within a few meters from the repository. In the NE-EDZ case, which has a permeable pathway through the shaft EDZ, some gas permeates up through the EDZ. Some dissolved gas also reaches the top of the Intermediate Groundwater Zone, in small amounts and at long times.
7. Methane is generally the dominant gas throughout the evolution of the repository, due to degradation of organic wastes and the consumption of hydrogen and carbon dioxide via the microbial methanogenic reaction. The balance of the initial inventories of metallic and organic wastes results in the repository atmosphere containing small levels of either hydrogen or carbon dioxide.
8. The repository remains largely unsaturated over the 1 million years evaluated in the normal evolution scenario. Slow gas dissolution and permeation allow eventual resaturation on very long time scales.

While all the cases for the Normal Evolution Scenario exhibit the same series of gas and water flow processes, they differ in the timing of these processes, as well as the magnitude of the repository response (both water saturation and pressure). Only the enhanced EDZ permeability case based on the DGR-1 and DGR-2 permeabilities (NE-EDZ) has bulk gas reaching the top of the Intermediate Groundwater Zone. As noted in Section 8.3, the simplified geometry of the gas model does not incorporate horizontal flow processes in the Silurian formations that would likely significantly reduce vertical flow through the Intermediate Bedrock Groundwater Zone.

Similar processes occur in the Severe Shaft Seal Failure Scenario. The main difference is that (as with the NE-EDZ case), gas reaches the top of the Intermediate Groundwater Zone. The SF-US case, with shaft failure only in the upper 400-m of Devonian and Silurian rocks, illustrates the effectiveness of the Ordovician sequence at limiting the transport of gas.

The results of the detailed gas modelling presented here are used in the assessment-level modelling to inform:

- the water level in the repository with time;
- the relative proportions of CO₂ and CH₄ and hence partitioning of gaseous C-14 between CO₂ and CH₄;
- the partitioning of radioactive gases between gas and groundwater in the repository;
- the release rates of radioactive gas entrained in bulk gas to the shaft and geosphere; and
- the bulk gas travel time from the repository to the ground surface via the shafts and geosphere.

Uncertainties have been minimized through use of sensitivity cases, conservative representation and a detailed gas generation model that incorporates the key processes for each waste stream. Sensitivity results highlight the following primary uncertainties and issues with a potential large impact on results.

- Variability in the gas generation repository system and gas generation behaviour at the limits of zero and complete water saturation. The introduction of variability in reaction rates is likely to smooth transitions and mitigate extremes of flux and pressure, while introducing more realism into the behaviour of the model in the limit of zero saturation is

likely to limit gas generation. The current model and results are expected to be conservative in both these respects; however, future studies should consider gas generation model refinements to further explore these uncertainties.

- Dimensional simplification of the actual three-dimensional repository to an equivalent two-dimensional radial axisymmetric system, primarily for model tractability. Future implementation of a fully 3D model as a sensitivity case could address any uncertainties related to this simplification.
- Geosphere permeabilities, initial gas pressures and initial gas saturations. Additional site characterization data will reduce the uncertainty of these parameters.
- Two-phase flow parameters (capillary pressure and relative permeability).
- Shaft and EDZ parameterization. The primary uncertainty is the characterization of the shaft EDZ hydraulic conductivities. The sensitivity cases provided in this report are conservative, and consequently provide bounding cases. Selection of appropriate capillary pressure and relative permeability functions for EDZ is another source of uncertainty.
- Additional significant geosphere uncertainties relate to gradients in the Silurian, the time dependence of the Cambrian overpressure, and the causal mechanism and characterization of the measured Ordovician underpressures. Further geosphere uncertainties relate to the hydromechanical response of the repository and geosphere system to glaciation events. These uncertainties are addressed with conservative conceptualization.

Other issues identified, which are not expected to have a large impact on results, but will improve the transparency of model results if considered in future work, include the use of methane or a combination of gases as the bulk gas, instead of air; and differentiating between uncontaminated and contaminated gases.

REFERENCES

- Avis, J., N. Calder and R. Walsh. 2009. Postclosure Safety Assessment: Groundwater Modelling. Nuclear Waste Management Organization (NWMO) Report DGR-TR-2009-06-R0. Toronto, Canada.
- Davies, P. B. 1991. Evaluation of the role of threshold pressure in controlling flow of waste-generated gas into bedded salt at the Waste Isolation Pilot Plant (WIPP). Sandia Report SAND 90-3246, Sandia National Laboratories, Albuquerque, USA.
- DGR. 2009. Estimated Low Hydraulic Conductivity Values from Preliminary DGR-3 & DGR-4 Test Results. DGR Project Data Release 5/3/09. NWMO Records: 00216N-01900-T7. Nuclear Waste Management Organization. Toronto, Canada.
- European Commission (EU). 1999. Gas Migration and Two-Phase Flow through Engineered and Geological Barriers for a Deep Repository for Radioactive Waste. A Joint EC/NEA Status Report. EUR 19122 EN. Pg 29, Luxembourg.
- Garisto, N., J. Avis, S. Fernandes, R. Jackson, R. Little, J. Rees, G. Towler, and R. Walke. 2009. Postclosure Safety Assessment (V1): Features, Events and Processes. Nuclear Waste Management Organization (NWMO) Report DGR-TR-2009-05-R0. Toronto, Canada.
- Gartner Lee Limited. 2008a. OPG's Deep Geologic Repository for Low and Intermediate Level Waste. Phase 1 Geosynthesis. Ontario Power Generation Report OPG 00216-REP-01300-00010-R00. Toronto, Canada.
- Gartner Lee Limited. 2008b. OPG's Deep Geologic Repository for Low and Intermediate Level Waste. Phase 1 Regional Geology, Southern Ontario. Ontario Power Generation Report OPG 00216-REP-01300-00007-R00. Toronto, Canada.
- Hatch. 2008. OPG's Deep Geological Repository For Low and Intermediate Level Waste: Conceptual Design Report. Hatch 323874DGR-RPT-CDR200-Rev01. OPG 00216-REP-03902-00004-R01. Toronto, Canada.
- Incropera, F. P. and D. P. DeWitt. 1996. Fundamentals of Heat and Mass Transfer. John Wiley and Sons, USA.
- Little, R., A. Bath, P. Humphreys, F. King, R. Metcalfe, J. Penfold, D. Savage, G. Towler and R. Walke. 2009. Postclosure Safety Assessment (V1): System and Its Evolution. Nuclear Waste Management Organization (NWMO) Report DGR-TR-2009-04-R0. Toronto, Canada.
- Marschall, P. 2006. Evolution of temperature and water content in the bentonite buffer: Scoping calculations in support of general THM process and system understanding (GL 05-54). NAGRA AN 06-190. Wettingen, Switzerland.
- Penfold, J. and R. Little. 2009. Postclosure Safety Assessment (V1): Analysis of Human Intrusion and Other Disruptive Scenarios. Nuclear Waste Management Organization (NWMO) Report DGR-TR-2009-03-R0. Toronto, Canada.

Penfold, J.S.S., R.H. Little, R.A. Bowden and M.J. Egan. 2003. Preliminary Safety Assessment of Concepts for a Permanent Waste Repository at the Western Waste Management Facility Bruce Site. Quintessa Report QRS-1027B-1 v1.0. Henley-on-Thames, UK.

Pruess, K., C. Oldenburg and G. Moridis. 1999. TOUGH2 User's Guide, Version 2.0. Lawrence Berkeley National Laboratory LBNL-43134. Berkeley, USA.

Quintessa, Intera and SENES. 2009. Postclosure Safety Assessment (V1) Report. Nuclear Waste Management Organization (NWMO) Report DGR-TR-2009-01-R0. Toronto, Canada.

Suckling, P., J. Avis, N. Calder, P. Humphreys, F. King, J. Rees and K. Sedor (2009). T2GGM Software Documentation. Nuclear Waste Management Organization (NWMO) Technical Memorandum DGR-01390-T10. Toronto, Canada.

Sykes, J.F., E.A. Sykes, S.D. Normani, Y. Yin and Y.-J. Park, University of Waterloo. 2008. Phase I Hydrogeologic Modelling. OPG Report 00216-REP-01300-00009-R00. Toronto, Canada.

Walke, R., L. Limer, R. Little and G. Towler. 2009a. Postclosure Safety Assessment (V1): Analysis of the Normal Evolution Scenario. Nuclear Waste Management Organization (NWMO) Report DGR-TR-2009-02-R0. Toronto, Canada.

Walke, R., A. Bath, A. Bond, N. Calder, P. Humphreys, F. King, R. Little, R. Metcalfe, J. Penfold, J. Rees, D. Savage, G. Towler and R. Walsh. 2009b. Postclosure Safety Assessment (V1): Data. Nuclear Waste Management Organization (NWMO) Report DGR-TR-2009-08-R0. Toronto, Canada.

APPENDIX A: T2GGM V1.3 COMPUTER PROGRAM ABSTRACT

A.1 INTRODUCTION

T2GGM Version 1.3 is a software package intended for use in modelling gas generation and transport for a deep geologic repository.

It is comprised of two coupled models: a Gas Generation Model (GGM) used to model the detailed generation of gas within a repository due to corrosion and microbial degradation of the various wastes present, and a TOUGH2 model for two-phase gas and water transport in the repository and the geosphere.

Specific measures that the code is required to predict are:

- the magnitude and timing of the peak gas pressure within the repository;
- the evolution of the repository saturation;
- the rates of gas and liquid generation within the repository; and
- the flux of gas through the geosphere.

A.2 OPERATING REQUIREMENTS

T2GGM is intended for operation on a computer running current versions of Windows, such as Windows Vista. The required computer capabilities depend on the size of the model.

The user is referred to TOUGH2 documentation (Pruess et al. 1999) for compiling requirements. GGM and its include files simply need to be included during the compilation process.

A.3 COMPONENTS

T2GGM v1.3 requires the following modules

- GGM version 1.3
- TOUGH2 v 2.0 including EOS3 module.

A.4 CAPABILITIES

This primary capabilities are:

- hydrogen gas generation from corrosion of steels and zirconium alloys under aerobic and anaerobic conditions;
- CO₂ and CH₄ gas generation from degradation of organic materials under aerobic and anaerobic conditions;
- methanogenesis from CO₂ and H₂
- biomass generation, decay and recycling;
- exchange of gas and water between the repository and the surrounding geosphere; and
- two-phase flow of water and gas in the geosphere.

Full details can be found in the theory section of the software documentation (Suckling et al. 2009).

A.5 LIMITATIONS

T2GGM is a complex code, modelling a range of coupled processes, from gas and liquid transport to microbial degradation and corrosion, over disparate length and time scales. This

makes running the code technically very difficult. The code has been designed and tested for the geometry and parameters relevant to the OPG DGR Version 1 Postclosure Safety Assessment.

Run times for the code can be anything from several days to a week depending on the parameters used. As a result, it may not be practical to use T2GGM to perform sensitivity studies with T2GGM without further simplifying assumptions and code development.

Significant limitations in T2GGM v1.3 include the following:

- water consuming reactions within the repository are not limited at low water levels;
- repository corrosion and gas reaction rates are first order in a primary reactant, and in particular are not dependent on the amount of microbial biomass;
- metal corrosion and organic decomposition is described by a constant corrosion rate for the relevant conditions (aerobic/anaerobic, saturated/unsaturated);
- organics are modelled as either cellulose or styrene;
- all gas in the geosphere is modelled as air; all gases released from the repository model are converted into air on an equivalent molar basis; and
- groundwater in the geosphere is modelled as freshwater.

A.6 DOCUMENTATION

Detailed documentation for T2GGM version 1.3, including a Theory Manual with supporting references, is contained in the Software Documentation (Suckling et al. 2009).

REFERENCES FOR APPENDIX A

Pruess, K., C. Oldenburg and G. Moridis. 1999. TOUGH2 User's Guide, Version 2.0. LBNL-43134. Earth Sciences Division, Lawrence Berkeley National Laboratory, Berkeley, California.

Suckling, P., J. Avis, N. Calder, P. Humphreys, F. King and J. Rees, K. Sedor (2009). T2GGM Software Documentation. Nuclear Waste Management Organization (NWMO) Technical Memorandum DGR-01390-T10. Toronto, Canada.

APPENDIX B: SIMPLE GAS PRESSURE CALCULATION

B.1 SUMMARY

This appendix documents a simple 'back of the envelope' calculation, designed to estimate the maximum gas pressures that could be observed within the repository, as waste is converted to gaseous forms during its evolution.

Based on the initial waste inventories (about 5.8×10^7 kg of metals and 2.2×10^7 kg of organics), this calculation estimates the total number of moles of iron (Fe), zirconium (Zr), and carbon (C) in the repository. These materials were assumed to degrade completely to generate mostly hydrogen (H_2), carbon dioxide (CO_2), and methane (CH_4) gases within the void volume of the repository. The following assumptions were made:

- no leakage of these gases;
- no oxygen, no nitrate, no sulphate;
- no biomass;
- unlimited supply of water;
- void space of 3.35×10^5 m³ in the repository, taken from Table 4-5 of the data report (Walke et al. 2009); and
- repository temperature of 20°C.

This simple calculation indicates maximum gas pressures of about **19 MPa** under the above assumptions. See Section B.2. This estimate does not take into account the following.

- $FeCO_3$ (siderite) formation from iron and H_2CO_3 (carbonic acid). This reaction could reduce gas pressure making less Fe available for the H_2 -producing Fe_3O_4 corrosion reaction.
- The methanogenic reaction, which converts 4 moles of H_2 with 1 mole of CO_2 to 1 mole of CH_4 .

These two reactions could reduce the gas pressure. The relative importance of these reactions was explored and the results are given in Section B.3-B.5. A summary of maximum gas pressures is given in Table B-1. Table B-1 shows that methanogenic reaction is the most important process for reducing gas pressure, followed by siderite formation. Case 4, which corresponds to the T2GGM base case (NE-BC), shows a maximum gas pressure of about **8 MPa**, consistent with T2GGM results. This pressure is slightly above the initial steady state pressure of about 7.6 MPa at the repository level, and significantly below the lithostatic pressure of about 17 MPa at the repository level.

Table B-1: Estimated Maximum Repository Gas Pressures

Gas Generation	Initial Mass of Metals or Organics (kg)	Maximum Gas Pressure (MPa)			
		Case 1	Case 2	Case 3	Case 4
		Anaerobic Corrosion & Degradation	Case 1 with FeCO ₃ Formation	Case 1 with Methanogenic Reaction	Case 1 with FeCO ₃ and Methanogenic Reactions
H ₂ from metal corrosion	5.8E+07	10.0	8.8	0.0	0.2
CO ₂ from organic degradation	2.2E+07	3.6	0.0	1.2	0.0
CH ₄ from organic degradation		5.3	5.3	7.8	7.6
N ₂ from initial air	-	0.1	0.1	0.1	0.1
Total	8.0E7	19.0	14.2	9.0	7.9

B.2 GAS GENERATION UNDER ANAEROBIC CORROSION & DEGRADATION WITH NO SIDERITE FORMATION AND NO METHANOGENIC REACTION (CASE1)

B.2.1 METAL CORROSION

The metals within the repository are categorised into unpassivated and passivated C-steels, passive alloys, and zircaloy. The first three are assumed to be composed of Fe. The zircaloys are assumed to be composed of Zr. See Table B-2 for their inventory. These metals are corroded under anaerobic condition according to the following equations:



Therefore, 1 mole of Fe generates 4/3 mole of H₂; 1 mole of Zr generates 2 moles of H₂. Based on the Fe and Zr total moles, the amount of H₂ generated from metal corrosion was calculated to be 1.4 x 10⁹ moles (Table B-2).

Table B-2: Iron and Zirconium Initial Inventory and Theoretical Amount of H₂ (Case 1)

Waste source	Initial Metal Mass* (kg)	Initial Fe Amount (mol)	Initial Zr Amount (mol)	Theoretical H ₂ Amount (mol)	Theoretical Fe ₃ O ₄ Amount (mol)
Unpassivated C-steel	2.3E+07	4.1E+08	-	5.5E+08	1.4E+08
Passivated C-steel	1.7E+07	3.0E+08	-	4.0E+08	1.0E+08
Passive alloys	1.7E+07	3.0E+08	-	4.0E+08	1.0E+08
Zircaloy	6.1E+05	-	6.7E+06	1.3E+07	-
Total	5.8E+07	1.02E+09	6.7E+06	1.4E+09	3.4E+08

*Table 4-12 from the data report (Walke et al. 2009).

B.2.2 DEGRADATION OF ORGANICS

The organic materials are categorised into cellulosic, plastics and rubbers, and ion-exchange resins. Cellulosic materials are modelled by $C_6H_{10}O_5$, and plastics and rubbers are modelled by C_8H_8 (styrene). The dry ion-exchange resins consist of cation and anion resins (assumed 50 mol% each). See Figure B-1 for cation resin structure. The molecular mass for dry cation and anion resin is 0.184 and 0.193 kg/mol respectively, averaged 0.1885 kg/mol. The resins have an average of 10 carbon (C) atoms per mole of resins.

Table B-3 shows the initial C amount (1.2×10^9 moles). Since 1 mole of C generates 1 mole of CO_2 or 1 mole of CH_4 , the theoretical total amount of CO_2/CH_4 from organic materials is 1.2×10^9 moles.

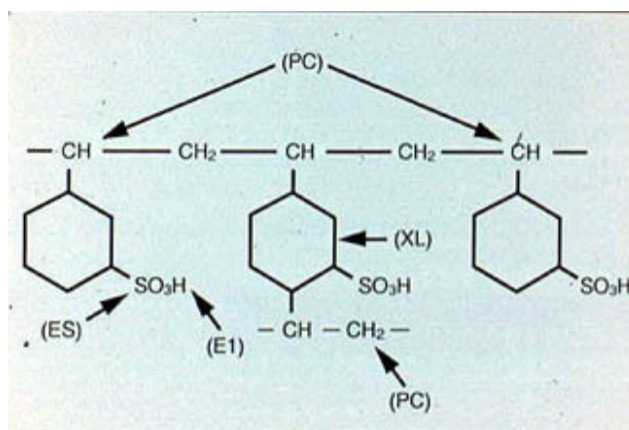


Figure B-1: Molecular Structure of Cation Resins (XL: cross link; PC, polymer chain; ES, exchange site; EI, exchangeable ion)

Table B-3: Carbon, Hydrogen and Oxygen Contributions from Organic Waste Sources (Case 1)

Waste source	Molecular Mass (kg/mol)	Initial Organic Mass (kg)*	Initial Carbon Amount (mol)	Theoretical CO_2+CH_4 Amount (mol)
Cellulosic materials	0.162	8.5E+06	3.1E+08	3.1E+08
Plastics and rubbers	0.104	7.9E+06	6.1E+08	6.1E+08
Ion-exchange resins (dry)	0.1885	5.8E+06	3.1E+08	3.1E+08
Total		2.2E+07	1.2E+09	1.2E+09

*Table 4-10 from the data report (Walke et al. 2009).

CO_2 and CH_4 can also be estimated from the following anaerobic degradation reactions. The results are shown in Table B-4. Rubber, plastics, and resins are treated as styrene (C_8H_8).



Table B-4: CO₂ and CH₄ Generation from Organic Waste Sources (Case 1)

Waste source	Theoretical CO ₂ Amount (mol)	Theoretical CH ₄ Amount (mol)	Theoretical CO ₂ +CH ₄ Amount (mol)
Cellulosic materials	1.6E+08	1.6E+08	3.1E+08
Plastics and rubbers	2.3E+08	3.8E+08	6.1E+08
Ion-exchange resins	1.2E+08	1.9E+08	3.1E+08
Total	5.0E+08	7.3E+08	1.2E+09

B.2.3 GAS PRESSURES

Metal corrosion and organic degradation mostly generate H₂, CO₂ and CH₄. In addition, initial air in the repository contains about 1.1 x 10⁷ mole of N₂. All O₂ in the initial air is quickly consumed by material degradation and is not considered in the scoping calculation. Based on the initial void space in the repository and repository temperature, the maximum gas pressure in the repository was calculated to be about 19 MPa using ideal gas law (Table B-5).

Table B-5: Maximum Repository Gas Pressure with No Siderite and No Methanogenic Reactions (Case 1)

	Theoretical Amount (mol)	Partial Pressure (MPa)
H ₂ from metal corrosion	1.4E+09	10.0
CO ₂ from organic degradation	5.0E+08	3.6
CH ₄ from organic degradation	7.3E+08	5.3
N ₂ from initial air	1.1E+07	0.1
Total	2.6E+09	19.0

B.3 GAS GENERATION UNDER ANAEROBIC CORROSION & DEGRADATION WITH SIDERITE FORMATION AND NO METHANOGENIC REACTION (CASE 2)

Because of the high HCO₃⁻ concentration, the stable corrosion product is FeCO₃ (siderite) rather than Fe₃O₄. The corrosion of carbon steel in CO₂-containing environments is given by



Therefore, 1 mole each of Fe and CO₂ will be converted to 1 mole each of FeCO₃ and H₂. Since there are 5.0 x 10⁸ moles of CO₂ (Table B-4), 5.0 x 10⁸ moles each of FeCO₃ and H₂ will be formed, and 5.0 x 10⁸ moles of Fe will be consumed. The remaining Fe (5.2 x 10⁸ moles) will be converted to Fe₃O₄ according to Equation (B-1). The theoretical amounts of iron corrosion products and H₂ are given in Table B-6.

Table B-6: Theoretical Amount of H₂ and Iron Corrosion Products (Case 2)

Waste source	Theoretical FeCO ₃ Amount (mol)	Theoretical Fe ₃ O ₄ Amount (mol)	Theoretical H ₂ Amount (mol)
Fe	5.0E+08	1.7E+08	1.2E+09
Zr	-		1.3E+07
Total	5.0E+08	1.7E+08	1.2E+09

Since 5.0×10^8 mole of CO_2 are converted to FeCO_3 , there will be no CO_2 . Therefore, Table B-4 can be simplified to Table B-7.

Table B-7: CO_2 and CH_4 Generation from Organic Waste Sources (Case 2)

Waste source	Theoretical CO_2 Amount (mol)	Theoretical CH_4 Amount (mol)
Cellulosic materials	0	1.6E+08
Plastics and rubbers	0	3.8E+08
Ion-exchange resins	0	1.9E+08
Total	0	7.3E+08

The total amount of H_2 and CH_4 are given in Table B-6 and B-7 respectively. Based on the ideal gas law, they can be converted to partial pressures. The total gas pressure was estimated to be 14 MPa (Table B-8).

Table B-8: Maximum Repository Gas Pressures under Anaerobic Corrosion & Degradation with Siderite and No Methanogenic Reaction (Case 2)

	Theoretical Amount (mol)	Partial Pressure (MPa)
H_2 from metal corrosion	1.2E+09	8.8
CH_4 from organic degradation	7.3E+08	5.3
N_2 from initial air	1.1E+07	0.1
Total	1.9E+09	14.2

B.4 GAS GENERATION UNDER ANAEROBIC CORROSION & DEGRADATION WITH METHANOGENIC REACTION AND NO SIDERITE FORMATION (CASE 3)

H_2 generated from anaerobic corrosion of metals can be combined with CO_2 to form CH_4 (Equation B-6).



There are a total of 1.4×10^9 moles of H_2 generated (Table B-2). It requires 3.4×10^8 moles of CO_2 to convert all H_2 to form 3.4×10^8 moles of CH_4 . Therefore, 1.6×10^8 moles of CO_2 will remain. See Table B-4 for total moles of CO_2 generated (5.0×10^8 moles). The total amount of CH_4 will be increased from 7.3×10^8 moles (Table B-4) to 1.1×10^9 moles. The total gas pressure was estimated to be 9 MPa (Table B-9).

Table B-9: Maximum Repository Gas Pressures under Anaerobic Corrosion & Degradation with Methanogenic Reaction and No Siderite Formation (Case 3)

	Theoretical amount (mol)	Partial Pressure (MPa)
H_2 from metal corrosion	0	0
CO_2 from organic degradation	1.6E+08	1.2
CH_4 from organic degradation	1.1E+09	7.8
N_2 from initial air	1.1E+07	0.1
Total	1.2E+09	9.0

B.5 GAS GENERATION UNDER ANAEROBIC CORROSION & DEGRADATION WITH METHANOGENIC REACTION AND SIDERITE FORMATION (CASE 4)

Case 4 considers both siderite formation and the methanogenic reaction. This case corresponds to the T2GGM base case (NE-BC).

CO₂ formed from the anaerobic degradation of organic materials can be consumed in the formation of FeCO₃ (Equation B-5) and in the methanogenic reaction (Equation B-6). The relative proportion of CO₂ consumption depends on the relative rate of these reactions. For the T2GGM base case, the amount of FeCO₃ formed was found to be 1.8 x 10⁸ moles for time greater than about 10,000 years (Figure 5-9). Therefore, 1.8 x 10⁸ mole of CO₂ (36% of total) was used in the siderite formation, leaving about 3.2 x 10⁸ mole of CO₂ (from 5.0 x 10⁸ moles in Table B-4).

H₂ is generated from metal corrosion (Equation B-1 and B-2) and siderite formation (Equation B-5). The total amount of H₂ was calculated to be 1.3 x 10⁹ moles (1.1 x 10⁹ moles from iron corrosion, 1.3 x 10⁷ moles from Zr corrosion, and 1.8 x 10⁸ moles from siderite formation). Based on Equation B-6, 1.3 x 10⁹ moles of H₂ are required to convert the remaining 3.2 x 10⁸ moles of CO₂ in the methanogenic reaction to form 3.2 x 10⁸ moles of CH₄. After siderite formation and methanogenic reactions, all CO₂ are consumed and about 2.8 x 10⁷ moles of H₂ remain. The total amount of CH₄ will be increased from 7.8 x 10⁸ moles (Table B-4) to 1.1 x 10⁹ moles.

The gas pressure was found to be about 8 MPa (Table B-10), consistent with the calculated gas pressure at long times (>10,000 years) for the NE-BC case (Figure 5-6). This pressure is slightly above the initial steady state pressure of about 7.6 MPa at the repository level, and significantly below the lithostatic pressure of about 17 MPa at the repository level.

Table B-10: Maximum Repository Gas Pressures under Anaerobic Corrosion & Degradation with Methanogenic and Siderite Reactions (Case 4)

	Theoretical Amount (mol)	Partial Pressure (MPa)
H ₂ from metal corrosion	2.8E+07	0.2
CO ₂ from organic degradation	0	0.0
CH ₄ from organic degradation	1.1E+09	7.6
N ₂ from initial air	1.1E+07	0.1
Total	1.1E+09	7.9

REFERENCES FOR APPENDIX B

Walke, R., A. Bath, A. Bond, N. Calder, P. Humphreys, F. King, R. Little, R. Metcalfe, J. Penfold, J. Rees, D. Savage, G. Towler and R. Walsh. 2009. Postclosure Safety Assessment (V1): Data. Nuclear Waste Management Organization (NWMO) Report DGR-TR-2009-08-R0. Toronto, Canada.